2010

The Mechanism of Mitochondrial Folate Transport by the Mitochondrial Folate Transporter

Scott Alan Lawrence
Virginia Commonwealth University

Virginia Commonwealth University
School of Medicine

This is to certify that the dissertation prepared by Scott Alan Lawrence entitled THE MECHANISM OF MITOCHONDRIAL FOLATE TRANSPORT BY THE MITOCHONDRIAL FOLATE TRANSPORTER has been approved by his committee as satisfactory completion of the dissertation requirement for the degree of Doctor of Philosophy.

Richard G. Moran, Ph.D., Director of Dissertation

Glen E. Kellogg, Ph.D., School of Pharmacy

Michael F. Miles, M.D., Ph.D., School of Medicine

Stephen T. Sawyer, Ph.D., School of Medicine

Shirley M. Taylor, Ph.D., School of Medicine

William L. Dewey, Ph.D., Chair, Department of Pharmacology and Toxicology

Jerome F. Strauss, III, M.D., Ph.D., Dean, School of Medicine

Dr. F. Douglas Boudinot, Dean of the Graduate School

April 29, 2010

THE MECHANISM OF MITOCHONDRIAL FOLATE TRANSPORT BY THE MITOCHONDRIAL FOLATE TRANSPORTER

A dissertation submitted in partial fulfillment of the requirements for the degree of Doctor of Philosophy at Virginia Commonwealth University.

by

SCOTT ALAN LAWRENCE
Bachelor of Science in Pharmacy, Ohio Northern University, 2004

RICHARD G. MORAN, PH.D.
PROFESSOR, DEPARTMENT OF PHARMACOLOGY AND TOXICOLOGY

Virginia Commonwealth University
Richmond, Virginia
April 29, 2010

Acknowledgements

I would like to recognize those who have fostered my scientific development throughout my graduate education. I would like to thank my advisor, Dr. Richard G. Moran, for the time, effort and research dollars he put forward in my training and for encouraging me to ask and answer my own questions. I will truly cherish the time I spent in his laboratory. I would also like to thank my committee members, Drs. Glen Kellogg, Michael Miles, Steve Sawyer, and Shirley Taylor for investing their time in my training. I would especially like to thank Dr. Shirley Taylor for her advice and guidance that covered all aspects of my research and beyond. I would like to thank Dr. John Hackett, who used our collaboration as an opportunity to teach me about molecular dynamics and computational chemistry. I also want to express gratitude to Drs. Jon Sprague and David Kinder at Ohio Northern University who mentored, advised, and encouraged me to pursue my interests in research. Finally, I would like to recognize and thank all of the members of the Moran and Taylor labs with whom I have worked: Dr. Dolores Arjona, Guoyan Gao, Amy Heineman, Cortney Heyer, Dr. Shane Kasten, Dr. T. Britt Langston, Dr. Erin Perchiniak, Erica Peterson, Dr. Alex Racanelli, Scott Rothbart, Lisa Shock, Prashant Thakkar, B. Ann Woodard, and Lin Xie. The conversations and interactions I had with all of you truly made difficult times and frustrating experiments easier.

Table of Contents

List of Tables

Page

List of Figures

Page

Abbreviations

5f-thf – 5-formyl-tetrahydrofolate

Å - angstroms

A_{280} – absorbance at 280 nm

AAC – ADP/ATP carrier

AICARFT – aminoimidazole ribonucleotide formyl transferase

Apo-MFT – molecular dynamics simulation with CHO MFT without tetrahydrofolate

bAAC – bovine ADP/ATP carrier

CATR - carboxyatractyloside

cFPGS – AuxB1 cell line transfected with the cytosolic isoform of FPGS

CHO – Chinese hamster ovary

CPK – Corey, Pauling, and Koltun coloring

cSHMT – cytosolic isoform of serine hydroxymethyltransferase

DHFR – dihydrofolate reductase

dox – doxycycline

FBS – fetal bovine serum

FPGS – folyl-poly-γ-glutamate synthetase

FR – folate receptor

GART – glycinamide ribonucleotide formyl transferase

GCS – glycine cleavage system

GFP – green fluorescent protein

K - kelvin

kb - kilobase

kDa – kilodalton

LAPAO – 3-laurylamido-N,N'-dimethylpropyl amine oxide

LB – Luria-Bertani

MCF – mitochondrial carrier family

MCS – multiple cloning site

MD – molecular dynamics

MEM – minimal essential medium

mFPGS - AuxB1 cell line transfected with the mitochondrial isoform of FPGS

MFT – mitochondrial folate transport protein

mSHMT – mitochondrial isoform of serine hydroxymethyltransferase

mutFPGS - AuxB1 cell line transfected with a mutated version of the mitochondrial isoform of FPGS

NPT – normal pressure and temperature

ns - nanoseconds

NVT – normal volume and temperature

PBS – phosphate buffer saline

PCFT – proton-coupled folate transport protein

PCR – polymerase chain reaction

PI – Roche EDTA-free protease inhibitors, proprietary mixture cat. # 11873580001

POPC – palmitoyl oleoylphosphatidylcholine

ps - picoseconds

PTP – phosphate transport protein

PVDF – polyvinylidene fluoride

RFC – reduced folate carrier

RNAi – RNA interference

SDS - sodium dodecyl sulfate

SDS-PAGE – sodium dodecyl sulfate-polyacrylamide gel electrophoresis

TBS-T – tris buffered saline with 0.05% Tween-20

TCA – trichloroacetic acid

T_D – doubling time

THF – tetrahydrofolate

THF-MFT - molecular dynamics simulation with CHO MFT and tetrahydrofolate

TMD – transmembrane domain

TS – thymidylate synthase

V - volts

Abstract

THE MECHANISM OF MITOCHONDRIAL FOLATE TRANSPORT BY THE MITOCHONDRIAL FOLATE TRANSPORTER

By Scott A. Lawrence, B.S. Pharmacy, R.Ph.

A dissertation submitted in partial fulfillment of the requirements for the degree of Doctor of Philosophy at Virginia Commonwealth University

Virginia Commonwealth University, 2010

Advisor: Richard G. Moran, Ph.D.
Professor, Department of Pharmacology and Toxicology

The mitochondrial folate transport protein (MFT) functions to transport folates into the mitochondrial matrix. The MFT is a member of a mitochondrial carrier family (MCF) of proteins that have a high degree of sequence and structural similarities, yet they transport vastly different substrates at high specificities. In this dissertation research, the folate-specific transport mechanism of the MFT was explored using experimental and computational techniques. MFT residues that differed from MCF consensus residues in conserved PxD/ExxK/R motifs and at a predicted substrate-binding site common to all MCF proteins were investigated. Site-directed mutagenesis of these anomalous residues in

the MFT revealed that these residues were adapted for optimal folate transport, and that the MCF consensus residues at these positions were incompatible with folate transport.

The structure of the MFT was predicted by homology modeling using the solved crystallographic structure of the ADP/ATP carrier as a template and this model was subjected to ~75 ns of molecular dynamics simulations. These simulations predicted a stepwise descent for the folate substrate into the MFT transport cavity and implicated several aromatic and basic residues in folate recognition and orientation. A predicted set of interactions at the base of the transport cavity between the MCF PxD/ExxK/R conserved motif residues did not appear static as previously hypothesized; these interactions appeared to be induced in the presence of the folate substrate. Therefore, we believe it is unlikely that these interactions form a barrier at the base of the transport cavity.

We also investigated the role of the MFT in the compartmentalization of folate metabolism. Cell lines were created that could be induced with doxycycline to express either the cytosolic or mitochondrial isoform of the enzyme folylpoly-γ-glutamate synthetase (FPGS). The constructed cell lines were used to study the flux of folylpolyglutamates across the mitochondrial membrane. It appeared that cellular folylpolyglutamates are not transported across the mitochondrial membrane in either direction. We also demonstrated that many antifolates, including methotrexate and pemetrexed, impaired mitochondrial folate uptake. We believe that these folate analogs competitively inhibit the MFT and have purified the MFT protein for future analysis in reconstituted transport systems.

CHAPTER 1 Introduction

Folate molecules are water-soluble B-vitamins that are required for cell growth and survival. Unlike bacteria, mammals are unable to synthesize folates and thus, must obtain folates from their diet. The United States Food and Drug Administration recommends a daily intake of 400 µg/day of folate for males and females over the age of 19 and 600 µg/day for pregnant women (66). Dietary folates can be separated into two groups: those that are naturally contained in food and those that are made synthetically. Dietary folates, or folates that are contained in food, are present in dark, leafy green vegetables, fruits, and beans. However, cooking destroys most of the naturally occurring folate in foods. More recently, synthetic folate, termed folic acid, has been added to many grain products in the United States and has also become available in pill-form supplements. Fortification of foods and the availability of supplements are responsible for increasing the folate status in the United States population (34). Despite this effort, folate deficiency, predominantly caused by insufficient intake and less commonly attributable to malabsorption, aberrant folate metabolism, or alcoholism, is still linked to diseases such as neural tube defects in pregnancy (135), anemia, and cancer.

Folate structure

Folate molecules are low molecular weight, anionic compounds that exist in a number of modified and conjugated forms within organisms. The basic folate chemical structure consists of a pteridine ring linked to a p-amino benzoate ring that has a glutamate residue attached via an amide bond (Figure 1-1). The structure of folic acid differs from the structure of tetrahydrofolate in that double bonds link the 5- and 6- and the 7- and 8-positions in the pteridine ring of folic acid. While this significantly enhances the stability of folic acid, in order for this compound to be biologically utilized the 6- and 7- positions in the structure of folic acid need to be reduced. In biological reactions 5,6,7,8-tetrahydrofolate derivatives serve to accept and donate 1-carbon units; the 5- and 10-position nitrogen atoms in the folate structure are the typical acceptors and donors of carbon groups. The vast majority of endogenous folates are modified on the glutamate end of the folate structure where 4-5 additional glutamate moieties are added. Folate molecules that contain multiple additions of glutamic acid are collectively referred to as folate polyglutamates. The purposes for and the function of these modifications will be discussed later in this chapter. In this thesis, use of term "folates" refers to all modified folate molecules unless otherwise stated.

Absorption and intracellular transport of folates

An understanding of folate structure and folate modification is important in understanding how ingested folates are utilized in the body. Folates that are naturally present in foods are folate polyglutamates and contain additional glutamate moieties linked

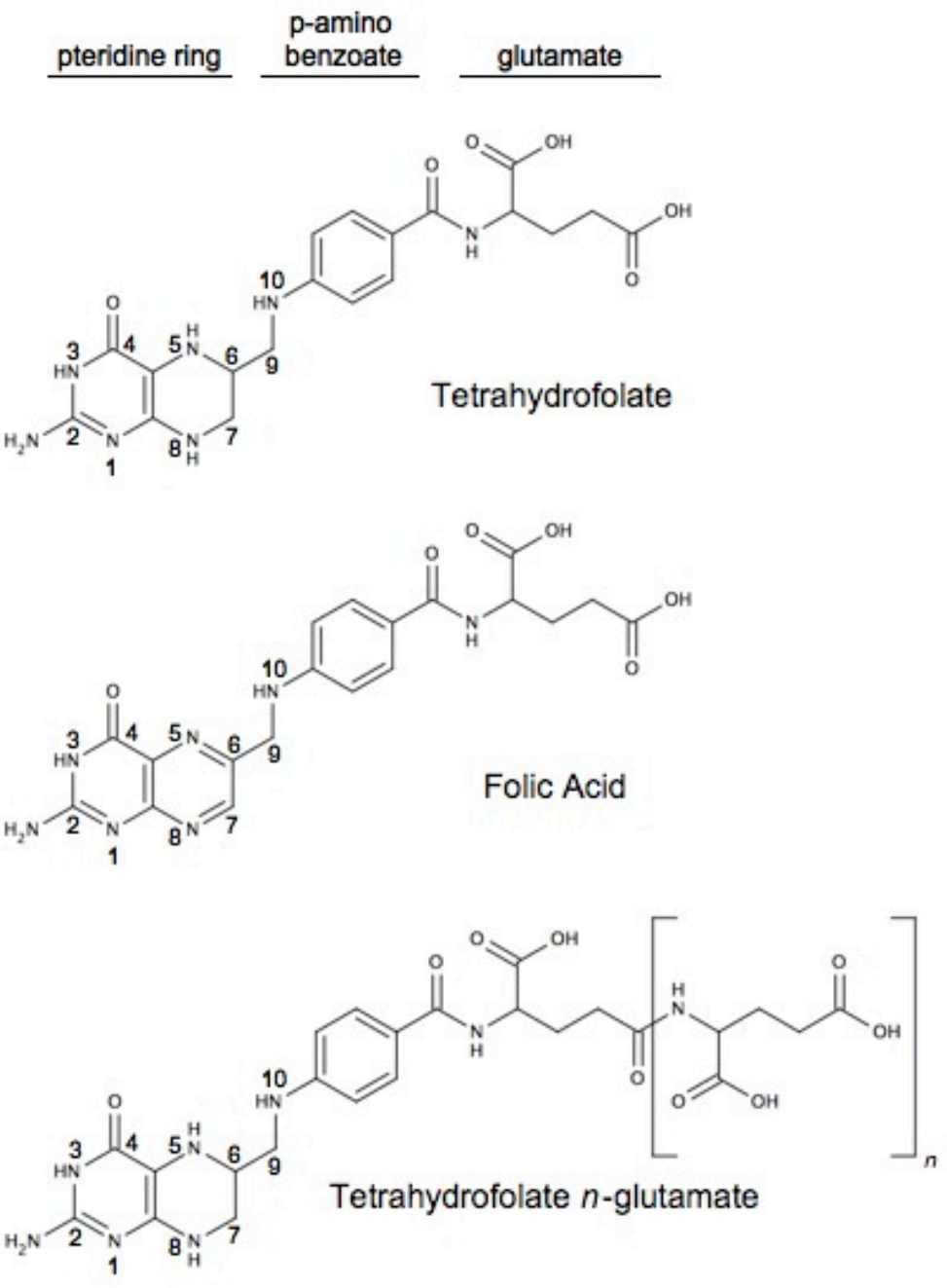

Figure 1-1 Structure of tetrahydrofolate, folic acid, and tetrahydrofolate polyglutamate.

γ-carboxyl group of the glutamate side chain of folate. Folate polyglutamates cannot be absorbed and depend on local enzymes, γ-glutamate carboxypeptidases (55, 146), to remove these additional glutamate moieties, leaving a single glutamate moiety on the folate molecule. Monoglutamyl tetrahydrofolate analogs do not contain any additional glutamate moieties and are absorbed into enterocytes without regard to carboxypeptidase activity. Folates are predominantly absorbed by the enterocytes in the small intestine by a proton-coupled folate transporter (PCFT) on the apical surface of the duodenum and proximal jejunum (115, 138). This transporter has a high affinity for folates (K_m (6S)-5-methyl-tetrahydrofolate = 0.53 μM) and synthetic folate (K_m folic acid = 0.83 μM) at a pH of 5.5 (138). A homozygous mutation has been identified in the PCFT and is linked to hereditary folate malabsorption (50, 138). The reduced folate carrier (RFC), another folate transport protein, is also present in the intestine, however, the RFC is pH-dependent and does not retain significant function at a pH below 6 (168), which is the pH at the apical surface in this area of the small intestine (94, 95). The mechanism of folate exit from enterocytes is less clear although it does appear evident that this process is carrier-mediated (144). Folate exit from enterocytes appears to be mediated by a multidrug-resistance protein, possibly MRP3 (78). Once transported across the basolateral membrane, folates enter the hepatic portal vein and travel to the liver, where they are stored or proceed to enter the systemic circulation as 5-methyl-tetrahydrofolate.

Folates, predominantly in the form of 5-methyl-tetrahydrofolate, circulating in the blood are transported into cells by either the reduced folate carrier (RFC) (51) or by a folate receptor (FR). The RFC and FR are both widely expressed in humans. The majority

of FR expression is localized to kidney and lung (126) with very low levels of expression elsewhere. The RFC appears ubiquitously expressed at moderate levels with increased expression in the liver (172). The PCFT also appears to be expressed on the cell surface, but is minimally active at a pH of 7.0 or above (138). The RFC and FR possess no homology to one another and exhibit different transport characteristics. The FR is suggested to be a high affinity, low capacity folate transporter (K_m 5-methyl-tetrahydrofolate = 3 nM) (21, 69, 167), that uses endocytosis-mediated receptor cycling to deliver folates into the cell (70). The RFC is a lower affinity folate transporter (Km 5-methyl-tetrahydrofolate = 1 μM) that is dependent on an electrochemical potential produced by the cellular export of anions, particularly organic phosphates, to transport folates into the cell (52). However, as the folate concentration increases, the RFC was shown to transport the majority of folate into the cell (151). Therefore, the RFC is currently thought to be the primary protein responsible for the transport of folates into cells. The role of the folate receptor in folate transport is less clear, although the expression of this receptor appears to be increased in a number of solid tumors and is currently being explored in targeted therapeutic approaches (93).

Intracellular folate metabolism

At the cellular level, an initial step in folate metabolism is the intracellular retention of folate molecules. A majority of the folates found in tissues contain multiple additions of glutamate molecules to the glutamate end of the folate (11). Polyglutamation of folates is attributed to the enzyme folylpoly-γ-glutamate synthetase (FPGS) (110, 111), which

enables cellular retention of folates (106). Two isoforms of FPGS have been identified in humans and these isoforms are transcribed from a single gene (45, 156); one in the cytosol and the other in mitochondria (90). Like FPGS, folates are found in the mitochondrial and cytosolic subcellular compartments (28, 155) and appear to be equally distributed between these two compartments (60). Chinese hamster ovary (CHO) cells that lack functional FPGS, known as AuxB1 cells, are unable to accumulate any cellular folates and therefore require an exogenous supply of purines, thymidine and glycine to the growth culture medium (106, 154). These studies suggested that the purpose of mammalian folate metabolism is to produce purines, thymidine and glycine.

Folate metabolism in mammalian cells is separated into reaction sequences that occur in the cytosolic and mitochondrial compartments and these reactions permit the recycling of folate molecules. Despite having all of the enzymes present in the cytosol to synthesize purines, thymidine, methionine and glycine, the cellular contributions of cytosolic folate metabolism are limited to purine, thymidine, and methionine synthesis. This was evidenced when the cytosolic isoform of FPGS was transfected into AuxB1 cells and relieved the purine and thymidine auxotrophy of these cells, but was unable to eliminate their requirement for exogenous glycine (45, 90). Furthermore, the glycine auxotrophy of AuxB1 cells was complemented only when the cells were transfected with a mitochondrially-targeted FPGS protein (45, 91). It would appear that mitochondrial folate metabolism serves to supply the cell with sufficient glycine and cytosolic folate metabolism is involved in purine and thymidine synthesis.

Cytosolic folate metabolism uses folate molecules as cofactors in reactions that contribute to the synthesis of purines, thymidine, and methionine (Figure 1-2). Cytosolic folate metabolism begins with the conversion of 5-methyl-tetrahydrofolate and homocysteine to tetrahydrofolate and methionine. Tetrahydrofolate can be converted to either 10-formyl-tetrahydrofolate or 5,10-methylene-tetrahydrofolate. The formyl carbon of 10-formyl-tetrahydrofolate is used by two folate-dependent enzymes of purine synthesis, glycinamide ribonucleotide formyltransferase (GART) and aminoimidazole carboxamide ribonucleotide formyltransferase (AICARFT). 5,10-methylene-tetrahydrofolate can be converted either to 5-methyl-tetrahydrofolate or to dihydrofolate. Dihydrofolate and thymidylate are produced by thymidylate synthase (TS) from 5,10-methylene-tetrahydrofolate and deoxyuridylate. The dihydrofolate produced during thymidylate synthesis is then converted to tetrahydrofolate by dihydrofolate reductase (DHFR).

Mitochondrial folates also participate in single carbon transfer reactions (Figure 1-3). The folate pools that participate in mitochondrial reactions are thought to be separated from those used in the cytosolic reactions (3). Of the molecules involved in folate metabolism, glycine, serine and formate appear to be exchanged between the mitochondrial and cytosolic compartments (127). Folates are cofactors in mitochondrial reactions that metabolize glycine. Specifically, the mitochondrial isoform of serine hydroxymethyltransferase (mSHMT) converts serine and tetrahydrofolate into glycine and 5,10-methylene-tetrahydrofolate. GlyA cells are CHO-derived cells that lack activity of the mSHMT isoform, but have an active cytosolic isoform (71). However, as a result of the

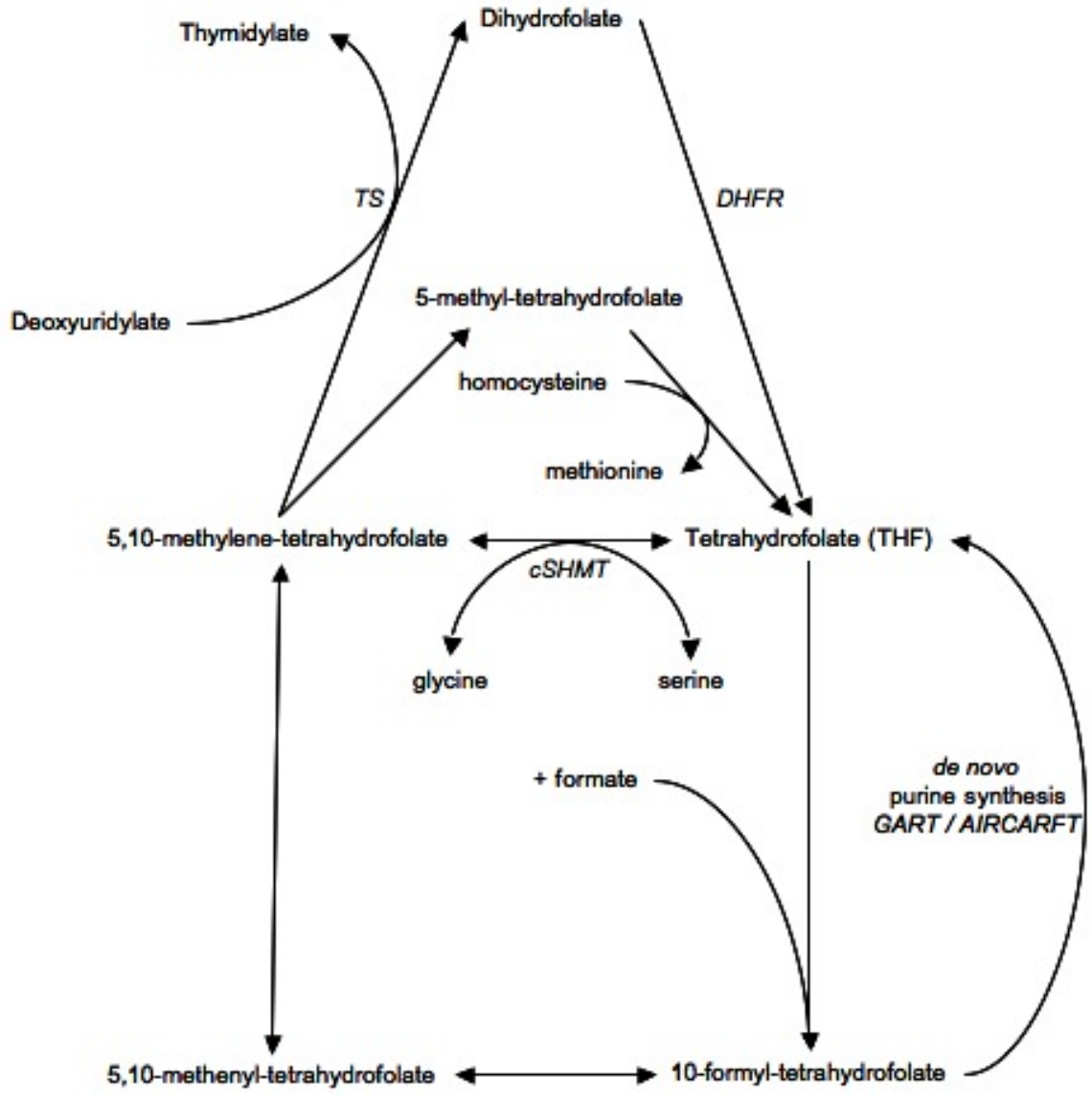

Figure 1-2 Schematic of folate metabolism and folate-dependent reactions that occur in the cytosolic subcellular compartment. Enzyme abbreviations are AICARFT – aminoimidazole carboxamide ribonucleotide formyltransferase ; cSHMT – cytosolic serine hydroxymethyltransferase isoform ; DHFR – dihydrofolate reductase ; GART – glycinamide ribonucleotide formyltransferase ; TS – thymidylate synthase. Single arrows represent the direction of irreversible reactions and double arrows represent reversible reactions.

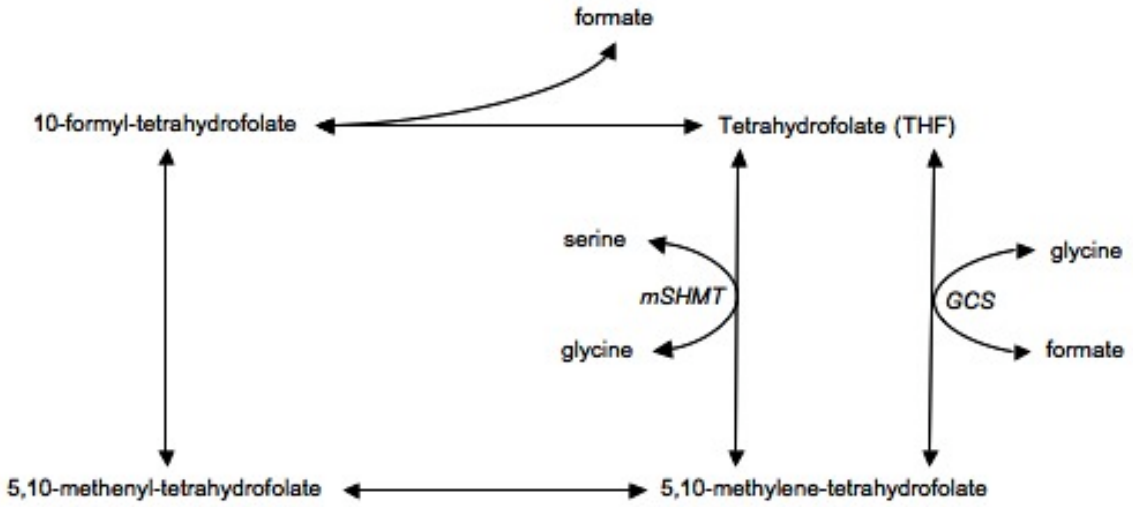

Figure 1-3 Schematic of folate metabolism and folate-dependent reactions that occur in the mitochondrial subcellular compartment. Enzyme abbreviations are GCS – glycine cleavage system ; mSHMT – mitochondrial serine hydroxymethyltransferase isoform. Single arrows represent the direction of irreversible reactions and double arrows represent reversible reactions. The two reversible reactions shown converting tetrahydrofolate to 5,10-methylene-tetrahydrofolate do not occur simultaneously; they are separate reactions that use the same molecules in different reactions with different enzymes.

mSHMT deficiency, glyA cells are auxotrophic for glycine. GlyA cells were later shown to have increased amounts of intracellular serine and decreased amounts of glycine when compared to wild-type CHO cells (116). Mitochondria also contain a unique glycine cleavage system (GCS) that uses tetrahydrofolate and NAD to catabolize glycine into formate, ammonia, 5,10-methylene-tetrahydrofolate and $NADH^+$ (76). Both the mSHMT and GCS reactions are reversible, but are predicted to run in the direction of tetrahydrofolate to 5,10-methylene-tetrahydrofolate (towards generation of 10-formyl-tetrahydrofolate) in mathematical models generated to simulate hepatic folate metabolism (120). Interestingly, these reactions oppose each other in terms of glycine regulation, but both reactions appear to eventually generate formate. The GCS directly generates formate from the catabolism of glycine. Additionally, 5,10-methylene-tetrahydrofolate can be converted to 10-formyl-tetrahydrofolate in two steps, and 10-formyl-tetrahydrofolate can be metabolized into formate and tetrahydrofolate. The importance of mitochondrial formate was shown in yeast, where ~25% of the carbon units used in purine synthesis were from mitochondrially-derived formate (127). Furthermore, a computational model of hepatic folate metabolism studied the effects of removing mitochondrial folate metabolism from the *in silico* system and found that thymidine and purine synthesis were reduced by ~40% and 60% respectively, and that other cytosolic folate-dependent processes were relatively unaffected (120). Thus, the role of mitochondrial folate metabolism may be to produce glycine that can be metabolized into formate for use in the cytosolic synthesis of purines and thymidine.

Mitochondrial uptake of folates

The importance of mitochondrial folate metabolism had been established, but prior to 1981, the mechanism of mitochondrial folate transport had not been studied. The importance of the metabolic events that occurred after mitochondrial folate transport was established in two mutant cell lines. AuxB1 cells, which harbored an inactivating mutation in the *fpgs* gene, were transfected with cytosolic FPGS, yet were still auxotrophic for glycine (45, 90). Likewise, glyA cells were deficient in mSHMT activity and were also auxotrophic for glycine (71). Cybulski and Fisher published a report in 1981 stating that mitochondria folate uptake could be saturated by increasing substrate, inhibited by structurally related folate molecules, and uptake was dependent on folate structure, as only non-reduced pteridine ring folates, i.e., folic acid and dihydrofolate, were shown to accumulate in isolated rat liver mitochondria (30). Eleven years later, the process of mitochondrial folate uptake was revisited. Studies were similarly carried out in isolated rat liver mitochondria and, in agreement with the earlier work of Cybulski and Fisher, these studies demonstrated that mitochondrial folate uptake exhibited characteristics of saturation and inhibition (61). The work by both groups suggested that mitochondrial folate accumulation was a carrier-mediated process. Horne *et al.* also demonstrated that mitochondrial folate uptake was pH-dependent, with a pH optimum of 5.5 at 37° C and 5-fold less activity at pH 7.4. Cybulski and Fisher examined folate uptake at pH 7.4 at 4° C and this may explain why these studies had discrepancies regarding the substrates for the carrier protein. Horne *et al.* showed that the carrier-mediated transport of mitochondrial folates was specific to pteridine ring-reduced folates, such as 5-formyl-tetrahydrofolate and

5-methyl-tetrahydrofolate. In addition, they reported that mitochondrial transport of reduced folates was hardly inhibited by competition with non-reduced folates. It was thought that the studies by Horne *et al*. were technically superior to those by Cybulski and Fisher and therefore, the prevailing concept is that reduced folates are optimal substrates for carrier mediated mitochondrial transport.

Discovery of the protein responsible for mitochondrial folate transport

The discovery of a protein responsible for mitochondrial folate transport was greatly facilitated by previous studies that created a somatic cell genetic mutant chinese hamster ovary (CHO) cell line, the glyB cell (71). The glyB cell line was generated when CHO cells were treated with mutagens to intentionally produce mutant cell lines that required glycine for survival (71). Four classes of mutants were identified: glyA, glyB, glyC, and glyD, each of which required an exogenous supply of glycine for cell growth and survival. One group, the glyA cell, was immediately identified to have only 5% of wild-type mSHMT activity. The other three groups were shown to maintain wild-type activity of mSHMT, and were suspected to have some other defect in mitochondrial folate metabolism. The cellular defects in the three other cell types, glyB, glyC, and glyD, remained unidentified for over 30 years. The mutations that are responsible for the observed glycine auxotrophy in glyC and glyD cell types are still unidentified.

GlyB cells were shown to be deficient in mitochondrial folate accumulation, despite having normal cytosolic folate metabolism (155). This suggested the possibility that glyB cells were deficient either in mitochondrial folate transport or in mitochondrial

folate retention. GlyB cells were characterized in this laboratory 31 years after they were first created (108, 160). Upon transduction with a human cDNA library in a retroviral vector, a colony of glyB cells was isolated that was able to sustain growth in the absence of glycine (160). The transduced cDNA sequence from this cell population was isolated and cloned into a mammalian expression vector that also encoded resistance to the selective agent, G418. GlyB cells were transfected with this mammalian expression vector and ~30% of the cells that were resistant to G418, were able to survive in the absence of glycine (160). Thus, the protein encoded by the transfected cDNA, which was later named the mitochondrial folate transport protein (MFT), complemented the defect in glyB cells that induced glycine auxotrophy. The isolated human *mft* cDNA sequence consisted of a 945 base pair sequence that encoded a 315 amino acid protein. Analysis of the MFT protein sequence demonstrated homology to a previously identified family of proteins that were embedded in the inner mitochondrial membrane and functioned to transport small, charged molecules into the mitochondrial matrix. The MFT contained three conserved motifs that were common to this family of transporters. In addition, a hydropathy plot analysis suggested that the MFT and this family of proteins had structural similarities (160).

The MFT was suggested to be an integral inner mitochondrial membrane protein that transported folates into mitochondria. MFT homologues from hamster, mouse, and zebrafish were identified based on sequence homology. These cDNAs were subsequently cloned into a mammalian expression vector and transfected into glyB cells (108). The predicted MFT proteins from hamster, mouse, and zebrafish all permitted glyB cell

survival in the absence of glycine, suggesting that the transfected putative MFT proteins restored mitochondrial folate accumulation in glyB cells. The concept of the transfected, wild-type MFT proteins restoring mitochondrial folate accumulation in glyB cells was studied using radiolabeled folic acid incubated with glyB and wild-type CHO cells followed by analysis of folate uptake into subcellular compartments. Untransfected glyB cells contained mitochondrial folates at levels that were 1-5% of that observed in the wild-type parental CHO cell line (108, 160). However, upon transfection of with either human or CHO *mft* cDNA, mitochondrial folate levels in these transfected glyB cells increased to 43% and 90% of wild-type CHO cells, respectively (108, 160). Thus, the MFT protein was able to restore mitochondrial folate accumulation in glyB cells.

It had been established that glyB cells were not capable of accumulating mitochondrial folates, but the mechanism of this defect was unknown. Northern blot analysis of glyB and CHO cells showed that the *mft* mRNA was present in both cells lines (108). Determination of MFT protein expression was not attempted, as there was no antibody available at that time to detect the endogenous MFT protein by western blotting. Fluorescence *in situ* hybridization analysis revealed that glyB cells only contained one copy of the *mft* gene in comparison to the two copies contained in wild-type CHO cells (108). This finding was complemented when the genomic DNA from glyB cells was sequenced and revealed a single in frame G to A point mutation in the only copy of the *mft* gene in glyB cells (108). This mutation in glyB DNA translated into a protein mutation that changed a glycine codon to a glutamate codon at position 192 in the glyB MFT protein. Hence, glyB cells were auxotrophic for glycine because their only copy of the *mft*

gene had a point mutation that mutated glyB MFT 192 from a glycine residue to a glutamate residue, a mutation that was incompatible with mitochondrial folate transport.

Understanding the defects in glyB cells enabled this cell line to become a valuable reagent in studying the function of the MFT. Since glyB cells are unable to accumulate any mitochondrial folates they are auxotrophic for glycine. This phenotype was utilized in discovery of the MFT where a functional MFT protein was shown to complement the glyB cellular requirement for glycine. Newly constructed MFT mutants could be studied in the same way: a mutation in the wild-type CHO *mft* cDNA could be constructed, transfected into glyB cells and the ability of these transfected cells to survive in the absence of glycine could be observed. If cells transfected with this mutated *mft* cDNA could survive without glycine supplementation, the encoded MFT mutant protein was assumed to have retained its function as a mitochondrial folate transport protein. Conversely, if the transfected glyB cells still required glycine for survival, the encoded MFT protein was assumed to be unable to restore mitochondrial folate uptake in glyB cells; the MFT mutant protein was devoid of folate transport activity. In addition to the utility of the glyB cell line in this glyB glycine complementation assay, glyB cells were also used as a negative control in folate transport studies. GlyB cells have proven to be an extremely useful and powerful cell line in studying the folate transport function of the MFT.

Focus of dissertation

The objectives of this research were to understand the folate-specific transport mechanism of the MFT and to explore the contributions of the MFT to cellular folate

metabolism. While the MFT belonged to a large family of structurally similar mitochondrial transport proteins, we were interested in how the MFT was able to specifically recognize and transport folate molecules. We wanted to understand why no other protein in this family was capable of folate transport and how the MFT evolved to serve this function. Because of the structural homology in this family of mitochondrial transporters, we believed that discrete residue differences within the transport cavity of the MFT shaped its substrate-specificity. In Chapter Two, we highlight some striking residue differences in the MFT and the impact of these residue differences on the MFT mechanism of folate transport. We were also interested in the molecular interactions that were required for folate recognition and folate transport by the MFT. We used molecular dynamics simulations, also presented in Chapter Two, to gain insight into these events. Finally, we wanted to further elucidate the role of the MFT in cellular folate metabolism. We knew that the MFT was responsible for mitochondrial folate transport, but we did not know what folates, folate conjugates or antifolates were transported by the MFT. Specifically, we investigated whether folate polyglutamates were as substrates for the MFT, as well as the effects of various antifolates on MFT function; these findings are presented and discussed in Chapter Three.

CHAPTER 2 The Mechanism of Folate Transport by the Mitochondrial Folate Transport Protein

The mitochondrial folate transporter (MFT) was discovered in 2000 and it was subsequently determined that this protein was responsible for folate transport into mitochondria (108, 160). Its discovery revived questions regarding the substrate specificity of mitochondrial folate transport and the molecular mechanisms involved in this process. The MFT was highly homologous to an established family of mitochondrial inner membrane proteins, the mitochondrial carrier family (MCF), which has been extensively investigated over the past 40 years. We used this growing body of literature to aid in the design of experiments to better understand the MFT mechanism of folate transport and gain insight into the substrate specificity of the MFT. In this chapter, the mitochondrial carrier family (MCF) is introduced and compared to the MFT. The differences between the MCF consensus sequence and the MFT were the foundation for our experimental designs. During the course of this dissertation, we have gained an enormous appreciation for the synergy achievable when combining experimental and computational approaches. Using these approaches, we studied the MFT and analyzed several evolutionary changes that have occurred apparently to create a folate-specific transport mechanism for folate uptake into mitochondria.

The mitochondrial carrier family (MCF)

The mitochondrial carrier family (MCF) is a subfamily of a larger solute carrier family, which consists of ~365 proteins organized into 48 subfamilies (56, 62). The mitochondrial carrier family, or SLC25, contains ~35 yeast and ~52 human nuclear encoded integral membrane proteins that are embedded in the inner membrane of mitochondria (62, 124). The number of human MCF members can increase dramatically to ~79, if one includes different isoforms of these transporters (173). All MCF proteins facilitate the transport of small, charged molecules from the mitochondrial inter-membrane space into the mitochondrial matrix; the mitochondrial outer membrane is freely permeable to molecules under 5000 daltons (121, 173). Substrates for MCF members include nucleotides, amino acids, keto acids and other co-factors such as NAD^+, FAD^+, and folate (Table 2-1). Of the ~52 human MCF proteins, substrates have been identified for ~33 of these (125, 173). Since almost all of the known substrates are involved in reaction sequences that ultimately produce energy for the cell, efficient transport by MCF proteins is required for mitochondrial function and cellular survival. Furthermore, amino acid mutations caused by single nucleotide polymorphisms in MCF proteins have been documented in humans and are linked to clinical diseases for eight of these transporters (reviewed in (125)). These diseases include AAC1 deficiency (ADP/ATP carrier in heart and muscle), Senger's syndrome (transcription of ADP/ATP carrier), PiC deficiency (phosphate carrier in heart and muscle), autosomal dominant progressive external ophthalmoplegia (ADP/ATP carrier in heart, muscle, and brain), CAC deficiency (carnitine/acylcarnitine carrier), HHH syndrome (ornithine carrier), AGC2 deficiency

Gene Name	Protein Name	Substrate(s)
SLC25A1	Tricarboxylate carrier	citrate, malate
SLC25A2	Ornithine carrier-2	ornithine, citrulline
SLC25A3	Phosphate carrier	phosphate
SLC25A4	ADP/ATP carrier-1	ADP, ATP
SLC25A5	ADP/ATP carrier-2	ADP, ATP
SLC25A6	ADP/ATP carrier-3	ADP, ATP
SLC25A7	Uncoupling protein-1	H+
SLC25A8	Uncoupling protein-2	H+
SLC25A9	Uncoupling protein-3	H+
SLC25A10	Dicarboxylate carrier	malate, succinate
SLC25A11	Oxoglutarate carrier	2-oxoglutarate
SLC25A12	Aspartate/glutamate carrier-1	aspartate, glutamate
SLC25A13	Aspartate/glutamate carrier-2	aspartate, glutamate
SLC25A14	Uncoupling protein-5	unknown
SLC25A15	Ornithine carrier-1	ornithine, citrulline, lysine, arginine
SLC25A16	Graves disease carrier	CoA
SLC25A17	PMP34	ATP
SLC25A18	Glutamate carrier-2	glutamate
SLC25A19	Deoxynucleotide carrier	thiamine pyrophosphate
SLC25A20	Carnitine/acylcarnitine carrier	carnitine, acylcarnitine
SLC25A21	Oxoadipate carrier	oxoadipate, oxoglutarate
SLC25A22	Glutamate carrier-1	glutamate
SLC25A23	Phosphate carrier-2	ATP, ADP, AMP, Pi
SLC25A24	Phosphate carrier-1	ATP, ADP, AMP, Pi
SLC25A25	Phosphate carrier-3	unknown
SLC25A26	S-adenosyl methionine carrier	S-adenosyl methionine, S-adenosyl homocysteine, S-adenosyl cysteine, S-adenosyl ornithine
SLC25A27	Uncoupling protein-4	unknown
SLC25A28	Mitoferrin-2	Fe2+
SLC25A29	Ornithine carrier-3	ornithine, acylcarnitine
SLC25A30	Kidney mitochondrial carrier-1	unknown
SLC25A31	ADP/ATP carrier-4	unknown (ATP, ADP?)
SLC25A32	Mitochondrial folate transporter	folate
SLC25A33	Bone marrow stromal cell derived carrier	unknown
SLC25A34	No name	unknown
SLC25A35	No name	unknown
SLC25A36	No name	unknown
SLC25A37	Mitoferrin-1	Fe2+
SLC25A38	Erythroid specific carrier?	glycine?
SLC25A39	No name	unknown
SLC25A40	No name	unknown
SLC25A41	SCaMC-3L	ATP-Mg, Pi
SLC25A42	No name	CoA, ADP
SLC25A43	No name	unknown
SLC25A44	No name	unknown
SLC25A45	No name	unknown
SLC25A46	No name	unknown

Table 2-1 Members of the mitochondrial carrier family. Identified human mitochondrial carrier family proteins are listed by the gene names given to them by the HUGO Gene Nomenclature Committee (62). The protein names and substrates are listed as identified.

(aspartate/glutamate carrier in liver), Amish microcephaly (thiamine pyrophosphate carrier), and neonatal myoclonic epilepsy (glutamate carrier). Most of these heritable diseases are autosomal recessive and, therefore, cases with severe deficiencies resulting from homozygous defects are rare. Nonetheless, the existence of diseases related to the deficiency of MCF transporters reinforces the essential metabolic requirement of these carrier proteins.

Mitochondrial carrier family proteins can be identified by similarities in their primary sequence. The first primary sequence discovered for a MCF protein was that of the ADP/ATP carrier in 1982 (5, 7) followed by the discovery of the phosphate carrier sequence in 1987 (6). Upon the discovery of the phosphate carrier sequence, it was suggested that these inner mitochondrial membrane transporters were part of a larger and homologous protein family (6). Hydropathy plot analysis of numerous MCF proteins predicted these proteins to have six transmembrane spanning regions (6, 65, 72, 165). In addition, studies on the tricarboxylate carrier indicated that the N- and C- termini extended into the inter-membrane space (24). The sequences of MCF proteins consist of three 100 amino acid repeats with each repeat predicted to contain two transmembrane domains (TMD). These repeats are sequentially connected to form a protein that consists of ~300-350 amino acids in total. The hallmark of MCF transporters is the conserved motif, Px(D/E)xx(K/R)x(K/R) - (20 to 30 amino acids) - (D/E)Gxxxx(Y/F/W)(K/R)G, commonly shortened to PxD/ExxK/R. This motif appears once every 100 amino acids for a total of three times per MCF protein. Each motif was initially thought to be located immediately after the 1st, 3rd, and 5th TMDs in MCF proteins. No other non-MCF protein has been

discovered to carry this repeated motif in its primary sequence. Therefore, proteins that contain this PxD/ExxK/R motif repeated thrice throughout their sequence are identified as MCF proteins. Functional identification and substrate analysis of MCF proteins is more difficult, explaining why there are ~20 MCF proteins with unknown functions and/or substrates at this time.

The structure and proposed transport mechanism of the MCF

The study of some MCF members dates back more than 40 years. Perhaps the most studied member of this family is the ADP/ATP carrier (AAC). Early studies on this protein were greatly facilitated by its prevalence in heart and liver and the discovery of two known classes of inhibitors, atractylosides and bongrekic acids (14, 15, 19, 79-81). The availability of radiolabeled forms of these two inhibitors further facilitated the isolation and purification of the AAC from mammalian tissues, as it enabled protein-inhibitor complex tracking throughout the purification process (4, 82). Even before the primary sequence of the AAC was known, it had been purified and reconstituted into liposomes and the kinetics and mechanism of this protein has been investigated (18, 147, 148). The biggest advancement in the MCF field to date was in 2003, when the three-dimensional coordinates of the bovine ADP/ATP carrier (bAAC) in complex with carboxyatractyloside (CATR) were solved by X-ray crystallography with a resolution of 2.2 Å (128). The structure showed that the N- and C- termini were present on the inter-membrane space side of the inner mitochondrial membrane. The protein did, in fact, contain six transmembrane spanning α-helices that were connected by hydrophilic loops: two loops that extended into

the inter-membrane space and three loops that protruded into the matrix (Figure 2-1) (128). The six TMDs were oriented such that the overall bAAC structure was conical and ~30 Å in length, with an apparent cavity that extended 20 Å deep into the protein (Figure 2-2). This transport cavity progressively narrowed from an initial opening diameter of ~20 Å down to ~8 Å at the bottom of the transport cavity where an apparent floor was formed.

The solved coordinates of the bAAC not only provided visualization of the structure of the bAAC, but also contained valuable insights that pertained to the transport mechanism. The exposed loops on both sides of the inner membrane were largely hydrophilic. Within the transport cavity, there was an asymmetric scattering of hydrophilic and aromatic residues. Aromatic residues were predominantly localized to the fourth TMD and formed what was formerly known as a tyrosine ladder (128), and more recently identified as an aromatic ladder (32). Hydrophilic residues were also found within the channel and the hydrophilic residues located at the floor of the cavity were probably the most intriguing characteristic in the bAAC structure. Interestingly, the PxD/ExxK/R conserved motifs were not located immediately after the 1st, 3rd, and 5th TMDs as previously thought, but rather were contained within the 1st, 3rd, and 5th TMDs about 2/3 of the distance through the lipid bilayer. The AAC crystal structure identified three basic and three acidic amino acids that corresponded to the D/E and K/R residues in the PxD/ExxK/R motifs; these residues were located at the base of the transport cavity. Prior to the crystallization of the AAC, mutagenesis of the charged, conserved motif residues in the AAC eliminated the ADP transport function of this protein (57, 58, 114, 117, 118). Thus, these charged, conserved motif residues had been previously shown to be an

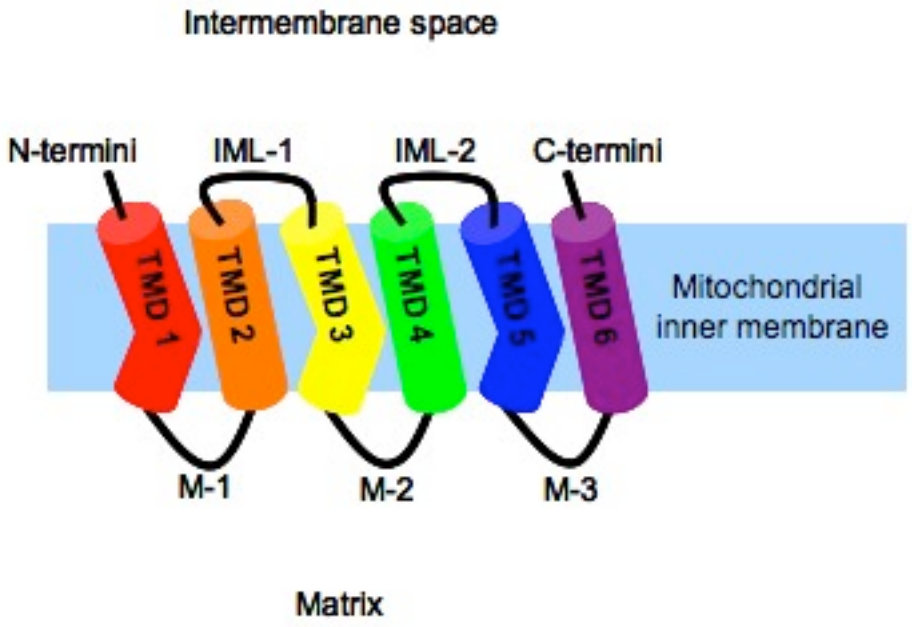

Figure 2-1 Orientation of the transmembrane domains of the ADP/ATP carrier. The structure of the bovine ADP/ATP carrier was solved by X-ray crystallography (128). The arrangement of the six transmembrane domains (TMD), N-and C-termini, inter-membrane space loops (IML), and matrix loops (M) are shown. Kinks were observed in the first (TMD 1), third (TMD 3), and fifth (TMD 5) transmembrane domains and were attributed to proline residues in a PxD/ExxK/R conserved motif.

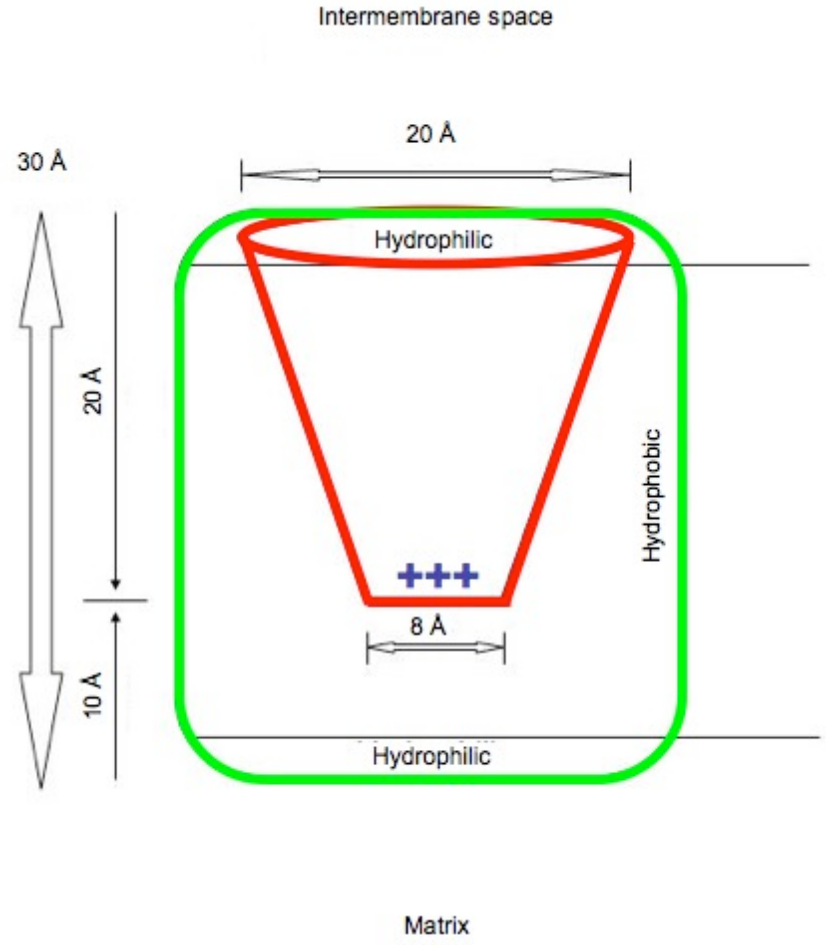

Figure 2-2 Depiction of the ADP/ATP carrier protein and transport cavity structure. This depiction is based on the solved crystal structure of the bovine AAC (128), a structure that is thought to be common to all MCF proteins. The cylindrical outline of the protein is in green. The cone-shaped transport cavity is shown in red and the positive charge at the base of the channel marked by +++ in blue. Distances are marked by arrows and are in angstroms (Å).

essential component in the transport function of the AAC, but the exact purpose of these residues was unknown before the crystallization of the AAC; they were speculated to constitute a charged-pair network that was essential for transport (119). The crystal structure showed that the residues in the PxD/ExxK/R motifs formed three symmetrical and interhelical bonds between the D/E in the conserved motifs on the 1st, 3rd, and 5th TMDs and the K/R within the conserved motifs on the 3rd, 5th, and 1st TMDs, respectively (128). Specifically in the AAC, three salt bridge interactions were formed between bAAC E29 and R137, D134 and R234, and D231 and K32 (Figure 2-3). Kinks were observed in the TMDs that contained the PxD/ExxK/R motifs and these kinks appeared to be induced by the proline residues in the PxD/ExxK/R motifs (Figure 2-1 and 2-3). It appeared that the function of the charged residues in the PxD/ExxK/R motifs was for the proline residues to provide helical flexibility and for the charged residues to form interhelical salt bridge interactions.

The static view of the crystallized AAC showed that the transport cavity floor, formed by the conserved motif interactions, was impenetrable. This suggested that a conformational change was necessary to remove the transport floor and to provide an opening within the transport cavity that would permit substrate passage into matrix. The crystal structure showed, and later molecular dynamics simulations with the AAC suggested, that bAAC conserved sequence residues E29, R137, D231 and R234 contacted the CATR inhibitor (68, 128). The same residues were predicted to contact ADP within the AAC transport cavity when ADP binding was simulated in two other molecular dynamics simulations (33, 169). Substrate contact with the residues in the PxD/ExxK/R motifs was

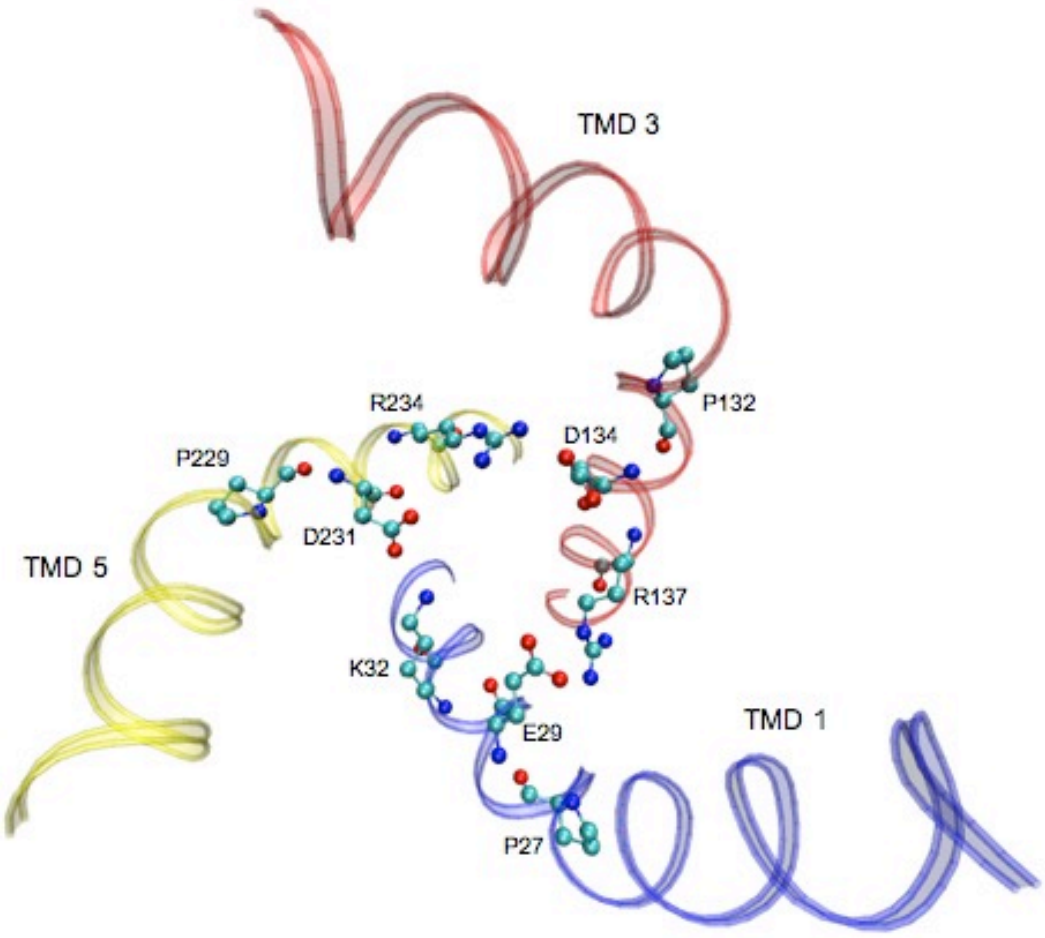

Figure 2-3 Orientation of the PxD/ExxK/R conserved motifs in the crystallized ADP/ATP carrier. The crystal structure of the bovine ADP/ATP carrier (128) (pdb accession 1okc) revealed the orientation of the conserved motif residues. The first, third and fifth transmembrane domains (TMD) are shown in transparent blue, red and yellow, respectively. The conserved motif residues are identified by their single letter amino acid abbreviation and numbered by their location in the amino acid sequence of the bovine ADP/ATP carrier. Salt bridge interactions were predicted between E29 and R137, D134 and R234, and D231 and K32.

proposed to disrupt the interactions that formed the transport cavity floor (128). The TMDs containing the PxD/ExxK/R motifs were then predicted to move about the conserved proline residues because the interactions between the charged PxD/ExxK/R residues, which held the TMDs in place, were disrupted. This movement about α-helical proline residues is not uncommon as this amino acid is often found in transmembrane helices of proteins and can destabilize α helices through steric hindrance and backbone bonding disruptions (29, 159). The role of the proline residues in the PxD/ExxK/R motifs was more recently examined in molecular dynamics simulations with the AAC. These simulations showed that the conformational change in the AAC was not mediated by proline isomerization or helical bending, but rather through deviations in swivel angles of the proline residues (40, 68). The movement about these conserved proline residues was proposed to remove the transport floor, leading to a momentary opening of a transport channel and substrate passage into the mitochondrial matrix.

In addition to the interactions that were anticipated to form at the base of the channel, residues that were positioned above the transport floor were also predicted to contact substrates within the AAC transport cavity. As shown in the AAC crystal structure, bAAC residues K22, N87, K91, R79, Y186, Y190, Y194 and R279 contacted the CATR inhibitor (128). These residues have also been suggested to contact either CATR or ADP within the AAC transport cavity in molecular dynamics simulations (33, 68, 169). The aromatic residues that were shown to be required for ADP transport by mutagenesis, bAAC Y186 and F191 (32), were speculated to participate in the coordination of the adenine ring of ADP based on the results of two molecular dynamics simulations using the

AAC (33, 169). Hydrophilic residues were also located above the cavity floor. Residues bAAC K22, R79, and R279 have all been shown to be required for AAC transport function in several mutagenesis studies (57, 58, 113, 117, 118). As shown in two separate molecular dynamics simulations, these residues are thought to coordinate the phosphate groups of ADP as it descends into the transport cavity (33, 169).

The sequence similarities between MCF proteins were thought to translate into structural and mechanistic similarities. Similar to the AAC, mutagenesis of the charged residues in the PxD/ExxK/R motifs resulted in other MCF proteins that lost their transport function (26, 96, 98, 132, 133). Because mutagenesis of the charged residues in the PxD/ExxK/R motifs resulted in severely impaired transport rates in nearly all MCF proteins, the function of the PxD/ExxK/R motifs in all MCF proteins was thought to be the same. The solved crystal structure of the AAC provided a structural scaffold that was used to predict the structures of other MCF proteins (112, 142, 166). Based on the AAC crystal structure, the predicted structures for nine MCF proteins were generated by homology modeling and the predicted substrate for each of these transporters was computationally docked into the transport cavity (142). The docking of these substrates led to the conclusion that all MCF proteins contain three common "substrate-binding sites" that corresponded to the residues in the AAC aromatic ladder for one contact point, K22 and R79 for another, and R279 as the third contact point (142). The residues contained in the proposed common substrate-binding sites had been previously mutated in the AAC (see above) and in the oxoglutarate (25), carnitine (64), and citrate (98) carrier proteins, and were shown to be required for transport function in all of these transporters. Thus, the

residues that constituted the proposed common substrate-binding sites were implicated in the transport function of various MCF proteins. It was then proposed that the role of these binding sites was to properly orient the substrate for interaction with the charged residues in the PxD/ExxK/R conserved motifs at the transport cavity floor and that the amino acids present at these common binding sites conferred the substrate specificity of the protein (142). The mechanism of MCF protein transport was proposed to involve substrate discrimination and positioning by residues at three locations within the transport cavities of these proteins (128, 142). The location of the substrate, held within the transport cavity, could disrupt the interactions between the charged residues of the PxD/ExxK/R motifs that formed the cavity floor (128). The disruption of the interaction network at the base of cavity would enable flexibility of the conserved proline residues in the PxD/ExxK/R motifs, which could induce the formation of different interactions with the transport cavity and permit substrate passage into the mitochondrial matrix (119).

The MFT possessed a striking deviation from the MCF consensus sequence in its second PxD/ExxK/R motif: the MFT had substituted a tryptophan residue for the typical D/E residue, changing the second motif in the MFT to PxWxxK. Even more interestingly, there were only four other MCF proteins that contained this same substitution. Because the residues in these PxD/ExxK/R motifs appeared to be intimately involved in the transport mechanism of MCF proteins, it was fascinating that the MFT and four other MCF proteins deviated from this highly conserved sequence. The function of this substitution had not been investigated. In fact, only once before the discovery of the MFT had this PI/LW motif even been acknowledged (119). This substitution was proposed to influence

both the mechanism of transport and the substrate specificity of the transporters that carried this tryptophan residue (119).

In this chapter, we examine the folate-specific transport mechanism of the MFT. We probed residues thought to be involved in the MFT mechanism of transport by site-directed mutagenesis. A CHO MFT homology model complemented and later directed mutagenesis experiments. Furthermore, a CHO MFT homology model was subjected to molecular dynamics simulations to predict interactions between a tetrahydrofolate molecule and the residues that line the MFT transport cavity. These studies aim to accomplish multiple goals. We want to better understand the transport mechanism of the MFT. Understanding this mechanism would also provide insight to the substrate specificity of the MFT. We aim to appreciate how and why folates were specifically recognized and transported by this MFT protein and not other molecules. We found it remarkable that MCF proteins were able to transport such a wide variety of substrates with high specificity. Most of the work in the MCF field had focused on the similarities between these proteins and how these commonalities translated into shared mechanisms in MCF proteins. We felt it was possible to contribute to the knowledge of these MCF proteins, their substrate specificities and their mechanisms by understanding the roles of the anomalous residues in the transport mechanism of the MFT.

MATERIALS AND METHODS

Alignment of MCF proteins

Sequences for MCF proteins were loaded into the MegAlign program (version 6.1) (27) and aligned by ClustalW (158) using the following NCBI protein accession numbers: NP_001142 - human ADP/ATP carrier, isoform 1 (HsAAC1); NP_110407 – human mitochondrial folate transporter (HsMFT); NP_012132 – yeast FAD^+ transporter (ScFlx1p); NP_009751 – yeast pyrimidine transporter (ScRim2p); NP_010910 – yeast NAD^+ transporter (ScYEL006W); NP_014316 – yeast Mg-ATP/P_i transporter (ScSal1p); NP_005975 – human citrate transporter (HsCTP); NP_003553 – human oxoglutarate carrier (HsOGC); NP_055067 – human ornithine transporter (HsORNT1).

Site-directed mutagenesis of the CHO MFT by overlap extension PCR

The CHO and glyB *mft* cDNA (~1,100 base pairs) had been previously cloned into the pcDNA 3.1(-) vector and contained a EQKLISEEDL *c-myc* tag directly downstream of the *mft* cDNA start codon (129). Within the pcDNA 3.1(-) vector, *Xho*I and *Hin*dIII recognition sites flanked the 5' and 3' full-length *myc-mft* cDNA, respectively, and were contained in the multiple cloning site (MCS) of the vector. Site-directed mutagenesis was accomplished by overlap extension polymerase chain reaction (PCR) (59, 145) using the *myc*-tagged CHO *mft* in pcDNA 3.1 (-). Overlap extension PCR consisted of two rounds of PCR (Figure 2-4). In the first round, the CHO *mft* template was placed in two separate reactions. One reaction involved a vector-specific primer that was upstream of the 5' *mft*

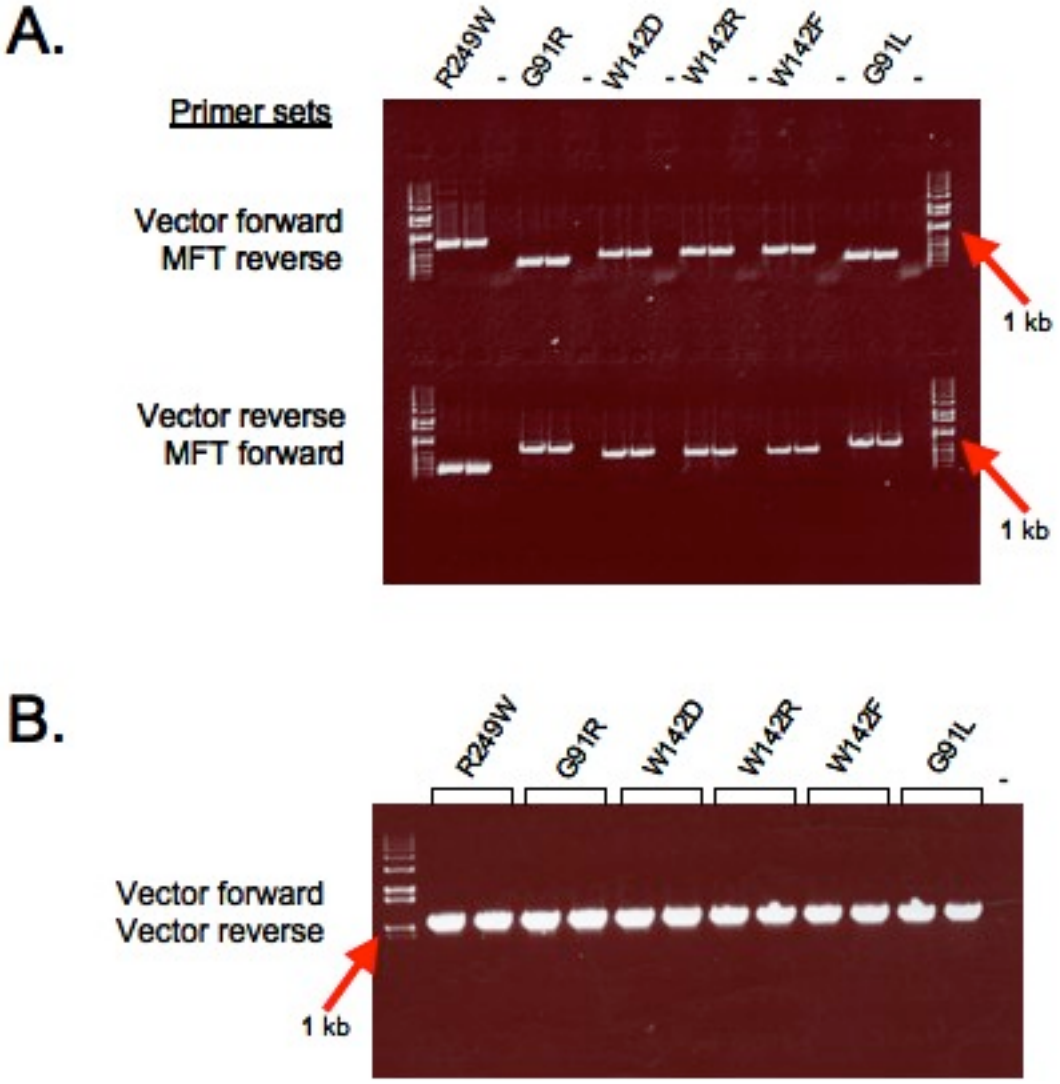

Figure 2-4 Generation of CHO *mft* mutant cDNAs by overlap extension polymerase chain reaction. A. Two fragments of a N-terminal *myc* tagged CHO *mft* cDNA (1.1 kilobases (kb)) that had been cloned into pcDNA 3.1(-) (100 ng) were amplified using two sets of primers. Each set of primers contained a vector-specific primer (vector forward and vector reverse) and a *mft*-specific primer (MFT forward or MFT reverse) that introduced a mutation into the CHO *mft* cDNA. The *mft*-specific primers used in separate reactions each introduced the same mutation and contained 15 base pairs of DNA sequence overlap. The fragments were amplified by polymerase chain reaction (PCR) and were visualized on a 1% agarose gel. B. The fragments produced and purified from the first PCR reaction were added (50 ng of each product) to a second PCR reaction. This reaction contained the same vector-specific primers as in the first PCR reaction. The 15 base pairs of overlap created by the *mft*-specific primers in the first round PCR hybridized to one another in the first cycle of PCR and the vector-specific primers inserted the missing base pairs to produce a full-length CHO *mft* cDNA (1.1 kb) that contained the introduced mutation. This full-length CHO *mft* cDNA was amplified by successive cycles of PCR and visualized on a 1% agarose gel. The "–" signs denotes lanes loaded with PCR reactions that did not receive any starting cDNA template.

start site that ran 5' to 3' and the other primer was located within the *mft* sequence, introduced the mutation and ran 3' to 5'. The other reaction used a similar *mft*-specific primer as in the first reaction; it contained ~15 base pairs of overlap with the first reaction primer, introduced the mutation, but ran 5' to 3'. The second primer in the other first round reaction was specific to the vector, was located downstream of the 3' stop and ran 3' to 5'. Following first round PCR, products were electrophoresed on a 1% agarose gel with ethidium bromide added and the fragment with the expected molecular mass was extracted, purified using the Promega Wizard SV gel and PCR clean up system kit, and the concentration of the purified PCR products was determined by sample absorbance at 260 nm. An aliquot containing 50 ng of product from each of the two first round reactions was added as template into the second round reaction. Due to the overlap designed into the *mft*-specific primers that introduced the mutation, these two products hybridized using the 15 base pair overlap site and were extended during the first PCR extension cycle to form a single double stranded DNA product. The primers used in the second round reaction were the 5' and 3' vector-specific primers from the first round reactions that flanked the *mft* cDNA. The second round PCR products were electrophoresed, extracted, purified and the concentrations of products were spectrophotometrically determined. Each PCR reaction had a total volume of 50 µL and contained 20 mM Tris-HCl, 50 mM KCl (pH 8.4 ; $MgCl_2$-free Taq polymerase buffer), 1.5 mM $MgCl_2$, 200 µM deoxynucleotides, 0.3 µM of each primer, 2 U Taq DNA polymerase, and 0.5 U PFU turbo polymerase (Stratagene). PCR reactions were initiated at 95° C for two minutes, followed by 20 cycles of 95° C for one

minute, 53° C for 1 minute, and 72° C for two minutes, and finished with a ten minute incubation at 72° C. The sequences of all of the primers used are shown in Table 2-2.

Cloning of mutant mft cDNA constructs into a mammalian expression vector

Mutant *mft* cDNA PCR fragments were cloned into a mammalian expression vector, pcDNA 3.1(-), for transfection into glyB cells. The PCR amplification of these cDNAs had been carried out so that the 5' *Xho*I and 3' *Hin*dIII recognition sites were preserved in the fragments. The pcDNA 3.1(-) vector also contained these restriction sites in its MCS. The vector and the mutant PCR-amplified *mft* cDNAs were digested with both *Xho*I and *Hin*dIII at 37° C for one hour. The total volume of each digest reaction was 20 µL and each reaction contained 10 mM Tris-HCl, 50 mM NaCl, 10 mM $MgCl_2$, 1 mM dithiothreitol (pH 7.9; NEB2), 0.1 µg/µL BSA, 20 U *Xho*I, and 20 U *Hin*dIII. Following digestion, these products were electrophoresed, extracted, purified, and the concentrations of purified products were determined as above. Ligation of the vector and mutant *mft* cDNA was carried out at 16° C for 16 hours. Each ligation reaction had a total volume of 10 µL that contained a 3:1 molar ratio of *mft* cDNA to vector pcDNA 3.1(-) (~5.4 kilobases ; 25 ng vector/reaction), 66 mM Tris-HCl, 5 mM $MgCl_2$, 1 mM dithiothreitol, 1 mM ATP (pH 7.5 ; Ligase Buffer), and 1 U T_4 DNA ligase.

Vector Specific Primers

Name	Sequence	Mutant	Direction
T7for	taatacgactcactatagggagaccc	-	Forward
pcDNA 3.1(-) rev.	gacagtgggagtggcaccttc	-	Reverse

MFT Specific Primers

Name	Sequence	Mutant	Direction
CHOMFTW142A-FM	acaaacccactggcggtgacgaaaact	W142A	Forward
CHOMFTW142A-RM	agttttcgtcaccgccagtgggtttg	W142A	Reverse
CHO MFT W142D FM	ccactggacgtgacgaaaactcg	W142D	Forward
CHO MFT W142D RM	cgtcacgtccagtgggtttgtg	W142D	Reverse
CHO MFT W142F FM	ccactgttcgtgacgaaaactcgccttatg	W142F	Forward
CHO MFT W142F RM	cgtcacgaacagtgggtttgtgatg	W142F	Reverse
CHO MFT W142R FM	ccactgagggtgacgaaaactcg	W142R W142R / R249W	Forward
CHO MFT W142R RM	cgtcaccctcagtgggtttgtgatgcag	W142R W142R / R249W	Reverse
CHO MFT R249W FM	tatcaagttgtgtgggcccgtcttcaggac	R249W W142R / R249W	Forward
CHO MFT R249W RM	gcccacacaccttgatacgg	R249W W142R / R249W	Reverse
CHO MFT G91R FM	gtatggagggcgggtttatcctg	G91R	Forward
CHO MFT G91R RM	acccgccctccatacatttgg	G91R	Reverse
CHO MFT G91L FM	gtatggcttgcgggtttatcctggggactc	G91L	Forward
CHO MFT G91L RM	acccgcaagccatacatttggggttac	G91L	Reverse
CHO MFT Q246E fp	tacccgtatgaggttgtgcgagcccg	Q246E	Forward
CHO MFT Q246E rp	tcgcacaacctcatacgggtatgttgc	Q246E	Reverse

Table 2-2 List of primers used for PCR reactions. All primers are listed from 5' to 3'

Transformation of E. coli with mutant mft cDNA ligated into pcDNA 3.1(-) for plasmid purification

Chemically competent TOP10 *E. coli* cells were stored at -80° C and thawed on ice for ~5 minutes. After thawing, 5 µL of each ligation reaction was added to ~50 µL TOP10 cells and this mixture incubated on ice for 30 minutes, after which it was placed at 42° C for 45 seconds. Following this heat-shock, the mixture was placed back on ice for 10 minutes to allow the TOP10 cells to recovery from the heat-shock. S.O.C. Media (2% tryptone, 0.5% yeast extract, 10 mM NaCl, 2.5 mM KCl, 10 mM $MgCl_2$, 10 mM $MgSO_4$, and 20 mM glucose) (250 µL), warmed to 25° C, was added to the mixture and the reaction tube was placed horizontally in a shaking incubator for one hour at 225 rpm and 37° C. The transformed TOP10 cells were plated on Luria-Bertani (LB) agar plates with 100 µg/mL of carbenicillin added and were incubated at 37° C overnight. The pcDNA 3.1(-) vector provided an ampicillin resistance cassette that permitted growth in the presence of carbenicillin to TOP10 bacteria that were transformed with this vector. Approximately five colonies were picked for further expansion, inoculated into 5 mL LB media containing carbenicillin and placed in a shaking incubator at 37° C and 225 rpm for ~16 hours. Bacterial cells were centrifuged at 4,000 x g to pellet the cells and the plasmid DNA was isolated using a Promega Wizard Plus SV Miniprep kit. A *Xho*I and *Hin*dIII restriction digest (as above) was used to check for the appropriate insert size and three clones containing the correct insert size were sequenced. Frozen stocks of these clones were made in LB broth with 10% DMSO and stored at -80° C. The same procedure was followed for large-scale plasmid isolations, only clones were initially inoculated in 5 mL

of LB agar with 100 µg/mL carbenicillin for ~4 hours at 37° C and then expanded into a total of 50 mL of the same media and grown for an additional 16 hours at 225 rpm and 37° C. Plasmid DNA was isolated using a Promega PureYield Plasmid MidiPrep kit.

Transfection of glyB cells with mutant mft cDNA in pcDNA 3.1(-)

Mft cDNAs cloned into pcDNA 3.1(-) that were confirmed by sequencing to contain only the intended mutations were transfected into glyB cells to test the function of the encoded mutant MFT protein. The normal growth media of glyB cells was MEM α media with deoxynucleosides and ribonucleosides, supplemented with 10% fetal bovine serum (FBS). GlyB cells were routinely grown at 37° C with 5% CO_2. GlyB cells were plated at 100,000 cells per 100 mm dish 48 hours prior to transfection with mutant *mft* cDNA in pcDNA 3.1(-). Plasmid DNA was diluted to 100 ng/µL over 1/10 the volume of chloroform, mixed well and placed at 4° C 24 hours before transfection. Transfection was carried out using a calcium phosphate-based method (53). For transfection of a single 100 mm dish, 700 µL of HEBES buffer (10 g/L HEPES, 16 g/L NaCl, 0.74 g/L KCl, 0.25 g/L, $Na_2HPO_4(7H_20)$, 2 g/L glucose, pH 7.04) was added drop-wise into an air-bubbled solution containing the pcDNA 3.1(-) vector that encoded a mutated CHO *mft* cDNA and $CaCl_2$ for a final volume of 1 mL/100 mm dish with 5 µg plasmid DNA per 100 mm dish and 135 mM $CaCl_2$. For transfection of multiple dishes with the same mutant MFT construct, the amounts of HEBES, DNA and $CaCl_2$ were proportionally increased, combined into a single solution and 1 mL portions were taken from this master solution for each plate. After HEBES was added, this solution was incubated at room temperature for 30 minutes.

Media was aspirated from the glyB cells and the transfection mix was placed directly on the cells for 30 minutes at room temperature with agitation every 10 minutes. After this incubation, 9 mL of fresh non-selective media (MEM α with deoxynucleosides and ribonucleosides supplemented with 10% FBS and 1% Penicillin and Streptomycin (Pen/Strep)) was added to each transfection dish and the plates were placed in an incubator at 37° C and 5% CO_2. The non-selective media containing the transfection mix was aspirated from the transfected dishes 24 hours later, 10 mL of fresh, non-selective media was added, and the dishes were placed at 37° C in a 5% CO_2 incubator for 24 hours. After a total of 48 hours after transfection, selective media was placed on the cells. Two different types of selective media were used in the glyB complementation assay, single selection media and double selection media. Both media types contained glycine-free MEM α media that was supplemented with 10% dialyzed FBS, 1% Pen/Strep, and 1 mg/mL G418. The difference between the two media types was that single selection media was also supplemented with 50 mg/L glycine, while double selection media did not contain any glycine. Selective media was replaced every other day for 8-10 days, after which the media was removed and the dishes were washed twice with phosphate buffered saline (PBS). Methanol was placed on the dishes for 15 minutes to fix any colonies. The methanol was removed from the plates and colonies were stained in 5% Wright-Giemsa stain for 15 minutes. The stain was removed, the dishes were washed with distilled water, the plates were allowed to air-dry and the colonies on each dish were manually counted. Every colony that was easily visible to the eye was counted. The data shown represents the average from three to six experiments with standard deviation bars. In each experiment,

three replicate dishes were used per selection condition. Statistical significance ($p < 0.001$) was determined for all data using a one-way ANOVA analysis followed by a Tukey/Kramer analysis. Selected stained plates are shown in Figure 2-5.

Generation of glyB cells stably transfected with mutant mft cDNA

GlyB cells were transfected as described above and colonies of transfected glyB cells were grown in single selection media. After 8-10 days of growth in single selection media, colonies were visualized under a microscope and their location was marked on the underside of their growth dish with a permanent marker. In a sterile environment, selective growth medium was removed from the 100 mm dishes and colonies were removed from dishes by touching sterile cotton swabs to the location of the dish that corresponded to the marked areas. Twelve colonies were randomly selected for each mutation without preference for colony size or morphology. These clones were grown in single selection media at all times.

Isolation of mitochondria and mitochondrial protein

Stably transfected cells lines were scraped from tissue culture dishes in phosphate buffered saline (PBS) with a commercial mixture of EDTA-free protease inhibitors (PI) (Roche, cat. #11873580001). The protease inhibitors in this mixture are a proprietary mixture of serine, cysteine, and metalloprotease inhibitors. All samples were kept on ice from herein. Cells were centrifuged and resuspended in 7.5 mL of homogenization solution (250 mM sucrose, 1 mM EDTA, pH 6.8) with protease inhibitors. Following a

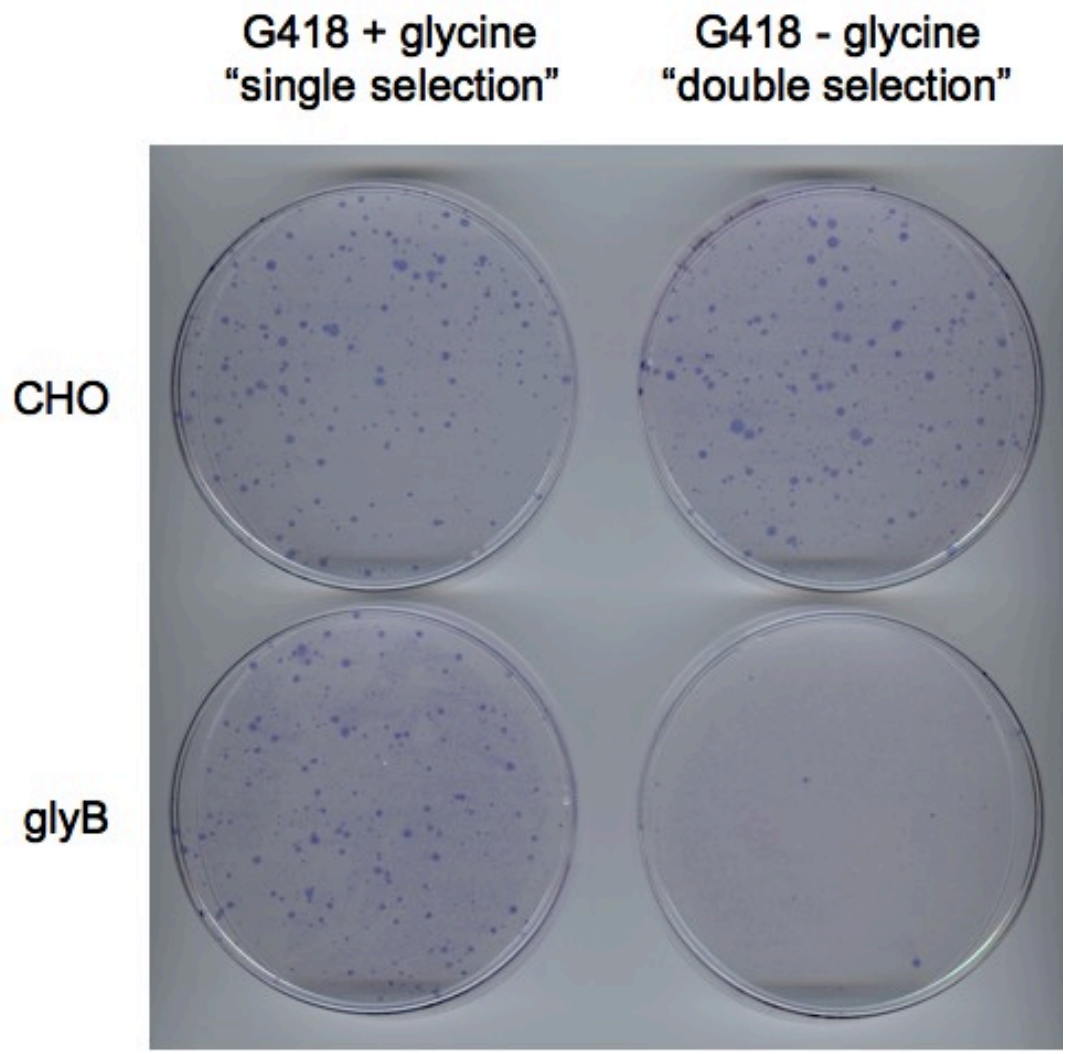

Figure 2-5 Stained transfection plates from glyB complementation assay. GlyB cells were plated on 100 mm dishes and transfected with CHO *mft* cDNA constructs in pcDNA 3.1(-) by a calcium phosphate-based method. Transfected cells were grown in media containing 1 mg/mL G418 in the presence (single selection) or absence (double selection) of glycine. After 8-10 days of growth in selective media dishes, cells were washed with phosphate buffered saline, the colonies that formed were fixed to the dishes with methanol and stained in 5% Wright-Giemsa. The dishes were then air-dried and colonies were manually counted. Data was expressed as a ratio of the number of colonies formed in the absence of glycine versus in the presence of glycine. The plates that are shown represent glyB cells transfected with either CHO or glyB *mft* cDNA.

five minute incubation in homogenization solution, cells were gently broken open using 15 strokes in a 7.5 mL dounce homogenizer using a "B" pestle. This homogenate was centrifuged at 2,000 x g at 4° C for 5 minutes to remove cell debris and unbroken cells. The post-nuclear supernatant was centrifuged at 11,000 x g at 4° C for 15 minutes and the pellet contained the mitochondria. For further mitochondrial protein analysis, the mitochondrial pellet was dissolved in lysis buffer (62.5 mM Tris, pH 6.8; 5% glycerol; 2% SDS; 5% 2-mercaptoethanol) formulated with protease inhibitors. Mitochondrial protein concentrations were determined by the Bradford reagent (Bio-Rad, cat. #5000006) as specified by the manufacturer against a standard of bovine serum albumin.

Western blot analysis of myc-MFT expression

Twenty micrograms of isolated mitochondrial protein was loaded into a freshly prepared 12% SDS-PAGE gel, subjected to electrophoresis, and the fractionated proteins were transferred to a PVDF membrane at 100 V over one hour in a buffer containing 192 mM glycine, 25 mM Tris, pH 8.3. Non-specific membrane binding was minimized by a one hour incubation with Starting Block T20 (Thermo Fisher Scientific, cat. #37543), followed by three vigorous washes in Tris buffered saline containing 0.05% Tween (TBS-T) for 5 minutes each. The membrane was incubated with rabbit anti-myc antibody (Sigma, cat. #C3956) in Starting Block T20 (1:2000 dilution) at 4° C for 16 hours. The membrane was washed three times for 15 minutes each in 0.05% TBS-T and placed in Starting Block T20 with peroxidase conjugated goat anti-rabbit IgG antibody (1:10,000 dilution, Thermo Fisher Scientific, cat. #31462) for one hour at 25° C, followed by three

washes for 15 minutes in 0.05% TBS-T. Protein IgG complexes were detected using a West-Dura chemiluminescent substrate kit (Pierce SuperSignal) that was incubated with the membrane in the dark and the membrane was then exposed to X-ray film so that the positions of and abundance of *myc*-tagged proteins could be visualized and documented on film. The abundance of MFT that was expressed in cultures expanded from individual colonies for each MFT mutation was compared, and clones of each mutant that expressed similar levels of *myc*-tagged MFT were selected for use in radiolabeled folate uptake experiments. The detection of *myc*-MFT expression in various MFT mutant clones is shown in Figure 2-6.

Mitochondrial uptake of ^{3}H-6S-5-formyltetrahydrofolate

GlyB cells stably expressing the transfected mutant MFTs were detached from 150 mm dishes using trypsin/EDTA and resuspended in MEM α media supplemented with 10% FBS, placed in a 37° C shaking incubator in suspension culture and allowed to recover from trypsin exposure for one hour. Cells were pelleted by centrifugation, resuspended in 0.25 mL RPMI 1640 media without folic acid or serum at 10-20 x 10^{6} cells/mL and placed in a 37° C shaking water bath for 5 minutes. An equal volume of RPMI 1640 media was added without folic acid, but containing 1 μM [3',5', 7, 9-^{3}H]-(6S)-5-formyl-tetrahydrofolate at a final specific activity of 2.5 μCi/mL. Uptake was stopped by the timed addition of 10 mL of ice cold PBS and samples were kept at 4° C thereafter. Cells were pelleted at 2000 x g at 4° C for 5 minutes, washed three times with 10 mL of PBS, and mitochondria were isolated by dounce homogenization and differential

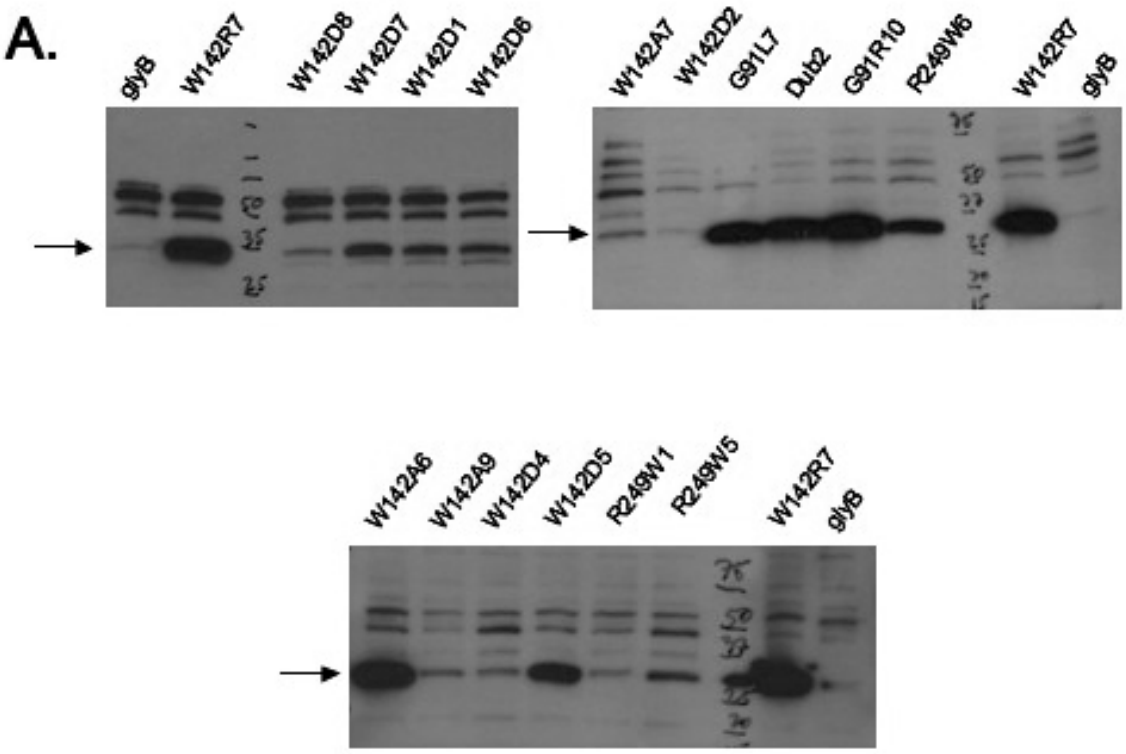

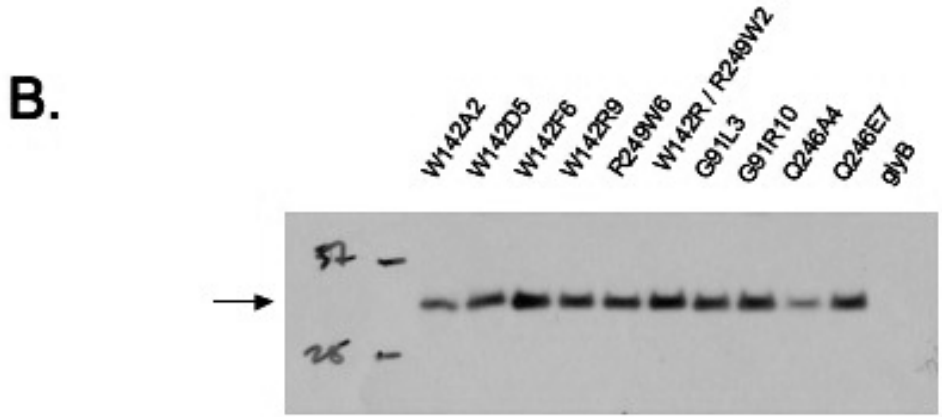

Figure 2-6 Probing MFT mutant clones for *myc*-MFT expression by western blotting. Ten colonies from glyB cells stably transfected with each mutant *myc*-MFT cDNA were randomly selected, isolated and expanded into ten mass cultures. Mitochondrial protein was isolated from mass cultures of up to ten clones per MFT mutation. In A. and B., mitochondrial protein from glyB cells was included as a negative control on these blots. The black arrows mark the expected size of the MFT, ~33 kDa. A. Ten micrograms of mitochondrial protein from the indicated MFT mutant clones was loaded onto a gel, electrophoresed, and the proteins in the gel were transferred to a PVDF membrane. This membrane was probed for *myc*-MFT expression using an antibody raised against *myc*. Mitochondrial protein from MFT mutant W142R, clone 7 was determined by western blotting (not shown) to contain a high amount of *myc*-MFT expression. Other MFT mutant clones were probed for *myc*-MFT expression similar to MFT mutant W142R, clone 7. It was later determined that *myc*-MFT expression in MFT mutant W142R, clone 7 was higher than was observed in most other MFT mutant clones and therefore, this clone was not used for further experimentation. B. Twenty micrograms of mitochondrial protein from clones of every constructed MFT mutant were loaded onto the same gel, the gel electrophoresed, and the proteins in the gel were transferred to a PVDF membrane. This membrane was probed for *myc*-MFT expression using an antibody raised against *myc*. All of the MFT mutant clones probed on this blot were expanded and used in the transport assays presented in the Results section of this chapter.

centrifugation, as described above. Isolated mitochondrial pellets were dissolved in 0.5 mL of 75 mM NaOH. The dissolved mitochondria were neutralized with a 0.5 mL addition of 100 mM HCl and a 1 mL addition of homogenization solution (250 mM sucrose, 1 mM EDTA, pH 6.8). Safety Solve scintillation cocktail (18 mL) was added into the 20 mL glass scintillation vials and the vials were placed in a Beckman Coulter LS 6500 multi-purpose scintillation counter for the determination of ^{3}H content. The counts per minute in each sample were analyzed for two cycles of counting for a total of 10 minutes each with no background input. The data shown represents the average of 3-4 experimental samples from two different experiments with standard deviation bars. Statistical significance ($p < 0.001$) was determined for all data using a one-way ANOVA analysis followed by a Tukey/Kramer analysis.

Generation of the CHO MFT homology models

Throughout the course of these studies, two CHO MFT homology models were created. Both models were generated using the CHO MFT primary sequence and the solved crystal structure of the bovine ADP/ATP carrier (128) (bAAC ; pdb accession: 1okc) as the structural template. The CHO MFT sequence was sent to the PSIPRED server (13, 22) to predict the secondary structure of the CHO MFT protein. The primary sequences of the CHO MFT and the bAAC were arranged so the predicted membrane-spanning domains and the PxD/ExxK/R motifs in the MFT were aligned with those in the bAAC crystal structure. The MFT and bAAC primary sequences were also aligned so the sequences of the predicted transmembrane domain regions did not contain any gaps in

sequence alignment. These regions were considered to be structurally conserved regions for MFT homology model generation. In the structurally conserved regions, the crystal structure of the AAC was used as the template to generate the MFT structure. We did not consider predicted random coil regions to be structurally conserved between the MFT and AAC. Therefore, gaps in the sequence alignment were permitted in the predicted loop regions of the MFT. Loop regions were modeled using an independent database that was contained within the Sybyl 7.1 COMPOSER program (161), in which the sequences of these MFT loop regions were paired to similar sequences in other proteins in which the structure was known. The first homology model was created in the COMPOSER module of Tripos Sybyl 7.1 (161). Following the generation of this model, the locations and orientations of all amino acid side chains were optimized using the SQWRL program (17).

A second model was created in the ORCHESTRAR module in Tripos Sybyl 8.0 (164) to improve the modeling of MFT loop regions using the enhanced libraries of loop structures and advanced prediction methods of that version. As in the generation of the first MFT homology model, the transmembrane domain regions were selected as the structurally conserved regions. The structure of these regions was created using the AAC crystal structure as the template. Predicted loop regions in the MFT were modeled independent of the AAC structure using an enhanced library of protein loop regions contained in the ORCHESTRAR program. Loops regions were searched using a combination of *ab initio*, fragment database (FREAD), and homolog comparison methods. Following the generation of the CHO MFT model, the model was inspected and contained no peptide bond breaks or distances > 1.60 Å between bonded atoms, no torsion angles that

were clearly outside of their allowable Ramachadran plot placement, and steric interactions of amino acid side chains were minimized.

Tetrahydrofolate docking into the CHO MFT homology model

A molecule of tetrahydrofolate was built in Sybyl 7.1, atom and bond types were checked, and the structure equilibrated to an energy minimum. The COMPOSER-generated CHO MFT homology model and the crystallography-derived structure of the bovine AAC (bAAC) (pdb accession: 1okc) were loaded into the Sybyl 7.1 program. The CHO MFT homology model and bAAC were aligned so that the common structural elements of these two proteins overlapped. Specifically, these proteins were aligned so that their transmembrane domains were superimposable. Initially two structure files existed, one contained the bAAC structure in complex with a carboxyatractyloside (CATR) inhibitor molecule in its transport cavity, and the other contained the CHO MFT homology model. The CATR inhibitor was then extracted *in silico* from the bAAC structure file. Three separate files now existed, one containing the bAAC, one containing the CHO MFT homology model, and one containing the CATR inhibitor, but the spatial locations and coordinates of all three structures did not change. The CATR inhibitor was then merged into the MFT homology model structure. The MFT homology model now contained the CATR molecule in the exact location and orientation as it was in the bAAC. Atoms in the MFT that were within 9.9 Å of the merged CATR were used as the active docking site for tetrahydrofolate using the FlexX program (161). Total Score and CSCORE were used to sort the resulting docked conformations of tetrahydrofolate.

Molecular dynamics simulation of tetrahydrofolate transport in the MFT homology model

A molecular dynamics simulation of the CHO MFT was run using the Ohio Supercomputer Center in collaboration with Dr. John C. Hackett of the department of Medicinal Chemistry at VCU. Dr. Hackett provided the following description of the molecular dynamics simulations methods.

A square 100 $Å^2$ palmitoyl oleylphosphatidylcholine (POPC) bilayer membrane slab was constructed using the Visual Molecular Dynamics (VMD) program (63) and an additional 30 Å and 20 Å of TIP3P water molecules were added to inter-membrane space and matrix sides, respectively. All molecular dynamics simulations were performed with the NAMD 2.6 suite of programs (134) and the CHARMM27 (99) force field for biomolecular simulations. The hydrated membrane was minimized for 5000 steps, followed by equilibration of the aliphatic lipid tails for 500 ps at constant volume and temperature (NVT; 300 K). After melting of the lipid tails, the entire membrane system was equilibrated in the NVT ensemble for an additional 500 ps.

The propKa module of the PDB2PQR suite of programs (10, 37, 74) was used to calculate estimates of pKa values for ionizable residues in the MFT homology model that were generated in the ORCHESTRAR module. These values were subsequently used to assign their protonation states at pH 7.4. After the appropriate adjustments in the protonation states, the homology model was oriented in the center of the pre-equilibrated POPC membrane. Overlapping lipid and water molecules, as well as those within 0.8 Å were removed from the simulation system. Nineteen chloride ions were added to neutralize the simulation cell resulting in a system containing ~100,000 atoms for molecular

dynamics simulation. The complete system was minimized for 5000 steps followed by equilibration of the lipid tails for 200 ps with the remainder of the system frozen. Melting of the lipid tails was followed by an additional 1000 steps of minimization and equilibration for 200 ps at constant temperature and pressure (NPT) using the Langevin piston method with a target pressure of 1.01325 bar, decay period of 100 fs, and piston temperature of 300 K. The area of the membrane was maintained constant during NPT simulations. The aforementioned minimization and equilibration protocol was then repeated, albeit with a harmonic restraint (5 kcal/mol/Å) applied to the protein backbone atoms. Moreover, in these preparative NPT MD simulations harmonic forces (0.1 kcal/mol/ Å) were applied between select water molecule oxygen atoms and the C21 atoms of the POPC lipids to prevent water molecules from entering the hydrophobic phase of the membrane during equilibration. Prior to production simulations, an additional 2 ns of NPT simulation was performed with these restraints applied between the water and lipid molecules to ensure appropriate equilibration and packing of the POPC membrane around the MFT protein. After completion of the preparative simulations, the MFT model was equilibrated for an additional 30 ns.

CHARMM parameters for tetrahydrofolate (THF) were derived from dihydrofolate parameters described by Garcia-Viloca and coworkers (48). Electrostatic potential charges were derived using the CHELPG scheme (20) from a geometry fully-optimized geometry at the B3LYP/6-31G* level of theory using the *Gaussian03* suite of programs (46). To simulate capture of tetrahydrofolate by the MFT model, this ligand was merged with a trajectory snapshot corresponding to t = 5 ns with the carboxylates oriented toward the

base of the channel. The molecule of tetrahydrofolate was manually placed above the MFT homology model transport cavity. Overlapping water molecules as well those within of THF 0.8 Å were removed from the simulation system. Furthermore, to compensate for the dianionic tetrahydrofolate and maintain electrical neutrality, two chloride ions were removed from the simulation cell.

RESULTS

A former graduate student in this laboratory who had worked on the mitochondrial folate transporter (MFT) project, Dr. Erin Perchiniak, submitted a manuscript for publication before she left the lab. In her work, she used insertion of a *c-myc* tag (EQKLISEEDL) to study the function of the N- and C- termini and the predicted inter-membrane space loop regions of the chinese hamster ovary (CHO) MFT. She also designed ten site-specific residue mutations in the MFT protein to study the roles of these residues in the transport function of the MFT. She was able to track these mutant proteins within the cell using the *c-myc* tag that was attached to the N-terminus of the constructed MFT mutant proteins. Dr. Perchiniak set up a survival assay to study the effects of regional *myc*-insertion in the MFT and of the site-specific mutations on MFT transport function in a MFT functionally-null, CHO-derived cell line, the glyB cell. The manuscript was returned from review and requested a more direct transport analysis of the site-directed mutants. With Dr. Perchiniak no longer in the lab, Dr. Moran and I devised an assay that more directly assessed the effects of mutations on MFT transport function by measuring

mitochondrial folate uptake in glyB cells transfected with mutant MFT constructs. Additionally, during the review and revision period, we generated a homology model of the CHO MFT, based on the solved three-dimensional coordinates of a related MCF protein, the ADP/ATP carrier (AAC). This homology model complemented the manuscript, helped explain the experimental data and aided in the design of future experiments.

Exploiting the glyB glycine auxotrophy phenotype to study MFT function

CHO-derived glyB cells have a single point mutation in their only allele that encodes for the MFT, which results in a G192E mutation and eliminates the transport function of the MFT (108). Thus, glyB cells are unable to accumulate any mitochondrial folates and, therefore, require an exogenous supply of glycine for survival. However, glyB cells could be relieved of this glycine auxotrophy phenotype by transfection with *mft* cDNA from human, hamster, mouse, zebrafish, even *Arabidopsis* because these cDNA constructs encoded a functional MFT protein that restored mitochondrial folate accumulation in the transfected cells (108, 160). MFT site-specific mutants could be studied in the same way; a mutation in wild-type CHO *mft* cDNA could be constructed, transfected into glyB cells and the ability of these transfected cells to survive in the absence of glycine could be observed. If cells transfected with this mutated cDNA could survive without glycine supplementation, the encoded MFT mutant protein retained function. Conversely, if the transfected glyB cells still required glycine for survival, it would be evident that the encoded MFT protein was unable to restore mitochondrial folate

uptake in glyB cells and the mutated MFT protein was considered to be devoid of folate transport activity.

Studying ten MFT residues conserved amongst MFT orthologs by mutagenesis

MFT site-specific mutations were designed during Erin Perchiniak's thesis work, and at that time, the crystal structure of the AAC was not available. Hence, there were no clues to the structure of the MFT protein in the literature. However, in the process of completing these studies, a crystal structure did become available and the MFT mutants that were initially designed are discussed with respect to their predicted locations in a CHO MFT homology model later in this section. Charged residues were hypothesized to contact and position the folate substrate within the channel. In addition, residues that were highly conserved in MFT orthologs but were altered in other MCF proteins suggested the potential involvement of these MFT residues in a folate-specific transport mechanism. The function of these residues was studied in a glyB complementation assay using the survival of glyB cells in the absence of glycine as an endpoint. The glyB complementation assay data is expressed as the number of colonies that are formed in the presence of G418 with and without glycine to control for transfection efficiency in each experiment. GlyB cells transfected with wild type CHO *mft* cDNA were able to form half of the colonies in the absence of glycine versus in the presence of glycine (Figure 2-7A). In contrast, glyB cells transfected with glyB *mft* cDNA (CHO MFT G192E) were unable to form colonies in the absence of glycine. Despite the conservation of these residues across MFT orthologs, eight of the ten site-directed mutations were capable of some level of folate transport, as

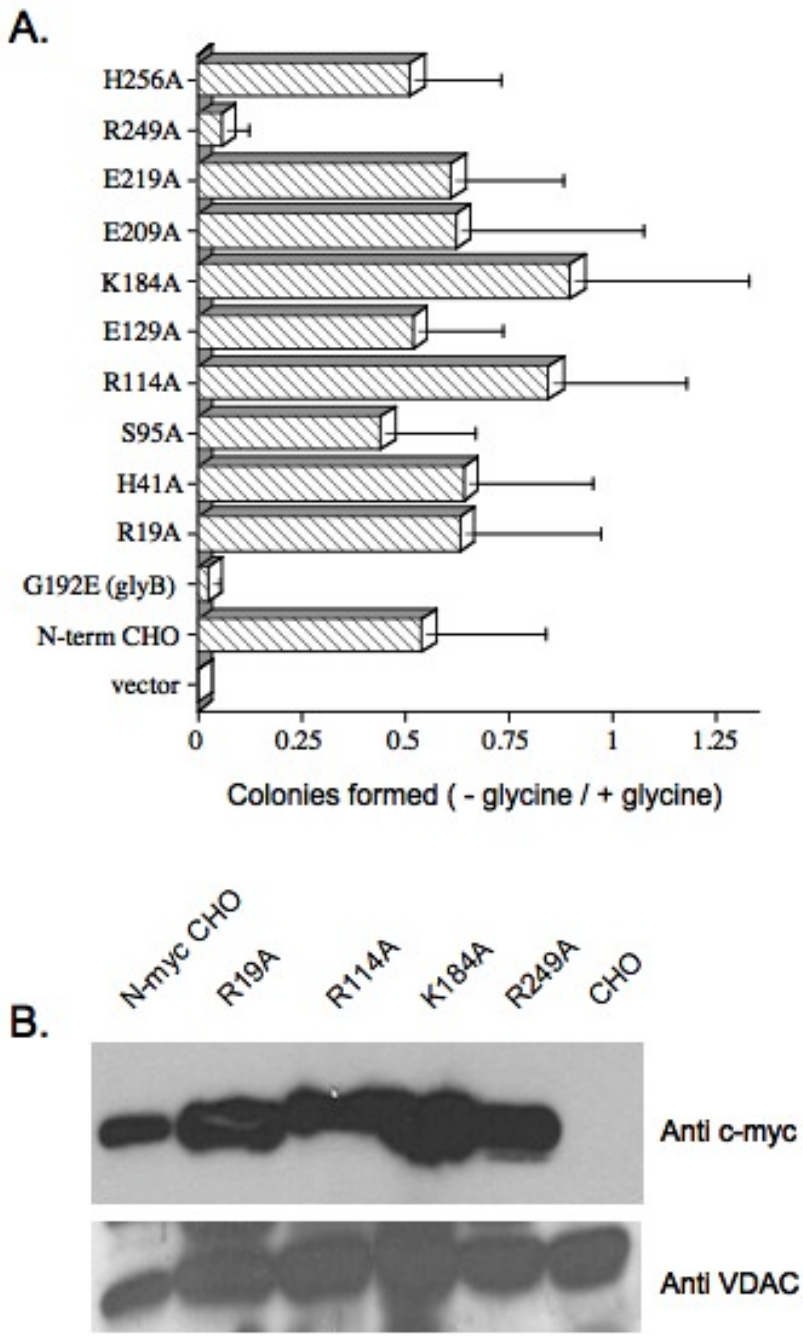

Figure 2-7 GlyB complementation and western blotting of MFT mutants. These studies are published in Perchiniak *et al.* (2007). A. Mutant *mft* cDNA constructs in pcDNA 3.1(-) were transfected into glyB cells and the ability of the transfectants to grow in the presence and absence of glycine was observed. B. Mitochondrial protein was isolated from stably transfected and pooled cell lines. Forty micrograms of protein from each cell line was probed for *myc*-MFT expression using an antibody raised against the *myc* epitope. Untransfected CHO cells and glyB cells transfected with a N-terminal *myc* tagged CHO *mft* cDNA were included as negative and positive controls, respectively.

suggested by the ability of the mutant transfectants to form colonies in the absence of glycine. Only two MFT mutations, CHO MFT R249A and G192E (mimicking the mutation in the glyB MFT) resulted in MFT proteins that were unable to restore mitochondrial folate accumulation in glyB cells (Figure 2-7A). All of the transfected MFT mutant proteins carried an N-terminal *myc* tag and western blot analysis of mitochondrial protein, probed for *myc* expression, confirmed that the MFT mutant proteins were expressed and localized to mitochondria (Figure 2-7B). This indicated that the glyB complementation data could be interpreted on the basis of MFT function without complications resulting from significant variance in MFT expression or an inability of the MFT to be properly targeted to mitochondria.

The endpoint in the glyB complementation assay was glyB cell survival in the absence of glycine, which was an indirect measure of the MFT transport. We did not know what level of mitochondrial folate accumulation was compatible with cell survival and how this level compared to wild type accumulation. For instance, it was possible that a MFT mutant protein could retain ~50% of its wild-type function, but this level of function would still permit enough mitochondrial folate accumulation to permit glyB cell survival in the absence of glycine. An assay was designed to more directly measure mitochondrial folate uptake and study the effects of these mutations on MFT transport function. This assay was not a direct measure of mitochondrial folate transport, but rather measured uptake of radiolabel into mitochondria when intact cells were exposed to ^{3}H-6S-5-formyl-tetrahydrofolate (5f-thf). To generate the cell lines used in this uptake assay, ten colonies of glyB cells that were transfected with the same mutant *mft* cDNA construct and

that survived G418 selection were expanded. Equal amounts of cells from each of the colonies were pooled together and the cells were used in this transport assay within three passages. In this assay, whole cells were incubated with 5f-thf. After 5f-thf uptake, cells were dounce homogenized and the mitochondrial and cytosolic compartments were isolated by differential centrifugation. The radioactivity in the mitochondrial fraction was determined and converted into units that represented mitochondrial folate uptake. CHO and glyB cells were incubated with 5f-thf for varying lengths of time up to one hour (Figure 2-8A). CHO cells actively and near linearly accumulated mitochondrial folates for 20 minutes, followed by a slower rate of accumulation for the remainder of the 60 minute incubation period. Mitochondrial folate uptake was observed in glyB cells, but was minimal when compared to CHO mitochondrial uptake. Based on this data, a 20 minute incubation with labeled 5f-thf was chosen for future experimentation; it appeared that mitochondrial folate accumulation was relatively linear up to this point and the uptake in CHO and glyB mitochondria was sufficiently separated to allow the interpretation of various levels of mitochondrial folate uptake in stably transfected MFT mutant cell lines. As was observed in the glyB complementation assay, CHO MFT R249A and G192E showed a distinct inability to uptake any mitochondrial folates (Figure 2-8B). Besides the R249A and G192 mutations, it appeared that all other MFT mutations studied were able to accumulate significant amounts of mitochondrial metabolites of 5f-thf.

Somewhat disappointingly, we had constructed ten MFT site-directed mutations and only two of these mutations appeared to affect the transport function of the MFT. Furthermore, of the two residues that were required for MFT transport, one residue

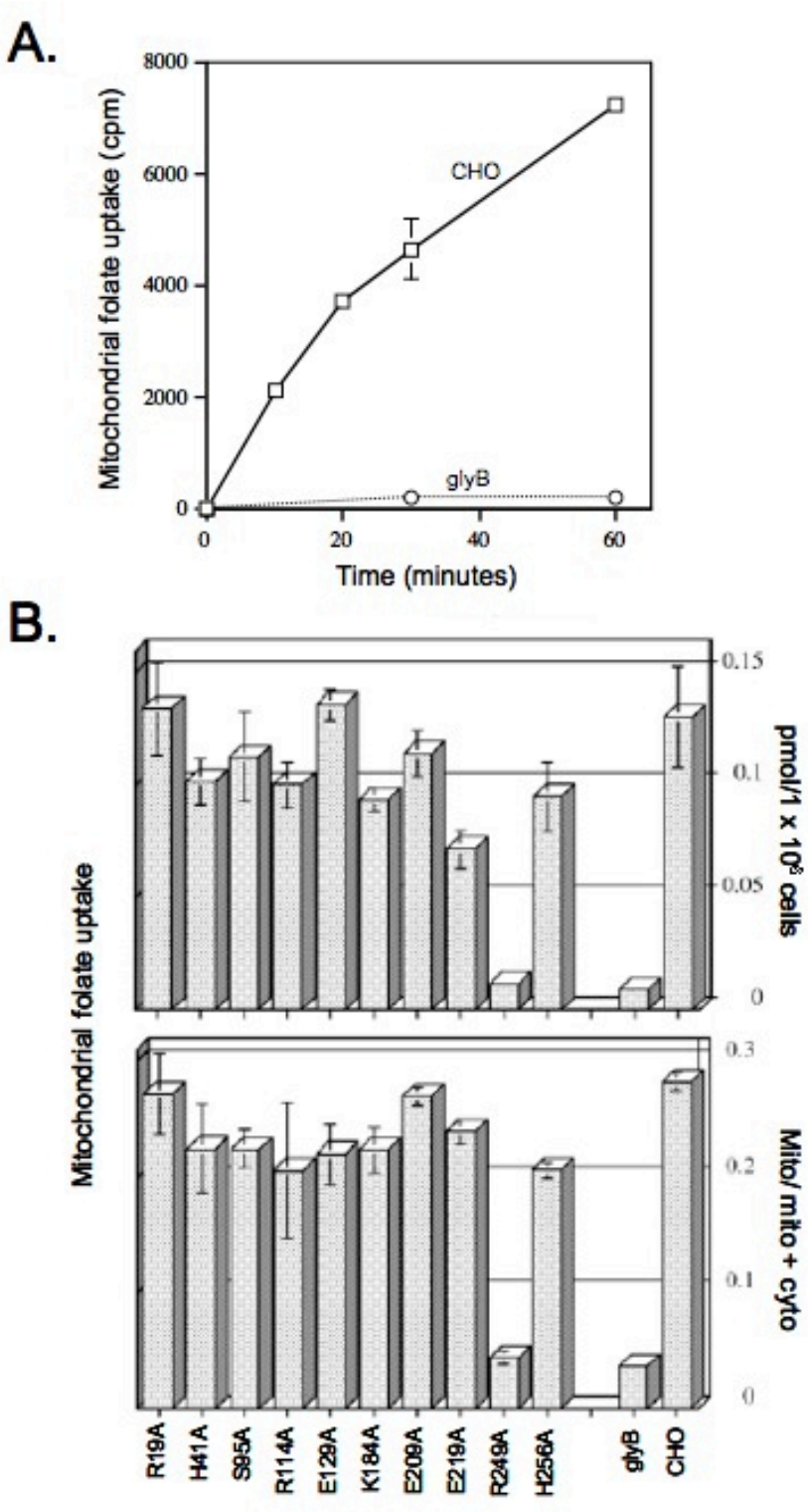

Figure 2-8 Mitochondrial folate uptake in CHO, glyB and MFT mutant cell lines. These studies are published in Perchiniak *et al.* (2007). A. CHO and glyB cells were incubated with 1 μM ^{3}H-6S-5-formyl-tetrahydrofolate for the indicated periods of time. Mitochondrial fractions were isolated from the cells and counted for radioactivity. B. GlyB cells were stably transfected with MFT mutant cDNAs and ten clones were randomly selected, expanded and equal amounts of cells were pooled together. These pooled lines were used in mitochondrial uptake experiments within three passages. Whole cells were incubated with 1 μM ^{3}H-6S-5-formyl-tetrahydrofolate for 20 minutes. Mitochondrial fractions were isolated from the cells and counted for radioactivity.

(G192) was previously established to be mutated in glyB cells and eliminated MFT function, and the other residue (R249) was located in a PxD/ExxK/R motif, common to all MCF proteins. Using residue conservation in MFT orthologs was an inefficient approach to design site-specific MFT mutant proteins to investigate the folate-specific transport mechanism in the MFT. We believed that a structural model of the CHO MFT would guide the hypothesis-driven design of future MFT mutations and also provide insight as to why the previously examined mutants were relatively uninformative. In the time it took to conduct studies on these ten MFT mutants, a high resolution (2.2 Å) crystal structure had become available for the ADP/ATP carrier, a MCF protein similar to the MFT. Using this structure, it was now possible to generate a structural model of the MFT.

Generation and application of a CHO MFT homology model

Upon its discovery in 2000, the MFT had both sequence and structural similarities with an identified mitochondrial carrier family (MCF) of integral membrane proteins (160). The solved crystal structure of one MCF member, the bovine ADP/ATP carrier (bAAC) (pdb accession: 1okc) (128), provided a template for the structural prediction of other MCF proteins. Furthermore, the technologies available for the prediction of membrane embedded helices are sufficiently advanced for accurate and reliable structural predictions (137). Structural predictions are even further enhanced when the structure of a related protein is available and the proteins contain functionally conserved residues or motifs, for example, the MCF PxD/ExxK/R conserved motif (137). The primary sequences of the CHO MFT and the bAAC were sent to the PSIPRED server (13, 22) for alignment

and prediction of secondary structure. While the CHO MFT and bAAC have only 26% sequence identity, there was a high degree of secondary structure homology predicted between the two proteins (Figure 2-9). To generate a predicted structure for the CHO MFT, the sequence of the CHO MFT and the protein database file containing the sequence and three-dimensional coordinates of the bAAC (pdb accession: 1okc) were loaded into the Composer module of Sybyl v7.1 (161). The bAAC and CHO MFT sequences were aligned similarly, but not identically, to the alignment shown in Figure 2-9. The conserved PxD/ExxK/R motifs of the CHO MFT and bAAC were aligned and the transmembrane spanning regions of the MFT, as predicted by the PSIPRED server, were arranged to have minimal sequence gaps and were selected as structurally conserved regions. These structurally conserved regions were specifically modeled using the AAC structure as a template, while loop regions were modeled using an independent loop search database within the Composer module. The resulting CHO MFT homology model structure superimposed with the crystallized AAC in most of the transmembrane domain (TMD) regions (Figure 2-10A-B). However, there was a noticeable break in the α-helical structure of the fourth TMD in the CHO MFT homology model. Variability between the bAAC structure and the CHO MFT homology model was most evident in the loop regions. This variability was expected because the loop regions of the CHO MFT were modeled using an independent loop search to build these regions of the CHO MFT homology model. The CHO MFT homology model is also shown with surface representation to visualize the local charges from the residue side chains throughout the protein (Figure 2-10C-D). The aqueous exposed edges contained a large number of polar (green) and

Figure 2-9 Alignment and secondary structure prediction of the CHO MFT and the ADP/ATP carrier by the PSIPRED server. The sequences of the CHO MFT (Query) and the bAAC (1okcA0) were aligned by the PSIPRED server (13, 22). Amino acids are shown in their single letter abbreviations. In this alignment, residues in green are identical in the CHO MFT and AAC, residues in red are conservative substitutions, and the residues in blue are unrelated. The PSIPRED server also made secondary structure predictions, which are shown above (AAC ; 1okc0) or below (MFT ; Query) the respective protein sequences. Amino acids predicted to be located in helical structures are marked by "H" and "C" marks random coil structures. Numbers outside of the secondary structure predictions, above for the AAC and below for the MFT, correspond to the amino acid sequence. Conserved motifs are located at MFT (Query) amino acid positions 42, 140, and 244.

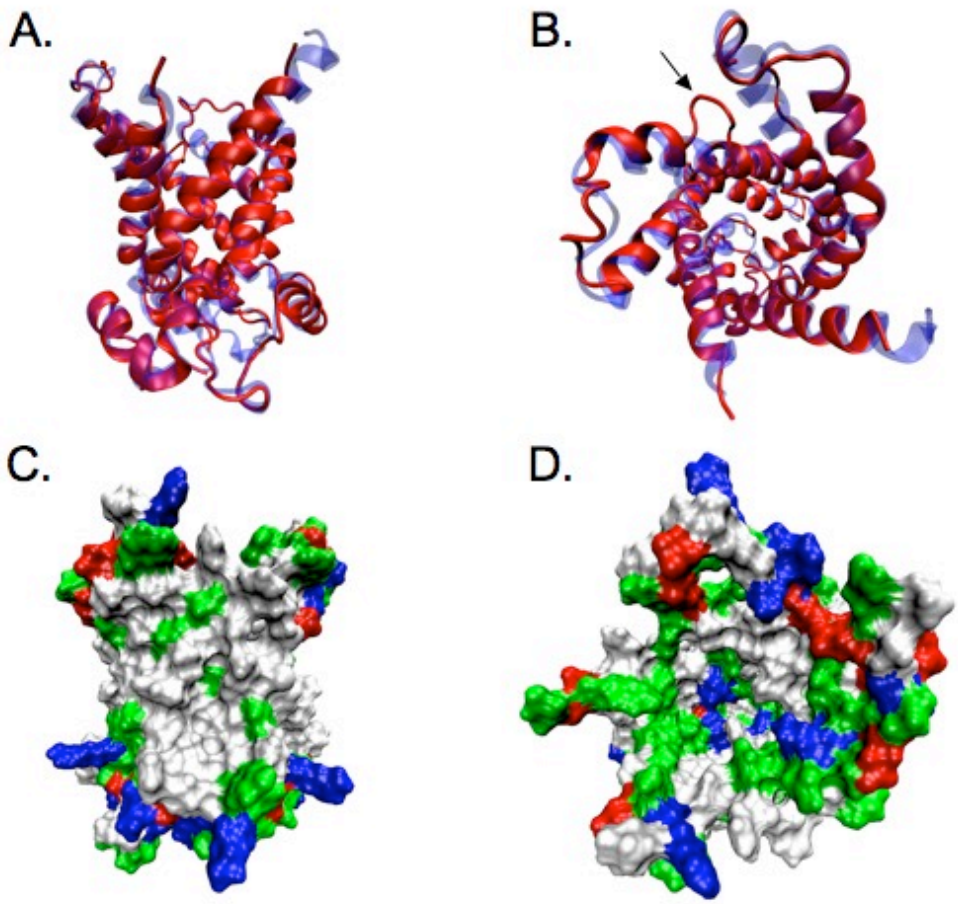

Figure 2-10 Predicted structure of the CHO MFT by homology modeling. A homology model for the CHO MFT was generated based on the solved crystal structure of the bovine ADP/ATP carrier (AAC). A. Cross sectional membrane view of the CHO MFT homology model (red) structurally aligned with the AAC (transparent blue). B. View from the inter-membrane space looking into the transport cavity of the CHO MFT homology model (red) with the AAC overlaid (transparent blue). The black arrow denotes a break in the α-helical structure of the fourth transmembrane domain in the MFT homology model. C. Cross sectional membrane view of the CHO homology model with a surface representation. Aromatic and aliphatic residues are shown in white, polar residues are in green, basic residues are shown in blue and acidic residues are in red. D. View from the inter-membrane space looking into the transport cavity of the CHO MFT homology model with a surface representation. Amino acids are color coded as indicated in C.

charged (red – acidic/negative and blue – basic/positive) residues. In addition, the base of the MFT transport cavity was highly charged, with basic amino acids predominating in this location. The charges associated with residues that lined the transport cavity above the cavity floor were mixed, with polar and neutral (white) side chain residues making up the majority of these residues. The middle portion on the outer surface of the CHO MFT homology model protein was largely neutral (white) and contained very few polar or charged amino acids, which would be predicted for a membrane embedded protein.

The CHO MFT homology model was then used to identify the locations of the ten mutations that were previously investigated in the glyB complementation assay (Figure 2-7A) and the mitochondrial uptake assay (Figure 2-8B). In these studies, CHO MFT R249A and G192E were shown to have a significant effect on MFT function. Observing the predicted locations of these residues in the CHO MFT homology model, provided an explanation for the mutagenesis data. CHO MFT R249 was located in the third conserved sequence of the MFT. The charged conserved sequence residues were shown in the crystal structure of the AAC to form interhelical interactions with one another (Figure 2-3). The orientations of CHO MFT R249 and the other residues in the PxD/ExxK/R motifs suggested that a similar network of interactions were occurring in the MFT as was observed in the AAC (Figure 2-11A). Specifically, the homology model predicted interactions between CHO MFT D44 and K145, W142 and R249, and Q246 and K47. Interestingly, the D/E residue (bAAC D134) in the PxD/ExxK/R motif of the AAC and in the vast majority of MCF proteins was a tryptophan in the MFT. While the ionic interaction that was found in the majority of MCF proteins did not appear likely in the

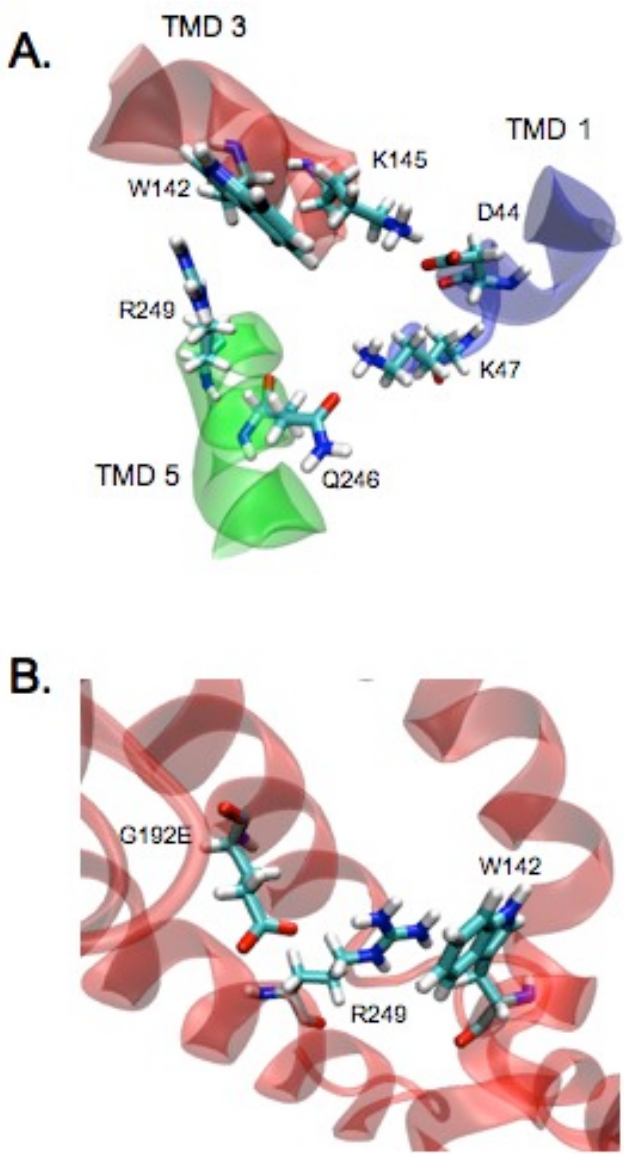

Figure 2-11 Orientation of R249 and G192E in the CHO MFT homology model. The CHO MFT homology model was used to aid in understanding the effects of CHO MFT R249A and G192E (glyB) mutations. A. The predicted orientation of conserved motif residues in the CHO MFT homology model. The first, third and fifth predicted transmembrane domains (TMD) in the CHO MFT are shown in transparent blue, red and green ribbon tube display, respectively. CHO MFT conserved motif residues are shown in CPK. CHO MFT R249 is suggested to interact with W142. B. The CHO MFT homology model is shown in transparent red ribbon tube display. The G192E mutation was created in the MacPyMOL program (157) and the side chain location of G192E was one of several predicted rotamers within the program.

MFT, we proposed that CHO MFT R249 and W142 participated in a cation-π interaction. If these two residues were to interact with one another, this would restore an important conserved motif interaction at the bottom of the MFT transport cavity that was present in the majority of other MCF proteins. This potential interaction was the subject of another set of studies that will be presented later in this section.

The mechanism by which CHO MFT G192E, or the glyB MFT mutation, eliminated the transport function of the MFT was unknown. To better understand the effects of the G192E mutation on MFT transport, the G192E mutation was created *in silico* in the MFT homology model. In one possible mutant rotamer, the G192E side chain projected down and into the transport cavity (Figure 2-11B). The negatively charged end of this glutamate side chain extended within 3 Å of the positively charged side chain of CHO MFT R249. We proposed that the G192E and R249 formed an ionic interaction. In forming this interaction, CHO MFT R249 was surrounded by W142 on one side and G192E on the other. We proposed that multiple interactions with CHO MFT W142 and G192E locked CHO MFT R249 in place. Thus, this stabilization appeared to eliminate any movement of CHO MFT R249, which inhibited the ability of the adjacent proline residue to induce a conformational change that was required for transport.

The CHO MFT homology model was also used to understand why most of the mutations previously studied did not affect the transport function of the MFT (Figures 2-7A and 2-8B). The predicted locations of these mutations were visualized in the CHO MFT homology model. Few residues were located within the MFT transport cavity in the CHO MFT homology model (Figure 2-12). One residue, CHO MFT S95, was located

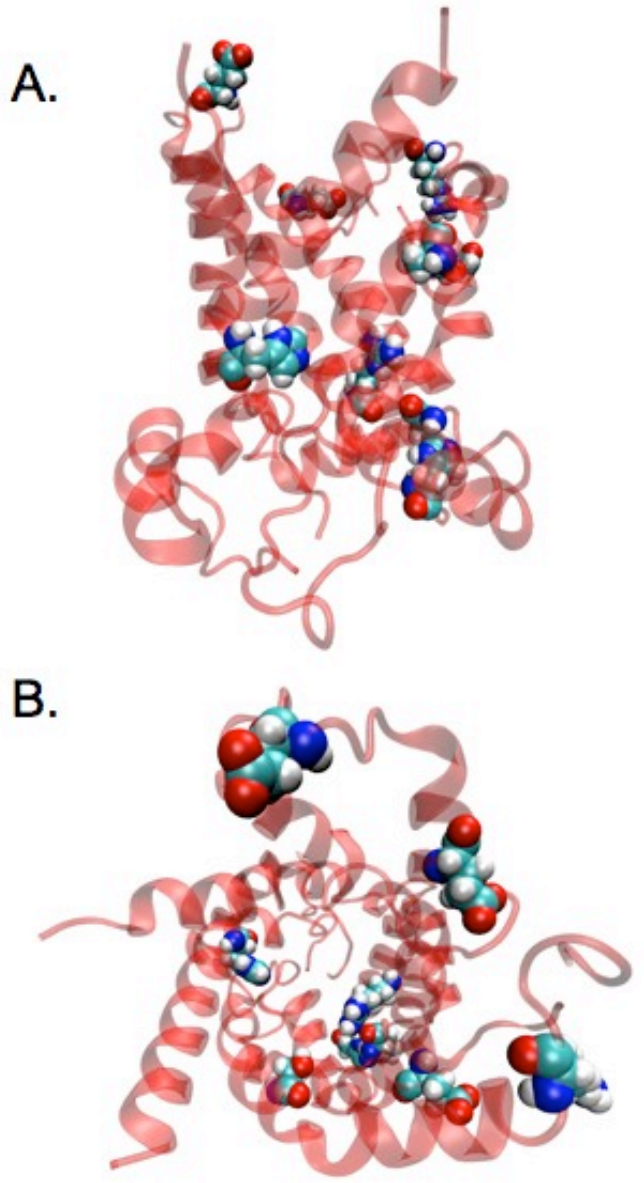

Figure 2-12 Predicted locations of mutated MFT residues in the CHO MFT homology model. A. Cross-sectional membrane view of the CHO MFT homology model in transparent red ribbon tube display with the residues that were mutated in the MFT shown in van der Waals representation. B. View from the inter-membrane space looking into the transport cavity of the CHO MFT homology model. Representations are the same as indicated in A.

within the MFT transport cavity just above the base of the cavity that was formed, in part, by R249. Residues K184 and H256 also appeared to be centrally located, but on the matrix side of the transport floor. While little is known about the roles of the matrix-associated regions of MCF proteins, these residues still could have had roles in assisting substrate passage into the mitochondrial matrix. Nevertheless, there was no evidence to suggest that these residues impaired the transport function of the MFT.

Computational docking of tetrahydrofolate into the transport cavity of the CHO MFT homology model

In addition to visually inspecting the residues that lined the transport cavity, computationally docking a folate molecule into the transport cavity was another way to gain insight into the folate-specific transport mechanism of the MFT. To accomplish this, the CHO MFT homology model and the crystallized AAC structure (pdb accession: 1okc) were structurally aligned as shown in Figure 2-10A-B. In addition to the structure of the AAC, the protein data bank file also contained the three dimensional coordinates of the carboxyatractyloside (CATR) inhibitor that co-crystallized within the transport cavity of the AAC. With the MFT and AAC structurally aligned, the CATR molecule was extracted from its location in the AAC with its orientation and three-dimensional coordinates retained. This CATR molecule was then merged into the MFT homology model so that the MFT now contained the CATR inhibitor within its transport cavity in the exact orientation as in the AAC. The MFT homology model containing CATR was loaded into the FlexX docking suite in Sybyl 7.1 as was a molecule of THF. The space occupied by

CATR and the surrounding 9.9 Å within the MFT transport cavity was selected as the docking site for the molecule of THF. The positions of the glutamate tail of THF in each of the two highest scoring conformations were nearly super imposable (Figure 2-13). In each of the two conformations, the glutamate tail of THF was equidistant (< 2 Å) from CHO MFT PxD/ExxK/R motif residues K47 and K145 (Figure 2-13B). The glutamate tail of THF was also the portion of the THF molecule that was located the deepest within the MFT transport cavity, suggesting that the monoglutamate tail of folate substrates enters the transport cavity first. Interestingly, the benzyl ring of THF in the two highest scoring conformations differed in their placement relative to the tryptophan residue (W142) proposed in the cation-π interaction (Figure 2-13C). The benzyl ring of the highest scoring THF conformation, THF1, was oriented such that further descent of the THF molecule in this conformation would place the benzyl ring of THF directly between CHO MFT W142 and R249. The benzyl ring of THF in the second highest scoring conformation was located on the opposite side of W142. Either of these THF orientations would likely be able to disrupt the conserved motif interactions in the MFT that formed the transport cavity floor; the glutamate group of THF would disrupt any interactions with K47 and K145, while the benzyl ring would disrupt any interaction with W142. This docking study suggested that the proposed cation-π interaction between CHO MFT W142 and R249 was implicated in an opening mechanism used for transport as well as substrate recognition through interaction with the benzyl ring of THF.

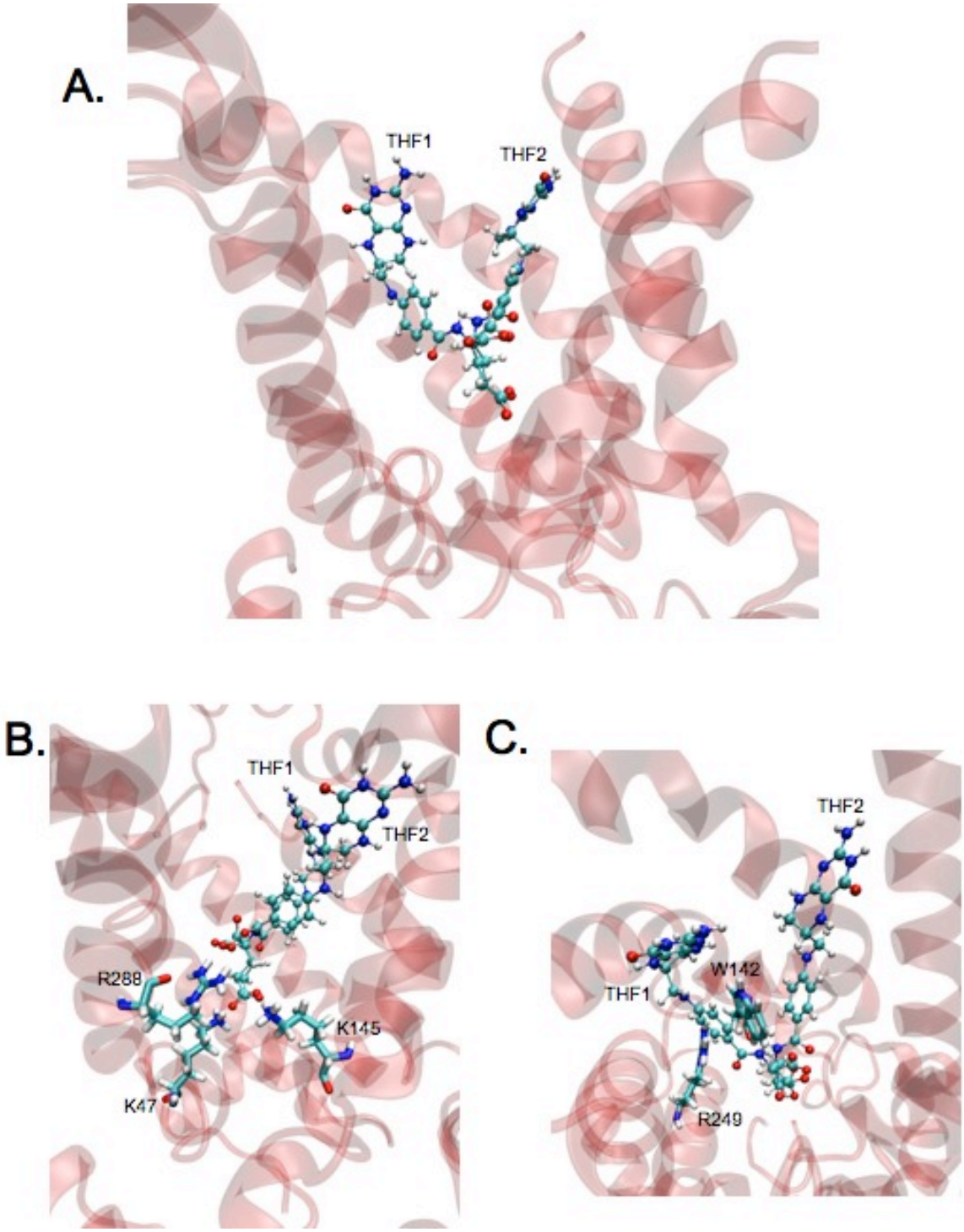

Figure 2-13 Docking of tetrahydrofolate into the CHO MFT homology model. Tetrahydrofolate was computationally docked into the CHO MFT homology model using the FlexX program and the two highest scoring tetrahydrofolate conformations are shown. A. The CHO MFT is shown in transparent red ribbon tube display and the orientations of the two highest scoring conformations of tetrahydrofolate, THF1 and THF2, respectively, are shown in ball and stick representation. B. Orientations of the two highest scoring tetrahydrofolate conformations as shown in A. with CHO MFT R288 and conserved motif residues K47 and K145 shown in CPK. C. Orientations of the two highest scoring tetrahydrofolate conformations as shown in A. with CHO MFT R249 and W142 shown in CPK.

MFT mutagenesis guided by sequence alignment and homology modeling

The generation of the CHO MFT homology model and the predicted conformations of tetrahydrofolate within the MFT transport cavity highlighted a tryptophan substitution in a PxD/ExxK/R motif in the MFT that was strikingly different from the MCF consensus at that position. The predicted orientations of the residues in the PxD/ExxK/R motifs showed that, of the three salt bridge interactions observed in the crystallized ADP/ATP carrier (AAC) structure (Figure 2-3), only one remained intact in the MFT. The MFT contained a tryptophan (CHO MFT W142) substitution in its second conserved motif and a Q (CHO MFT 246) in its third conserved motif, both in place of a D/E residue typically found in the PxD/ExxK/R motif in most MCF proteins. These two substitutions are rarely observed in other MCF proteins and are fascinating considering the proposed roles of the conserved PxD/ExxK/R motifs in a shared mechanism of transport among MCF members. The design of a second mutagenesis study benefited from the direction given by the CHO MFT homology model and the growing body of literature in the MCF field. Four residues were selected for site-specific mutagenesis in the MFT. These were residues that either vastly differed from MCF consensus residues (CHO MFT G91, W142, and Q246) or that appeared to have an altered function in the MFT; for instance, participation in a cation-π interaction (CHO MFT R249). MFT proteins carrying these mutations were studied in a glyB complementation assay and a transport assay, similar to the previously presented MFT mutants. We then performed a molecular dynamics simulation on a modified version of the CHO MFT homology model to complement our mutagenesis data and to gain a

more comprehensive perspective on the phenomena that enable mitochondrial folate transport.

Studying the function of the anomalous residues in the MFT

The MFT contains striking deviations in its conserved motifs compared to the MCF consensus sequence. However, these substitutions are not completely unique to the MFT. The MFT and four yeast MCF proteins all contain PI/LWxxK/R in their second conserved motif in place of the MCF consensus, PxD/ExxK/R sequence. Because this change is located in a conserved motif and because these conserved motifs are proposed to be involved in a shared transport mechanism, the tryptophan substituted, PI/LW subfamily has been proposed to form a functionally distinct group (119). The sequences of the PI/LW subfamily of transporters and several other MCF transporters were aligned in the Lasergene MegAlign program (27) using ClustalW (158) (Figure 2-14). The PI/LW subfamily matches the MCF consensus residues in the first conserved motif. The tryptophan substitution that distinguishes this PI/LW subfamily is evident in the second conserved motif. Another interesting residue substitution that is common to all PI/LW proteins is the glycine residue observed at the location homologous to bAAC R79 (human AAC R80). While most MCF proteins have a basic residue at this position, the PI/LW subfamily unanimously carries a glycine at this position. Mutation of the position homologous to bAAC79, typically an R, but interestingly in one case a G, has been shown to impair the transport function of several MCF proteins (25, 64, 97, 117). This position also constitutes one of the three MCF regions previously proposed to be common

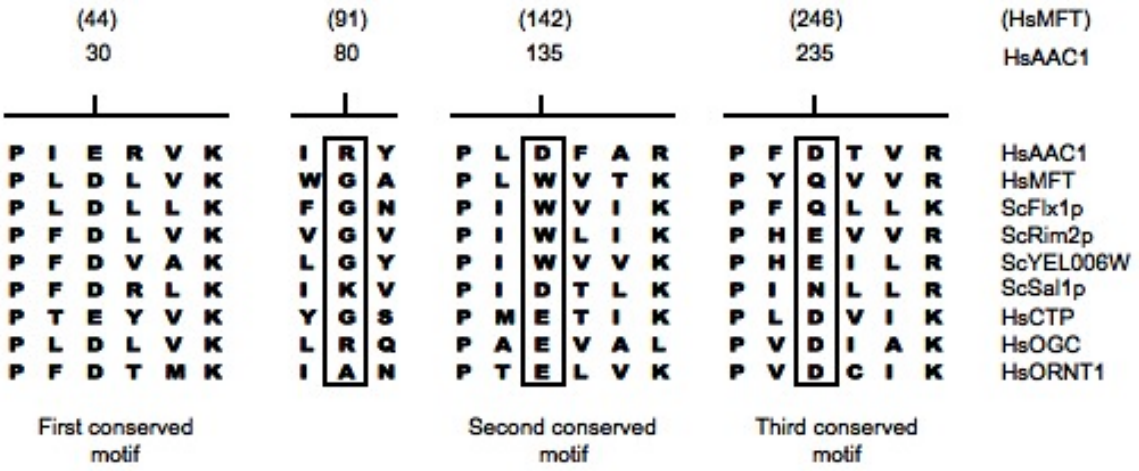

Figure 2-14 Alignment of MCF members. Selected regions of nine MCF proteins were aligned by ClustalW in the Lasergene Megalign program. The abbreviations are: HsAAC1 – human ATP/ADP carrier, isoform 1; HsMFT – human mitochondrial folate transporter; ScFlx1p – yeast FAD transporter; ScRim2p – yeast pyrimidine transporter; ScYEL006W – yeast NAD transporter; ScSal1p – yeast Mg-ATP/P_i transporter; HsCTP – human citrate transporter; HsOGC – human oxoglutarate carrier; HsORNT1 – human ornithine transporter. The residue numbering for the HsAAC1 and HsMFT is shown above the alignment. Key differences in the PxD/ExxK/R sequence motifs that are observed in the HsMFT protein are boxed at HsAAC1 positions 135 and 235, as well as a difference at HsAAC1 80.

substrate-binding sites based on extensive molecular modeling and computational docking studies (142). The MFT also has a less common substitution in its third conserved motif where the typical D/E residue has changed to a glutamine (CHO MFT Q246). This change is not specific to any particular subset of MCF proteins and only two other proteins contain this substitution. Interestingly, one of the two other proteins that carry this substitution, ScFlx1, also contains a tryptophan in its second conserved motif. The goal of these studies was to understand why these residues changed in the MFT and how they impacted the folate-specific transport mechanism of the MFT. In addition, as most of the work in the MCF field has focused on the similarities between MCF proteins, by studying these anomalous residues in the MFT, we could learn more about aspects of the transport mechanism common to all MCF members by understanding the differences in this mechanism in the PI/LW subfamily proteins.

Mutagenesis of W142 provides evidence of a cation-π interaction

We previously showed that CHO MFT R249 was required for the transport function of the CHO MFT, although the precise step in the transport process for which it was required was not clear. Based on its orientation in the CHO MFT homology model, we proposed that R249 and W142 formed a cation-π interaction (Figure 2-15A) (39). Furthermore, computational docking of tetrahydrofolate within the CHO MFT homology model transport cavity suggested that this cation-π interaction participated in the coordination of the benzyl ring of tetrahydrofolate within the MFT transport cavity. We proposed that this cation-π interaction was required for folate transport. If this cation-π

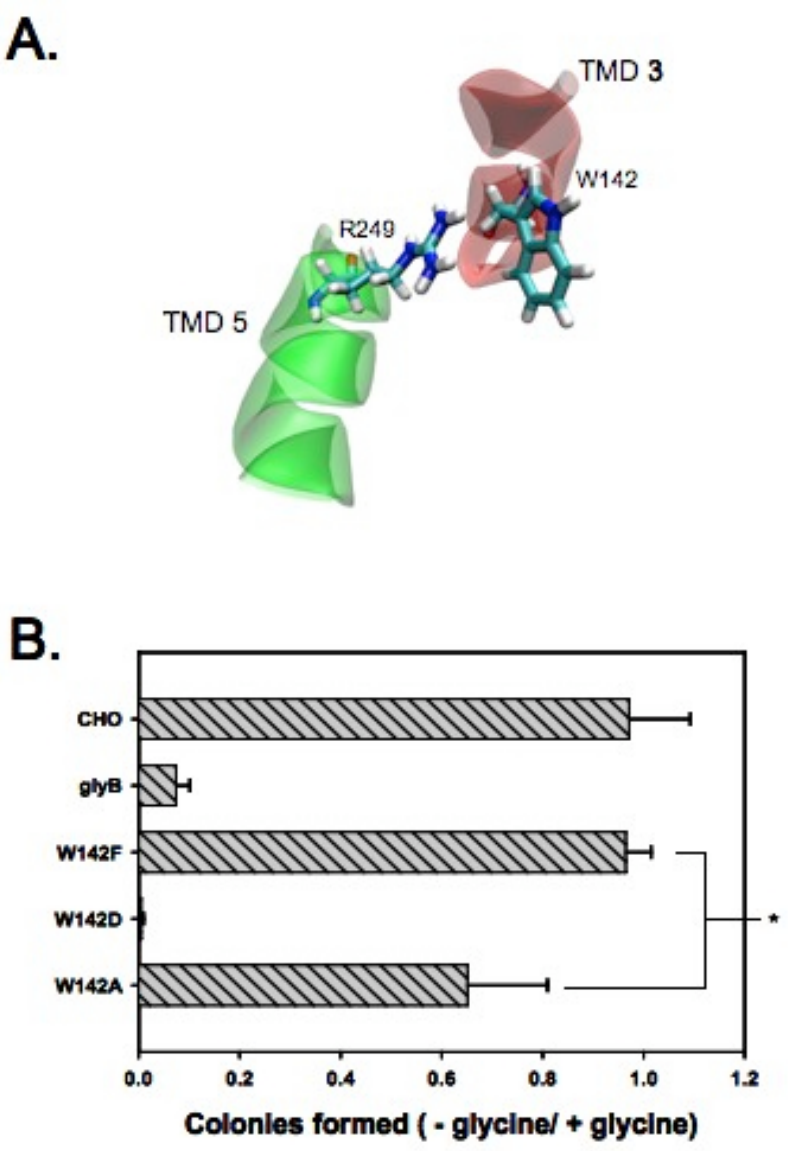

Figure 2-15 Investigating the role of CHO MFT W142 in a proposed cation-π interaction. A. Orientations of CHO MFT R249 and W142 in the CHO MFT homology model suggested that these residues could form a cation-π interaction. The third and fifth predicted transmembrane domains (TMD) of the CHO MFT are shown in transparent red and green ribbon tube display, respectively, with R249 and W142 shown in CPK. B. GlyB complementation assay with W142 MFT mutants. GlyB cells were transfected with the indicated mutant *mft* cDNA constructs and cells were grown in 1 mg/mL G418 and in the presence or in the absence of glycine. Data is expressed as a ratio of the number of colonies formed in the absence of glycine versus the number of colonies formed in the presence of glycine. Statistical significance ($p < 0.001$) was determined for all data using a one-way ANOVA analysis followed by a Tukey/Kramer analysis and data determined to be statistically different are marked by "*".

interaction was required for folate transport, then CHO MFT W142 would be as functionally important in the MFT transport mechanism as its binding partner, CHO MFT R249. The residue requirement at this position in the MFT was investigated in the glyB complementation assay and a folate uptake assay. Three mutant MFT proteins, W142A, W142D, and W142F, were generated at this position. All three mutations were designed to investigate the proposed cation-π interaction and to understand why the MFT changed the highly conserved D/E residue in its second PxD/ExxK/R motif to a tryptophan. An alanine mutation (W142A) was designed to probe the requirement for the tryptophan residue in the MFT transport mechanism, a phenylalanine mutation (W142F) was made to investigate the requirement of a aromatic side chain residue at this location, and a aspartate (W142D) mutation would revert this position to the MCF consensus and examine the necessity of this deviation, which had come about during the divergence of the MFT. The W142F mutant protein retained MFT function, as glyB cells transfected with this mutant protein were able to survive in the absence of glycine (Figure 2-15B). Interestingly, glyB cells transfected with the W142D construct were not able to survive in the absence of glycine. The MFT apparently cannot function with a D/E residue at this position that is typical of almost all MCF proteins; a tryptophan residue is required for mitochondrial folate transport. Surprisingly, glyB cells transfected with a W142A mutant *mft* cDNA were able to survive in the absence of glycine, suggesting that W142 was not required for MFT function.

The survival of glyB cells transfected with W142A *mft* cDNA in the absence of glycine was unexpected and difficult to explain given the proposed roles of the charged

residues in the PxD/ExxK/R motifs in the function of MCF proteins. It was anticipated that studying MFT function in a survival-based assay such as the glyB complementation assay, could under-report the functional effects of the transfected mutant MFT proteins. Specifically, cells may be able to grow and survive with significantly less mitochondrial folates than are normally found in mitochondria. It is unknown exactly how much mitochondrial folate a cell requires for normal growth and survival. To better assess the effects of MFT mutations on the transport function of the MFT, glyB cells stably transfected with these mutant MFT constructs were studied in an assay that more directly reflected mitochondrial transport. In contrast to the previous mitochondrial uptake assay (Figure 2-8), which allowed uptake in whole cells for 20 minutes, this assay was modified to allow mitochondrial uptake in cells for only four minutes. We suspected that given enough time, MFT mutant proteins with an impaired mechanism of transport would exhibit wild-type mitochondrial folate accumulation. Therefore, examining mitochondrial folate uptake for a shorter duration would hopefully better separate and differentiate fully functional MFT proteins from ones with impaired transport function. CHO and glyB cells were incubated with ^{3}H-6S-5-formyl-tetrahydrofolate (5f-thf) for varying periods of time. A large separation in the time-dependent uptake of 5f-thf was observed between CHO mitochondria and glyB mitochondria (Figure 2-16). Mitochondrial uptake in the CHO cell line appeared linear at least through six minutes of incubation and there appeared to be sufficient separation between CHO and glyB cells at four minutes that would allow the interpretation of various levels of 5f-thf uptake in MFT mutant transfected cell lines.

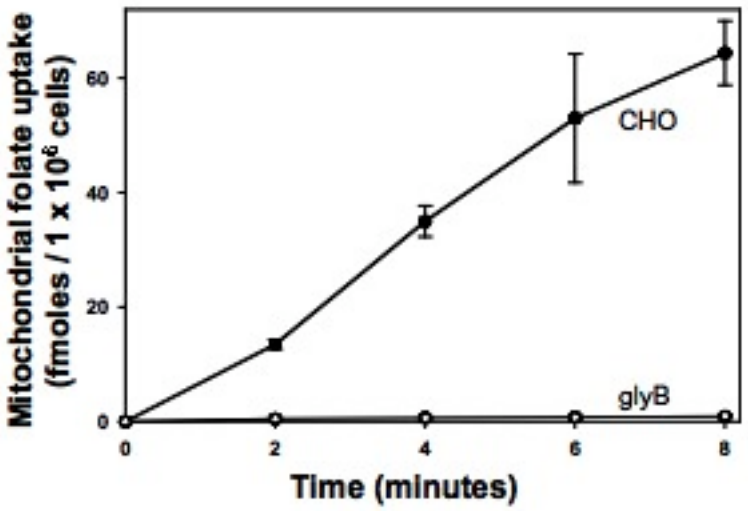

Figure 2-16 Mitochondrial folate uptake in CHO and glyB cells. CHO and glyB cells were incubated with 1 μM ^{3}H-6S-5-formyl-tetrahydrofolate for the indicated periods of time, after which mitochondria were isolated from these cells and these mitochondrial fractions were counted for radioactive content.

Another variable that was addressed in this mitochondrial folate uptake assay was the level of mutant MFT protein expression. In this mitochondrial folate uptake assay, stable MFT mutant cell lines were established from individual colonies (ten colonies were picked per mutation), these colonies were separately expanded and probed for *myc*-MFT expression (see Materials and Methods). Stably transfected, isolated clones that expressed *myc*-MFT mutant proteins at similar levels as detected by western blotting were selected for use in this uptake assay. MFT expression in the mutant W142 clones chosen for study in the folate uptake assay was nearly equivalent, although the MFT W142F protein appeared to be expressed at a slightly higher level than W142A or W142D MFT proteins. (Figure 2-17A). Mitochondrial uptake of folate derivatives of ^{3}H-5f-thf was then measured in these mutant cell lines (Figure 2-17B). The W142F MFT protein was fully capable of mitochondrial folate uptake, while the W142D protein was completely incapable of any mitochondrial folate uptake, as suggested in the glyB complementation assay. Mitochondrial folate accumulation in cells transfected with MFT W142A was impaired by >75% when compared to uptake in CHO cells. While the glyB complementation assay demonstrated that the W142A protein was capable of transporting an amount of folate that was sufficient for cell survival, a more direct analysis of mitochondrial folate uptake demonstrated that the transport function of this mutant MFT protein is limited. This reinforces the proposed concept of cation-π interaction and the role of the tryptophan substitution in the MFT. This finding also warned us that cells could survive perfectly well with only a fraction of wild-type MFT transport function. We benefited from studying this MFT W142A mutation in two separate experimental designs as the interpretation of

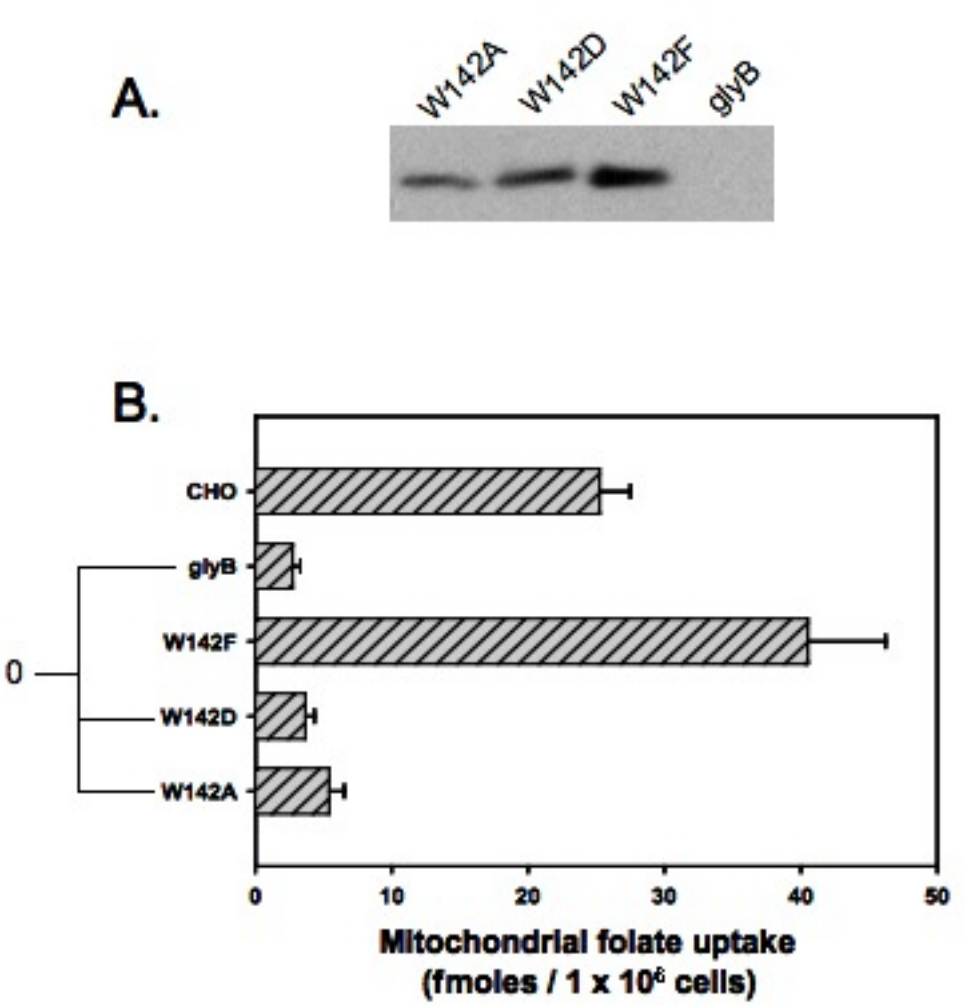

Figure 2-17 Western blotting and mitochondrial folate uptake in W142 mutants. GlyB cells were transfected with N-terminally *myc*–tagged mutant *mft* cDNAs in pcDNA 3.1(-) and grown in selective media containing 1 mg/mL G418 and glycine. Transfectant colonies were selected and expanded in selective media. A. Mitochondrial protein was isolated from each MFT mutant clone and 20 μg of total mitochondrial protein was loaded into a gel, electrophoresed and the protein contents of the gel were transferred to a PVDF membrane. This membrane was probed for *myc*-MFT expression using an antibody raised against *myc*. B. Stably-transfected clones that expressed similar amounts of each mutant MFT protein (shown in A.) were incubated with 1 μM ^{3}H-6S-5-formyl-tetrahydrofolate at 37° C for 4 minutes. Following whole cell uptake, mitochondria were isolated from each mutant cell line and counted for radioactive content. Statistical significance ($p < 0.001$) was determined for all data using a one-way ANOVA analysis followed by a Tukey/Kramer analysis and selected data that were not statistically different are marked by "0".

these mutations differed depending on the assay used. The differences between these two assays that led to these significantly different interpretations are analyzed in the Discussion section of this chapter.

Informative W142R/R249W double mutant suggests folate interposition between the cation-π interacting residues

The MCF PxD/ExxK/R motifs are proposed to be essential in a MCF shared mechanism of opening that generates a temporary transport channel through the disruption of PxD/ExxK/R motif interactions that form the transport cavity floor. Incoming substrate was proposed to disrupt these barrier-forming interactions at the base of the MCF protein transport cavity, but it was not known whether substrate disruption occurred by proximity or by direct positioning between the interacting residues. Docking studies predicted the benzyl ring of tetrahydrofolate in the two highest scoring docking conformations to occupy different locations, but both were in the vicinity of a proposed cation-π interaction between CHO MFT W142 and R249 (Figure 2-18A). Mutations were made in the CHO MFT to investigate if the incoming folate substrate interposed directly between the proposed cation-π interaction of W142 and R249. A double mutation, W142R/R249W, was constructed that theoretically permitted the formation of a cation-π interaction, but flipped the location of two residues involved in this bond. These residues were also mutated separately to control for any effects observed in the double mutant that were attributable to mutation of a single residue. The CHO MFT W142R/R249W double mutation permitted a level of mitochondrial folate accumulation compatible with the survival of glyB cells in the

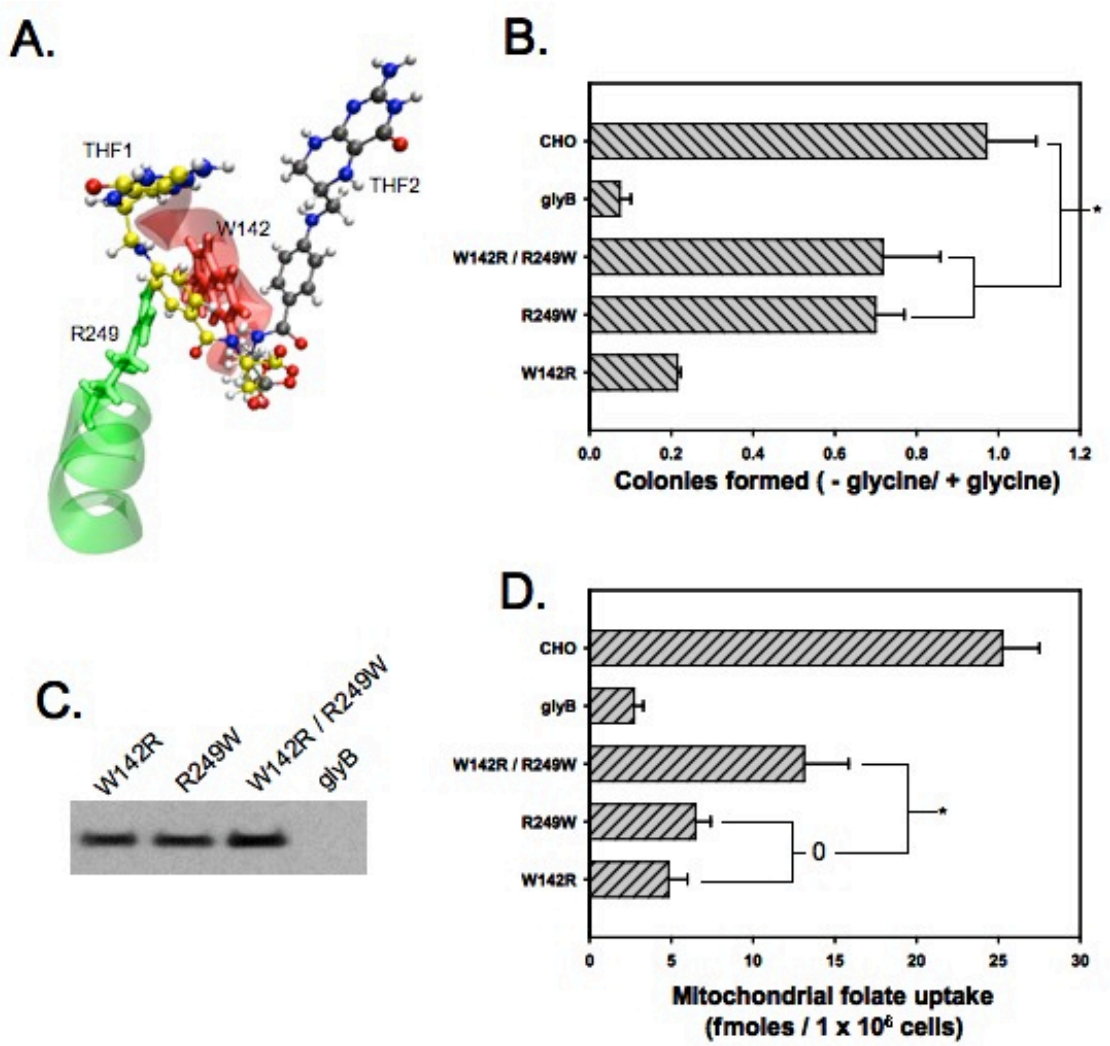

Figure 2-18 Investigating the participation of CHO MFT R249 in a proposed cation-π interaction. A. Tetrahydrofolate was computationally docked into the transport cavity of the CHO MFT homology model using the FlexX program. The docked conformations were sorted by Total score and cScore and the two highest scoring conformations, THF1 (yellow) and THF2 (gray) respectively, are shown in ball and stick representation. CHO MFT W142 (licorice representation) and the third transmembrane domain (transparent ribbon tube display) are shown in red and CHO MFT R249 (licorice representation) and the fifth transmembrane span (transparent ribbon tube display) are shown in green. B. GlyB cells were transfected with the indicated MFT constructs in pcDNA 3.1(-) and grown in media containing 1 mg/mL G418 with or without glycine. Data is expressed as a ratio of the number of colonies formed in the absence of glycine versus the number of colonies formed in the presence of glycine. C. Mitochondrial protein was isolated from glyB cells stably transfected with the indicated mutant MFT constructs. Twenty micrograms of mitochondrial protein was loaded into a gel, electrophoresed, proteins in the gel were transferred to PVDF membrane and the membrane was probed for *myc*-MFT expression with an antibody raised against *myc*. D. Stably transfected glyB cells that expressed similar amounts of the mutant MFT protein (shown in C.) were incubated with 1 μM ^{3}H-6S-5-formyl-tetrahydrofolate at 37° C for 4 minutes. Following whole cell uptake, mitochondria were isolated from each mutant cell line and counted for radioactive content. Statistical significance ($p < 0.001$) was determined for all data using a one-way ANOVA analysis followed by a Tukey/Kramer analysis and selected data that were determined to be statistically different are marked by "*". Selected data that were not statistically different are marked by "0".

absence of glycine (Figure 2-18B). However, both individual mutations, CHO MFT W142R and R249W, were also capable of some level of mitochondrial folate transport as evidenced by the ability of glyB cells transfected with W142R or R249W to survive in the absence of glycine. The stably transfected MFT mutant cell lines that were selected for uptake studies had no apparent differences in MFT expression (Figure 2-18C). In the mitochondrial folate uptake assay, none of the MFT mutant proteins were able to uptake folates into mitochondria to the same extent as CHO cells (Figure 2-18D). However, it does appear that the W142R/R249W mutant was able to accumulate more mitochondrial folates than the MFT R249W mutant alone. There was some level of MFT function that was restored by reinstating this cation-π interaction, even with the residues in flipped orientations. Furthermore, we believed that if the folate substrate was not directly interposing between CHO MFT W142 and R249, the W142R/R249W double mutation would not have provided this added transport advantage over the individual residue mutations. Based on this data, we concluded that the folate substrate was interposing between a cation-π interaction formed between CHO MFT R249 and W142 at the base of the transport cavity. Interestingly, the MFT R249W mutant protein provided sufficient mitochondrial folate accumulation to permit transfectant cell survival in the absence of glycine. The apparent low level functioning of this protein could be explained by the aromatic side chain of the R249W mutant forming a π-π interaction with W142. This could restore a vital conserved motif interaction between R249W and W142 that permits some level of folate transport.

A glycine substitution at a proposed MCF substrate-binding site is required for MFT function

CHO MFT residue G91 is located at one of the three previously proposed substrate-binding sites that are suggested to be common to all MCF proteins based on the results of homology modeling and computational docking studies (142). Interestingly, all PI/LW subfamily proteins contain a G at this position, while the vast majority of other MCF proteins have a lysine or arginine residue at this position. Because this position was shown to be essential in the transport function of other MCF proteins (25, 64, 97, 117), the requirement of a glycine residue at this position in the MFT was investigated. An arginine was inserted *in silico* at this position in the CHO MFT homology model, creating a G91R mutant MFT. In the CHO MFT homology model containing the G91R mutation, the side chain of the selected arginine (G91R) rotamer was predicted to extend into the MFT transport cavity within close proximity to W142 (Figure 2-19A). Based on the visualization of this G91R mutation in the CHO MFT, we hypothesized that the positively charged side chain of an arginine residue at this position could form an additional cation-π interaction with CHO MFT W142. By CHO MFT G91R interacting with W142 in addition to R249, W142 would be locked in its position in the MFT transport cavity and the proline residue in the second conserved motif in the MFT would not be able to induce the conformational change proposed to remove the transport cavity floor and permit substrate passage into the mitochondrial matrix. However, based on the orientation of the second highest scoring docking conformation of tetrahydrofolate within the MFT transport cavity (Figure 2-13C), this glycine substitution could have occurred to create a substrate-binding

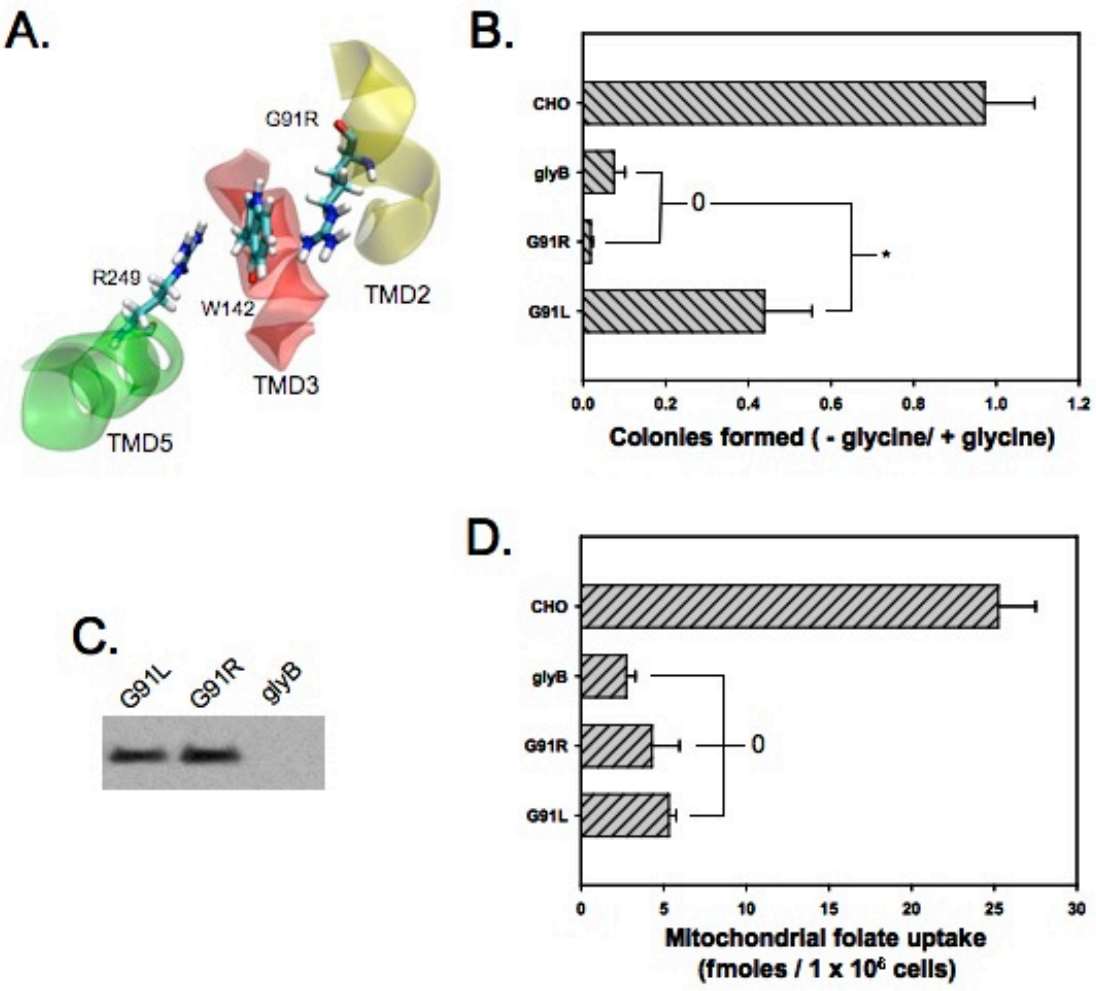

Figure 2-19 Investigating a glycine substitution at a proposed substrate-binding site in the CHO MFT. A. Orientations of CHO MFT G91R, W142, and R249 within the CHO MFT homology model transport cavity are shown in CPK. The second (yellow), third (red), and fifth (green) CHO MFT transmembrane domains (TMD) are shown in transparent ribbon tube display. The G91R mutation was created in the MacPyMOL program (157) and the orientation of G91R was one of several side chain rotamers predicted within the program. B. GlyB cells were transfected with the indicated MFT constructs in pcDNA 3.1(-) and grown in media containing 1 mg/mL G418 with or without glycine. Data is expressed as a ratio of the number of colonies formed in the absence of glycine versus the number of colonies formed in the presence of glycine. C. Mitochondrial protein was isolated from glyB cells stably transfected with the indicated mutant MFT constructs. Twenty micrograms of mitochondrial protein was loaded into a gel, electrophoresed, proteins in the gel were transferred to PVDF membrane and the membrane was probed for *myc*-MFT expression with an antibody raised against *myc*. D. Stably transfected glyB cells that expressed similar amounts of the mutant MFT protein (shown in C.) were incubated with 1 μM ^{3}H-6S-5-formyl-tetrahydrofolate at 37° C for 4 minutes. Following whole cell uptake, mitochondria were isolated from each mutant cell line and counted for radioactive content. Statistical significance ($p < 0.001$) was determined for all data using a one-way ANOVA analysis followed by a Tukey/Kramer analysis and selected data that were determined to be statistically different are marked by "*". Selected data that were not statistically different are marked by "0".

pocket on the side of CHO MFT W142 that was opposite R249 and the cation-π interaction. In addition, the idea of this substitution forming a substrate-binding pocket corroborated the homology modeling and computational docking studies of Robinson and Kunji that predicted this location to be a common substrate-binding site for all MCF proteins (142). A mutation was made at this position (G91R) that tested whether or not the MCF consensus residue (K/R) was compatible with MFT transport function. In addition to its positive charge, arginine also has a fairly large side chain. A G91L mutation was designed to control for this size as leucine also has a large chain, but without the positive charge (Figure 2-20). GlyB cells transfected with the MFT G91L were able to survive in the absence of glycine, suggesting some level of function by this mutant MFT protein (Figure 2-19B). The level of cell survival in the absence of glycine in G91L transfectants was about 40% of that observed with glyB cells transfected with the CHO *mft* cDNA. In contrast, cells transfected with MFT G91R, the MCF consensus residue, were completely unable to survive in the absence of glycine. MFT expression levels did not appear to differ between MFT G91L and G91R stably transfected cell lines (Figure 2-19C). Interestingly, mitochondrial folate uptake in both G91L and G91R transfected glyB cells was inefficient (Figure 2-19D). While both mutations appeared to impair MFT function in the mitochondrial folate uptake assay, the inability of G91R *mft* cDNA transfectants to survive in the absence of glycine suggests that the G91R mutation may inhibit the MFT. Additionally, G91L *mft* cDNA transfectants were able to survive in the absence of glycine, suggesting that this mutant MFT protein is impaired but not inhibited. It appears that the

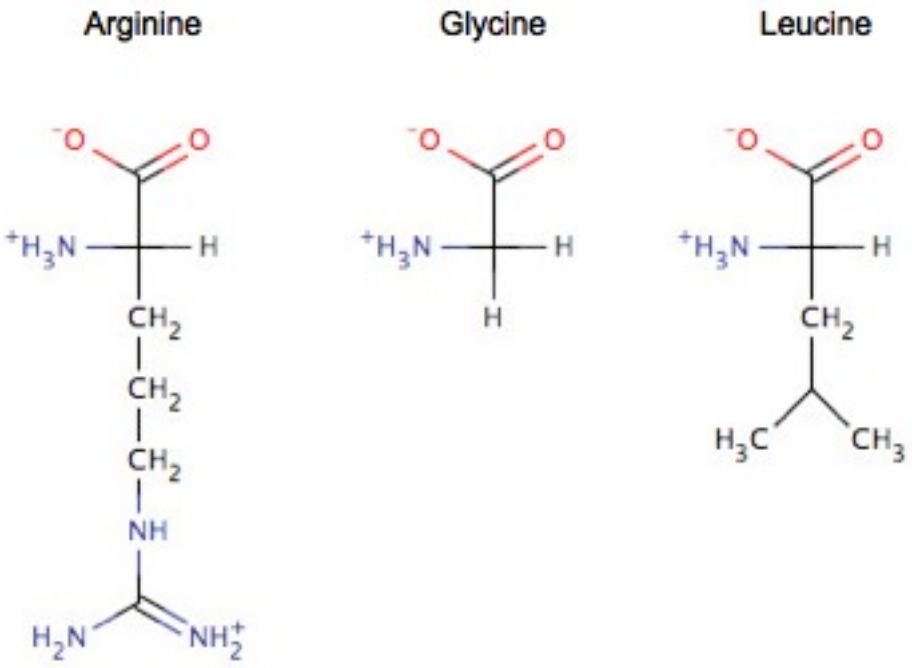

Figure 2-20 Chemical structures of arginine, leucine and glycine.

MFT has inserted a glycine at this position because a basic residue, present in the majority of MCF transporters, will not permit mitochondrial folate transport.

Another MFT conserved motif residue, Q246, does not appear to be required for MFT transport function

The MFT has substituted a glutamine residue in the D/E position of its third conserved motif. Instead of the salt bridge interaction that is typical in most MCF members at this location, this substitution in the MFT was proposed to form a hydrogen bond with CHO MFT D44 based on the orientations of these two residues in the CHO MFT homology model (Figure 2-21A). Thus, an interaction between the two conserved motifs could be maintained. Two mutations, Q246A and Q246E, were designed to probe this interaction to understand the role of this glutamine substitution in MFT transport function and how a glutamine residue aided in the adaptation of a folate-specific transport mechanism. We expected that MFT Q246E would function like the wild-type CHO MFT as this mutation was predicted to restore a salt bridge interaction with D44 in the MFT, and that the Q246A mutation would result in complete disruption of a vital interaction and eliminate MFT function. However, both mutant MFT proteins appear to retain some level of function as both mutant MFT proteins enabled glyB transfectants to survive in the absence of glycine (Figure 2-21B). Both of these mutant constructs were stably transfected into glyB cells and individual clones were probed for MFT expression (Figure 2-21C). Expression of the Q246A MFT protein appears less than the expression of the Q246E MFT protein in the respective cell lines. The *myc*-MFT expression observed in this

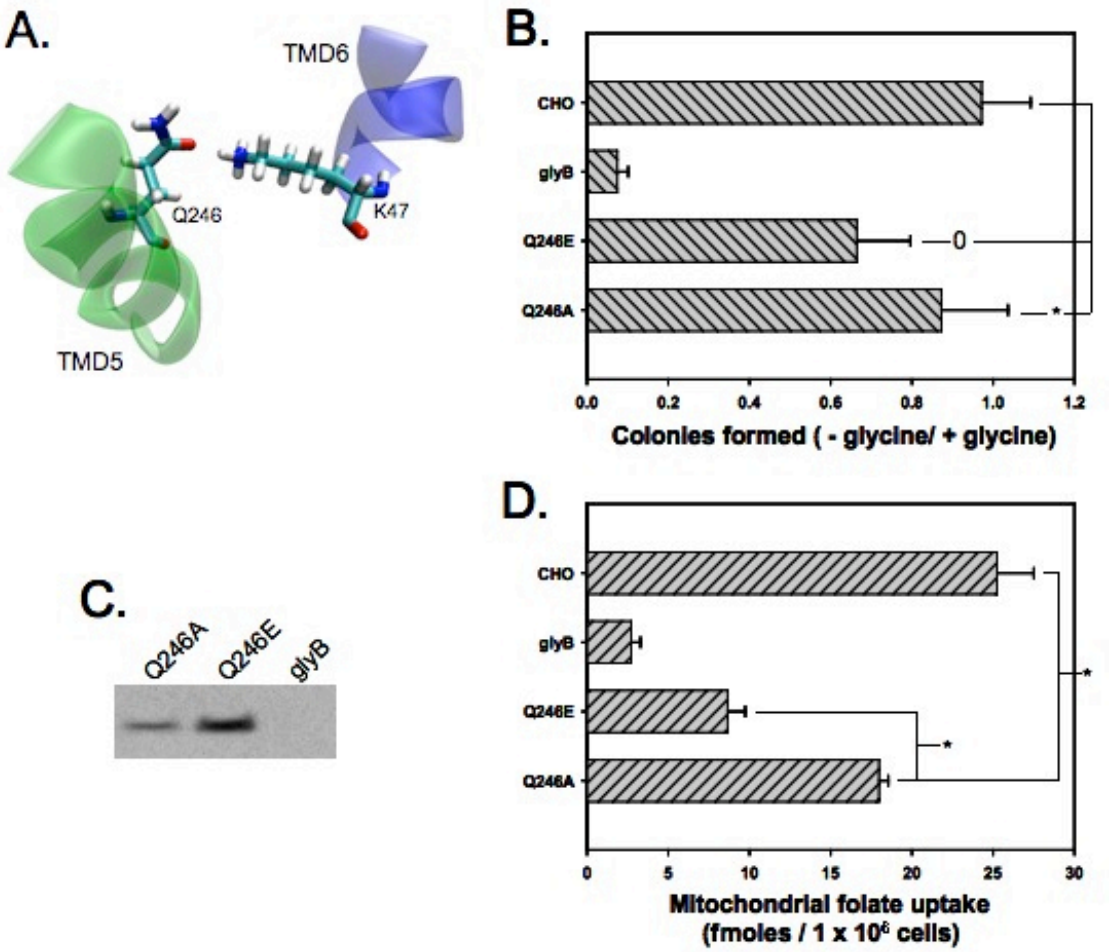

Figure 2-21 Investigating the requirement of CHO MFT conserved motif residue Q246. A. Orientations of CHO MFT Q246 and K47 in the MFT homology model transport cavity shown in CPK. The fifth (green) and sixth (blue) CHO MFT transmembrane domains (TMD) are shown in transparent ribbon tube display. B. GlyB cells were transfected with the indicated MFT constructs in pcDNA 3.1(-) and grown in media containing 1 mg/mL G418 with or without glycine. Data is expressed as a ratio of the number of colonies formed in the absence of glycine versus the number of colonies formed in the presence of glycine. C. Mitochondrial protein was isolated from glyB cells stably transfected with the indicated mutant MFT constructs. Twenty micrograms of mitochondrial protein was loaded into a gel, electrophoresed, proteins in the gel were transferred to PVDF membrane and the membrane was probed for *myc*-MFT expression with an antibody raised against *myc*. D. Stably transfected glyB cells that expressed similar amounts of the mutant MFT protein (shown in C.) were incubated with 1 μM ^{3}H-6S-5-formyl-tetrahydrofolate at 37° C for 4 minutes. Following whole cell uptake, mitochondria were isolated from each mutant cell line and counted for radioactive content. Statistical significance ($p < 0.001$) was determined for all data using a one-way ANOVA analysis followed by a Tukey/Kramer analysis and selected data that were determined to be statistically different are marked by "*".Selected data that were not statistically different are marked by "0".

CHO MFT Q246A clone was the highest detected MFT expression level out of six Q246A clones that were screened (data not shown). Nonetheless, mitochondrial folate uptake was observed in both stably transfected cell lines (Figure 2-21D). Despite the discrepancy in apparent MFT expression levels, cells transfected with CHO MFT Q246A were able to accumulate ~50% more mitochondrial folate than CHO MFT Q246E transfectants. The MFT demonstrated a surprising mutational tolerance at this position, suggesting that Q246 may not be an essential residue in the transport mechanism of the MFT.

Modification and generation of a new CHO MFT homology model for molecular dynamics simulations

Several MFT mutations were quite interesting, yet difficult to interpret. The glyB complementation assay data suggested that the MFT retained some level of transport with a variety of mutations. On the other hand, many of the mutations that were apparently tolerated by the MFT in the glyB complementation assay were shown to be incompatible with optimal folate transport in the mitochondrial folate uptake assay. To aid in the interpretation of this data, we used molecular dynamics simulations to better understand the effects of these mutations and the roles of these residues in the MFT transport mechanism. However, the structure of the MFT was unknown, which meant that these simulations would have to occur in a simulation system that included a MFT homology model. If there were errors, inaccurate structural elements, or inappropriate side chain orientations in the homology model, the resulting molecular dynamics simulation data and the interpretation of this data could be skewed. While the initial MFT homology model

was useful in generating hypotheses that were testable by mutagenesis, the model needed to be improved before it could be used for computational experiments. We generated a new MFT homology model using the ORCHESTRAR program (162), which was shown to produce homology models with better geometries and orientation of side chains that are more complete and more accurate when homology is <30% when compared to Composer (163), the program used to generate the initial MFT homology model (36). The newly generated MFT model corrected a disruption in the α-helical structure of the predicted fourth transmembrane domain in the CHO MFT homology model generated in Composer (Figure 2-22). In addition, the ORCHESTRAR program was able to better predict the structure of N- and C- terminal regions and therefore, more amino acids were modeled in these regions in the CHO MFT homology model generated by the ORCHESTRAR.

The molecular dynamics simulation was set up with the newly generated MFT homology model. A palmitoyl oleaylphosphatidylchloine (POPC) bilayer membrane was constructed in the Visual Molecular Dynamics (VMD) program (63), and water molecules were added on both sides of the membrane. The newly generated MFT homology was inserted into the center of the membrane slab and nineteen chloride ions were added to obtain a neutral charge within the simulation box. The complete molecular dynamics system is shown in Figure 2-23.

Molecular dynamics simulations of the apo-MFT

A molecular dynamics (MD) simulation was initially run without a tetrahydrofolate (THF) substrate. In this simulation, a chloride ion was almost immediately attracted to the

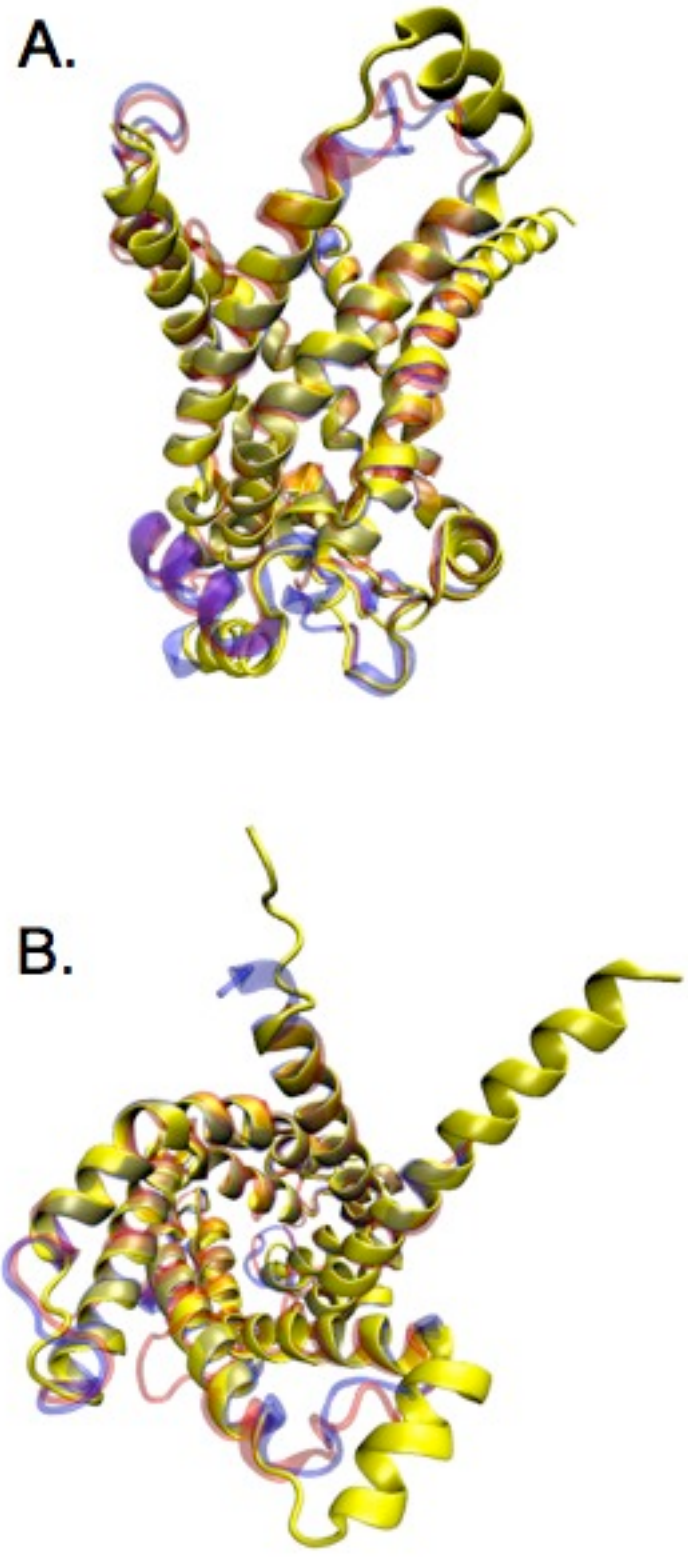

Figure 2-22 Generation of a new CHO MFT homology model for use in molecular dynamics simulations. A second CHO MFT homology model was created in Sybyl ORCHESTRAR to more accurately model MFT loop regions. A. Cross-sectional membrane view of the crystallized ADP/ATP carrier (AAC ; transparent blue), initial CHO MFT homology model (transparent red), and the newly generated CHO MFT homology model (yellow) in ribbon tube display. B. View from the inter-membrane space looking into the transport cavity of the crystallized AAC (transparent blue), initial CHO MFT homology model (transparent red), and the newly generated CHO MFT homology model (yellow) in ribbon tube display.

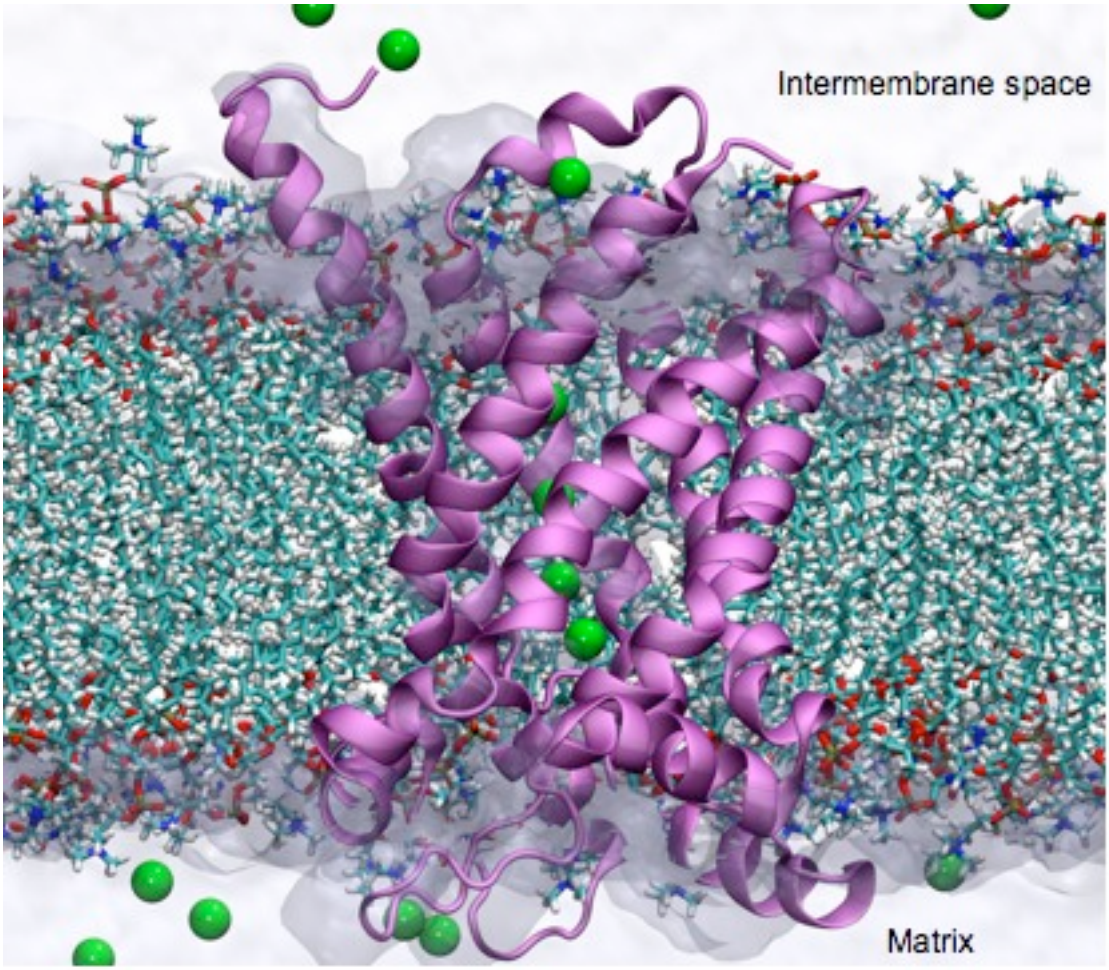

Figure 2-23 Visualization of the molecular dynamics system. The CHO MFT homology model is shown in purple ribbon tube display and was inserted in a POPC lipid bilayer membrane that was created in the VMD program and is shown in CPK. An additional 30 Å of water molecules were added to the inter-membrane space side and 20 Å of water molecules were added to the matrix of the MFT homology model, but are not shown. The aqueous environment surrounding the lipid bilayer also included 19 chloride ions, which are shown in green van der Waals representation. The presented figure represents the molecular dynamics system after 30 nanoseconds of equilibration. This figure was provided by Dr. John C. Hackett.

base of the transport cavity and within t = 15 ns a total of four chlorides resided and remained in the MFT transport cavity for the duration of the simulation. However, no chloride ions appeared to be fixed in their location. The residence of these chloride ions hinted at a strong electrostatic potential within the MFT transport cavity. Indeed, the electrostatic potential within the MFT reaches a maximum +1.9 V potential at the base of the transport cavity and maintains +1.5 V surface around the conserved motif basic residues K47, K145, and R249 (Figure 2-24). The positive electrostatic surface potential and the attraction of chloride ions within the transport cavity of the MFT is similar to that observed in molecular dynamics simulations in the AAC (33, 86, 169). Interestingly, the AAC was predicted to generate a maximum electrostatic potential of +1 V at its base (33, 169). Nonetheless, it is this large electropositive potential located at the transport cavity floor that is thought to be the driving force for substrate attraction deep within the transport cavity of MCF proteins.

We next examined the orientations of the conserved motif residues and explored their interaction throughout the apo-MFT simulation. Throughout the duration of the 30 ns simulation, the distance between the PxD/ExxK/R motif residues that were predicted to interact was followed. The residues that were predicted to interact, based on the orientations of homologous residues in the AAC crystal structure and the predicted orientations of these residues in the CHO MFT homology model, were CHO MFT D44 and K145, W142 and R249, and Q246 and K47. The only predicted interaction in which the residues remained within 4 Å for a majority of the MD simulation was between CHO MFT Q246 and K47 (Figure 2-25). Residues W142 and R249 maintained a distance of ~5

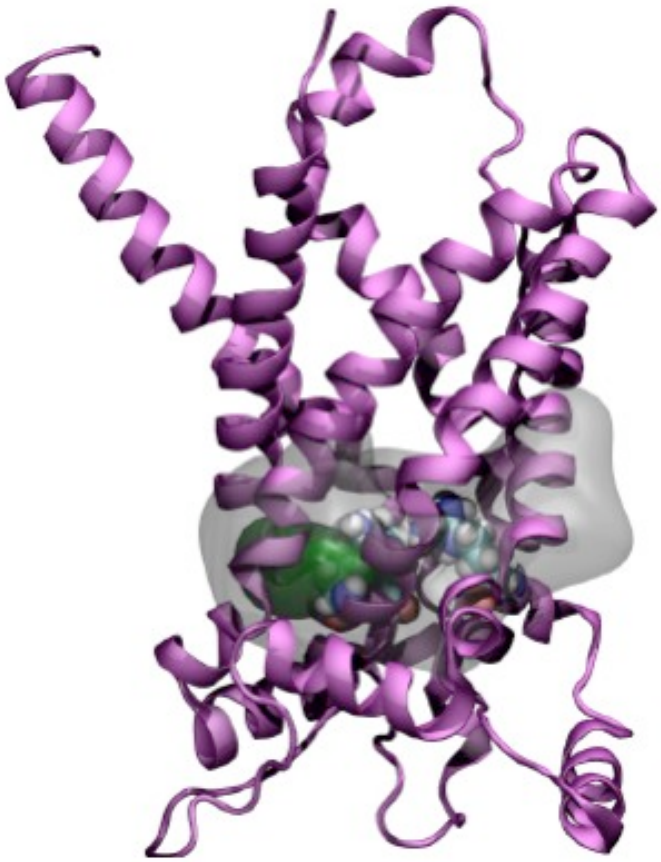

\

Figure 2-24 Electrostatic potential in the transport cavity of the CHO MFT homology model. The time-averaged electrostatic potential surface of the initial 2.5 ns of the apo-MFT simulation was computed using the PMEPot (2) plugin of VMD. The CHO MFT homology model (cross-sectional membrane view) is shown in purple ribbon tube and residues K47, K145 and R249 are shown in van der Waals representation. The surface corresponding to a +1.0 V electrostatic potential is shown in transparent gray and is symmetrically located around the base of the transport cavity. The surface corresponding to a +1.5 V electrostatic surface potential is shown in green at the base of the cavity localized around CHO MFT K47, K145 and R249. This figure was provided by Dr. John C. Hackett.

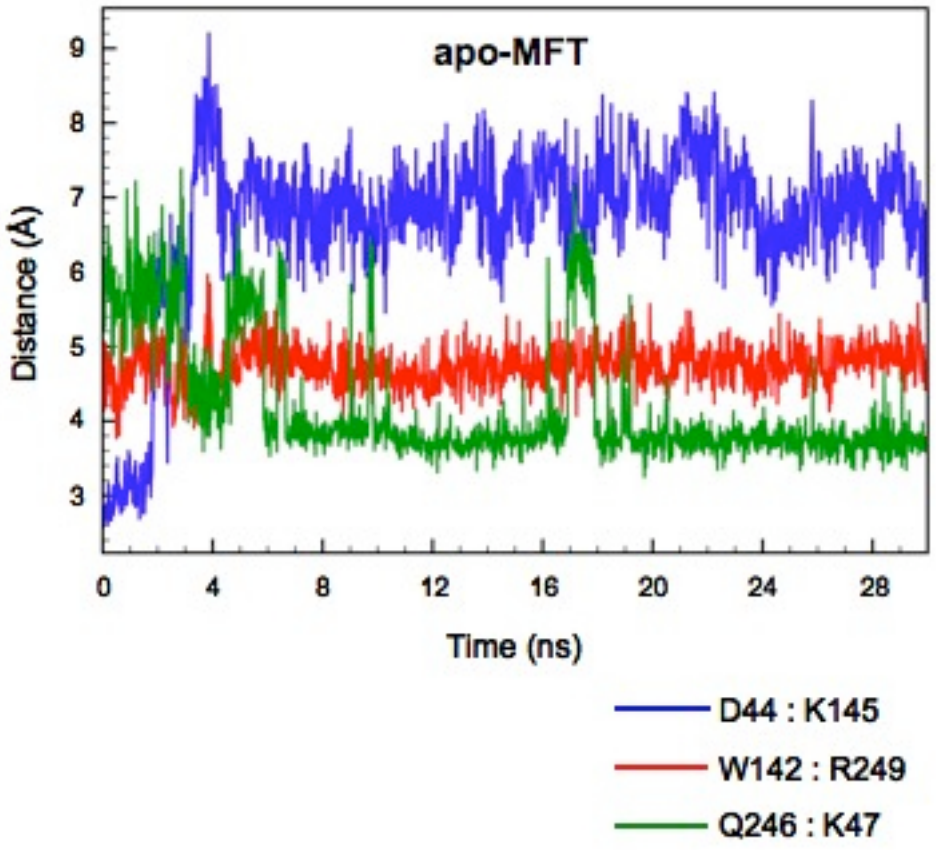

Figure 2-25 Distance between the PxD/ExxK/R motif residues during the apo-MFT molecular dynamics simulation. CHO MFT conserved motif residues, D44 and K145, W142 and R249, and Q246 and K47 were predicted to interact based on the crystal structure of the AAC and the orientations of these residues in the CHO MFT homology model. Molecular dynamics (MD) simulations were run with the CHO MFT homology model without a molecule of tetrahydrofolate (THF). During these simulations, the distance, in angstroms (Å), between conserved motif residues that were predicted to interact were measured. The CHO MFT homology model was subjected to 30 nanoseconds (ns) of a molecular dynamics simulation without THF. The distances between CHO MFT D44 and K145 (blue), W142 and R249 (red), and Q246 and K47 (green) are shown throughout the simulation.

Å throughout the entire simulation. Of the residue pairs that were predicted to interact, the distance between R249 and W142 was the most stable of the three throughout the MD simulation; the distances between CHO MFT D44 and K145 and Q246 and K47 fluctuated throughout the simulation. Whereas most MCF proteins contain three salt bridge interactions between the charged residues of the PxD/ExxK/R conserved motifs, the only salt bridge interaction predicted to be in the MFT was between CHO MFT D44 and K145. Surprisingly, these residues were separated by > 6 Å for the duration of the MD simulation and, hence, an interaction was not observed between these two residues that would reinforce their proposed role in the formation of a transport barrier.

The flexibility of the conserved sequence residues in the apo-MFT MD simulation was striking. We further examined CHO MFT D44 and K145 and the possibility that they were interacting with other residues in the MFT transport cavity. There seemed to be more potential for D44 to have another binding partner because the transport cavity contained more basic residues for D44 to interact with than acidic residues for K145 to interact with. The flexibility that was observed for CHO MFT D44 was quite remarkable; it appeared to contact three different residues during the apo-MFT simulation (Figure 2-26). Initially, MFT D44 interacted with K145. However, because bAAC E29 and R137 were within 2 Å in the bAAC crystal structure (see Figure 2-3 for AAC conserved sequence residue orientations), the homologous residues in the MFT, D44 and K145, were predicted to assume a similar orientation in the CHO MFT homology model. This would explain why an interaction between CHO MFT D44 and K145 was initially observed in the CHO MFT homology model. Next, D44 briefly contacted K47 to form an intrahelical interaction,

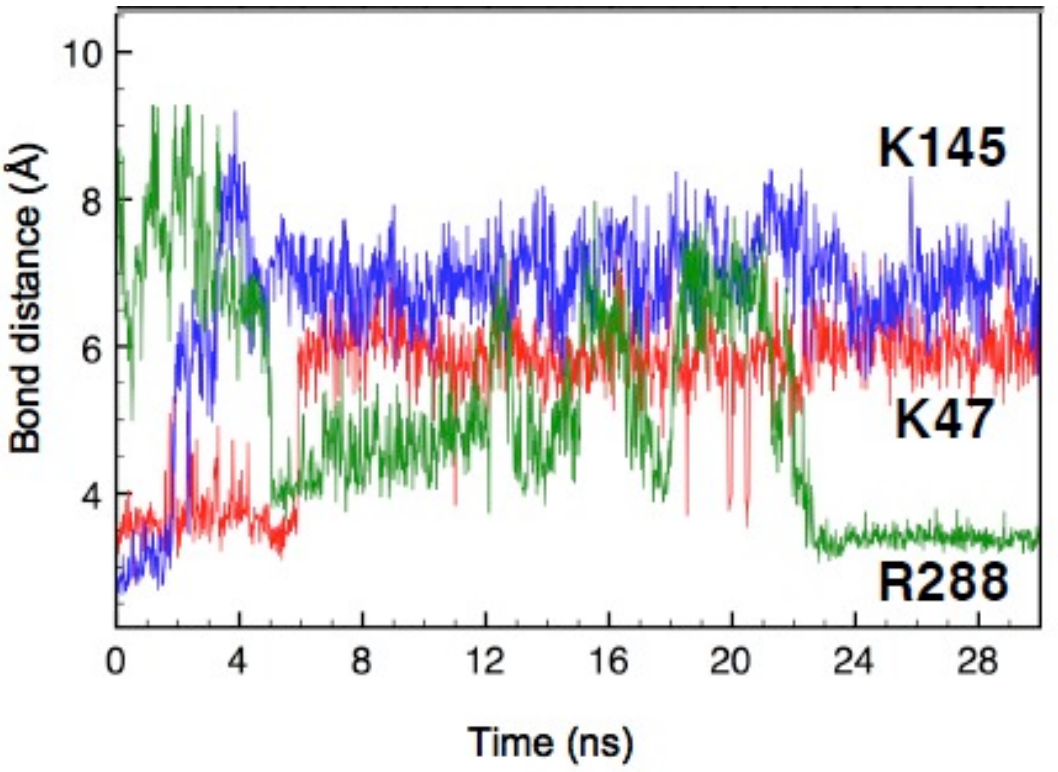

Figure 2-26 Interactions of CHO MFT K47, K145 and R288 with D44 in the MFT transport cavity during the apo-MFT MD simulation. The CHO MFT homology model was subjected to 30 nanoseconds (ns) of a molecular dynamics simulation without THF. Throughout this simulation, the distance (in angstroms (Å)) between CHO MFT D44 and three basic residues within the MFT transport cavity, K47 (red), K145 (blue) and R288 (green), was measured.

followed by a period of apparent freedom (Figure 2-26). Finally, D44 settles to form a stable interaction with CHO MFT R288 (homologous to AAC R279), a residue that constitutes a substrate-binding site proposed to be common to all MCF proteins. It is also interesting to note the variation in distance between MFT K47 and Q246 during this simulation (Figure 2-25). Initially these residues were separated by ~6 Å and gradually moved towards each other. At t = 6 ns, these residues appeared to form a stable interaction. However at t = 16 ns, K47 and Q246 were momentarily separated, but this distance eventually re-stabilized at 4 Å after a few nanoseconds. Nonetheless, this demonstrated the dynamic flexibility of these residues and interactions in the MFT that could not be observed in a homology model. This flexibility of the conserved motif residues and the apparent distances between them have also been observed in MD simulations with the apo-AAC (33, 40, 68, 169). Despite substitutions that changed residues involved in two of the three predicted conserved motif interactions in the MFT, the apo-MFT appears to behave like the apo-AAC in MD simulations.

Progress of tetrahydrofolate down the MFT transport cavity

In addition to the simulation of the apo-MFT, we also designed a molecular dynamics simulation to visualize the interactions of tetrahydrofolate (THF) within the MFT transport cavity. A molecule of THF was manually placed in the visual center of the inter-membrane space opening of the CHO MFT homology model. Tetrahydrofolate was oriented vertically with the glutamate portion of the molecule extending down into the MFT transport cavity. This orientation was chosen based on previous MD simulations that

demonstrated the AAC positioned the ADP substrate vertically with the phosphate groups of ADP pointing towards to the base of the AAC cavity, independent of the starting orientation of ADP (33, 169). Computational docking studies also predicted that the THF molecule was vertically oriented within the MFT transport cavity with the glutamate portion of THF located the closest to the cavity floor (Figure 2-13). Initially, a molecule of THF was placed above the MFT transport cavity in the *in silico* inter-membrane space. This placement of THF caused the THF molecule to diffuse into the aqueous space above the lipid bilayer and away from the transport cavity when the simulation was started. We then moved the THF molecule further down towards the MFT transport cavity so that the glutamate tail of THF was even with the outermost loop regions of the MFT homology model. As the simulation began with THF in this location, the THF molecule was immediately drawn to the loop regions of the MFT homology model and was not released. The molecule of THF was then placed in the MFT transport cavity ~20 Å above the transport cavity floor. This placement of THF resulted in the successful capture of the substrate and its descent to the MFT transport cavity floor.

The descent of THF through the MFT transport cavity was simulated for 40 ns and THF moved through the MFT transport cavity in a step-wise fashion (MD movies 1 and 2 – supplemental material). The distance between functional groups in the THF molecule and residues within the MFT transport cavity were followed over the duration of the simulation (Figure 2-27 ; MD movies 3 and 4 – supplemental material). The initial orientation of THF biased the γ-carboxyl of THF to immediately contact MFT CHO K235 and this interaction was evident at the start of the simulation (Figure 2-27C). The

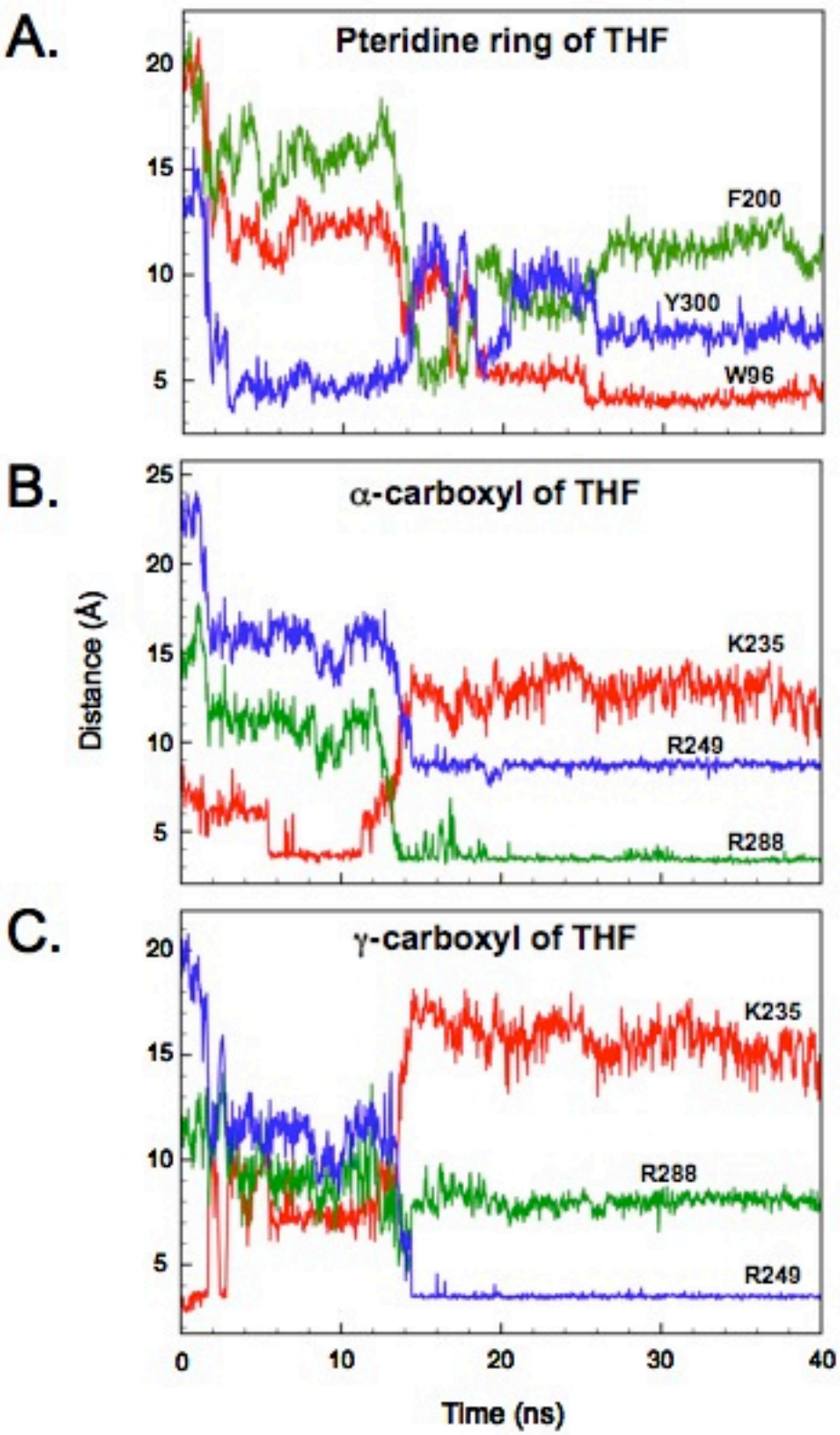

Figure 2-27 Interaction of tetrahydrofolate with residues lining the CHO MFT homology model transport cavity as predicted in molecular dynamics simulations. A molecule of tetrahydrofolate (THF) was placed in the transport cavity of the CHO MFT homology model and subjected to 40 nanoseconds (ns) of molecular dynamics simulations (MD movies 1 and 2 in supplemental material). Distances, in angstroms (Å), between the indicated groups of THF and CHO MFT residues were measured throughout the simulation. A. The distance between the pteridine ring of THF and CHO MFT W96 (red), F200 (green), and Y300 (blue) is shown (MD movie 4 in supplemental material). B. The distance between the α-carboxyl of the glutamate portion of THF and CHO MFT K235 (red), R288 (green), and R249 (blue) is shown (MD movie 3 in supplemental material). C. The distance between the γ-carboxyl of the glutamate portion of THF and CHO MFT K235 (red), R288 (green), and R249 (blue) is shown (MD movie 3 in supplemental material).

interaction between MFT K235 and the γ-carboxyl of THF was weakened (t = 2 ns) and THF dropped further into the transport cavity. MFT K235 released the γ-carboxyl of THF and later formed an interaction with the α-carboxyl of THF (t = 6 ns) (Figure 2-27B). During this exchange, the pteridine ring of THF formed a π stacking interaction with Y300 (t = 3 ns) (Figure 2-27A). This π-π interaction held the pteridine portion of THF in place so that the α-carboxyl of THF could rotate and contact MFT K235. These two interactions were maintained until t = 14 ns, when MFT R249 attracted the γ-carboxyl of THF deeper within the transport cavity to the cavity floor (Figure 2-27C). Simultaneously, the α-carboxyl of THF descended from MFT K235 to R288 (Figure 2-27B) and both carboxyl groups of THF were held in place for the remainder of the simulation. As the carboxyl groups of THF moved deeper into the cavity, the interaction between Y300 and the pteridine ring of THF was broken and THF contacted MFT F200 (Figure 2-27A). However, the interaction of THF with MFT F200 was brief and the substrate ultimately interacted with W96 instead. At t = 18 ns, the pteridine ring of THF was within 5 Å of W96 (Figure 2-27A). The indole nitrogen of MFT W142 then contacted the keto group adjacent to the benzyl ring of THF at t = 20 ns. This interaction caused the pteridine ring of THF and W96 to move closer together (t = 25 ns). Although the simulation lasted for 40 ns, no further interactions were observed after t = 25 ns of the simulation.

Orientations of the CHO MFT conserved motif residues in the presence of THF

The molecular dynamics simulation predicted THF to interact with two residues, W142 and R249 that were located in the conserved motifs of the CHO MFT (Figure 2-28).

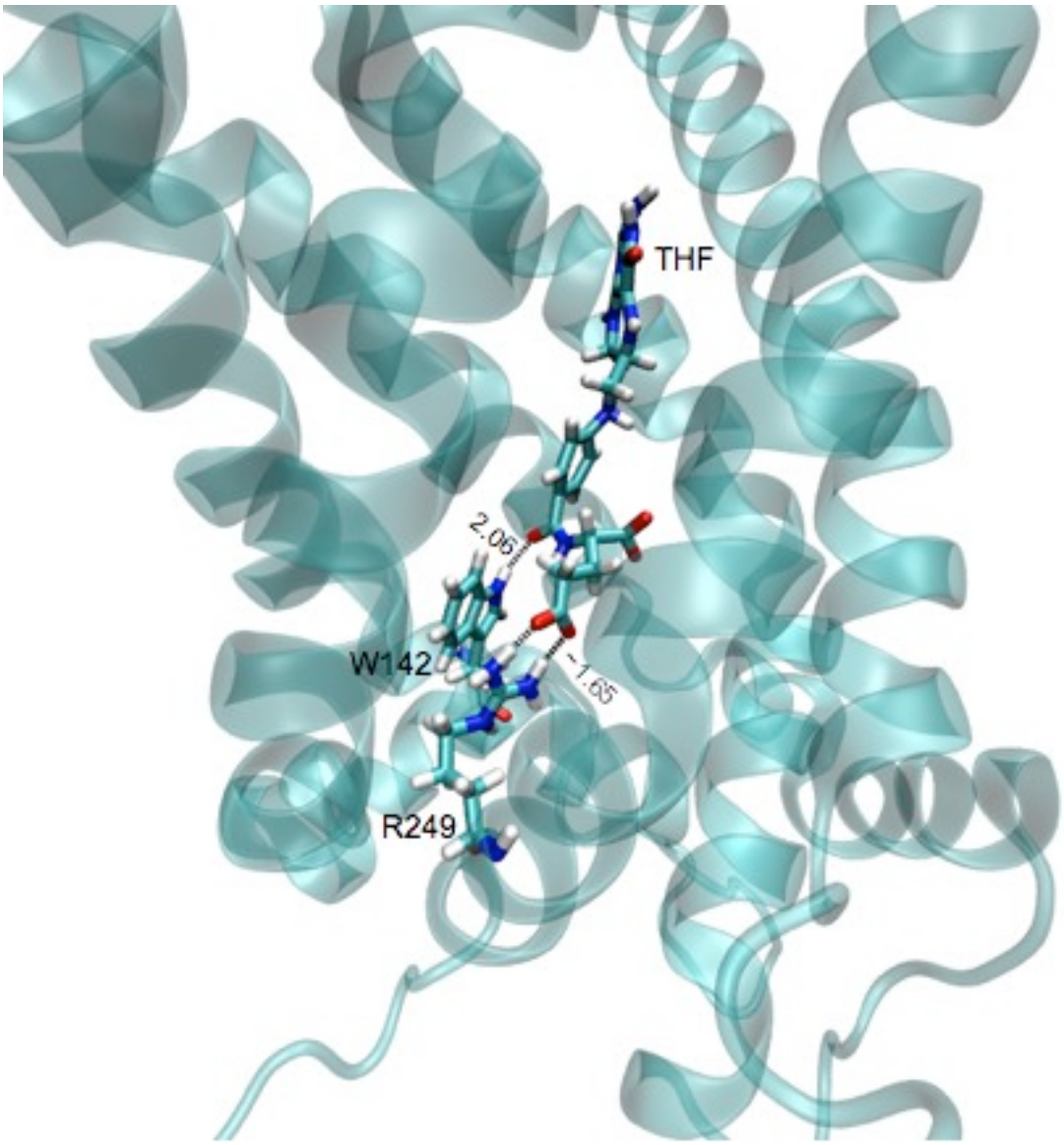

Figure 2-28 Interaction of tetrahydrofolate with CHO MFT W142 and R249 at the end of the MD simulation. The CHO MFT homology model is shown in transparent blue ribbon tube display. The orientations of tetrahydrofolate (THF) and CHO MFT W142 and R249 at the end of the 40 ns THF-MFT MD simulation are shown in CPK. The dashed black lines represent potential interactions with bond distances measured in angstroms (Å).

No interactions were observed between THF and other conserved motif residues, but these interactions may occur at times beyond our computational reach. At the end of the 40 ns simulation, the α-carboxyl was bound to MFT R288 and was equidistant from K47 and K145, the basic residues in the first and second conserved motifs in the MFT (Figure 2-29). These residues may play a role in events that occur later in the folate transport process, but were not implicated in transport on the time scale used in our MD simulation. The distances between the conserved motif residues that were predicted to interact in the MFT were followed for the duration of the THF-MFT MD simulation. Despite the THF substrate only interacting with CHO MFT W142 and R249, the substrate appeared to decrease the flexibility of all of the residues in the PxD/ExxK/R motifs of the MFT (Figure 2-30 ; MD movie 5 – supplemental material). As THF moved deeper within the MFT transport cavity and encountered the transport cavity floor (t = 20 ns), it appeared that the presence of substrate caused the charged residues in the conserved motifs to move closer together. This was in contrast to what was observed in the apo-MFT simulation, where the conserved motif residues had a large degree of flexibility (Figure 2-25). The distances between the PxD/ExxK/R motif residues that were predicted to interact in the MFT fluctuated in the first half of the simulation with THF (t = 0-20 ns), as was observed in the apo-MFT simulation. However, these residues converged at t = 25 ns in the presence of THF. The propensity of these residues to come together and form these interactions did not occur until THF had completely settled within the channel. Hence, it appeared that these conserved motif residues in the MFT interacted only in the presence of substrate. Consistent with our finding, four other molecular dynamics simulations with the AAC

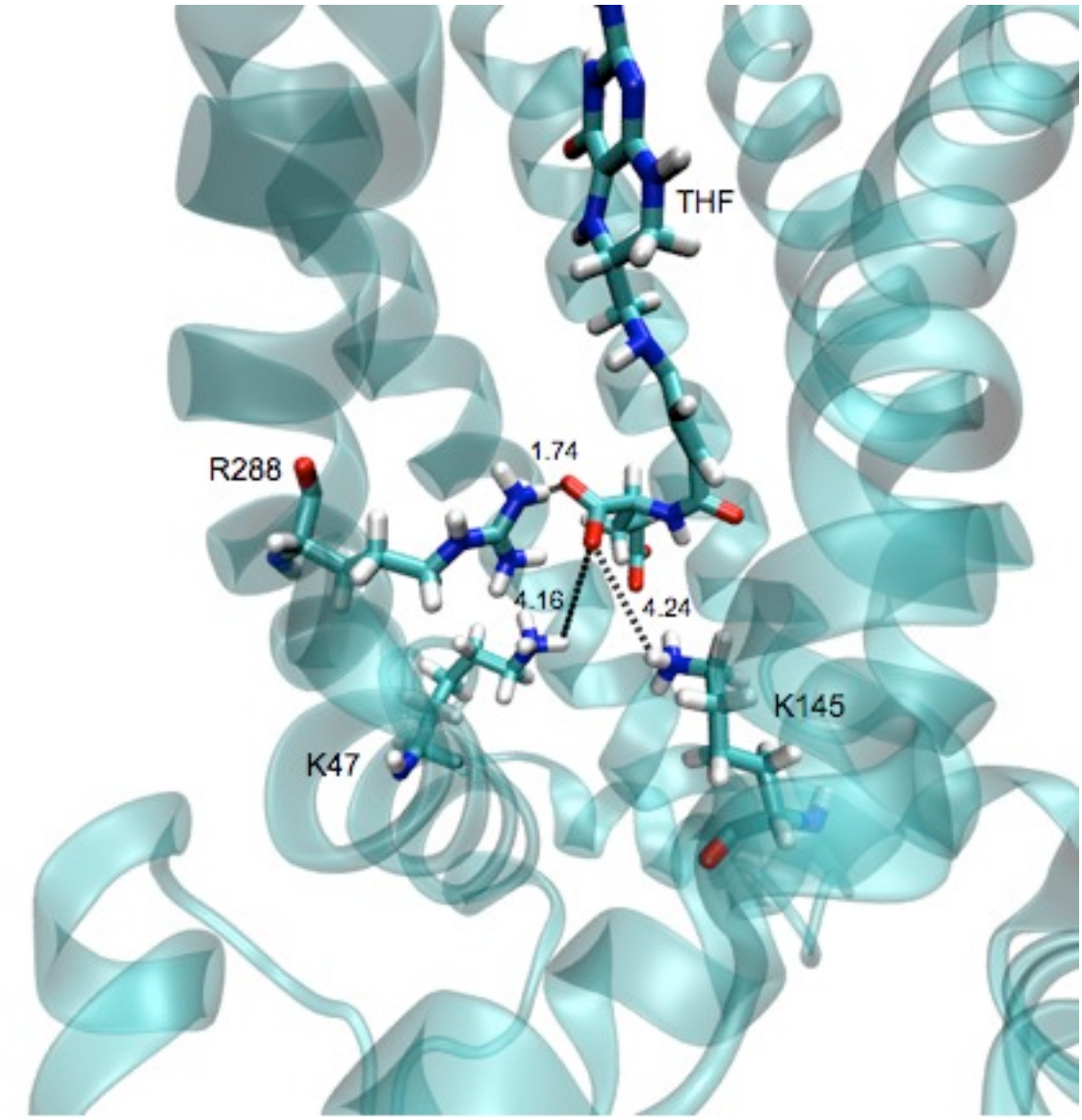

Figure 2-29 Interaction of tetrahydrofolate with CHO MFT K47, K145 and R288 at the end of the MD simulation. The CHO MFT homology model is shown in transparent blue ribbon tube display. The orientations of tetrahydrofolate (THF) and CHO MFT K47, K145, and R288 at the end of the 40 ns THF-MFT MD simulation are shown in CPK. The dashed black lines represent potential interactions with bond distances measured in angstroms (Å).

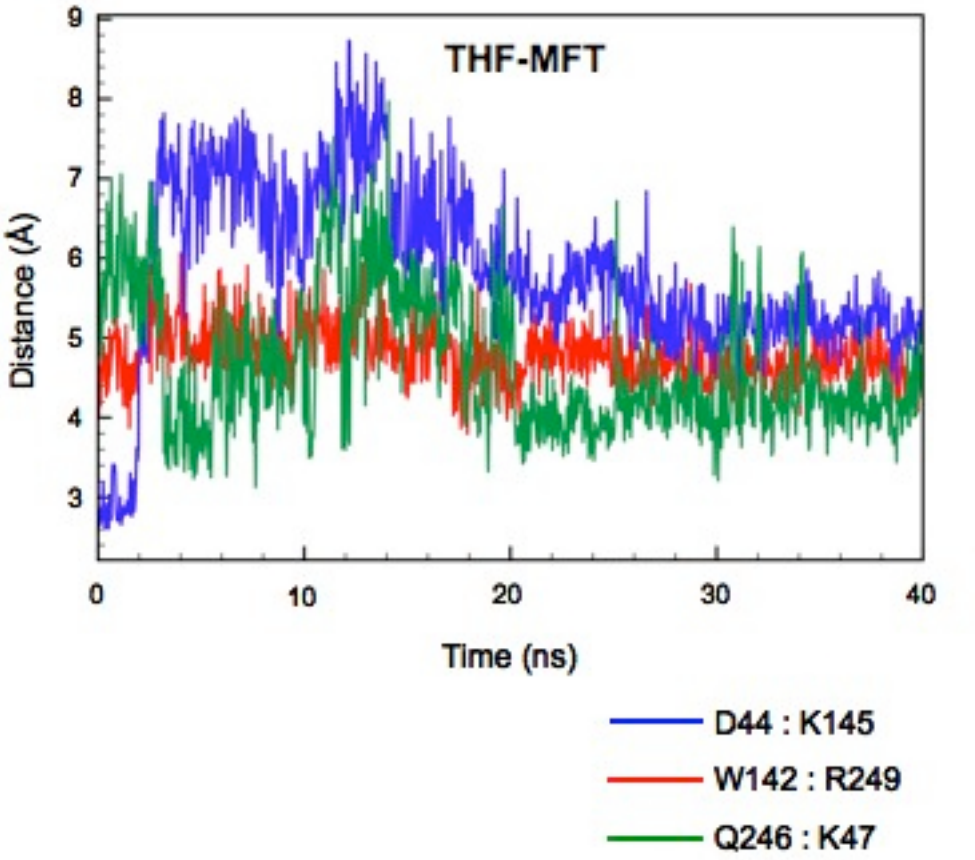

Figure 2-30 Distance between PxD/ExxK/R motif residues during the THF-MFT molecular dynamics simulation. CHO MFT conserved motif residues, D44 and K145, W142 and R249, and Q246 and K47 were predicted to interact based on the crystal structure of the AAC and the orientations of these residues in the CHO MFT homology model. Molecular dynamics (MD) simulations were run with the CHO MFT homology model and with a molecule of tetrahydrofolate (THF) (MD movie 5 in supplemental material). During these simulations, the distance in angstroms (Å), between conserved motif residues that were predicted to interact was measured. The CHO MFT homology model was subjected to 40 nanoseconds (ns) of a molecular dynamics simulation with a molecule of THF placed within the CHO MFT homology model transport cavity (THF-MFT). The distances between CHO MFT D44 and K145 (blue), W142 and R249 (red), and Q246 and K47 (green) are shown throughout the simulation.

showed that these conserved sequence interactions were also induced in the presence of substrate or inhibitor, and that these interactions were not present in the apo-AAC simulations (33, 40, 68, 169). Therefore, the conserved motif interactions that are induced in the presence of substrate, likely reflect an event that occurs in all MCF proteins. We concluded that these conserved motif interactions are not static in MCF proteins and that these interactions are induced by substrate as part of an intermediate step that is common to all MCF proteins during the transport process.

DISCUSSION

Studying MFT mutants using multiple approaches provided a more holistic understanding of the functional effects caused by the constructed MFT mutations, in turn, leading to a better understanding of the transport mechanism of the MFT. The purposes for the studies in this chapter were to understand the mechanism of mitochondrial folate uptake and the changes that occurred in the MFT that evolved a folate-specific transport mechanism. An initial set of mutations was made without the guidance of a homology model and yet still identified two informative mutations that severely affected the transport function of the MFT. However, it was the application of the homology model that was used *post facto* to understand what these mutations were doing to the MFT protein. The second set of mutations was guided by the CHO MFT homology model and computational docking studies that focused our attention on a few residues in the MFT that had anomalous substitutions fixed during the evolution the folate transport mechanism.

Mutagenesis of these residues indicated that mitochondrial folate transport could not occur with the MCF consensus amino acids at most of the studied positions; these changes apparently evolved out of necessity for mitochondrial folate transport. We turned back to computational approaches to further examine the trajectory of tetrahydrofolate (THF) down the MFT transport cavity and the interaction of THF with residues of the transport cavity floor in molecular dynamics (MD) simulations. Once again, the computational approach enhanced our understanding of the effects observed in the mutant MFT proteins and implicated several residues in the coordination of folates in early transport events. These residues, CHO MFT W96, K235, R288, and Y300, would be excellent new targets for new mutagenesis studies (See Chapter Four). Hence, combining the glyB complementation and mitochondrial folate uptake assays with computational methods provided a more inclusive perspective than using either of these approaches alone. The techniques, interpretation of the results in these assays, and their impact on our current understanding of MFT and MCF mechanism of transport are discussed below.

Investigating MFT function in a survival-based glyB complementation assay

The glyB complementation assay took advantage of the glycine dependence of glyB cells, and MFT function was crudely measured in this assay by the disappearance of this glycine auxotrophy. The disappearance of the glyB phenotype is thought to correspond to the re-establishment of mitochondrial folate transport. A number of mutations were made in the MFT that were able to complement the glyB glycine auxotrophy. We did not predict that all of these mutations would provide some level of glyB complementation. It

was quite possible that even a severe level of impairment of MFT function would still suffice for glyB survival in the absence of glycine so long as some fractional level of transport remained (see below). Furthermore, complementation could also be observed in MFT mutants with minimal transport efficiency if they were expressed at higher levels. However, it should not be overlooked that many of these mutations permitted some level of glyB cell survival in the absence of glycine. The fact that these proteins were still able to transport mitochondrial folates suggests that the proteins were still functional as mitochondrial folate transporters.

While the complementation assay did not exactly correlate with the uptake of folates into mitochondria at incremental levels of MFT function, this assay can be interpreted to indicate function versus no function in MFT mutant proteins. There were four mutations, CHO MFT G192E, R249A, W142D, and G91R that did not complement the glycine auxotrophy of glyB cells at any level. We believe that the inability of these mutant proteins to provide any complementation suggests that mitochondrial folate transport is completely prevented and not just impaired by these mutations. Interestingly, all of the mutations involved the introduction or removal of a charged side chain. The G192E, W142D and G91R mutations added charged side chain residues into the MFT. The W142 position was also mutated to W142A, W142F, and W142R; yet only the anionic nature of the aspartate side chain in the W142D mutant was unable to provide any glyB cell survival in the absence of glycine. This implies that the negative charge associated with the aspartate residue inhibits the MFT, and interestingly, this negative charge is present in a majority of MCF members. Also, the G91L MFT was a mutation made to

control for the size of the arginine side chain of G91R, without the positive charge. There was a 40% level of complementation in glyB cells transfected with MFT G91L, suggesting that the positive charge associated with the arginine side chain was responsible for some of the loss of function observed with G91R. The only mutation that involved the removal of a charge and subsequent failure to transport mitochondrial folates was CHO MFT R249A. Since CHO MFT R249 was located in the third PxD/ExxK/R motif in the MFT, it was thought that this mutation abolished the residue required to participate in a cation-π interaction with W142. Interestingly, when this position was mutated to R249W, this MFT protein complemented the glycine auxotrophy in glyB cells. It seemed likely that this mutation resulted in the formation of a π-π interaction with W142 and that such an interaction was fulfilling the function served by the cation-π between W142 and R249. However, given the MFT inhibition observed with the W142D mutant, this W142:R249 interaction appears to be more complex than originally thought.

Examining mitochondrial folate uptake in cell-based transport experiments

There was a need to more directly study the capability of mutant MFT proteins to transport folates into mitochondria. The protocol used to study mitochondrial folate uptake in the first set of mutants, published in *Biochemistry* in 2007, was slightly different than that used to study the second set of MFT mutants. The first set of experiments studied uptake of ^{3}H-6S-5-formyl-tetrahydrofolate in a pooled population of transfectants for 20 minutes. The second set of experiments examined mitochondrial folate uptake for four minutes in cell lines expanded from single clones in which MFT expression was similar.

The data produced in these experiments was subtly different. In the first set of uptake experiments, only the MFT mutants that did not permit glyB cell survival in the absence of glycine were unable to accumulate mitochondrial folates. In contrast, the second set of mutations included a number of MFT mutant proteins that were unable to efficiently accumulate mitochondrial folates, despite all but two mutant proteins complementing the glyB phenotype. When comparing the two sets of experiments, it appears that studying mitochondrial folate uptake for shorter intervals in stably transfected clones with known and relatively similar amounts of MFT protein provides a more accurate indication of MFT transport function.

Nevertheless, the mitochondrial uptake data corroborated our interpretation of data from the glyB complementation assay regarding the impairment of some mutated MFT proteins. In the second set of mutations, we observed that a majority of the mutated MFT proteins retained some level of MFT function. While these stably transfected cell lines appeared to inefficiently transport folates in this assay, the only mutant protein that appeared to exhibit uptake comparable to wild-type was W142F. In contrast to the glyB complementation assay, this uptake assay was useful for separating functionless or impaired transporters from fully functional proteins. Overall, we concluded that the glyB complementation assay over-predicted the transport function of mutant MFT proteins, presumably because cells can survive with only a fraction of the mitochondrial folate transport observed in wild-type cells. Also, the mitochondrial uptake assay may tend to underestimate the transport function of mutant MFT proteins, as these mutated proteins may be able to transport folates at a slower rate.

Impact of experimental techniques on determining functional effects of mutant MFT and MCF transporters

In the studies presented in this chapter, we had the advantage of studying the function of mutations in the MFT proteins in two different assays. Using these methods, our data suggested that survival assays tend to underestimate functional effects, while direct transport studies may overestimate the impact of certain mutations. This combination of assays that measure survival and direct transport are rarely combined to study other MCF proteins. Of the five MCF proteins that have been examined by mutagenesis, only two, the AAC and phosphate transport protein (PTP), have been examined using both survival and direct transport studies. The study of the PTP in this manner has shown similar results to those that we have produced with the MFT. Transport analysis over 20 seconds in reconstituted liposomes showed that mutation of some charged conserved motif residues in the PTP drastically impaired its transport function (132). However, transfection of these mutant PTP proteins into a PTP-null yeast strain showed that they retained some level of transport activity as evidenced by decreased colony sizes formed by these mutants (132). Nonetheless, the interpretation of the mutational effects changed depending on the assay in which the mutant proteins were studied. Functional interpretations become increasingly important as the proposed mechanism of opening common to all MCF members and the proposed common substrate-binding sites have relied heavily on mutagenesis data.

MCF mutations are more commonly studied using methods that involve protein purification, typically from recombinant expression systems, and reconstitution into

liposomal transport systems. These systems are advantageous because they allow the direct analysis of transport events. Liposomal systems are designed to contain a single protein of interest incubated with a single substrate. This design eliminates the possibility of substrate transport by another, non-specific protein and removes other proteins that could modify the substrate. Thus, the study of transport in liposomes is an ideal system to obtain direct kinetic data and substrate analysis. However, there is one shortcoming with these systems that has been largely ignored and will be briefly addressed. In these studies, purified transport protein is mixed with lipids that were subjected to sonication and passed over an amberlite column to facilitate the formation of intact, spherical vesicles that contain the purified protein embedded in a re-formed lipid membrane (123). The major shortcoming with liposomal systems is that the protein appears to randomly orient itself in the lipid vesicle membrane. There is some percentage of purified protein that is inserted with the N- and C- termini facing outside of the liposomes and some percentage is inserted with the terminal regions protruding into the vesicles; the protein appears to be randomly inserted into the membrane (54). This would imply that even if an equal amount of protein were incorporated into liposomal membranes, the amount of protein available for import might not be equivalent when comparing different liposomal preparations because of the random orientation of the protein in the membrane.

Nonetheless, liposomal transport is the gold standard in the mitochondrial carrier field. Similar to the mitochondrial folate uptake assay presented in this chapter, we believe that studying the transport function of MCF proteins in proteoliposomes also over exaggerates the effects of mutations on the transport function of these proteins. For

example, the mechanism of transport was probed in the oxoglutarate transporter by mutating nearly every amino acid predicted to be a transmembrane domain to a cysteine residue (25, 26). Recombinant mutant proteins were purified and reconstituted into proteoliposomes and transport was allowed for 30 seconds at 25° C. Uptake of ^{14}C-oxoglutarate into proteoliposomes containing mutant oxoglutarate transporters was observed and numerous residues inhibited the transport rate of the oxoglutarate carrier by at least 75%. Residues that were found to inhibit transport function were spaced at intervals of 3-4 residues apart and these residues were not specifically associated with charged, polar, aromatic, or aliphatic side chains, suggesting that every transport cavity-lining residue was involved in the transport process. While we tend to believe there is a strict organization that occurs within the transport cavity of MCF proteins, it seems unlikely that each of these mutations would impact cell growth and survival in the same fashion.

Generation and application of a CHO MFT homology model

The crystallization of the AAC was a monumental breakthrough in the mitochondrial carrier field. It was one of the first integral membrane proteins to be crystallized and the X-ray crystallographic analysis that followed was performed at a remarkably high resolution (2.2 Å). Since then, numerous labs have used the solved coordinates of this protein to predict the structures of other MCF proteins using homology modeling (112, 142, 166). In fact, one group generated homology models for nine MCF members and computationally docked the respective substrates into each of these models

(142). As a result, they analyzed the binding of substrates within the transport cavities of nine homology-modeled MCF proteins. The results of this study led the authors to propose that all MCF proteins contain three common substrate-binding sites and the amino acids that were present at these proposed common binding sites dictated the substrate specificity of each transport protein (142). We also generated a homology model using the solved coordinates of the AAC. This model aided in the interpretation of experimental results, predicted the molecular organization in the MFT structure, provided a basis for experimental design, and allowed visualization of the predicted locations of residues within the MFT transport cavity. Initial application of this homology model involved the inspection of the residues involved in the PxD/ExxK/R motifs in the MFT. With each use, the homology model was able to provide insights and possible explanations for experimental phenomena. Additionally, the homology model suggested additional experiments that evolved into an iterative process between experimental and computational approaches.

We decided to push the limits of our computational reach by using the CHO MFT homology model in molecular dynamics (MD) simulations. In order to run simulations on our MFT model, we needed to ensure that the structure was as accurate as possible. Thus, we generated a second homology model in a newer module contained within the Sybyl program, ORCHESTRAR, that was shown to be superior in generating more complete and more accurate homology models when the sequence is < 30% identical, and in producing homology models with better geometries and side chain orientations (36). The first homology model that we generated was a good model, but it had some flaws in the loop

regions and in the C-terminal region of the fourth transmembrane domain. These flaws were largely corrected in the second generation CHO MFT homology model. We were initially concerned that any errors in the homology model would potentially be amplified and erroneous regions could produce flawed interpretations of the MD simulations. We now feel that MD simulations circumvent some of the limitations of homology modeling by equilibrating the MD system before simulations were run.

Molecular dynamics simulations of the apo-MFT

The apo-MFT simulations were just as valuable and contained as much information as the THF-MFT simulations regarding the transport mechanism of the MFT. These simulations demonstrated a large electrostatic potential at the base of the MFT transport cavity and extreme flexibility of the residues in the MFT conserved motifs. The average +1.5 V electrostatic charge found at the base of the MFT was greater than that (+1.0 V) calculated for the AAC (33, 169). The conserved motif residues that are altered in the MFT are all in the D/E positions, where two typically acidic residues have been changed to an aromatic residue, W142, and to a polar residue, Q246. Not only are these changes suspected to contribute to the substrate specificity and transport mechanism of the MFT, but they may also increase the electrostatic potential responsible for drawing the folate substrate deep into the cavity. The electrostatic potential in the AAC may be sufficient to attract the highly electronegative phosphate groups of ADP, but it is possible that the less electronegative carboxyl groups on a folate molecule require more electrostatic pull for efficient capture.

We observed a large degree of flexibility in the PxD/ExxK/R motif residues in the apo-MFT simulation. On the basis of the X-ray crystallography of the AAC, the interactions between the conserved sequence pairs were thought to be sustained MCF transporters in the absence of substrate. However, our apo-MFT simulation predicted that this was not the case. In fact, it suggests that CHO MFT D44, W142 and Q246 may form a number of temporary interactions with intrahelical residues and other charged residues located higher within the MFT transport cavity. We showed that D44 prefers to interact with CHO MFT R288 in the apo-MFT simulation and predict that K145 is stabilized by W142, a residue that is located on the same transmembrane domain. The flexibility we observed in the MFT conserved motif residues was also observed in molecular dynamics simulations with the AAC and in an oxoglutarate transporter homology model (33, 40, 68, 112, 169). In addition, early mutagenesis on the yeast AAC suggested that conserved motif residues in the AAC were interacting with intrahelical residues as well as non-conserved sequence residues (119). In this study, second-site revertants were established that indicated an interaction existed between AAC residues homologous to CHO MFT D44 and R288 (118). Later, it was discovered that the AAC residue homologous to MFT K145 had two second-site revertants at positions homologous to CHO MFT D44 and W142 (119). This data, combined with what has been demonstrated in numerous MD simulations of apo-MCF proteins, suggests that these conserved motif interactions are not constantly maintained in these proteins. We believe that the presence of the carboxyatractyloside inhibitor within the transport cavity of the bAAC crystal structure induced a conformation where bAAC E29 and R137, D134 and R234, and D231 and K32 formed interactions and

that the apparent stability of these interactions was an artifact of crystallography with a tight-binding inhibitor.

Initial positioning of tetrahydrofolate in the MFT transport cavity for molecular dynamics simulations

The tetrahydrofolate (THF) substrate was placed ~25 Å above the MFT cavity floor, oriented with the carboxyl groups facing down into the MFT transport cavity for molecular dynamics (MD) simulations. MD simulations with the AAC demonstrated that despite the initial orientation of the substrate, ADP quickly adopted a position within the AAC transport cavity with its phosphate groups pointing down towards the cavity floor (33, 169). Therefore, it was unlikely that this initial orientation of THF in the MFT transport cavity would bias the MD simulation. Initially, the THF substrate was placed higher above the MFT transport cavity. However, if the THF was placed too high in the channel, it either diffused into the aqueous space above the membrane or it interacted with a loop from the MFT that extended into the inter-membrane space. In a previous simulation with the AAC, it was shown that ADP molecules contained in the aqueous inter-membrane space were spontaneously attracted into the AAC transport cavity (33). However, the computational time required to visualize this event was significantly longer than that needed to simulate binding using a biased substrate placement. Substrate binding to an external loop of the MFT may also be an event required to recruit the folate substrate into the transport cavity. We previously showed that insertion of a *myc* tag into the first inter-membrane space loop of MFT inhibited its function as evidenced in the

inability of glyB cells transfected with this construct to grow in the absence of glycine (129). Furthermore, studies on the homologous region in the yeast AAC demonstrated that four amino acids in the first inter-membrane space loop were vital for AAC transport (75). Therefore, it seems likely that this loop region initially attracts substrate from the aqueous inter-membrane space environment.

Molecular dynamics simulations predict residues that contact and guide tetrahydrofolate down into the MFT transport cavity

The tetrahydrofolate substrate was passed down to the cavity floor of the MFT by the step-wise and sequential interaction with residues that lined MFT transport cavity. The step-wise nature of THF passage indicated the strict organization of residues and side chains that protruded into the MFT transport cavity. MD simulations showed that a majority of the residues predicted to contact THF at the cavity floor were charged with one aromatic residue (W142) and the majority of the residues predicted to contact THF above the cavity floor were aromatic with one anionic residue (K235). The arrangement of residues in this manner is also consistent with the THF substrate moving into the transport cavity with its charged carboxyl groups first. The charged residues that were predicted to contact the THF substrate were CHO MFT R249, R888, and K235. Residues R249 and R288 are highly conserved among proteins in the MCF, while K235 was an interesting discovery peculiar to the MFT. PI/LW subfamily proteins all contain a lysine residue at this location. Interestingly, the amino acid homologous to CHO MFT K235 in the vast majority of non-PI/LW MCF proteins is a glycine, while the AAC contains a threonine at

this position. This conserved lysine residue reinforces the belief that these PI/LW transporters are functionally distinct from the rest of the MCF.

Four aromatic residues were predicted to contact THF during the MD simulations. CHO MFT W96, F200, Y300 all contacted the pteridine ring of THF and were located high up in the transport cavity near K235, while W142 is a conserved motif residue at the base of the transport cavity that is the hallmark of the PI/LW subfamily. CHO MFT F200 is homologous to AAC F191, a residue located in an "aromatic ladder" in the AAC. This AAC aromatic ladder consists of four residues, AAC Y186, Y190, F191, and Y194. Of these residues, Y186 and F191 were shown to be required for optimal transport in the AAC by mutagenesis (32). The MFT and the rest of the PI/LW subfamily only contain aromatic residues in locations homologous to AAC F191 and Y194. It is unclear if the MFT requires an aromatic ladder for folate transport. However, as the folate substrate reaches the cavity floor in the molecular dynamics simulations, the THF substrate samples the MFT region homologous to the AAC aromatic ladder, specifically CHO MFT F200. However, this sampling is short-lived and the pteridine ring of THF interacts with W96 on the opposite side of the transport cavity instead. This may suggest that the MFT does not require an aromatic ladder in the homologous position as in the AAC. Additional mutagenesis studies would clarify the role of these residues in the MFT. CHO MFT W96 is also quite interesting. While it is not conserved amongst the entire PI/LW subfamily, the NAD^+ (ScYEL006W) and FAD^+ (ScFlx1p) transporters also contain this amino acid. An aromatic amino acid is not found at this position in any other MCF member besides these three; the position homologous to CHO MFT W96 is mostly polar residues throughout

MCF proteins. The polar residue at this position in the bAAC, Q84, was predicted to contact the ADP substrate in molecular dynamics simulations with the bAAC (bAAC Q84) (33), while mutagenesis of the homologous residue in the oxoglutarate carrier, T95C, was shown to impair transport by ~75% in reconstituted liposomes (T95C) (25). Although the residues are different between MCF transporters, these locations appear to be important in other MCF proteins.

The most striking or, at least, most obvious changes that have occurred in the MFT are substitutions contained within the PxD/ExxK/R conserved motifs and the behavior of the residues in these motifs in the molecular dynamics simulations was of particular interest. It was apparent that as the THF substrate moved through the MFT transport cavity and migrated closer to the cavity floor, the conserved motif residues moved closer to one another. It appeared that the conserved motif interactions predicted to form and maintain the cavity floor were actually induced by substrate. Interestingly, this same phenomenon was observed in other molecular dynamics simulations with the AAC (33, 68, 169), but little attention was given to this in these simulations. Recalling that the AAC was co-crystallized with a CATR inhibitor within the transport cavity, it was possible that the solved structural coordinates of the AAC were altered by in the presence of this inhibitor. We believe that binding of the transport substrate deep in the transport cavity of MCF proteins induces these interactions; they do not contribute to a transport barrier, but rather represent an intermediate conformation required for transport.

The hypothesis that the charged residues of the PxD/ExxK/R motif do not form a transport barrier would explain the enigmatic effects observed with mutation of the

charged PxD/ExxK/R residues. It was previously thought that the charged residues in the PxD/ExxK/R motifs participated in three interactions that formed a transport cavity floor, an apparent transport barrier. To initiate transport, the substrate was thought to disrupt or rearrange these three interactions. If the purpose of these residues were to form three interactions that solidified a transport barrier, then removal of one of these interactions by mutating an involved residue would seemingly weaken this barrier. In addition, the substrate would have one less interaction to disrupt before initiating transport. Therefore, removing one barrier-forming interaction by mutagenesis would theoretically facilitate substrate transport. Transport of substrate by MCF proteins is not facilitated when the charged residues in the PxD/ExxK/R motifs are mutated; mutant proteins display impaired transport, at the least, and, in most cases, the transport function of the MCF proteins is completely eliminated ((26, 57, 58, 96, 98, 114, 117, 118, 132, 133), data presented in this thesis). If we consider the interactions of the PxD/ExxK/R motifs to exist as an intermediate transport step, the effects by mutagenesis of the charged residues in PxD/ExxK/R motifs are more easily explained. We propose that the purpose of this intermediate step and the interaction of these charged residues is for the D/E residue of the interacting pair to position and maintain the location of the K/R residue. The K/R residue becomes immobilized by this interaction with the D/E residue, but the location in which the K/R residue is held enables this cationic residue to contact the anionic groups of the substrate more efficiently. Therefore, we believe that the K/R residues of the PxD/ExxK/R motifs are absolutely required for substrate transport because these K/R residues interact with substrate at locations deep within the transport cavity. The binding of substrate to the

K/R residues of the PxD/ExxK/R motifs may constitute the penultimate binding step in substrate translocation into the matrix (see Perspectives section).

Speculation and working hypothesis of the mitochondrial folate transport mechanism of the MFT

We have done considerable work on the mechanism of folate transport that, I believe, justifies the following speculation about this transport process. We consider folate molecules to be freely permeable through the voltage dependent anion channel pores in the outer mitochondrial membrane. Folates randomly diffuse throughout the mitochondrial inter-membrane space and are expected to be initially recruited to the first inter-membrane space loop of the MFT. As all of the loop regions in the MFT are hydrophilic, this attraction is likely between the loop region and the carboxyl groups of the folate. As the carboxyl groups interact with residues on this MFT loop in the inter-membrane space, the pteridine and benzyl rings of folate are free to move. It is anticipated that these aromatic groups, specifically the pteridine ring, interact with residues on the opposite side of the MFT. Perhaps this interaction occurs with the second inter-membrane space loop or the C-terminal region, which were shown to complement the glycine auxotrophy of glyB cells by 35% and 50%, respectively (129). The folate molecule would now be horizontally oriented above the opening to the cavity floor. As an interaction is established with one of the aromatic groups of the folate substrate, the carboxyl groups are freed from interactions with the loop regions and move down into the channel to make contact with CHO MFT K235. With the carboxyl groups held in place once again, the pteridine ring is stabilized

and is predicted to contact CHO MFT Y300. As the folate molecule progresses down the transport channel and the molecular dynamics simulation finishes, the γ-carboxyl of the folate is in contact with CHO MFT R249 and the α-carboxyl is in contact with R288. The benzyl ring resides in a substrate-binding pocket between W142 and G91, and the pteridine ring is coordinated by W96. The next step, which was not observed over the time-scale accessible by our molecular dynamics simulations, is proposed to be the passage of the α-carboxyl group from CHO MFT R288 to K47 and K145, which are equidistant from R288. As demonstrated in the molecular dynamics simulations, when substrate is not present in the transport cavity, CHO MFT D44 interacts with R288. However, the presence of the folate substrate induces D44 to interact with K145 and we hypothesize that this stabilization attracts the α-carboxyl to K145. This would result in the rotation of the benzyl ring from the binding pocket between to G91 and W142 to the other face of W142, which was predicted to interact with R249. This is consistent with the observed function of the CHO MFT W142R/R249W mutant that we examined. Additionally, this movement would break the interaction between the γ-carboxyl of the folate and CHO MFT R249, moving this part of the folate molecule closer to the matrix. As the folate substrate progresses closer to the mitochondrial matrix, the proline residues in the PxD/ExxK/R motifs likely provide sufficient flexibility to the 1st, 3rd, and 5th transmembrane domains so that the substrate is accommodated in the spatially constrained region of the MFT at and below the transport cavity floor. Little is known about the events that correspond to translocation and passage into the mitochondrial matrix. However, it has been suggested that second and third matrix-exposed loops in the AAC possess the flexibility to protrude

back into the membrane bound portion and play a role in gating transport in the AAC (100, 101). These loops may be important in accepting the γ-carboxyl of the folate and leading the remainder of the folate molecule into the mitochondrial matrix. However, we believe that the substrate-induced conserved motif interactions are prerequisites for the stabilization and proper orientation of the matrix-associated loop regions that eventually guide the folate into the mitochondrial matrix.

CHAPTER 3 Role of the MFT in the Compartmentalization of Folate Metabolism

An aspect that has been largely ignored up to this point in this thesis is that some of the MCF transporters function as exchangers. For instance, the AAC is thought to exchange cytosolic ADP for mitochondrial ATP in a 1:1 ratio (130, 131). Exchange has also been noted for the oxoglutarate carrier (malate for oxoglutarate) (122), citrate carrier (malate for citrate) (143), and the glutamate carrier (glutamate for aspartate) (88). It is highly controversial whether this exchange occurs through a conformational change within a single protein, or if these proteins exist as dimers, in which one subunit transports substrate into the matrix and the other sequentially transports substrate out of the matrix. Nonetheless, these proteins are predicted to cycle through conformations known as the *c*-state, where the transporter is open to the inner membrane space and accepts substrates from the cytosol, and the *m*-state, where the protein may accept and transport substrates from the mitochondrial matrix. These *c*- and *m*-states have been most clearly defined in the AAC because of the availability of two different classes of inhibitors, bongkrekates and atractylates that lock the carrier in these two different conformational states (reviewed in (19, 83). In the absence of inhibitors, there is thought to be equilibrium between the *c*- and the *m*-states of the AAC. Mechanistically, ADP is thought to bind to the *c*-state AAC and

the events that permit release of ADP into the matrix induce a conformational change that transitions the AAC to its *m*-state. The conformational switching between these two states in other transporters or whether two distinguishing states even exist in other MCF transporters is poorly understood. However, if this switching occurs, it is thought to enable substrate exchange between the cytosol and mitochondrial matrix.

Folate exchange and transport of folate polyglutamate molecules across the mitochondrial membrane

The exchange function of the MFT remains to be determined. In the two published experiments that have examined mitochondrial folate uptake, both have studied only the uptake of monoglutamate folate molecules in purified mitochondria (30, 61); uptake of folate polyglutamate forms has not been directly examined. However, there is evidence to suggest that cytosolic folate polyglutamates are unable to cross into the mitochondrial matrix. In a study published by others, AuxB1 cells were transfected with *Escherichia coli (E. coli)* FPGS and > 95% of the FPGS protein was localized in the cytosolic compartment of the transfectants (90, 91). In these transfectants, > 95% of the total cellular folates were located in the cytosol and ~85% of the cytosolic folate pool was triglutamate conjugates. Despite the transfectants accumulating cytosolic folates at wild-type levels, mitochondria of cells transfected with *E. coli* FPGS contained 90% less folates than mitochondria of wild-type cells. This suggested that the folate polyglutamate forms found in the cytosol were unable to enter mitochondria. Considering that the vast majority of mitochondrial folates are polyglutamated forms (28), these polyglutamated folates would be the most

likely candidates for efflux from mitochondria if folate exchange were to occur. However, the efflux of mitochondrial folates through the MFT is not comparable to the efflux of ATP through the AAC. Where a single phosphate group is added to ADP to form ATP, mitochondrial folate molecules typically contain up to six additional glutamate residues and few folates contain ≤ 3 glutamate moieties (28, 90). Whether or not mitochondrial folates efflux from mitochondria and enter the cytosolic folate pool is a fundamental question surrounding the function of the MFT and the design of the compartmentalization of folate metabolism.

The findings of two previous experiments suggested that mitochondrial folates were able to efflux into the cytosol (45, 91). One experiment attached a sequence encoding a mitochondrial leader peptide to an *E. coli fpgs* cDNA and transfected this construct into FPGS-null AuxB1 cells under the control of a CMV promoter (91). The transfected cells accumulated both mitochondrial and cytosolic folate polyglutamates and did not require any supplementation with glycine, purines, or thymidine for cell survival. This suggested that this mitochondrially-targeted FPGS protein was able to retain mitochondrial folates, as evidenced by complementation of glycine auxotrophy, and provide cytosolic folates within the cell, as evidenced by purine and thymidine auxotrophy complementation. The second study determined the sequence of the mitochondrial isoform of FPGS and discovered that two human mRNA transcripts were produced from a single *fpgs* gene (45, 156). When a cDNA encoding the mitochondrial isoform of FPGS was transfected into AuxB1 cells under the control of a CMV promoter, the mitochondrial isoform of FPGS complemented purine, thymidine, and glycine auxotrophy in AuxB1

cells. These studies suggested that the mitochondrial isoform of FPGS was capable of supplying the entire cell with sufficient folate molecules for cellular folate metabolism, although other explanations were possible (see below).

The cytosolic and mitochondrial isoforms of human FPGS are translated from two different RNA species that are transcribed from the same genetic locus (45, 156). The only difference between the mitochondrial and cytosolic FPGS proteins is that the mitochondrial isoform contains an extra 42 amino acid sequence, which appears to target this isoform to mitochondria (45). In addition, the transcript encoding the mitochondrial isoform of FPGS contains the start codon used to translate the cytosolic isoform of FPGS. Whereas two previous studies can be interpreted to suggest the mitochondrial isoform of FPGS was capable of supplying the entire cell with folate polyglutamates (45, 91), the cytosolic protein could be translated from the mitochondrial *fpgs* transcript if the downstream start codon was available for translation. This could be especially possible in engineered cell lines that produce high amounts of full-length *fpgs* transcript from strong viral promoters (CMV). In addition, it was also possible that a high amount of FPGS protein was being translated in these engineered cells and this amount of protein saturated one of the steps of protein import into mitochondria. This could result in catalytically active FPGS protein remaining in the cytosol, awaiting import into mitochondria. Neither of the published studies ruled out the presence of cytosolic FPGS protein. In fact, one study showed that ~25% of the total cellular FPGS activity and ~14% of the total cellular FPGS protein was located in the cytosol despite being transfected with a protein that was

targeted to mitochondria (91). Overall, these studies did not prove that folate polyglutamates were transported out of the mitochondrial matrix.

Mammalian cell lines were recently generated in this laboratory that were designed to directly answer the question of mitochondrial folate polyglutamate efflux. *Fpgs* cDNA was cloned into a mammalian expression vector in which transcription was only active in the presence of doxycycline (Clontech Tet-On expression system). The Tet-On expression system required the transfection of two vectors into FPGS-null AuxB1 cells. One vector, the regulatory vector, encoded a doxycycline-binding protein using a promoter that was constitutively active. The other vector, the response vector, contained the *fpgs* cDNA, in which expression was controlled by a promoter that was active only when doxycycline bound the doxycycline-binding protein and the complex resided at the promoter. Under ideal conditions, this promoter will not initiate transcription in the presence of unbound doxycycline or doxycycline binding protein. In this doxycycline-inducible expression system, varying levels of expression were achievable, in principle, by adjusting the amount of doxycycline that the transfected cells were exposed to.

Three *fpgs* cDNA constructs were generated, cloned into the doxycycline-inducible expression system, and transfected into AuxB1 cells. The first cDNA construct, cFPGS, allowed translation from an ATG that encoded a cytosolic FPGS protein only (Figure 3-1). Another construct, mFPGS, contained *fpgs* cDNA with both mitochondrial and cytosolic FPGS isoform translational start sites, and would possibly allow translation of both FPGS isoforms if the downstream (cytosolic) ATG was available for use by an internal ribosomal entry site or by ATG-skipping. The third cDNA construct, mutFPGS, encoded a FPGS

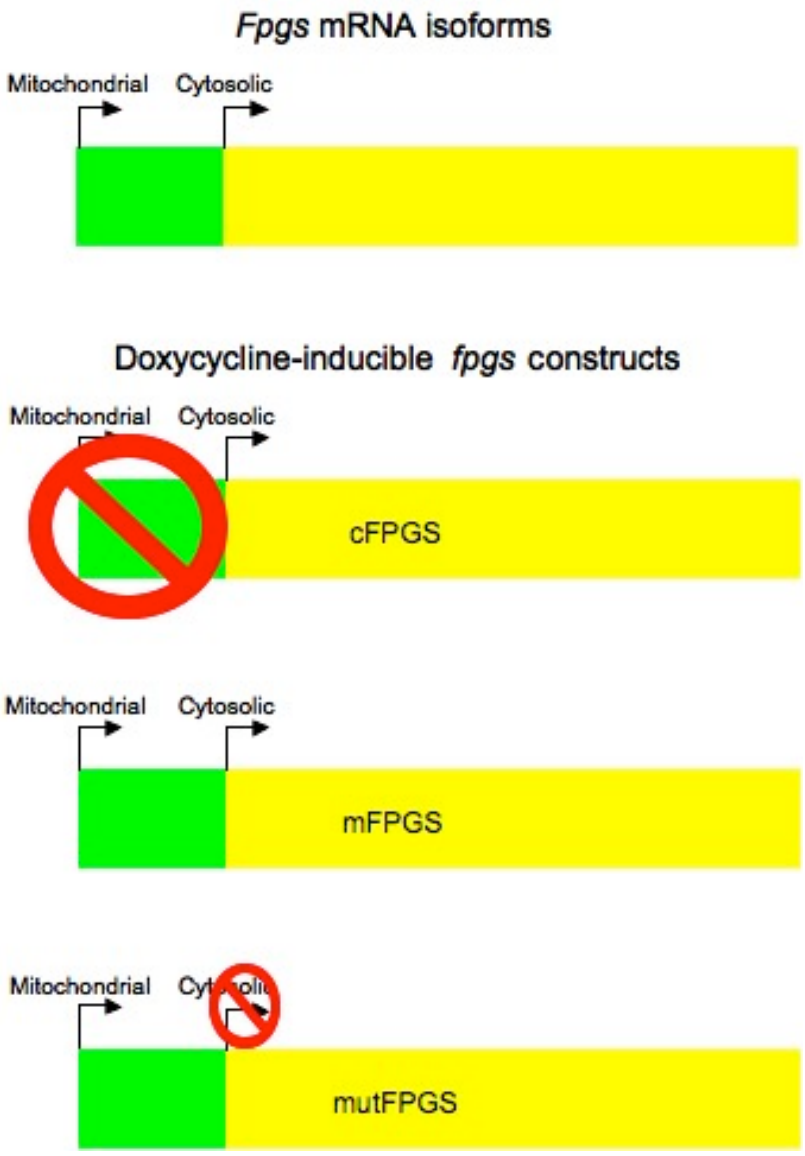

Figure 3-1 Schematic representations of FPGS isoforms and transfected constructs. The full-length *fpgs* mRNA is depicted in green and yellow, and start sites are marked with arrows. The mitochondrial leader peptide that distinguishes the mitochondrial isoform and targets this isoform to mitochondria is shown in green. The sequences of both cytosolic and mitochondrial isoforms are identical in the yellow region. The cFPGS construct does not contain the mitochondrial leader peptide (green region). The mFPGS construct retains both cytosolic and mitochondrial start sites. The mutFPGS construct contains the start site for the mitochondrial FPGS isoform, but has mutated the downstream start site for the cytosolic isoform to ATT.

protein with the mitochondrial FPGS isoform start site intact, but mutated the downstream ATG site to ATT. Therefore, this mutFPGS construct would encode the mitochondrial FPGS isoform only. Hence, these FPGS-inducible cell lines should allow controllable and compartmental expression of the FPGS protein. This controllable and compartmental FPGS expression, when coupled with detection of the FPGS protein, should enable the definitive study of folate polyglutamate flux across the mitochondrial membrane for the first time.

Potential for antifolate inhibition of the MFT

Antifolates have been developed to exploit the cellular dependence on folate metabolism. The utility of folate analogs as therapeutic agents dates back to the late 1940's where treatment with 4-aminopteroyl-glutamic acid (aminopterin) was discovered to induce remission in children with acute lymphocytic leukemia (41). The success of this compound was followed by the development of a less toxic structural analog, methotrexate (4-amino-N^{10}-methyl-pteroyl-glutamic acid) (42). Methotrexate was later found to inhibit dihydrofolate reductase (171), an enzyme that recycles tetrahydrofolate from dihydrofolate after thymidylate synthesis. After this monumental discovery, the development of antifolates progressed along with the increasing knowledge and understanding of cellular folate metabolism. Antifolate development eventually shifted to focus on thymidylate synthase, where raltitrexed (D1694, N-(5-[(N-(3,4-dihydro-2-methyl-4-oxoquinazolin-6-ylmethyl)-N-methylamino]-2-thenoyl)-L-glutamic acid) emerged as a potent inhibitor of thymidylate synthesis (67). Later, folate dependent enzymes in *de novo* purine synthesis

were identified as targets for antifolate development and DDATHF (lometrexol, 5,10-dideaza-5,6,7,8-tetrahydrofolate) was discovered to be an inhibitor of glycinamide ribonucleotide formyl transferase (GART) (12). AG2034 (4-[2-(2-amino-4-oxo-4,6,7,8-tetrahydro-3H-pyrimidino[5,4-6] [1,4]thiazin-6-yl)-(S)-ethyl]-2,5-thienoyl-L-glutamic acid) and AG2037 were developed to inhibit GART as well (16). Another antifolate, pemetrexed (N-[4-[2-(2-amino-3,4-dihydro-4-oxo-7H-pyrrolo[2,3-*d*]pyrimidin-5-yl)ethyl] benzoyl-L-glutamic acid), was part of a second series of compounds that were designed and targeted to inhibit GART. Interestingly, pemetrexed was discovered to inhibit multiple folate-dependent targets, with thymidylate synthase being the primary target of this antifolate (153). It was later shown that pemetrexed in its pentaglutamated form inhibited thymidylate synthase (K_i = 1.3 nM), dihydrofolate reductase (K_i = 7.2 nM), GART (K_i = 65 nM), and aminoimidazolecarboxamide ribonucleotide formyl transferase (AICARFT) (K_i = 260 nM), the other folate-dependent enzyme in *de novo* purine synthesis (149). Recently, AICARFT has been identified as the secondary target of pemetrexed inhibition in intact tumor cells (139). Of these antifolates, methotrexate and pemetrexed are clinically used throughout the world and raltitrexed is used only in Europe and Asia. Methotrexate is used in the treatment of leukemia, psoriasis and arthritis, while pemetrexed and raltitrexed are used in cancer chemotherapy for lung cancers and colon cancer, respectively.

The potency of antifolates not only depends on inhibition of intracellular target enzymes, but also depends on transport across the cell membrane and polyglutamation by FPGS. Like endogenous folates, most antifolates are transported into the cell by the

reduced folate carrier (51, 105). Pemetrexed also appears to be a substrate for the proton-coupled folate transporter (PCFT) at physiological pH (177). Once inside the cell, polyglutamation of folate analogs by FPGS is important because it results in the intracellular retention of antifolates and enhances the inhibitory potency of these agents (8, 67, 149, 153). Decreases in membrane transport and polyglutamation by FPGS are also implicated in antifolate resistance mechanisms (35, 109, 136, 176). Because antifolates rely on many of the same proteins that facilitate and coordinate cellular folate metabolism, these folate analogs may be substrates for or inhibitors of the MFT, which could result in unknown or undesirable mitochondrial toxicities.

Understanding if these folate analogs are substrates for or inhibitors of the MFT is an important question because these agents could potentially disrupt mitochondrial folate metabolism. The two studies published on carrier-mediated mitochondrial folate uptake reported that methotrexate was a weak inhibitor of mitochondrial folate transport (30, 61). However, the effects of other folate analogs on mitochondrial folate transport have not been examined. Inhibition of the MFT would result in decreased or abolished mitochondrial folate accumulation. Disrupting mitochondrial folate metabolism has been shown in three other cases to result in cellular toxicity in the absence of exogenous glycine supplementation (45, 71, 90, 160). In the absence of glycine, almost all glyB cells die within 24 hours (107), hence, dysfunctional mitochondrial folate transport initiates a rapid cellular response that ultimately ends in the death of the cell. The potential effects of antifolates on the MFT will be examined in this chapter.

MATERIALS AND METHODS

Culture of AuxB1 cells stably transfected with doxycycline-inducible fpgs cDNA constructs

Three stable cell lines were previously generated in our lab by Amy Heineman to express various isoforms of the FPGS protein under the control of a doxycycline-inducible promoter. These AuxB1-derived cells were routinely grown in MEM-α media supplemented with 10% tetracycline-free fetal bovine serum (FBS), 1% Penicillin and Streptomycin (Pen/Strep), 500 µg/mL G418 and 200 µg/mL hygromycin at 37° C with 5% CO_2. MEM α media contains all of the ribo- and deoxyribonucleosides and, hence, is not selective for deficiencies in folate metabolism.

Preparation of whole cell lysates from CEM, HCT116, H460 and transfected AuxB1 cells

Expression of FPGS in transfected AuxB1 cells was induced by the addition of 1 µg/mL doxycycline 48 hours prior to cell harvesting. During this period of exposure to doxycycline, cells were maintained in active growth phase. Cells were scraped from dishes using ice-cold phosphate buffered saline (PBS) with protease inhibitors (PI) (Roche complete EDTA-free protease inhibitors, proprietary – cat. # 11873580001) as previously described in Chapter Two. Cells were centrifuged at 2,000 x g for five minutes at 4° C. The resulting supernatant was aspirated and the pellet was washed with an additional 5 mL of PBS with PI, placed in a pre-weighed tube and centrifuged at 2,000 x g for five minutes at 4° C. The supernatant was aspirated and a volume of lysis buffer (62.5 mM Tris, pH 6.8; 5% glycerol; 2% SDS; 5% 2-mercaptoethanol) ten times the cell pellet weight (10 µL :

1 mg) was added to the cell pellet. This solution was then repeatedly passed through a 19G or 21G needle ~30 times to shear any DNA and centrifuged at 20,000 x g for five minutes at 4° C. Because of the SDS in the lysis buffer, passing this solution through a needle created bubbles. These bubbles made it difficult to get efficient shearing using a needle. Therefore, centrifugation at 20,000 x g for five minutes at 4° C was used to collapse the bubbles and return the solution to a liquid phase versus foam phase. The process of passing the solution through a needle 30 times followed by centrifugation was repeated for a total of four times. Protein concentrations were determined using the Bradford reagent according the manufacturer's specifications.

Preparation of cytosolic and mitochondrial protein lysates from CEM, HCT116, H460 and transfected AuxB1 cells

Expression of FPGS in transfected AuxB1 cells was induced by the addition of 1 µg/mL doxycycline 48 hours prior to cell harvesting. Active cell growth was maintained during this period by keeping the cultures subconfluent. Cells were scraped from dishes using ice-cold PBS with PI as previously described. Harvested cells were centrifuged at 2,000 x g for five minutes at 4° C. Cell pellets were resuspended in 7.5 mL of homogenization solution (250 mM sucrose, 1 mM EDTA, pH 6.8) with protease inhibitors. Following a five minute incubation in homogenization solution, cells were gently broken open using 15 strokes in a 7.5 mL dounce homogenizer with a "B" pestle and the homogenate was centrifuged at 2,000 x g at 4° C for five minutes. The supernatant was kept and centrifuged at 11,000 x g at 4° C for 15 minutes. The pellet that resulted from this

centrifugation contained mitochondria and the supernatant contained cytosolic protein. Mitochondria were immediately dissolved in lysis buffer (62.5 mM Tris, pH 6.8; 5% glycerol; 2% SDS; 5% 2-mercaptoethanol). To dissolve mitochondrial protein and shear any mitochondrial DNA, this solution was rapidly pipeted up and down for a total of 100 times. A manual pipet was used because the volume was typically too small to use a needle to shear DNA. This solution was then centrifuged at 4,500 x g for three minutes at 4° C. The pipeting and centrifugation steps were repeated for a total of four times. The cytosolic fraction was combined with trichloroacetic acid (TCA) at a final concentration of 6% TCA to precipitate and concentrate the cytosolic protein. This solution was mixed by inversion and incubated on ice for 30 minutes. After incubation, this solution was centrifuged at 7,800 x g for 15 minutes at 4° C. The pellet was washed with 1 volume (initial volume of the cytosolic fraction plus TCA) of ice-cold acetone and centrifuged at 7,800 x g for five minutes at 4° C. This acetone wash was repeated for a total of three times, after which, the pellet was dried by inversion for one minute and lysis buffer was added to the precipitated protein. Heat, sonication, or passage through a needle were used to assist in dissolving the TCA precipitated protein, but the protein must be resuspended in a sufficient volume of lysis buffer to aid in the solubilization of the precipitated protein. In this case, passage through a 19G or 21G needle was used as previously described. Protein concentrations were determined using the Bradford reagent according to the manufacturer's specifications.

Detection of the FPGS protein by western blotting

The cytosolic isoform of human FPGS had been previously purified in this lab and was included (3 ng) throughout western blotting procedures as a positive control. Tubes containing the samples to be loaded were placed in boiling water so that all of sample volume was immersed in the boiling water for five minutes and loaded into a freshly prepared 7.5% SDS-PAGE gel, electrophoresed in a buffer containing 192 mM glycine, 25 mM Tris, and 0.1% SDS, pH 8.3, and the protein contents of the gel were transferred to a nitrocellulose membrane at 100 V for 45 minutes in a fresh portion of the buffer in which the gel was run. Non-specific protein binding to this membrane was blocked using Blotto blocking solution containing 5% nonfat dry milk (Bio-Rad, cat. #170-6404XTU), 10 mM Tris pH 7.4, 0.14 M NaCl, and 0.1% Tween 20. The membrane was incubated with Blotto solution for one hour at room temperature, followed by three washes of five minutes each in Tris buffered saline with 0.05% Tween 20 (TBS-T). The membrane was then incubated in a TBS-T solution with 5% nonfat dry milk and a dilution of an antibody against the FPGS protein at 4° C for ~16 hours. The membrane was washed for five minutes for a total of three times in TBS-T and was incubated for one hour at room temperature in a TBS-T solution containing 5% nonfat dry milk and a dilution of an antibody raised against the IgG of the organism in which the primary antibody was raised. This incubation was followed by three washes of five minutes each in TBS-T. Protein complexes were detected using a West-Dura chemiluminescent substrate kit (Pierce SuperSignal, cat. # 34075) that was incubated with the membrane in the dark and the protein complexes on the membrane were exposed and documented on X-ray film.

Two different antibodies were used in these studies; one was obtained from a group in Toronto (150) and the other was obtained from Lilly Research Laboratories (38). The Toronto antibody was raised in rabbit against a peptide from the human FPGS protein that corresponded to residues 275-290 and was used at a dilution of 1:500. The secondary antibody used with the Toronto antibody was raised in goat against rabbit IgG (Pierce ImmunoPure, cat. # 31462) and diluted at 1:7,500 in a solution of TBS-T with 5% nonfat dry milk. The antibody obtained from Lilly Research Laboratories is antibody 4-18 as referenced by Dotzlaf *et al.* (38). This antibody was raised in mouse against a peptide from human FPGS corresponding to residues 521-550 and recognizes the FPGS amino acid sequence RDPIFAPPSPP (38). The antibody obtained from Lilly Research Laboratories was diluted 1:600 in a TBS-T solution with 5% nonfat dry milk. The secondary antibody that was used to detect the Lilly antibody was raised in goat against mouse IgG (Pierce ImmunoPure, cat. # 31438) and diluted at 1:15,000 in a TBS-T solution with 5% nonfat dry milk.

Colony formation of AuxB1 cells transfected with fpgs cDNA constructs under doxycycline control and in the presence of various growth supplements

These studies were done by Ms. Guoyan Gao of this laboratory. Doxycycline was added to the cell culture media at the indicated concentrations 48 hours prior to the plating of cells. Cells were centrifuged, pelleted and resuspended in MEM-α media without purines, thymidine, or glycine, and supplemented with 10% dialyzed tetracycline-free FBS, 1% Pen/Strep, 500 µg/mL G418, and 200 µg/mL hygromycin. This was the basal

media (no additions) for this experiment. Cells were placed in 24-well plates with each well containing ~150 cells in the basal media as described above with the corresponding growth supplements and the indicated concentrations of doxycycline. Inosine was added to the medium of some cultures at 100 µM, thymidine at 5.6 µM, and glycine at 50 mg/L. Media was changed and fresh media containing identical supplementation was fed to the cells every other day for ~10 days. After 10 days, cells were washed twice with PBS, fixed to the plates with methanol, and stained with 5% Wright-Giemsa stain for visualization and colony counting. All visible colonies were manually counted and none were excluded based on size.

Pulse treatment with ^{3}H-6S-5-formyl-tetrahydrofolate and retention of folate polyglutamates in AuxB1 cells transfected with fpgs cDNA constructs under doxycycline control

This study was designed to follow the subcellular retention and distribution of folate polyglutamate molecules. A diagram of the experimental setup is included in the Results section of this chapter in Figure 3-5. [3', 5', 7, 9-^{3}H]-6S-5-formyl-tetrahydrofolate was obtained from Moravek Radiochemicals. All cells were grown at 37° C and 5% CO_2. CHO cells were included as a positive control in this experiment and were grown in a similar media as described below, but without G418 and hygromycin additions. Cells were plated 48 hours before time t = 0 hours in 100 mm dishes at 2 x 10^4 cells / dish in MEM-α media supplemented with 10% tetracycline-free FBS, 1% Pen/Strep, 500 µg/mL G418, and 200 µg/mL hygromycin. Also, 1 µg/mL of doxycycline was added to the indicated cells at

this time. Twenty-four hours prior to time t = 0 hours, media was removed and all cells were fed with 3.5 mL of RPMI 1640 folate-free media that was supplemented with 10% tetracycline-free FBS, 1% Pen/Strep, 500 µg/mL G418, 200 µg/mL hygromycin, and 1 µg/mL doxycycline where indicated. This media was also supplemented with 0.5 µM of ^{3}H-6S-5-formyl-tetrahydrofolate at 0.25 µCi/mL. The media containing the radiolabeled folate was incubated with the cells for a total of 24 hours. After 24 hours, the media containing the radiolabeled folate was removed, cells were washed with 10 mL of PBS, and the cells were fed with 10 mL of MEM-α media supplemented with 10% tetracycline-free FBS, 1% Pen/Strep, 500 µg/mL G418, 200 µg/mL hygromycin, and 1 µg/mL doxycycline where indicated. After this time (t = 0 hours), the cells were not exposed to any further isotope for the remainder of the study. Cells were harvested at 12 hour intervals after isotope exposure and the cytosolic and mitochondrial cell fractions were isolated as described above. However, after the final centrifugation step at 11,000 x g for 15 minutes a 4° C, cytosolic fractions containing cytosolic protein in homogenization solution were placed in pre-weighed tubes and total cytosolic volumes were estimated by the weight of the liquid in these tubes. A total of 1 mL of the cytosolic fraction was added to 20 mL glass scintillation vials. The mitochondrial pellet was dissolved in 500 µL of 75 mM NaOH, after which 500 µL of 100 mM HCl was added to neutralize the solution containing dissolved mitochondria. A total of 1 mL of the solution containing dissolved mitochondria was added to 20 mL glass scintillation vials. Vials containing the mitochondrial fractions then received 1 mL of homogenization solution and the vials containing the cytosolic fractions received 500 µL of 75 mM NaOH and 500 µL of 100

mM HCl so that all samples had exactly the same salt concentrations to simplify counting efficiency. The total sample volume in each scintillation vial was 2 mL, to which 18 mL of SafetySolve scintillation cocktail was added. The vials were then counted for radioactivity in a Beckman LS 6500 multi-purpose scintillation counter. Cells from replicate plates that had been identically treated, other than they were not exposed to radioactivity were counted for each experimental condition. Compartmental retention of ^{3}H-6S-5-formyl-tetrahydrofolate metabolites throughout the experiment was normalized to the initial cell number at time t = 0. Counts per minute, obtained from scintillation counting, were converted to fmoles of ^{3}H-6S-5-formyl-tetrahydrofolate metabolites by counting duplicate aliquots of the radiolabel-containing medium and dividing by the concentration of 5-formyl-tetrahydrofolate in the medium. Total fmoles of ^{3}H-6S-5-formyl-tetrahydrofolate metabolites retained in cells was obtained by adding the radioactivity detected in the cytosolic and mitochondrial compartments at each time point.

Supplemental rescue of antifolate toxicity in folate-depleted L1210 cells

L1210 cells are suspension cells that were routinely grown in RPMI 1640 media supplemented with 10% FBS. For folate depletion of L1210 cells, cells were grown in folate-free MEM media supplemented with 10% dialyzed FBS, 1% solution A (solution A = 2.5 g/L L-alanine, 5 g/L L-asparagine, 3 g/L L-aspartic acid, 10 g/L L-cysteine HCl-H_20, 7.5 g/L L-glutamic acid, 4 g/L L-proline, and 2.5 g/L L-serine), 1% solution B (solution B = 11 g/L sodium pyruvate, 20 mg/L lipoic acid, 5 g/L L-ascorbic acid, 10 mg/L biotin, and 0.14 g/L cyanocobalamin), 100 µM hypoxanthine, 5.6 µM thymidine, and 50 mg/L glycine

for at least three passages prior to experimental use. Under these growth conditions the folate content of the cells diminished to < 0.1%, but the cells were still healthy. For experimentation, folate-depleted cells were centrifuged and resuspended in fresh MEM media supplemented with 10% dialyzed FBS, 1% solution A, 1% solution B, 20 mM HEPES and 10 mM MOPS at a pH of 7.4, and growth supplements where indicated. The concentrations of these supplements were 100 µM hypoxanthine, 5.6 µM thymidine, and 50 mg/L glycine. Cells were added to the wells of 24 well plates containing folic acid and drug for a final volume of 1.5 mL and at a final concentration of ~3 x 10^4 cells / mL, 2.28 µM folic acid and the indicated antifolate concentrations. Cells were incubated for 72 hours at 37° C and 5% CO_2, after which 1 mL of the cell suspension was counted twice and the average cell number recorded. Cell growth in the presence of drug is expressed as a percentage of the growth of untreated cells and each data point represents duplicate samples.

Uptake of ^{3}H-6S-5-formyl-tetrahydrofolate in isolated mitochondria

Mitochondria from CHO and glyB cells growing in ten 150 mm dishes were isolated as previously described. However, after the final centrifugation step at 11,000 x g for 15 minutes at 4° C, the mitochondrial pellet was resuspended in a mitochondrial isolation buffer containing 300 mM trehalose, 10 mM HEPES, 10 mM KCl, 0.1 g / 100 mL bovine serum albumin, 1 mM EGTA, 1 mM EDTA, and 2 mM ADP at a pH of 7.4; 50 µL of this solution containing mitochondria was added to experimental tubes. The tubes were placed in a shaking water bath at 37° C for 3 minutes. Transport in isolated

mitochondria was initiated by the additional of 50 µL of a solution containing ^{3}H-6S-5-formyl-tetrahydrofolate. The final transport solution contained 100 µL of isolated mitochondria, 1.5 µM 6S-5-formyl-tetrahydrofolate at 7.5 µCi/mL, 300 mM trehalose, 10 mM HEPES, 10 mM KCl, 0.1 g / 100 mL bovine serum albumin, 1 mM EGTA, 1 mM EDTA, 2 mM ADP, 2 mM ATP, 5 mM succinate, 10 mM creatine phosphate, and 100 µg/mL creatine kinase. Transport was stopped by the timed addition of 10 mL of ice-cold homogenization solution. Samples were then loaded onto 0.45 μm HA membrane filters (Millipore, cat. # HAWP02500) in a vacuum manifold and a vacuum was applied to pull liquid through the filters. The filters were then washed three times with 10 mL of ice-cold homogenization solution. The filters were removed from the vacuum manifold and placed in 1 mL of 75 mM NaOH in 20 mL glass scintillation vials for ~16 hours, after which 1 mL of 100 mM HCl and 15 mL of SafetySolve scintillation fluid were added and the samples were counted for radioactivity in a scintillation counter. The error bars in the presented experiment represent the range of two duplicate samples from a single experiment.

Uptake of ^{3}H-5-formyl-tetrahydrofolate was also examined in isolated CHO mitochondria in the presence of 5 µM of various folate analogs. Uptake in isolated mitochondria from glyB cells was included as a negative control in this experiment. The design of this experiment was identical to the experiment in mitochondria isolated from CHO and glyB cells as described above. Uptake was permitted for three minutes in all samples after which 10 mL of ice-cold homogenization solution was added to the experimental tubes to stop any further mitochondrial uptake. Samples were processed as

previously described and the error bars in the presented experiment represent the range of two duplicate samples from a single experiment.

G418 toxicity in L1210 cells

L1210 cells were plated in 24-well plates at densities ranging from 3.3 x 10^2 cells / mL to 1 x 10^6 cells / mL in RPMI 1640 media supplemented with 10% dialyzed FBS, 1% Pen/Strep, 20 mM HEPES, 10 mM MOPS, and 10 µM 2-mercaptoethanol. Each density of L1210 cells was exposed to different concentrations of G418. The concentrations were 0, 250, 500, 750, 1250, and 2000 µg/mL of G418. The growth of G418-treated L1210 cells was followed over the course of 11 days and the media was not changed over this time course. Cell growth estimates were based on subjective estimates of well confluence after daily visualization of the cells under a microscope.

Addition of a $His^{(6)}$ tag to the CHO MFT and cloning into the pcDNA 3.1(-) mammalian expression vector

The CHO MFT was previously cloned into a mammalian expression vector with an N-terminal *myc* tag (129). For purification, a His tag was added to the C-terminal end of the *mft* cDNA that encoded six tandem histidine residues immediately followed by a stop codon. This was accomplished in two successive PCR reactions. Each PCR reaction used the same vector-specific forward primer that was located upstream of a *Xho*I restriction site and the 5' *mft* start codon. In the first PCR, the 3' reverse primer added six His codons (CAC) immediately followed by a stop codon. This product was electrophoresed on a 1%

agarose gel containing ethidium bromide, extracted from the gel and purified using a Promega Wizard SV gel and PCR clean up system kit. The reverse primer in the second reaction recognized the sequence added by the first primer and added 6 base pairs, a *Hin*dIII restriction site, and another 3 base pairs. This PCR product was electrophoresed, visualized and purified identical to the first PCR reaction. This final PCR product and pcDNA 3.1(-) were digested using *Xho*I and *Hin*dIII, the digested products were ligated together, cloned into TOP10 cells, and the vector was purified from a transformed TOP10 clone and sequenced as described in Chapter Two.

Transfection of L1210 cells with the CHO MFT in pcDNA 3.1(-) and selection of clones

L1210 cells were transfected using the Nucleofector II device (Amaxa) following the manufacturer's specifications. A cell line optimization nucleofector kit (Amaxa, cat. #VC0-1001) was obtained for nucleofection of L1210 cells. For transfection, 3 x 10^6 actively growing L1210 cells were centrifuged and the cell pellet was resuspended in 105 µL of pre-warmed nucleofector solution V. The cell solution then received 3 µg of purified plasmid, either pmaxGFP (contained in optimization kit) or pcDNA 3.1(-), which contained the CHO *mft* with an N-terminal *myc* tag and a C-terminal $His^{(6)}$ tag. From this solution, 100 µL was added into an Amaxa certified cuvette that was provided in the optimization kit and was compatible with the Nucleofector II device. This cuvette was inserted into the Nucleofector II device and nucleofection proceeded using the S-018 program in the device. After nucleofection, 500 µL of pre-warmed RPMI 1640 supplemented with 10% FBS and 1% Pen/Strep was added to the cells. The cells were

removed from the cuvette using a plastic pipet and transferred into a single well in a 12-well plate in a total volume of 1.6 mL of RPMI 1640 supplemented with 10% FBS and 1% Pen/Strep. The cells were incubated at 37° C and 5% CO_2 for 24 hours. L1210 cells that were transfected with 3 µg of the pmaxGFP construct were visualized 24 hours after nucleofection using a fluorescent microscope and the captured images are presented with and without fluorescent exposure. L1210 cells that were transfected with the CHO *mft* in pcDNA 3.1(-) were collected by centrifugation 24 hours after nucleofection and resuspended at 28,000 cells / mL in RPMI 1640 supplemented with 10% FBS, 1% Pen/Strep, 20 mM HEPES, 10 mM MOPS, 10 µM 2-mercaptoethanol, and 500 µg/mL G418. Media was removed and fresh media was added every other day for 18 days.

Some L1210 cells were able to grow and survive in the presence of 500 µg/mL of G418; this population became evident after 18 days of G418 selection. These cells were centrifuged and resuspended in selective media (RPMI 1640 supplemented with 10% FBS, 1% Pen/Strep, 20 mM HEPES, 10 mM MOPS, 10 µM 2-mercaptoethanol, and 500 µg/mL G418) at a density of 0.5 cells / mL; 200 µL of this cell suspension was plated in individual wells in a 96-well plate to isolate clones from this population. After 7 days, six wells were observed to contain an actively growing L1210 cell population. The cells in these wells were expanded and examined for MFT expression.

Isolation of mitochondrial protein from transfected L1210 cells

Transfected L1210 cells were routinely grown in selective media (RPMI 1640 supplemented with 10% FBS, 1% Pen/Strep, and 500 µg/mL G418). Mitochondrial protein

was isolated from these cells using dounce homogenization and differential centrifugation as described in Chapter Two, except that L1210 cells grow in suspension, so that removal of adherent cells from dishes by scraping was not necessary. The concentration of isolated mitochondrial protein from each L1210 cell clone was determined using the Bradford reagent.

Detection of CHO myc-MFT expression in transfected L1210 cells by western blotting

Tubes containing 40 µg of mitochondrial protein were immersed in boiling water for 5 minutes so that the volume in the tube was covered by water and then loaded into a freshly made 12.5% SDS-PAGE gel. The gel was electrophoresed in a buffer containing 192 mM glycine, 25 mM Tris, and 0.1% SDS, pH 8.3. The protein contents in the gel were transferred to a PVDF membrane in a buffer containing 192 mM glycine and 25 mM Tris, pH 8.3 at 100 V for 45 minutes. After the transfer of proteins to the PVDF membrane, non-specific protein binding to the membrane was blocked using Blotto blocking solution containing 5% nonfat dry milk, 10 mM Tris pH 7.4, 0.14 M NaCl, and 0.1% Tween 20. The membrane was incubated with Blotto for one hour at room temperature, followed by three washes of five minutes each in Tris buffered saline with 0.05% Tween 20 (TBS-T). After these washes, the membrane was incubated with a rabbit anti-*myc* antibody (Sigma, cat. #C3956) at a dilution of 1:2000 in a TBS-T solution with 5% nonfat dry milk for 16 hours at 4°C. The membrane was washed three times for 15 minutes each in TBS-T and incubated with a peroxidase conjugated goat anti-rabbit IgG antibody (Thermo Fisher Scientific, cat. #31462) diluted to 1:10,000 in a TBS-T solution

with 5% nonfat dry milk, for one hour at 25° C. Incubation with this secondary antibody was followed by three washes of 15 minutes in TBS-T. Protein complexes were detected using a West-Dura chemiluminescent substrate kit (Pierce SuperSignal, cat. # 34075) that was incubated with the membrane in the dark and the protein complexes on the membrane were exposed and documented on X-ray film. Mitochondrial protein isolated from untransfected L1210 cells was included as a negative control.

Purification of CHO MFT from a transfected L1210 clone

Clone #4 from the above transfection was selected for expansion and purification based on the high level of MFT expression that was detected by western blotting. Before expansion and purification, these cells were adapted to grow in 5% FBS instead of 10% FBS over the course of seven days in the selective media (RPMI 1640 supplemented with 5% FBS, 1% Pen/Strep, and 500 µg/mL G418). These cells were routinely grown at densities between 1 x 10^5 cells / mL and 2 x 10^6 cells / mL in selective media. Two 3 L spinner flasks were used to culture ~1.5 L of L1210 cells, equally divided between the two flasks. Cells were centrifuged at 1,000 x g for 15 minutes at 4° C. The cell pellet was resuspended in 7.5 mL of homogenization solution with added EDTA-free protease inhibitors (Roche, cat. #11873580001). Cells were broken open with 25 strokes in a 7.5 mL dounce homogenizer with a "B" pestle, followed by centrifugation at 1,000 x g for 5 minutes and collection of the post-nuclear supernatant. The pellet was resuspended in 7.5 mL homogenization solution and received an additional 25 strokes in a 7.5 mL dounce homogenizer. This procedure was repeated for a total of 100 strokes of dounce

homogenization and a total volume of 30 mL of post-nuclear supernatant. The pellet that remained after four cycles of dounce homogenization and centrifugation was collected, dissolved in lysis buffer and represents the nuclear fraction in the purification table and western blots. The pooled post-nuclear supernatants from dounce homogenization were centrifuged at 1,000 x g for 5 minutes at 4° C, the supernatant was collected and centrifuged at 10,000 x g for 15 minutes at 4° C. The supernatant was collected into a pre-weighed tube and the volume was estimated based on the weight of the supernatant liquid. A portion of this fraction was subjected to protein precipitation with TCA as previously described and represents the cytosolic fraction in the purification table and western blots. Mitochondria were contained in the pellet, and the pellet was resuspended in a buffer containing 1% 3-laurylamido-N,N'-dimethylpropyl amine oxide (LAPAO) (85), 0.1 M $NaSO_4$, 10 mM Tricine-KOH, 1 mM EDTA pH 7.5, and protease inhibitors (Roche, cat. #11873580001). Solubilization of mitochondria in this buffer occurred for 30 minutes at 0° C with gentle mixing by a magnetic flea. After 30 minutes, this solution was centrifuged at 15,000 x g for 15 minutes at 4° C. The pellet was collected, dissolved in lysis buffer and represents the LAPAO insoluble fraction in the purification table and western blots. The supernatant (LAPAO soluble fraction) was collected and batch purified by the addition of a slurry of hydroxyapatite resin with an equal amount (w/v) of a buffer containing 1% LAPAO, 10 mM MOPS and 100 mM NaCl, pH 7.2. This slurry was placed on a rotational shaker at 4° C for 30 minutes and centrifuged at 15,000 x g for 15 minutes at 4° C. The supernatant contained proteins that were not bound to hydroxyapatite (hydroxyapatite unbound fraction) and was collected for further purification by a talon

metal-affinity column (Clontech, cat. #635501). The hydroxyapatite resin with bound proteins was then resuspended in an equal volume of a buffer containing 1% LAPAO, 10 mM MOPS and 100 mM NaCl, and 1 M KHPO4, agitated and centrifuged as above, and the collected supernatant represents the hydroxyapatite eluate fraction in the purification table and western blots. The hydroxyapatite unbound fraction was run over a talon metal-affinity column that was prepared with 1 mL of packed resin volume in a buffer containing 1% LAPAO, 100 mM NaCl, and 50 mM $NaHPO_4$, pH 7.0. Once the hydroxyapatite unbound fraction was loaded onto the talon column, fractions were collected every 30 seconds, each with a volume of ~1 mL. The column was then washed three times with five bed volumes each of a buffer containing 1% LAPAO, 100 mM NaCl, and 50 mM $NaHPO_4$, pH 7.0 and fractions were collected every 30 seconds. After three column washes, five bed volumes of a buffer containing 1% LAPAO, 100 mM NaCl, 50 mM $NaHPO_4$, and 5-10 mM imidazole (10 mM imidazole in the first purification and 5 mM imidazole in the second purification), pH 7.0 was run over the column and fractions were collected every 10 seconds for the first 30 seconds and then every 30 seconds thereafter. A final elution buffer containing 1% LAPAO, 100 mM NaCl, 50 mM $NaHPO_4$, and 150 mM imidazole, pH 7.0 was run over the column and fractions were collected every 10 seconds for the first 30 seconds and then every 30 seconds thereafter. Small aliquots were collected from each step throughout the purification process and dissolved in lysis buffer for further analysis of protein concentration and western blotting. Protein concentrations from representative portions that were collected throughout the purification process, but not fractions collected from the talon column, were determined using the Bradford reagent.

Protein concentrations in fractions obtained from the talon column were determined by absorbance at 280 nm, assuming a solution with A280 = 1.00 has 1 mg/mL protein.

Detection of the CHO MFT in purification fractions

The CHO *myc*-MFT was detected by western blotting as previously described. All western blots used fractions collected from the first of the two purification attempts. Each lane was loaded with 40 µg of protein when available. The protein concentrations in the collected fractions from the talon column were not determined. Talon column fractions from each wash or elution, typically 5 bed volumes (5 mL), were pooled together and TCA precipitated with 6% TCA as previously described and ~25% of the total fraction was loaded into the gel.

The fractions collected from the talon column in the second CHO MFT purification attempt were TCA precipitated and ~50% of the total fraction volume was loaded into a freshly prepared 12.5% SDS-PAGE gel that was electrophoresed in a buffer containing 192 mM glycine, 25 mM Tris, and 0.1% SDS, pH 8.3. Following electrophoresis, the gel was washed three times in ~200 mL of 18.2 mΩ H_2O for 15 minutes each and then incubated with ~25 mL of Bio-Safe coomassie stain (Bio-Rad, cat. #161-0786) for one hour with gentle agitation. The gel was then incubated with ~200 mL of 18.2 mΩ H_2O for ~16 hours. Water was changed and a fresh 200 mL of 18.2 mΩ H_2O was added every hour for the first four hours of this 16 hours incubation.

RESULTS

I. Interplay between FPGS isoforms, folate polyglutamates and the MFT in the compartmentalization folate metabolism

Analysis of doxycycline-inducible FPGS expression in AuxB1 transfectants

AuxB1 cells do not express any functional FPGS protein and therefore require exogenous supplies of purines, thymidine and glycine for growth and survival. This cell line provides an excellent system for studying the cellular and compartmental requirements of the FPGS protein. Cells were transfected with either a cDNA encoding the full-length *fpgs* with an endogenous mitochondrial leader peptide (mFPGS) or a cDNA that did not contain this leader peptide and encoded a protein thought to strictly localize to the cytosolic compartment (cFPGS). The cDNA constructs were transfected into the AuxB1 cells under the control of a doxycycline-inducible promoter. It was necessary to first understand the process of FPGS expression induced by doxycycline. The stably generated cell lines transfected with either the mitochondrial *fpgs* cDNA (mFPGS) or the cytosolic isoform of FPGS (cFPGS) were induced with 1 μg/mL of doxycycline and probed for FPGS expression (Figure 3-2A). In both cell lines, it appeared that FPGS was not expressed in the absence of doxycycline. In the presence of doxycycline, there was robust expression of FPGS in both cell lines. This expression level appeared greater than FPGS expression levels in other cultured, but not transfected, cell lines: a human leukemic cell line (CEM), a colon carcinoma cell line (HCT116), and lung cancer cell (H460).

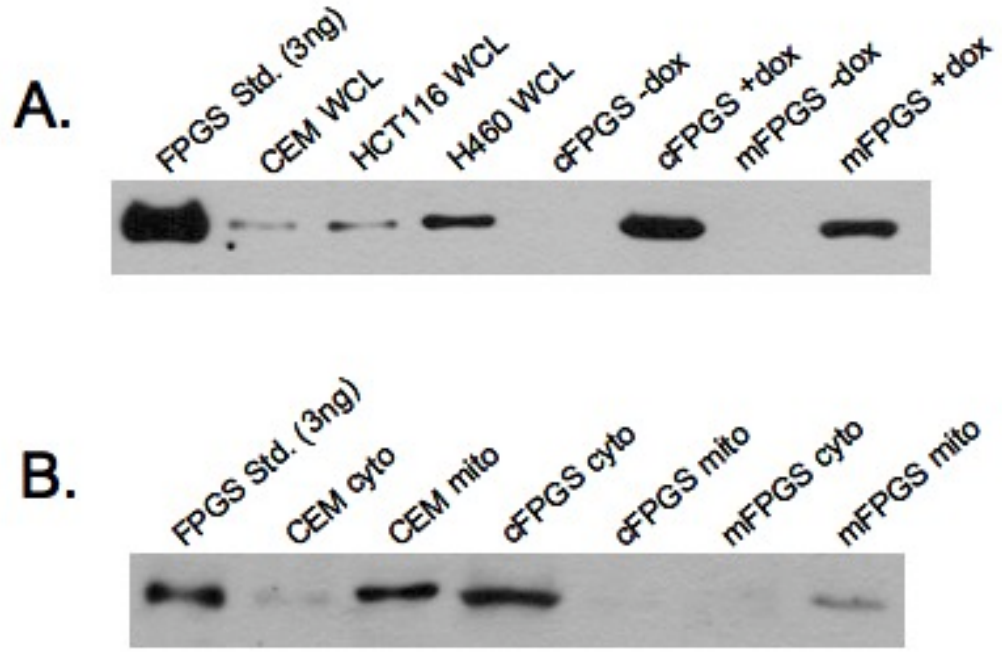

Figure 3-2 Detection of FPGS expression by western blotting. A. Detection of FPGS in 30 µg of whole cell lysates in CEM, HCT116, and H460 human cancer cell lines and in AuxB1 cells transfected with cytosolic (cFPGS) and mitochondrial (mFPGS) *fpgs* cDNA. Whole cell lysates were collected from cFPGS and mFPGS cells in the presence (+dox) and absence (-dox) of 1 µg/mL doxycycline. Purified human cytosolic FPGS (3 ng) is included as a positive control. B. Cytosolic and mitochondrial localization of the FPGS protein in CEM cells and in cFPGS and mFPGS cells in the presence of 1 µg/mL doxycycline. Lanes were loaded with 30 µg of total cytosolic protein and 10 µg of total mitochondrial protein. Blots in both A. and B. were probed with the FPGS antibody from Sohn *et al.* (2004).

Nonetheless, it appeared that the expression of FPGS in these transfected cell lines was inducible with doxycycline without any detectable basal expression in the absence of doxycycline.

It was then necessary to probe the compartmental expression of these doxycycline-inducible isoforms of FPGS. It is important to understand that the mitochondrial *fpgs* cDNA still contained an intact translational start site for the cytosolic isoform of FPGS that could theoretically be used to translate the cytosolic protein (Figure 3-1). We used doxycycline to induce FPGS expression in both constructed cell lines and examined the compartmental localization of the FPGS protein (Figure 3-2B). The first few experiments that examined the subcellular location of FPGS in these cells suggested that the FPGS protein was expressed in the intended compartment when expression was induced with doxycycline; the cytosolic construct resulted in FPGS expression that was only detected in the cytosol and the full-length mitochondrial construct resulted in FPGS expression that was only observed in the mitochondrial fraction. The controllable and compartmental expression of the FPGS protein in these cell lines appeared to make them ideal constructs to separate the contributions of these compartmentalized FPGS isoforms to cellular folate metabolism. However, later experiments indicated that a small amount of FPGS was present in the cytosolic compartment of the mFPGS cells (see below).

The dose-responsive nature of this doxycycline-dependent expression was also investigated. This system was originally selected for use based on its control over protein expression, a desirable feature when attempting to examine exogenous protein expression near endogenous levels. FPGS expression in both mFPGS and mutFPGS constructs varied

with doxycycline concentrations (Figure 3-3), indicating control over the amount of FPGS protein that was expressed. Interestingly and centrally important to this project, cytosolic FPGS was detected in both mFPGS and mutFPGS cell lines at increasing exposures. The cDNA for the mutFPGS construct contained the upstream ATG and the endogenous mitochondrial leader peptide, but mutated the downstream ATG to ATT. This construct was designed to control for the possible translational use of the downstream start codon in the mFPGS construct. Therefore, this mutFPGS construct was thought to encode only a mitochondrial FPGS protein. Because no cytosolic FPGS protein should be made from the mutFPGS cDNA construct, we believe this data suggests that import of the FPGS protein into mitochondria can become a limiting factor in these experiments.

Both FPGS isoforms appear to be required for cell survival

Deficiencies in cellular folate metabolism manifest as auxotrophic phenotypes in cells and the complementation of these phenotypes can be used to understand the reactions and requirements of cellular folate metabolism. Various concentrations of doxycycline were used to induce FPGS expression in AuxB1 cells stably transfected with the three *fpgs* cDNA constructs (cFPGS, mFPGS, and mutFPGS) and the growth requirements of these cell lines were studied (Figure 3-4). Basal medium supplemented with inosine, as a source of purines, thymidine and glycine permitted the survival of AuxB1 cells transfected with all three constructs at all doxycycline concentrations. This was expected as AuxB1 cells survive without any FPGS protein when given these supplements. It also indicated that concentrations of doxycycline up to 2 μg/mL did not significantly effect AuxB1 colony

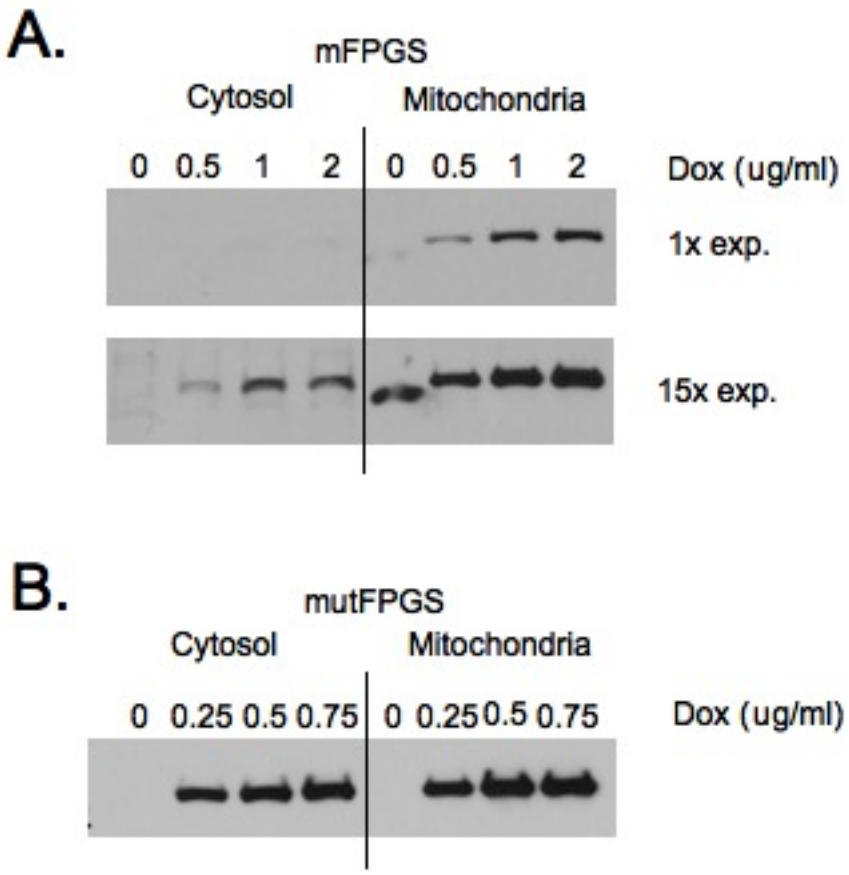

Figure 3-3 Doxycycline-dependent expression of FPGS in the cytosolic and mitochondrial compartments of mFPGS and mutFPGS transfected AuxB1 cells. A. FPGS expression in the cytosol and mitochondria of mFPGS transfected AuxB1 cells as a function of doxycycline concentration. Lanes were loaded with 32 µg of cytosolic protein and 16 µg of mitochondrial protein. A short exposure (1X) and a longer exposure (15X) are shown. The long exposure was exposed to film 15 times longer than the short exposure. B. FPGS expression in the cytosol and mitochondria of mutFPGS transfected AuxB1 cells as a function of doxycycline concentration. Lanes were loaded with 32 µg of cytosolic protein and 16 µg of mitochondrial protein. Blots in both A. and B. were probed with the FPGS antibody from Lilly Research Laboratories.

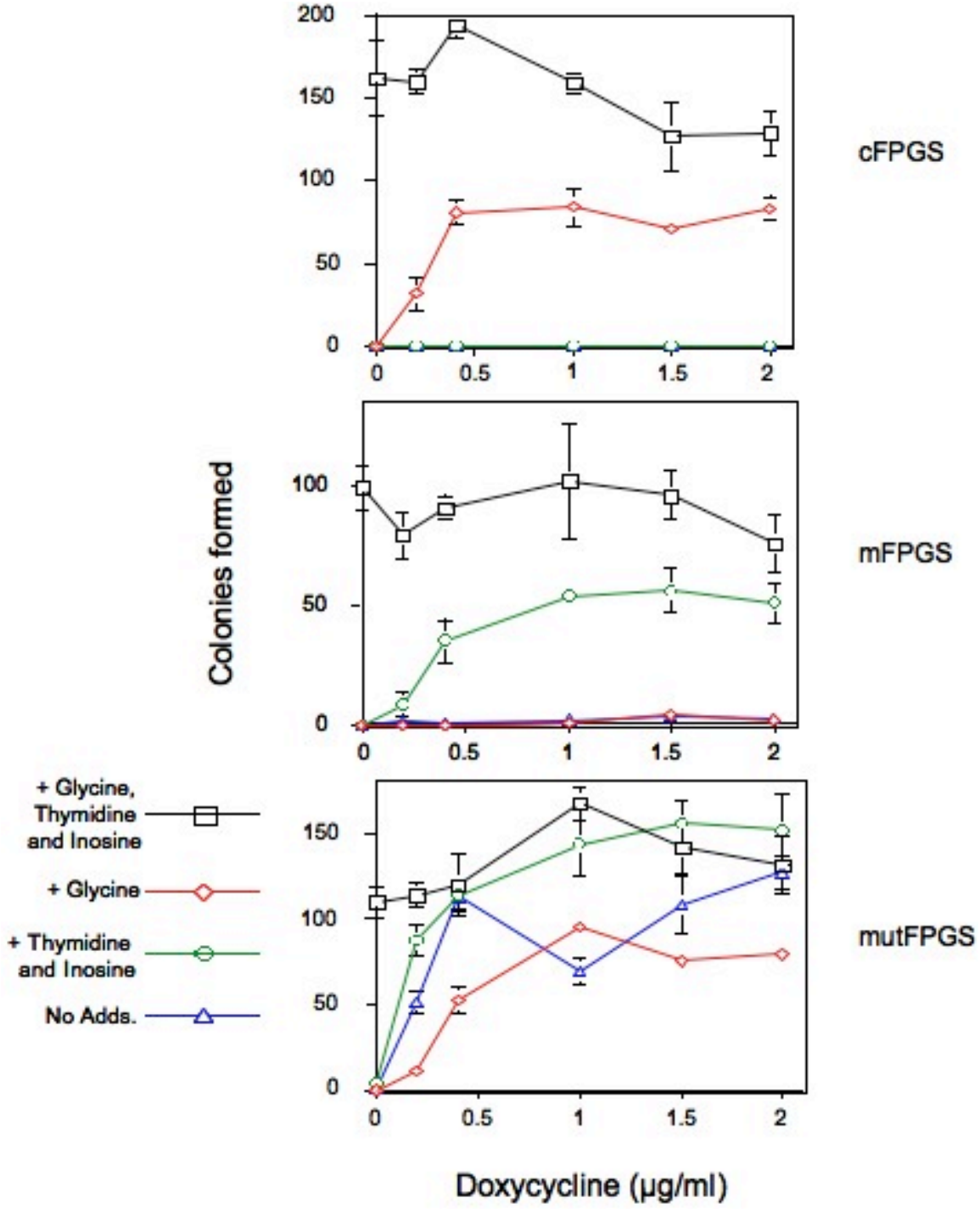

Figure 3-4 Growth requirements of AuxB1 cells transfected with FPGS constructs. Colony formation of cFPGS, mFPGS and mutFPGS cell lines in the presence of different growth supplements and at various doxycycline concentrations. Black lines with open squares represent colonies formed with inosine, thymidine, and glycine supplementation, green lines with open circles represent colonies formed with inosine and thymidine supplementation, red lines with open diamonds represent colonies formed with glycine supplementation, and blue lines with open triangles represent colonies formed with no supplementations. This experiment was performed by Ms. Guoyan Gao.

formation. None of the AuxB1 transfectants were able to survive without inosine, thymidine, and glycine supplementation in the absence of doxycycline, consistent with the western blots that indicated FPGS expression is dependent on doxycycline. AuxB1 cells transfected with cFPGS were able to survive when supplemented with glycine at doxycycline concentrations $\geq$ 0.5 µg/mL. This indicates that the cytosolic expression of FPGS supplies sufficient folates for the production of purines and thymidine in the cytosol, but these cells are deficient in folate-dependent glycine production, a function assigned to mitochondria. Conversely, AuxB1 cells transfected with mFPGS required exogenous thymidine and purines for survival, suggesting that these cells were deficient in cytosolic folate metabolism. This effect was observed in spite of the small amount of FPGS that was detected in the cytosol of this cell line. The level of cytosolic FPGS expression was apparently insufficient to sustain optimal cytosolic folate metabolism. However, it was noted that small colonies formed in plates of mFPGS transfectants without any supplementations when treated with 1 µg/mL doxycycline, possibly related to the low level of FPGS protein detected in the cytosol of this cell line. AuxB1 cells transfected with the mutFPGS construct were able to form colonies without any supplementations when in the presence of doxycycline. This can be explained by the detection of a substantial amount of FPGS in both cytosolic and mitochondrial compartments at low doxycycline concentrations in this cell line.

Intracellular retention and distribution of folates in doxycycline-inducible cell lines

The colony formation assay (above) indicated that cells expressing the mitochondrial isoform of FPGS contained, at the least, diminished cytosolic folate pools as evidenced by their requirement for exogenous supplies of purines and thymidine. We then wanted to directly address the intracellular distribution of folates in these stably transfected cell lines. An experiment was designed to incubate cells with ^{3}H-6S-5-formyl-tetrahydrofolate for 24 hours (t = -24 to 0), after which cells were not exposed to the isotope again (Figure 3-5). The cytosolic and mitochondrial compartments were isolated from the exposed cells at various time intervals up to 48 hours after this treatment with ^{3}H-6S-5-formyl-tetrahydrofolate and examined for radioactive content. It was assumed that only the subcellular compartments that contained the FPGS protein would be able to retain labeled folates and that labeled folates could not be retained in compartments that were devoid of FPGS activity. The total amount of radiolabeled folates that were present in all experimental cell lines immediately after pulse treatment (time = 0 hours) was the same as the amount present 48 hours after pulse treatment (Figure 3-6), indicating a long term retention of intracellular folate polyglutamates. CHO cells, the parental cell line of AuxB1 cells, contain FPGS in both compartments and retained radiolabeled folates in the cytosolic and mitochondrial compartments throughout the experimental time course. AuxB1 cell lines stably transfected with mFPGS or cFPGS were unable to accumulate any folates in either compartment in the absence of doxycycline. This is consistent with the finding that these cell lines do not express any FPGS in the absence of doxycycline. In the presence of doxycycline, differences were observed in the mitochondrial retention of folates between

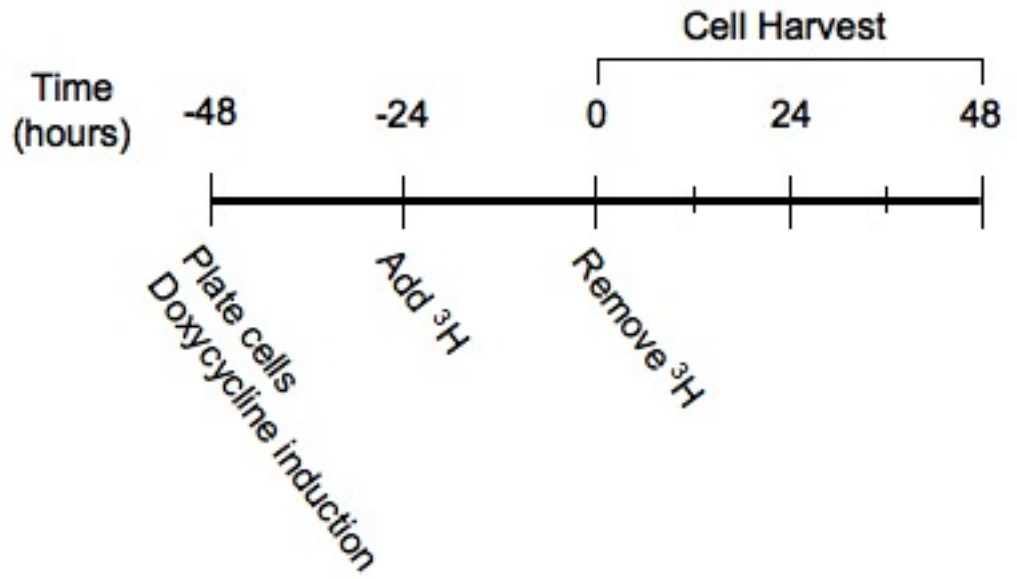

Figure 3-5 Experimental setup of assay following the intracellular retention and distribution of folates in doxycycline-inducible cell lines. Cells were plated at t = -48 hours and 1 µg/mL doxycycline was added to the indicated cell lines to induce FPGS expression. Doxycycline was present in the media for the duration of the experiment. At t = -24 hours, media containing 0.5 µM ^{3}H-6S-5-formyl-tetrahydrofolate at 0.25 µCi/mL, as the only folate source, was added to the cells. Cells were exposed to ^{3}H-6S-5-formyl-tetrahydrofolate for 24 hours, after which the label was removed (t = 0 hours), cells were thoroughly washed to remove any residual media containing the radiolabel, and normal growth media was added was to the cells. After t = 0 hours, cells were not exposed any further isotope. Cells were harvested at t = 0 hours and every 12 hours thereafter. The cytosolic and mitochondrial compartments were isolated from each cell line and the radioactive content in each subcellular fraction was determined.

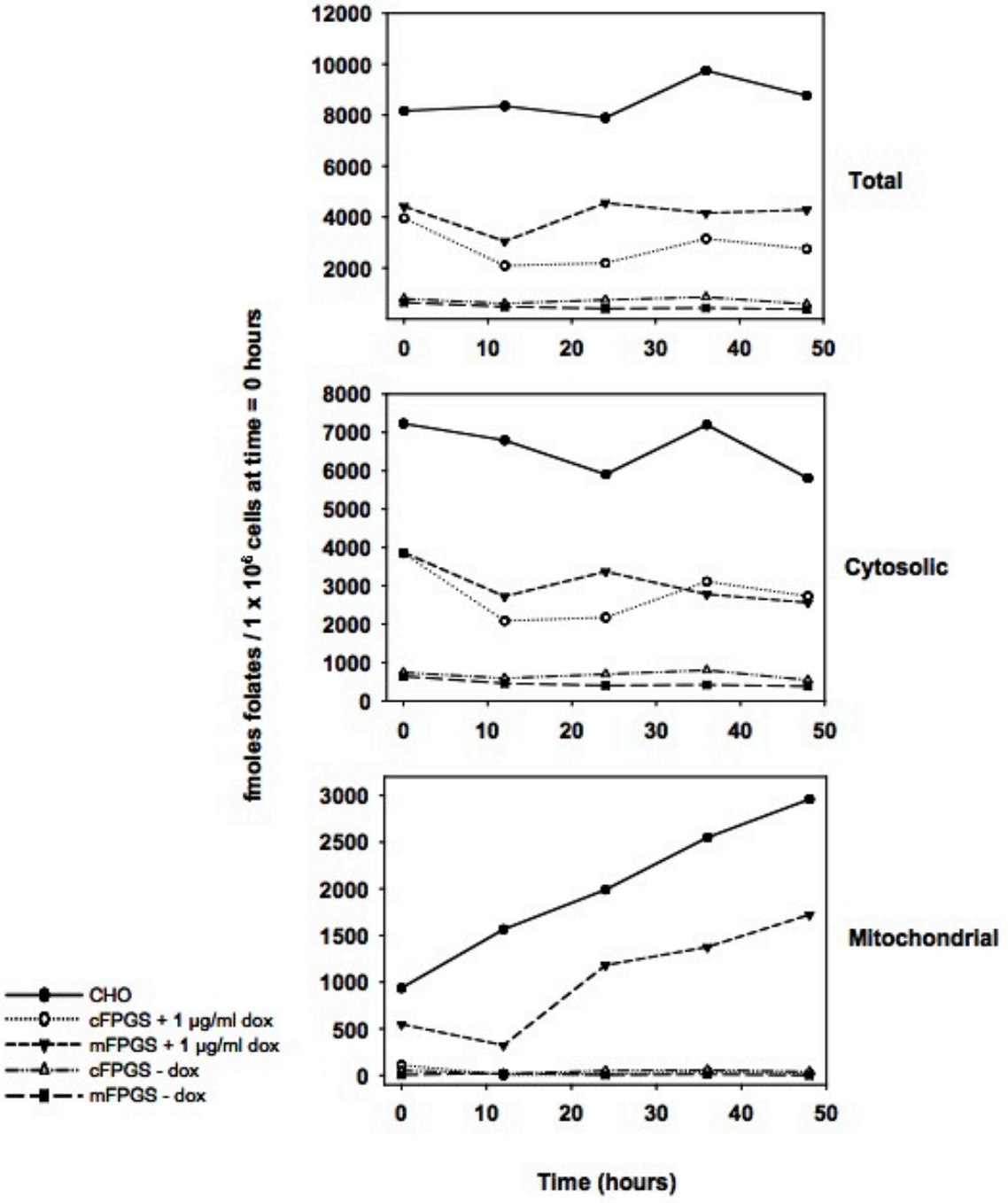

Figure 3-6 Compartmental retention and distribution of folates in AuxB1 cells transfected with *fpgs* cDNA constructs. FPGS expression was induced in cFPGS and mFPGS cell lines with 1 µg/mL doxycycline 48 hours prior to time t = 0 hours. Cells were incubated with 0.5 µM ^{3}H-6S-5-formyl-tetrahydrofolate at 0.25 µCi/mL 24 hours prior to t = 0. Radiolabeled 5-formyl-tetrahydrofolate was removed at time t = 0 hours and cells were not exposed any additional radioactivity after time t = 0. Cells were collected at time t = 0 and every 12 hours thereafter for a total of 48 hours. The cytosolic and mitochondrial cell fractions were collected at each time point and the radioactive content in these fractions was determined. The radioactive content in each subcellular compartment was normalized to the number of cells on replicate plates at time t = 0 hours.

the cFPGS and mFPGS cell lines; only the mFPGS cell line was able to retain mitochondrial folates. Not only were folates able to be retained in mitochondria of the mFPGS cell line, but these metabolites also accumulated in this organelle. This was also observed in mitochondria of CHO cells and presumably reflects mitochondrial retention of folate polyglutamates, suggesting that mitochondrial folates do not efflux into the cytosol from the mitochondrial matrix. In addition, no mitochondrial folates were observed in mitochondria of the cFPGS cell line, despite the establishment of a cytosolic folate pool in the cFPGS cell line. We believe this cytosolic folate pool is strictly polyglutamated folate metabolites; this strongly suggests that polyglutamated folates are not transported into mitochondria by the MFT. Interestingly, in the presence of doxycycline, both cell lines appeared to form and retain folate polyglutamates in the cytosol to the same extent. We previously showed that the mFPGS cell line contained some FPGS protein in the cytosol (Figure 3-3) and had expected some level of cytosolic folate retention in this compartment. However, because the mFPGS cell line still required exogenous purines and thymidine for full survival in a colony formation assay (Figure 3-4), we thought the cytosolic folate pools would be reduced. Both cFPGS and mFPGS cell lines appear to retain the same amount of cytosolic folates, yet only the mFPGS cell line remains auxotrophic for purines and thymidine. This interesting combination of data is considered in the Discussion section of this chapter.

II. Effects of folate analogs on mitochondrial folate transport

Secondary glycine toxicity is observed during antifolate treatment of folate-depleted L1210 cells

Due to structural similarities, folate analogs may be substrates for, or inhibitors of, the MFT. Given that we knew inhibition of mitochondrial folate transport would create a cellular dependence on glycine, the possibility of folate analogs interfering with normal mitochondrial folate transport was examined by cell growth and complementation of drug-induced auxotrophic phenotypes. Folate-depleted L1210 cells were treated with various concentrations of folate analogs. At each concentration, cells received different supplementations to alleviate any drug-induced phenotype. Without any supplementation, pemetrexed rapidly killed folate-depleted L1210 cells, a mouse leukemia cell line, with an IC_{50} of ~20 nM (Figure 3-7, closed circles). The primary target of pemetrexed is thymidylate synthase (153). Hence, it was expected that an exogenous supply of thymidine could restore growth and alleviate the inhibition of thymidylate synthase in pemetrexed-treated cells. When thymidine is provided to pemetrexed-treated L1210 cells, it relieves the effects from thymidylate synthase inhibition and increases the IC_{50} of pemetrexed in folate depleted L1210 cells to 100 nM (Figure 3-7, open circles). Pemetrexed, to a lesser extent than thymidylate synthase, also inhibits aminoimidazole carboxamide ribonucleotide formyltransferase (AICARFT), an enzyme in *de novo* purine synthesis (139). If both thymidine and hypoxanthine are provided to pemetrexed-treated, folate-depleted L1210 cells, pemetrexed should not incur any toxicity in L1210 cells as

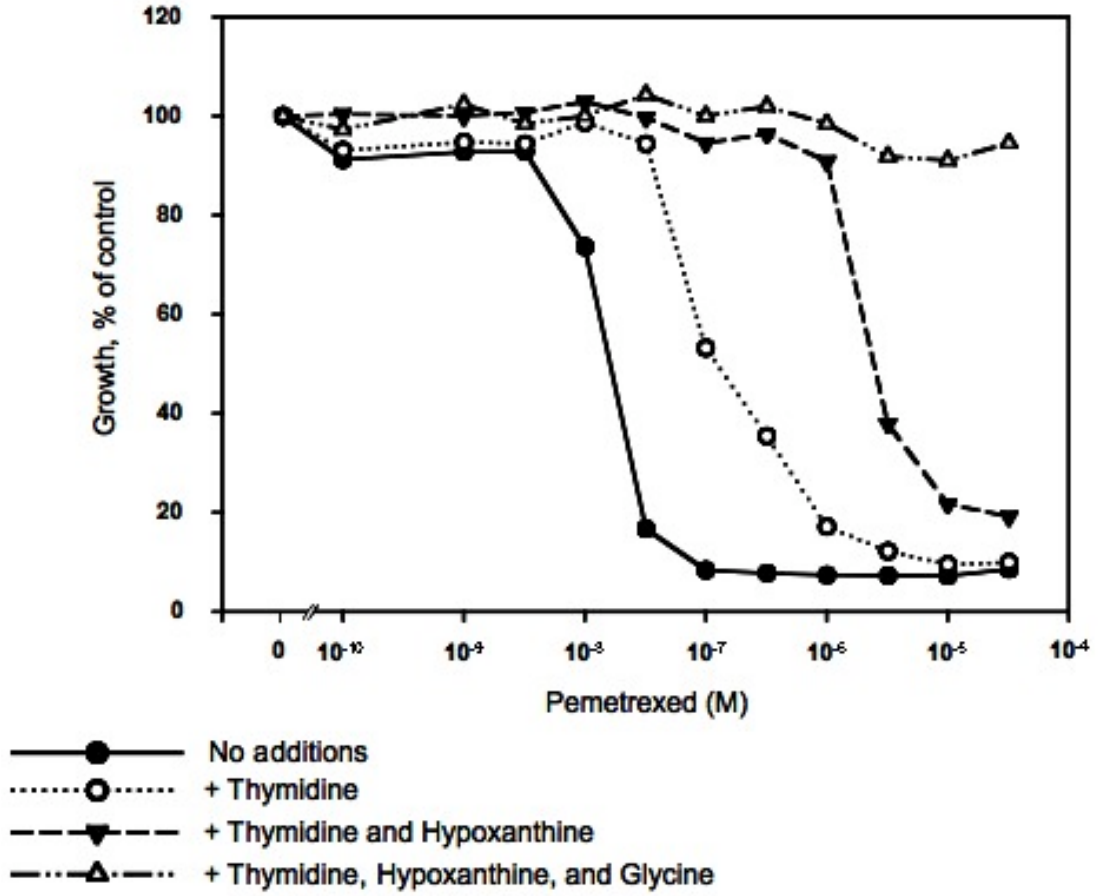

Figure 3-7 Underlying glycine toxicity in folate-depleted L1210 cells treated with pemetrexed. L1210 cells depleted of folates were treated with various concentrations of pemetrexed. Across these pemetrexed concentrations, supplements were provided to alleviate pemetrexed inhibition of intracellular targets. Concentrations of these rescue agents were 100 µM hypoxanthine, 5.6 µM thymidine, and 50 mg/L glycine. Data is expressed as a percentage of cell growth compared to untreated (control) cells.

supplementation with hypoxanthine and thymidine relieves the L1210 cell requirement for cytosolic folate metabolism. However, the IC_{50} of pemetrexed in folate-depleted L1210 cells supplemented with thymidine and hypoxanthine is ~1.8 μM (Figure 3-7, closed triangles). If pemetrexed-treated cells are also supplemented with glycine, in addition to thymidine and hypoxanthine, no toxicity is observed in folate-depleted L1210 cells at pemetrexed concentrations up to 32 μM (Figure 3-7, open triangles). It appears that concentrations of pemetrexed at and above 1.8 μM interfere with glycine metabolism, a folate-dependent process that occurs in mitochondria. This glycine toxicity is observed with some, but not all, folate analogs in similar experiments (Table 3-1). As a working hypothesis, we considered the possibility that some antifolates were inhibiting mitochondrial folate transport.

Antifolates interfere with mitochondrial folate transport

The underlying glycine auxotrophy that was observed when folate-depleted L1210 cells were treated with various antifolate agents suggested that some of these agents disrupted mitochondrial folate metabolism, which we believed to result from inhibition of mitochondrial folate transport. The effects of these folate analogs on mitochondrial folate transport were examined in mitochondria isolated from CHO and glyB cells and incubated with 1 μM ^{3}H-6S-5-formyl-tetrahydrofolate (5f-thf) for up to 15 minutes (Figure 3-8). Uptake was observed in both CHO and glyB mitochondria with over 60% of the total uptake occurring in the first three minutes. Folate transport in isolated CHO mitochondria was then examined in the presence of 5 μM of various antifolates for three minutes (Figure

	IC_{50} (μM)	
	Growth	Mitochondrial Toxicity
DDATHF	0.019	0.26
Methotrexate	0.01	0.05
Pemetrexed	0.018	1.8
Raltitrexed	0.018	Not observed
AG2034	0.18	3.2
AG2037	0.02	Not observed

Bronder, Lawrence and Moran

Table 3-1 Toxicity of antifolate agents in folate-depleted L1210 cells. Folate depleted L1210 cells were treated with various concentrations of each folate analog. IC_{50} values were recorded for antifolate growth suppression in cells with no added supplements. The IC_{50} for mitochondrial toxicity was observed when glycine was added in addition to agents that would reverse the inhibitory effects of the drug and provided a growth advantage over the rescue agents without glycine. Some of these experiments were done by Dr. Julie Bronder.

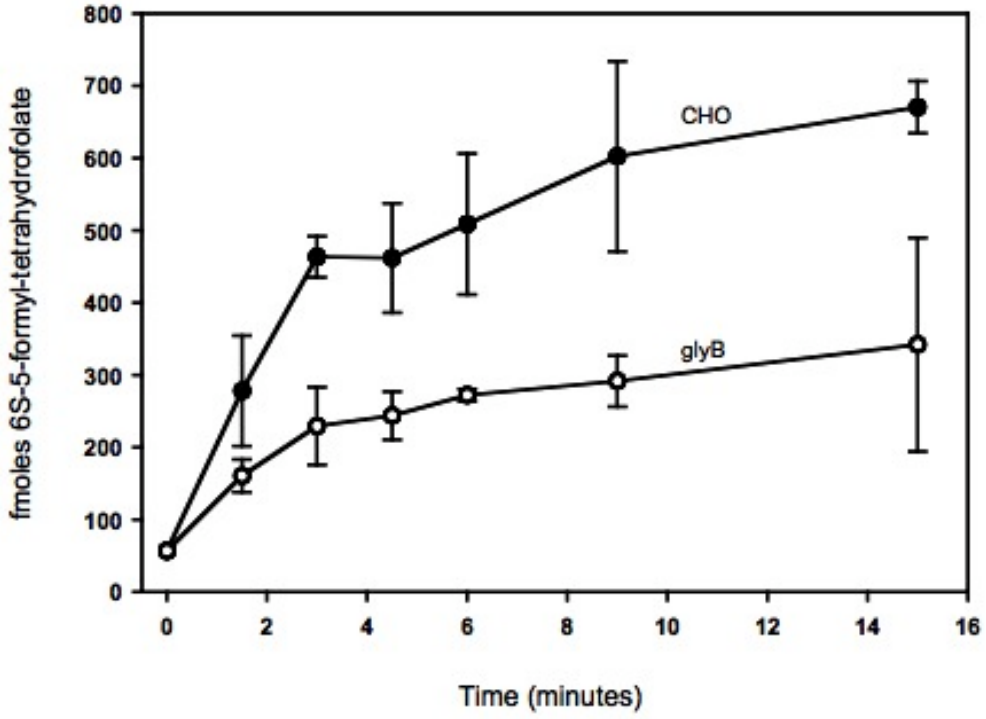

Figure 3-8 Uptake of ^{3}H-6S-5-formyl-tetrahydrofolate into isolated mitochondria from CHO and glyB cells. Mitochondria isolated from CHO and glyB cells were incubated with 1.5 µM of ^{3}H-6S-5-formyl-tetrahydrofolate for varying amounts of time. Following transport, mitochondria were collected onto 0.45 µm membrane filters by vacuum filtration and the filters were counted for radioactivity. Error bars represent variance of duplicate samples from a single experiment.

3-9). All antifolates appeared to decrease the transport of 5f-thf into CHO mitochondria, but none of the antifolates examined appeared to decrease mitochondrial folate transport to the level of deficiency observed in glyB cells. Interestingly, glyB mitochondria demonstrated a surprising ability to transport 5f-thf, a phenomenon not observed in previous whole cell transport assays (Figures 2-8A and 2-16). This uncharacteristic transport of 5f-thf in glyB mitochondria raised concerns that the integrity of the mitochondrial membranes may have been compromised by the isolation procedure.

Expression and purification of the MFT from a mammalian cell line

Due to the difficulties we experienced in obtaining reliable transport data for kinetic analysis using carefully isolated mitochondria, we decided that purification of the MFT and reconstitution into proteoliposomes was the best alternative to directly study MFT transport. A mouse leukemic cell line, the L1210 cell, was available that grew in suspension and doubled rapidly (T_D = 10 hours). This cell line could be adapted to grow in spinner flasks and, hence, could be rapidly expanded into large mass cultures. A C-terminal $His^{(6)}$ tag was added to the CHO MFT that also contained an N-terminal *myc* tag in the mammalian expression vector pcDNA 3.1(-). This vector also contained a gene that encoded G418 resistance. The sensitivity of L1210 cells to G418 was determined in order to appropriately choose the conditions for selection of L1210 transfectants. Various concentrations of G418 were incubated in a total volume of 1 mL containing 10,000 L1210 cells (Figure 3-10) for 10 days. Each well was microscopically examined every ~24 hours and given a rank (1-10) based on a subjective interpretation of cellular confluence. In the

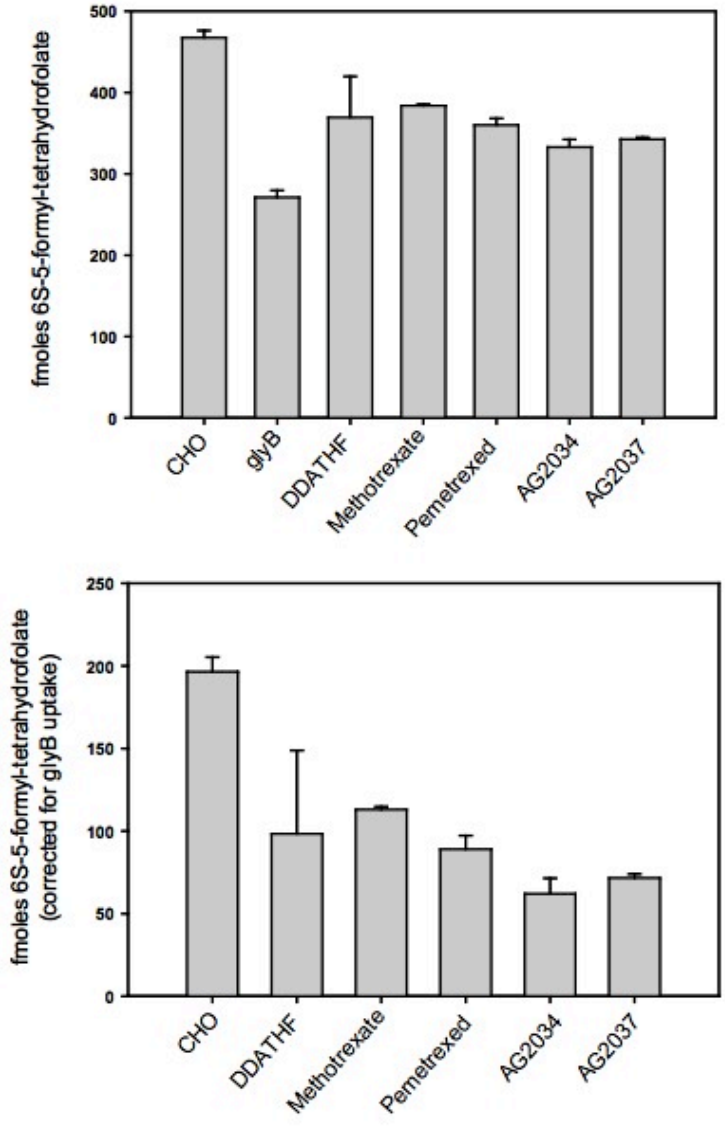

Figure 3-9 Uptake of ^{3}H-6S-5-formyl-tetrahydrofolate into mitochondria isolated from CHO cells in the presence of folate analogs. A. Mitochondria were isolated from CHO cells and incubated for 3 minutes with 1.5 µM of ^{3}H-6S-5-formyl-tetrahydrofolate in the presence of various folate analogs. Uptake in isolated CHO mitochondria in the absence of any antifolate was included as a positive control and uptake in isolated glyB mitochondria was included as a negative control. Following transport, mitochondria were collected onto 0.45 µm membrane filters by vacuum filtration and the filters were counted in a scintillation counter for radioactivity. Error bars represent variance of duplicate samples from a single experiment. B. The same data presented in A. with the uptake observed in glyB mitochondria subtracted from all experimental samples.

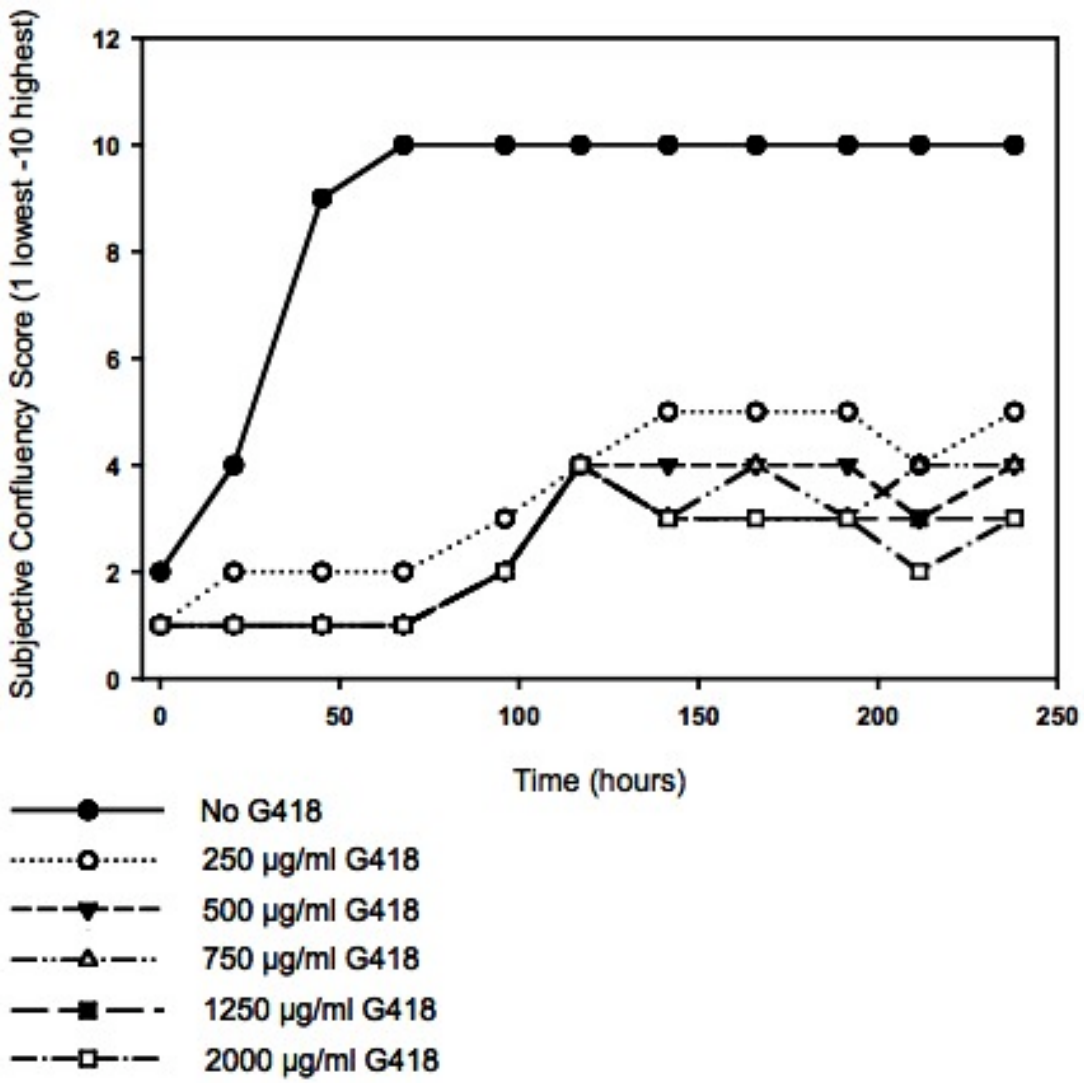

Figure 3-10 G418 toxicity in L1210 cells. Indicated concentrations of G418 were incubated with L1210 cells at a density of 1 x 10^4 cells/mL for 10 days. Confluence of L1210 cells was examined under a microscope daily and given a subjective score to reflect the observed density, with a rank of 1 representing almost no cells visible and 10 representing complete well confluence.

absence of G418, L1210 cells grew rapidly. Nearly every concentration of G418 inhibited the growth of L1210 cells; 500 µg/mL of G418 was chosen to be the selection concentration in the transfection experiment.

Because they grow in suspension, transfection of L1210 cells is considered difficult. Initial attempts were made to transfect L1210 cells using calcium-phosphate based and reagent-based (Superfect - Qiagen) methods, but did not produce any transfectants that survived G418 selection. Nucleofection of L1210 cells with the CHO MFT was to be attempted, but because of the time commitment involved in selecting for stable cell lines, L1210 cells were initially nucleofected with a green fluorescent protein (GFP) vector to examine and establish the efficiency of the nucleofection procedure. After 24 hours, L1210 cells transfected with a vector encoding GFP were visualized using a fluorescent microscope and it appeared that some L1210 cells had transiently taken up and were expressing GFP from the vector (Figure 3-11).

Based on the transient expression of GFP observed in nucleofected L1210 cells, L1210 cells were transfected with the pcDNA 3.1(-) vector encoding the CHO MFT with an N-terminal *myc* tag and a C-terminal $His^{(6)}$ tag. Nucleofected L1210 cells were exposed to 500 µg/mL G418 24 hours after nucleofection. On day 18 post-transfection, L1210 cells that had been growing in the presence of G418 were distributed into well plates at 0.1 cells/well to establish stably transfected single cell clonal lines. After 7 days of growth in selective media in 96-well plates, cell growth was observed in six wells out of a total of 192 wells. These clones were expanded and MFT expression was analyzed by western blotting of mitochondrial protein. All clones that were able to grow in the presence of 500

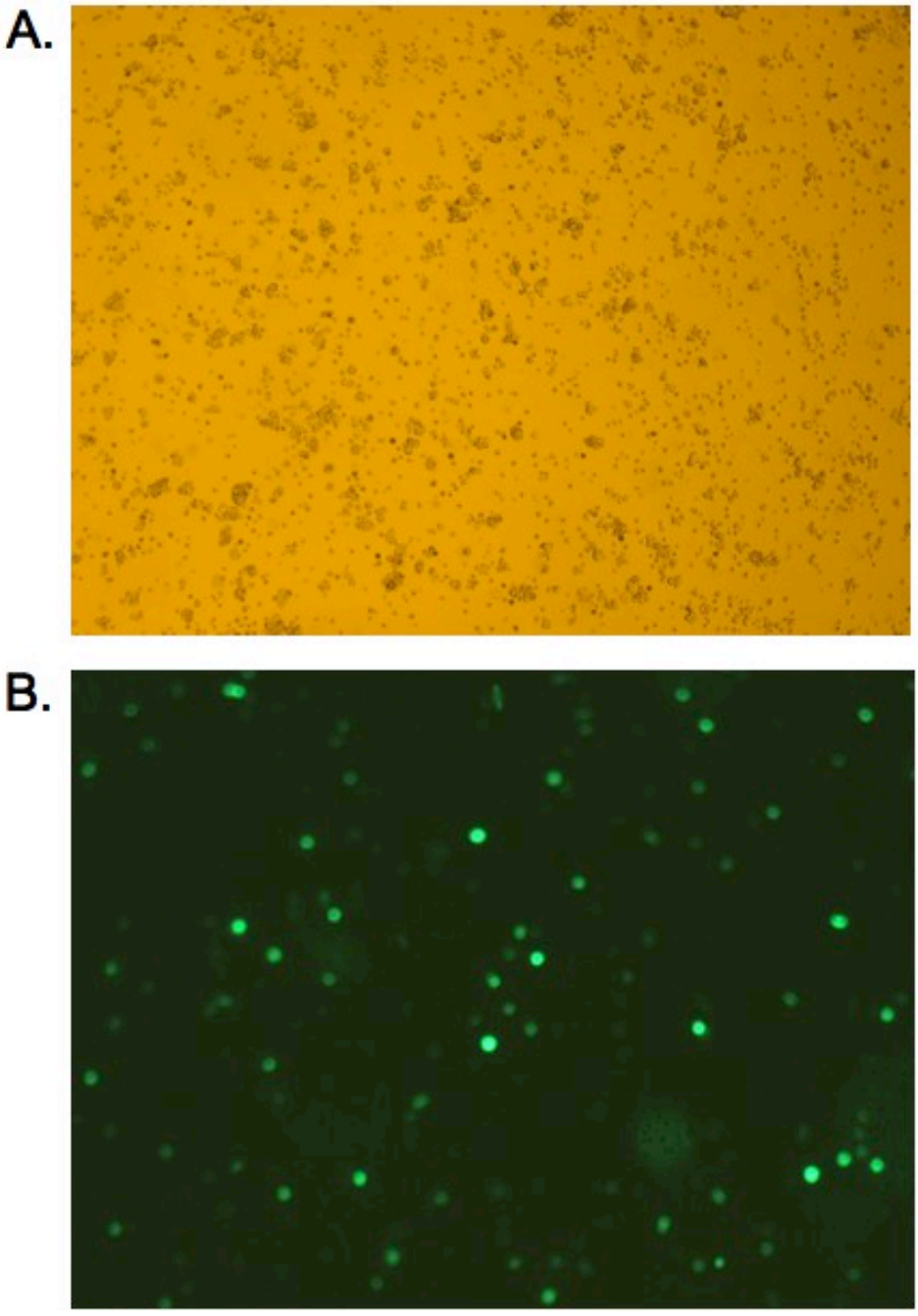

Figure 3-11 Transfection of L1210 cells with pmaxGFP to establish nucleofection efficiency. L1210 cells were transfected with pmaxGFP using the Nucleofector II device to optimize the transfection procedure. Twenty-four hours after transfection, cells were examined for GFP expression using a fluorescent microscope. The pictures presented are from the same viewing field under A. normal light conditions and B. a xenon light source at 495nm.

µg/mL G418 appeared to express a *myc*-tagged protein that was ~33 kDa in size, which corresponded to the size of the MFT (Figure 3-12). This protein was not detected in the mitochondrial fraction isolated from untransfected L1210 cells. Clone #4 was selected for further MFT purification based on its apparent highest level of MFT expression.

Two attempts were made to purify the MFT from a stably transfected L1210 clonal cell line. The purification procedure followed protocols established for other MCF proteins (85, 123, 140, 141). These protocols isolated mitochondrial followed by solubilization of mitochondrial proteins using a nonionic detergent. The soluble protein fraction was further purified using a hydroxyapatite resin. We added a C-terminal $His^{(6)}$ tag to the MFT protein and used talon column chromatography as a final purification step. Fractions were collected from each purification step and a purification table lists the total protein recovery for each purification experiment and purification steps up to the final purification using talon column chromatography (Table 3-2). Less than 50% of the total starting protein was recovered in the cytosolic, nuclear and mitochondrial compartments after dounce homogenization. This was the only step throughout the purification process in which significant protein loss was observed. Western blotting of these subcellular fractions indicated that the MFT protein was present only in the mitochondrial protein fraction (Figure 3-13). Mitochondrial protein, which was less than 15% of the total cellular starting protein, was then incubated with 3-laurylamido-N,N'-dimethylpropyl amine oxide (LAPAO) to solubilize mitochondrial protein. LAPAO was chosen for use based on its use in purification of the AAC (85, 128). Despite the fact that a large portion of mitochondrial protein remained insoluble in LAPAO (Table 3-2), western blotting indicated that the MFT

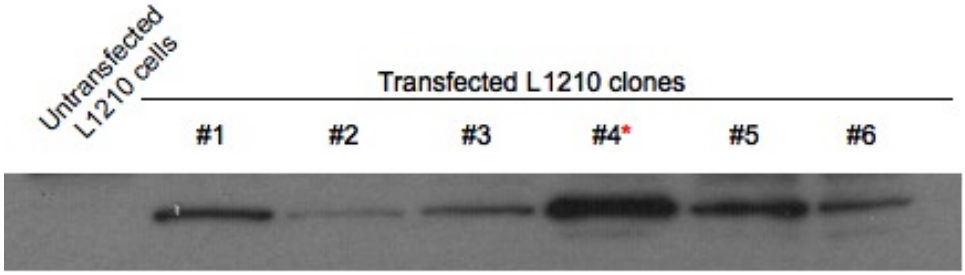

Figure 3-12 MFT expression in transfected L1210 cells detected by western blotting. The transfected CHO MFT contained a N-terminal *myc* tag. Forty micrograms of mitochondrial protein isolated from transfected L1210 cell clones was loaded into a 12% SDS-PAGE gel. Proteins in the gel were transferred to a PVDF membrane and the membrane was incubated with an antibody against *myc* to probe for *myc*-MFT expression. Mitochondrial protein from untransfected L1210 cells was included as a negative control. The red star marks the clone that was selected for use in MFT purification experiments.

	Purification #1	Purification #2
Total cell number	1.5×10^9	9.95×10^8
mg/million cells	0.096	0.091
Total Protein	143.34	90.7
Cell Fractions	67.01 (46.7%)	39.02 (43%)
Cytosolic	47.04 (32.8%)	25.86 (28.5%)
Nuclear	3.22 (2.2%)	0.46 (0.5%)
Mitochondrial	16.75 (11.7%)	12.7 (14%)
LAPAO fractions		
Soluble	9.98 (7.0%)	5.31 (5.9%)
Insoluble	6 (4.2%)	7.39 (8.1%)
Hydroxyapatite fractions		
Unbound	2.4 (1.7%)	Not Determined
Eluate	7.37 (5.1%)	2.113 (2.3%)

Table 3-2 Purification of the CHO MFT from L1210 cells. The total volume of each purification step of the MFT purification protocol was recorded. A fraction of the total volume from each purification step was collected. The protein content in each of the fractions was determined and multiplied by the total volume of the corresponding purification step. The total protein recovered is represented in milligrams. The percentages that are shown are percentages of the total protein.

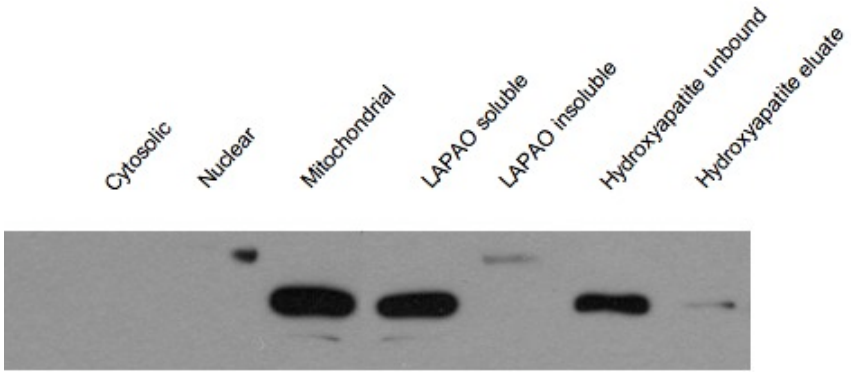

Figure 3-13 Detection *myc*-MFT in purification fractions by western blotting. A fraction was collected from each purification step. The protein concentration in each fraction was determined and 40 µg of protein from each fraction was loaded into a 12% SDS-PAGE gel. The protein contents of this gel were transferred to a PVDF membrane and the membrane was probed for the N-terminally *myc*-tagged MFT with an antibody raised against the *myc* epitope.

was completely soluble in LAPAO (Figure 3-13). The LAPAO-soluble protein was then batch purified using a hydroxyapatite resin. Hydroxyapatite was previously reported to not bind MCF proteins, but to adsorb a majority of other intracellular proteins (123). The exclusion of MCF proteins by hydroxyapatite is thought to be due to the hydrophobic nature of these proteins and the detergent that encompasses them. Western blotting demonstrated that the MFT is mostly unbound in the presence of hydroxyapatite resin (Figure 3-13). The protein fraction that was unbound by hydroxyapatite constituted ~2% of the total starting protein and was loaded onto a talon metal-affinity column. A majority of the protein loaded onto the talon column, ~90%, does not bind to the column (Figure 3-14A; fractions 1-12). However, about 10% of the protein loaded onto the column appears to bind to the talon column and is specifically eluted by imidazole (Figure 3-14; fractions 22-41). This small percentage of protein, ~0.2% of the total starting protein, is thought to be the MFT protein. The presence of the MFT in the imidazole-eluted fractions is demonstrated by western blotting (Figure 3-14B). Additionally, when talon column fractions were loaded onto a SDS-PAGE gel and proteins were visualized with coomassie stain (Figure 3-15), a number of proteins were observed in the talon column flow through (lane 1). After 5 bed volumes of wash buffer were run over the column three times, the column was washed with the same buffer, but with 5 mM imidazole added (lane 2). No protein appeared to elute with 5 mM imidazole. The column was finally washed in the same buffer, but with 150 mM imidazole and a dominant protein band appears in this fraction (lane 3) that is ~33kDa in size. We believe that the major protein species in this

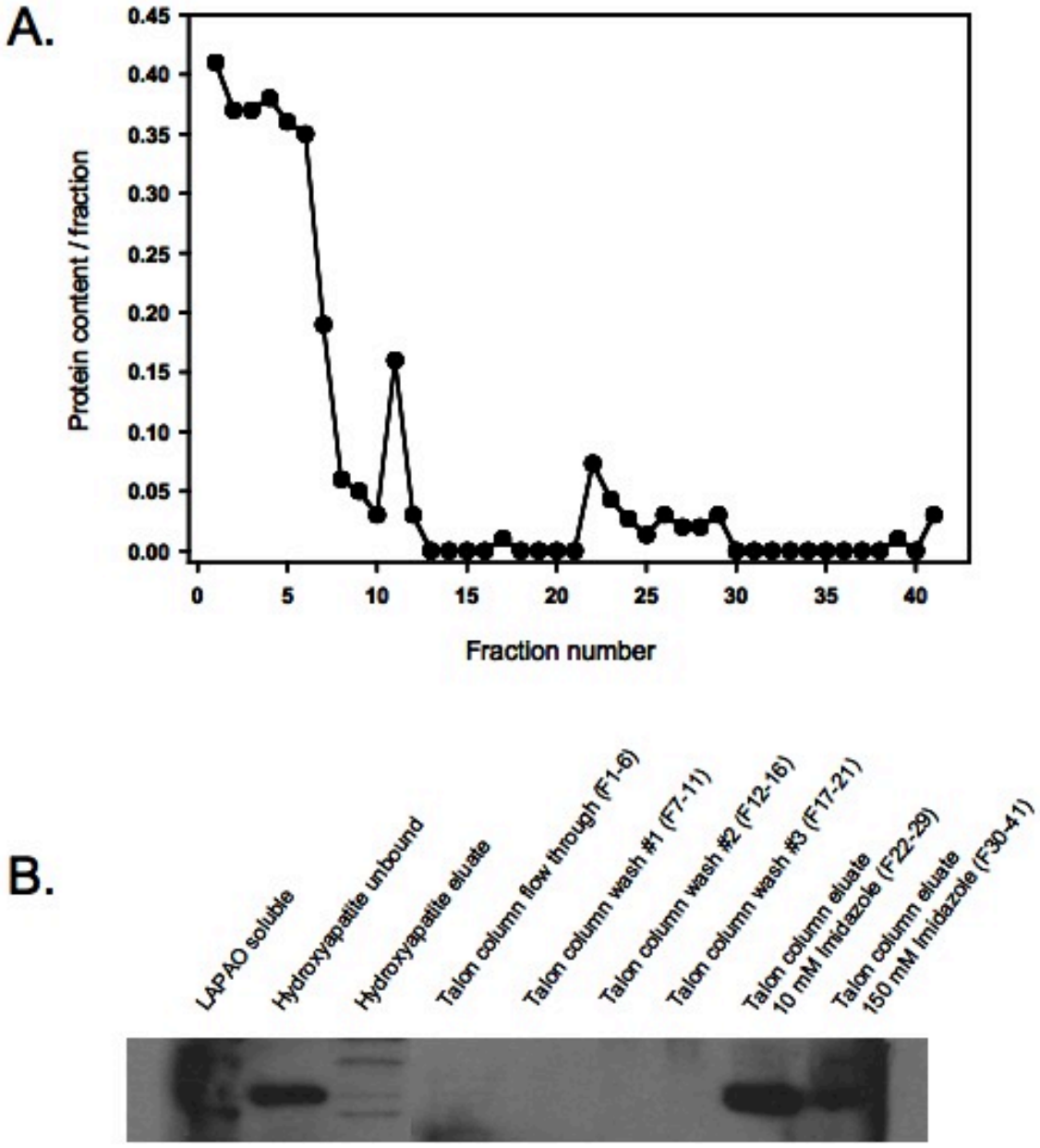

Figure 3-14 Protein and western blot detection of *myc*-MFT in talon column fractions. The protein that remained unbound in the presence of hydroxyapatite resin was loaded onto a talon metal-affinity column. Fractions 1-6 represent the total flow through volume that was obtained without allowing the bed resin to dry out. Fractions 7-11, 12-16 and 17-21 represent three separate column washes in 5 mL of a buffer containing 1% LAPAO, 100 mM NaCl, and 50 mM $NaHPO_4$, pH 7.0. Fractions 22-29 and 30-41 represent elutions in the above wash buffer but with the indicated amount of imidazole added. A. Individual fractions were collected and the absorbance a 280 nm was determined for each fraction. Protein content of each fraction was estimated assuming A_{280} of 1.00 = 1 mg/mL protein. B. After recording the absorbance at 280 nm for each fraction, fractions were pooled together and the protein in these pooled fractions were precipitated in 6% TCA. Approximately 25% of the total protein content in each pooled fraction was loaded into a SDS-PAGE gel, the protein contents of the gel were transferred to a PVDF membrane, and the membrane probed for the N-terminally *myc*-tagged MFT with an antibody raised against the *myc* epitope.

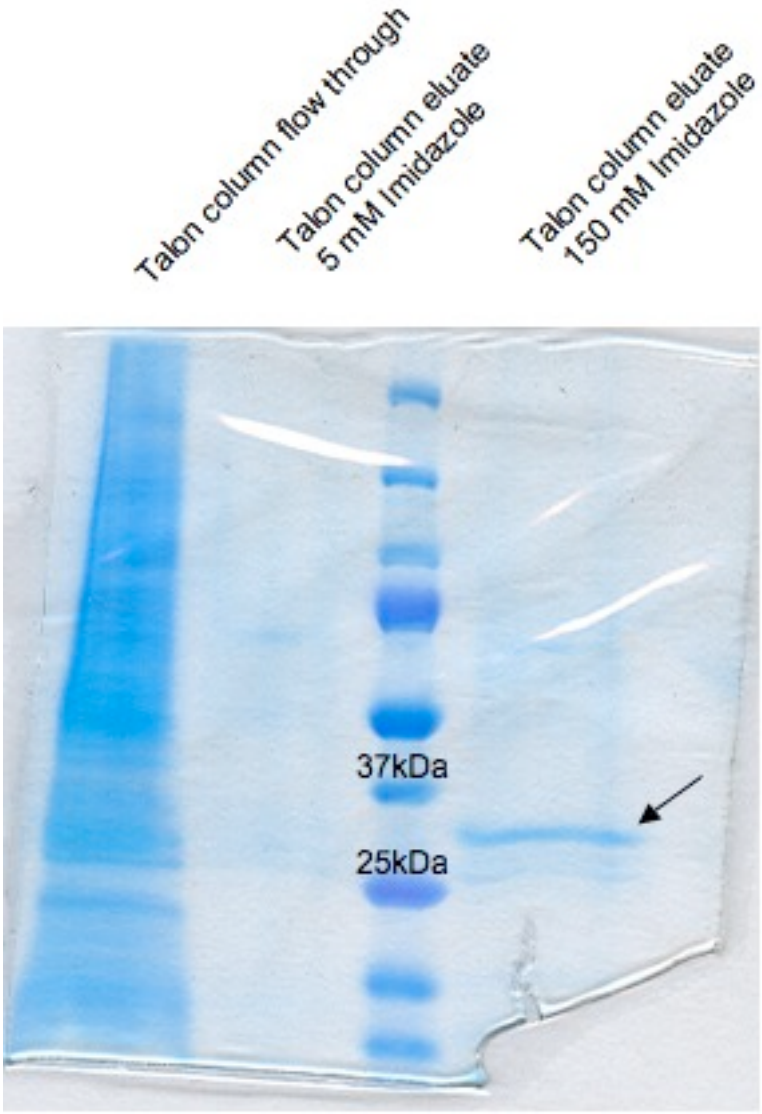

Figure 3-15 Protein staining of talon column fractions from MFT purification. Fractions were collected from a talon metal-affinity column and proteins in these fractions were precipitated in 6% TCA. Fifty-percent of the resolubilized, TCA precipitated protein from the flow through, 5 mM imidazole, and 150 mM imidazole fractions was loaded onto a SDS-PAGE gel. Following electrophoresis, the gel was washed in water and incubated in Coomassie BioSafe stain. The stain was removed from the gel and the gel was incubated in water for 16 hours.

fraction is the MFT. While the procedure yields ~0.2% of the total starting protein as MFT purified protein, it appears that the MFT has been highly purified.

DISCUSSION

Limitations of studies on the doxycycline-inducible expression of FPGS isoforms

The goal of using an inducible expression system was to recreate the expression of each of the isoforms of FPGS involved in the compartmentalization of folate metabolism in FPGS-null AuxB1 cells at endogenous levels. We did not have an efficient or reproducible method to detect the FPGS protein until recently, when we obtained a highly specific antibody against FPGS from colleagues at Lilly Research Laboratories (38). Prior to obtaining this antibody, colony formation assays similar to those in Figure 3-4 were used to screen and select for clones with the desired characteristics. Clones were selected because they did not appear to express FPGS in the absence of doxycycline, evidenced by the inability of the cloned cells to form colonies in the absence of doxycycline and without supplementation of purines, thymidine, and glycine. The induction dose of 1 μg/mL doxycycline was chosen based on the results in Figure 3-4; cells did not form more colonies when exposed to doxycycline concentrations above 1 μg/mL. To more closely mimic endogenous levels of FPGS expression, each line may require individual optimization of the induction dose of doxycycline. In particular, the mutFPGS cell line grossly overexpressed FPGS at every doxycycline concentration that we studied and a

level of doxycycline < 0.1 µg/mL would probably be required for the induction of FPGS at levels equivalent to endogenous FPGS expression.

Initially, it appeared that the cytosolic and mitochondrial *fpgs* cDNA constructs were expressing FPGS solely in their respective subcellular compartments. However, when FPGS expression as a function of doxycycline concentration was probed by western blotting, a small amount of FPGS protein was detected in the cytosolic fraction of the mFPGS cell line. We considered two possibilities that would explain the detection of FPGS protein in the cytosol of the mFPGS cells: 1) the downstream ATG in the mFPGS cDNA construct was available for use or, 2) import of the FPGS protein into mitochondria was limiting. If the downstream ATG on the mFPGS cDNA construct was available for use either by an internal ribosomal entry site or by ATG-skipping, then mutation of this downstream ATG in the *fpgs* cDNA should have eliminated cytosolic expression of FPGS. It did not do so; the presence of cytosolic FPGS was clearly shown in the mutFPGS cell line, a cell line that was transfected with the mFPGS cDNA, but with the downstream ATG mutated to ATT (isoleucine). It appeared that the cytosolic protein detected in the mFPGS cell line resulted from inefficient import of a mitochondrially-targeted protein. Hence, expression of the FPGS protein in this system had intrinsic limitations and we were not entirely successful in creating a cell line solely expressing FPGS in mitochondria.

FPGS expression was induced with 1 µg/mL doxycycline in mFPGS cells and these cells struggled to survive, but nonetheless formed small colonies in the absence of any additional media supplementations. In contrast, mFPGS cells exposed to 1 µg/mL doxycycline, purines, and thymidine were able to form larger colonies. The tiny colonies

formed by doxycycline-induced mFPGS cells in the absence of purines and thymidine may be attributable to the small amount of cytosolic FPGS protein detected in these cells, but we cannot eliminate the possibility that folate polyglutamates made in mitochondria contributed to the cytosolic folate pool. Nonetheless, we interpreted this to mean that both isoforms of FPGS were required for cellular folate metabolism and optimal cell growth. This interpretation opposes the impression lent by two previous studies, which suggested that the mitochondrial isoform of FPGS alone could complement the cellular requirement for purines and thymidine (45) and establish a pool of cytosolic folate polyglutamates (91). The expression of FPGS in both of these studies was driven by a strong CMV promoter, which undoubtedly caused overexpression of the FPGS protein in transfectants. Therefore, it was likely that these transfectants contained FPGS protein in the cytosol that had not been imported into mitochondria, similar to that seen in highly expressing mutFPGS cells. In one of the previous studies, ~ 25% of the total cellular FPGS activity was, in fact, located in the cytosol (91). Moreover, in several studies in which antifolate resistant populations were selected, there was a > 90-95% decrease in FPGS activity, and yet the resistant cells grew normally (89, 109, 176). This suggests that the ~ 25% residual activity of FPGS in the cytosol as seen by Lin *et al.* was more than sufficient for cytosolic folate retention and normal growth phenotypes in cells. It appears that to have an effect on cytosolic folate retention, FPGS activity must be substantially decreased (>90-95%).

The most confounding piece of data in this set of experiments related to the identical cytosolic retention of folate polyglutamates in doxycycline-induced cFPGS and mFPGS cell lines. Because FPGS can be detected in the cytosolic fraction of induced

mFPGS cells, one would anticipate some level of cytosolic folate retention in this cell line. The amount of FPGS protein that was detected in the cytosol of doxycycline-induced cFPGS and mFPGS cells was not the same (Figure 3-2B), and yet cFPGS and mFPGS cells were shown to retain equivalent amounts of folate polyglutamate metabolites in the cytosol (Figure 3-6). In spite of the fact that both cFPGS and mFPGS cell lines retained identical amounts of folate metabolites in the cytosolic compartments, mFPGS cells required thymidine and purines for optimal growth and cFPGS cells did not when in the presence of 1 μg/mL doxycycline (Figure 3-4). There is no reason to believe that there are differences between the folate polyglutamate metabolite pools in cytosolic compartments of the mFPGS and cFPGS cells lines. Obtaining a clear answer to the question of folate polyglutamate efflux from the mitochondrial matrix was seriously hindered by the small amount of cytosolic FPGS protein found in mFPGS cells. While it appears that optimal cell growth requires both cytosolic and mitochondrial folate metabolism, it is still unclear if cells can sustain survival through metabolism of mitochondrial folates alone.

Passage of folate polyglutamates through the mitochondrial membrane

We complemented the colony formation data by following the folate distribution of intracellular folates in the cytosol and mitochondria in these doxycycline-inducible cell lines as a function of time. This assay assumed that folates would be retained in the cell for the duration of the experiment once polyglutamation occurred and directly examined the subcellular distribution of folate polyglutamates in the mFPGS and cFPGS cell lines. The total radioactivity counted in both subcellular compartments of all cell lines remained

the same for 48 hours, despite the fact that cells were not exposed to any isotope after time t = 0. CHO cells grow with a doubling time of ~15 hours, so three generations elapsed during this experiment, yet we could not detect any loss of folates from the cells. Two effects were clear in these experiments: 1) there were no folate metabolites detected in the mitochondrial fraction isolated from doxycycline-induced cFPGS cells. Hence, folate polyglutamates made in the cytosol cannot penetrate the mitochondrial membrane and be sequestered into the mitochondrial matrix. 2) There was a noticeable accumulation of folates in the mitochondria of CHO cells and in doxycycline-induced mFPGS cells that appeared to occur at the expense of the cytosolic folate pool. While cytosolic folate polyglutamates do not appear to be transported into mitochondria, cytosolic folate polyglutamates may be metabolized back to folate monoglutamates, in which case, some of these monoglutamate folate forms appeared to be shuttled into mitochondria. The only intracellular enzyme capable of folate polyglutamate degradation is γ-glutamyl hydrolase, which is a lysosomal enzyme that removes glutamate moieties from folate polyglutamates, restoring them to their monoglutamate forms (47, 175). The accumulation of folates in mitochondria indicated that once folates enter mitochondria and are polyglutamated, they do not escape. There are no enzymes capable of digesting the poly-γ-glutamyl side chain of folates polyglutamates known in mammalian mitochondria. Therefore, this data suggests that mitochondrial folate polyglutamates do not efflux from mitochondria.

In silico predictions of folate polyglutamate acceptance by the MFT

As shown in the molecular dynamics (MD) simulation with the MFT in Chapter Two, the tetrahydrofolate (THF) molecule was vertically oriented during transit down the MFT transport cavity. It appeared that the γ- and α-carboxyl groups, the benzyl ring and the pteridine ring of the THF were contacted at every step of THF descent to the transport cavity floor by residues spaced at exact distances within the transport cavity. We predicted that CHO MFT K145 and W142 simultaneously positioned the α-carboxyl and the benzyl ring of the THF, respectively, at the transport cavity floor. We predict that additional glutamate moieties on folate molecules would disrupt the recognition of the functional groups of folate by the residues that line the MFT transport cavity at nearly every step of the folate trajectory. If the terminal glutamate on a folate polyglutamate was located at the base of the MFT transport cavity, the α- and γ-carboxyl groups of the terminal glutamate would be coordinated within the MFT transport cavity by CHO MFT R288 and R249, the same as was observed for the monoglutamate THF molecule in the MD simulation in Chapter Two. However, the benzyl ring of the THF monoglutamate molecule, which was contacted by CHO MFT W142 in the MD simulation, would be replaced by another glutamate residue for a folate polyglutamate. These extra glutamate residues on folate polyglutamates would interfere with almost every interaction that occurred with the benzyl and pteridine groups of the folate molecule because of the increased size of the glutamate tail. It would therefore appear that a glutamate moiety alone is not sufficient to successfully initiate transport of folates by the MFT; the MFT must also recognize the other ring structures in the folate molecule and these structures must be located at exact

distances from the γ-carboxyl group. This would not be the case for a folate polyglutamate molecule.

Examining the effects of antifolates on the MFT

Cell culture experiments demonstrated that antifolate agents were capable of disrupting mitochondrial folate metabolism, as evidenced by their underlying glycine-reversible toxicity. An underlying glycine-related toxicity was observed in folate-depleted L1210 cells that were treated with DDATHF, methotrexate, pemetrexed and AG2034, but not with raltitrexed or AG2037. These differences are likely indicative of the substrate specificity and the kinetics of substrate binding within the transport cavity of the MFT. Two pieces of data suggest that MFT inhibition by antifolates is competitive: 1) the underlying glycine-toxicity was most evident in cells exposed simultaneously to folate and drug and was much more muted in cells with pre-existing folate pools, and 2) uptake of ^{3}H-6S-5-formyl-tetrhydrofolate into CHO isolated mitochondria was impaired by AG2037, an antifolate agent that did not induce glycine auxotrophy in folate-depleted L1210 cells. Indeed, depletion of cellular folates is often observed in various pathological conditions and in cells exposed to antifolate agents under clinical conditions (23, 170). Any conditions that induce folate depletion may exacerbate antifolate inhibition of the MFT.

Since it appeared that antifolate inhibition of the MFT was competitive and concentration dependent, a kinetic analysis of MFT inhibition by various antifolates was desired. However, an isolated transport system was needed before kinetic studies could advance. Mitochondria isolated from CHO and glyB cells were an ideal pair of matched

cells and we had already shown enormous differences in the mitochondrial uptake of these two cell lines, albeit in a whole cell transport assay (Figures 2-8A and 2-16). The study of folate transport in isolated mitochondria was guided by two studies that addressed mitochondrial isolation and transport (87, 174). One of these studies demonstrated that mitochondria isolated using trehalose instead of mannitol or sucrose produced superior mitochondria that maintained outer membrane integrity even after freezing and thawing (174). The second study investigated the transport of heme into mitochondria that were isolated in a sucrose buffer and previously frozen (87). Following the procedures for mitochondrial isolation and transport outlined in these manuscripts, attempts were made to study ^{3}H-6S-5-formyl-tetrahydrofolate transport in previously frozen mitochondria. These attempts were unsuccessful; the uptake in CHO mitochondria was low and there was a much higher than expected uptake in glyB mitochondria. We suspected that subjecting the isolated mitochondria to a freezing and thawing process was compromising the integrity of the mitochondrial membranes. Therefore, folate uptake was analyzed in freshly isolated mitochondria from CHO and glyB cells. The uptake in CHO mitochondria increased two-fold, but the uptake in glyB mitochondria remained higher than expected. Subsequent transport studies used only freshly isolated mitochondria. However, the lack of separation between uptake in CHO mitochondria and glyB mitochondria made interpretation of this transport data difficult. It was unclear if the uptake observed in glyB mitochondria was real or an artifact of damaged mitochondria, but we favored the hypothesis that the level of uptake in glyB mitochondria was due to damaged mitochondria. Because we had previously shown that mitochondrial folate uptake in *glyB* cells was nominal ((108, 160),

data presented in this thesis), the uptake that occurred in glyB mitochondria was subtracted from the other experimental samples. With glyB uptake subtracted out, it appeared that all of these antifolates were impairing mitochondrial folate uptake to some extent. However, the subtraction of such a large negative control value was unsatisfactory.

On the other hand, perhaps the conditions used in these transport studies were not optimal for transport to occur in CHO mitochondria. Folate transport into isolated rat liver mitochondria was previously shown to pH sensitive with three to five-fold more uptake occurring at a pH of 5-6 than at a pH of 7-8 (61). This reported pH-sensitivity of folate transport was not factored into the design of these transport experiments in isolated mitochondria from CHO and glyB cells; our studies used a transport buffer at a pH of 7.4. Nonetheless, transport in isolated mitochondria became a frustrating and inefficient method to study the kinetics of MFT transport and we opted to move on with attempts to purify the MFT and study transport in reconstituted proteoliposomes.

Expression and purification of the CHO MFT

In order to study MFT transport in reconstituted systems, the purification of the MFT was required. Many of the MCF proteins that have been purified and reconstituted into liposomal systems were expressed in bacteria (1, 25, 26, 43, 44, 58, 65, 72, 103, 123, 132). Previous attempts were made to express and purify the MFT from bacteria and insect cells in this lab, but purification of an active MFT protein was not achieved (107). A mammalian cell line, the L1210 cell, was selected as the host for MFT expression in my studies. The L1210 cell made for an ideal host cell for MFT expression and purification as

this cell line grew rapidly in suspension and was compatible with the production of a large amount of protein. Nucleofection was chosen for DNA delivery into L1210 cells because of the difficulty encountered in previous attempts to transfect these cells using Lipofectamine (Invitrogen), Superfect (Qiagen), or a calcium phosphate-based method. While the characteristics of the cell largely determine their transfection efficiency, nucleofection appears to be a superior method for DNA delivery giving higher transfection efficiency with lower toxicity when compared to other transfection methodologies (104).

The MFT purification scheme used reagents and followed protocols that were used in the purification of other MCF proteins. The first step of purification from mammalian tissues involved the isolation of mitochondria following the solubilization of mitochondrial proteins. We used LAPAO because it was also used to solubilize the AAC protein in previous purification experiments (85, 128). We found that 1% LAPAO was able to completely solubilize the MFT. It may be of interest to revisit MFT expression in bacteria and test the solubility of the recombinant protein this LAPAO detergent. Hydroxyapatite has been found useful in the purification of other MCF proteins because it does not bind the non-denatured forms of these proteins (85, 123). Very few other purification procedures used further purification steps past hydroxyapatite chromatography. However, most other proteins are highly expressed in bacterial inclusion bodies and therefore, isolation of the inclusion bodies from bacteria served as a significant purification step. The purification of the MFT was not complete after hydroxyapatite chromatography and therefore, the hydroxyapatite unbound fraction was loaded onto a talon metal-affinity column for further purification.

The total amount of protein that was recovered in fractions of each step of the MFT purification scheme was consistent with protein recovery in the purification of other MCF proteins. Inexplicably yet consistently, only half of the expected total protein was recovered in the subcellular fractions. It is unclear why this loss of protein was observed, but it most likely reflected an artifact caused by interference with the Bradford assay. In contrast, very little protein was unaccounted for throughout the rest of the purification procedure. The protein contained in the hydroxyapatite fraction was slightly less than 2% of our total starting protein, and ~15% of the total mitochondrial protein. This is consistent with protein recovery observed in other MCF protein purifications from mammalian cells (9, 85, 92, 152). The concentrations of the fractions eluted from the talon column were too low to easily quantitate, but we estimated that this purification scheme yielded ~300-500 µg of purified MFT protein, or ~0.3-0.5% of the total starting protein and ~2% of the starting mitochondrial protein. This estimate is consistent with purified protein recovery in other purifications of MCF proteins from mammalian cells (84, 92). If our estimates were accurate, this quantity would be sufficient for reconstitution into proteoliposomes (123). In addition, if we are able to use this purification procedure and obtain similar protein recovery at each step, expanding the culture of transfected L1210 cells to five liters should yield over 1 mg of purified MFT protein that could be use for structural analysis.

The distribution of the MFT protein in purification fractions was also followed throughout the purification procedure. All of the MFT protein was found in the mitochondrial subcellular fraction and was soluble in buffer containing the detergent LAPAO as detected by western blotting. It appeared that the problems previously

encountered with MFT solubility were no longer a problem. However, it was unclear if this was due to the LAPAO detergent or the mammalian expression system. Nonetheless, very little MFT protein was insoluble. A majority of the MFT protein was detected in the protein fraction that did not bind to hydroxyapatite. The small amount of MFT that bound to hydroxyapatite is reminiscent of AAC protein binding to this resin; the protein that binds hydroxyapatite was shown to be in denatured form (85). Therefore, it also appears that the MFT protein solubilized in LAPAO was not denatured in the process. All of the MFT protein that was loaded onto the talon metal-affinity column appeared to bind to the column and this protein eluted from the column with imidazole. The stained gel showed that the major protein species in the imidazole eluate was a ~33 kDa protein that appeared to be of high purity. The protein is believed to be the MFT. Future studies will focus on reconstituting this protein into proteoliposomes.

CHAPTER 4 Perspectives

The work presented in this thesis has built on previous efforts in this laboratory to understand the mitochondrial folate transport protein, its mechanism, substrates and inhibitors and its niche in folate metabolism. The synergistic combination of mutagenesis and computational technology was prominent throughout this work. Mutagenesis experiments demonstrated that the investigated MFT residues diverged from the MCF consensus residues to evolve a folate-specific transport mechanism. A high quality homology model of the CHO MFT was constructed and subjected to extensive molecular dynamics (MD) simulations. These MD simulations predicted a stepwise descent for the tetrahydrofolate molecule into the recesses of the MFT transport cavity. These simulations also suggested that residues in the PxD/ExxK/R conserved motifs were not forming interactions in the absence of folate transport substrate. Hence, these simulations refuted a previously proposed barrier-forming role for the interactions between the residues in the PxD/ExxK/R motifs. Potential substrates and inhibitors of the MFT were also experimentally examined in cell-based assays and in isolated mitochondria. We presented evidence that suggested folate polyglutamate conjugates do not cross the mitochondrial membrane in either direction. This is the first evidence ever presented that implies mitochondrial folate polyglutamates are unable to efflux from mitochondria. In addition,

folate analogs, including methotrexate and pemetrexed, were shown to impair mitochondrial folate transport in isolated mitochondria. However, the desire to obtain direct transport data for kinetic analysis with various folate molecules was not obtained from experiments in isolated mitochondria. In order to obtain data for kinetic analysis and to characterize the substrates and inhibitors of the MFT, we attempted to purify the MFT for transport studies in reconstituted liposomal systems. We stably transfected a mammalian cell line with CHO *mft* cDNA and, for the first time, we have purified at least ~250 ng of soluble MFT protein. Purification of the MFT from this cell line now presents opportunities for the identification of the substrates and inhibitors of the MFT protein in reconstituted systems and for future structural analysis of the MFT protein. These studies have also advanced our understanding of the transport mechanism of the MFT protein and the compartmentalization of folate metabolism, which gives rise to a new series of fascinating questions for future investigation.

Why are cells that lack mitochondrial folate metabolism glycine auxotrophs?

One of the most interesting observations related to the MFT is that cells deficient in mitochondrial folate transport are glycine auxotrophs. GlyB cells rapidly die within 24 hours in media lacking glycine (107). The same phenomenon is observed in cells harboring inactivating mutations in folate-dependent enzymes (FPGS and mSHMT) in mitochondria. Hence, mitochondrial folate metabolism is assumed to be required for the synthesis of glycine, but it is not understood why cells deficient in mitochondrial folate metabolism are auxotrophic for glycine. Mammalian mitochondria contain two reversible

reactions that are capable of synthesizing glycine, mediated by either the glycine cleavage system (GCS) or the mitochondrial isoform of serine hydroxymethyltransferase (mSHMT). The cytosolic compartment in mammalian cells also contains one reversible reaction capable of glycine synthesis, mediated by the cytosolic isoform of serine hydroxymethyltransferase (cSHMT). It is not understood why the reversible cytosolic serine hydroxymethyltransferase (cSHMT) reaction is unable to compensate for decreases in mitochondrial glycine synthesis. In cells with (CHO) and without (glyA) mSHMT, the activity of cSHMT is unchanged, yet cells lacking mSHMT produce 10-fold less glycine than cells with mSHMT (116). Furthermore, in a computational model of hepatic folate metabolism the glycine concentration was predicted to remain relatively stable even when a large excess of serine was added to the *in silico* system (120). This may suggest that although it is reversible, the cSHMT reaction is not capable of fully complementing mitochondrial glycine synthesis. Despite being isoforms, human cSHMT and mSHMT are encoded by separate genes and have protein sequences that are only 63% identical (49). Analysis of the SHMT isoforms in yeast showed that the specific activity of mSHMT isoform was two-fold higher than the cSHMT isoform (73). However, why cSHMT is unable to optimally or efficiently catalyze the synthesis of glycine from serine is still unknown.

The role of and requirement for mitochondrial glycine is largely unknown. It is speculated that glycine metabolism is necessary for formate production and export to the cytosol. Mitochondrial formate has been estimated to account for at least 25% of the one-carbon units used in cytosolic purine synthesis (127). When either mSHMT or glycine

were removed from a computational model of hepatic folate metabolism, the flux of formate to the cytosol remained "normal" (120). However, when both mSHMT and glycine were removed from the system, the export of formate to the cytosol was halved. This suggested that both reactions that produce formate must be impaired before any phenotypic effects or growth impairments are observed. In the absence of mitochondrial folate metabolism in a computational model of hepatic cellular folate metabolism, no formate is exported to the cytosol, yet cytosolic folate metabolism continues and only thymidylate synthesis and purine synthesis are predicted to be drastically impaired; the rates of these processes are decreased by 40% and 60%, respectively (120). This reinforces the hypothesis that the purpose of mitochondrial folate metabolism is to supply formate to the cytosol for purine and thymidylate synthesis. However, it is interesting to note that glycine supplementation is able to rescue cells that lack mitochondrial folates (71, 106) even though mitochondrial folates appear to be cofactors in reactions that metabolize glycine. Thus, it is unclear how glycine supplementation relieves the requirement for mitochondrial folate metabolism.

Does the MFT transport folate polyglutamates?

The data presented in this thesis suggests that the MFT does not transport folate polyglutamate conjugates across the mitochondrial membrane in either direction. It had been previously shown that folate polyglutamates are not transported from the cytosol into mitochondria (91), and we presented data in this thesis that supports this concept. We also presented data that suggested for the first time, that folate polyglutamates do not efflux

from mitochondria. In spite of the considerable effort described in Chapter Three, a cell line that only expresses FPGS in mitochondria has yet to be contrived. Even at the lowest doxycycline induction level used in these studies, FPGS was still detected in the cytosol of mFPGS cells apparently because a step in the mitochondrial import of FPGS becomes a limiting factor. Future studies could examine FPGS expression induced by a lower concentration of doxycycline. According to the product manual, the Tet-on system is responsive to doxycycline concentrations as low as 10 ng/mL, a concentration that is 25-fold lower than the lowest concentration used in these studies. In the studies presented in Chapter Three, cells were continuously exposed to doxycycline to induce FPGS expression. However, in the Tet-on system, cells continuously exposed to doxycycline continue to transcribe FPGS from the doxycycline response vector. If the mitochondrial import of the FPGS protein was limiting, it may be possible to temporarily induce expression of FPGS with a pulse treatment of doxycycline so that transcription would not be as robust, less protein would be translated, and all of the expressed protein could be imported in mitochondria. Another possibility to directly determine if folate polyglutamates efflux from the mitochondrial matrix would be to knock down the MFT using RNA interference (RNAi) in the mFPGS cells. The mFPGS cell line expresses a small amount of FPGS in the cytosol and because we detect FPGS in the cytosol, we are unable to eliminate the possibility that this protein is responsible for the cytosolic retention of folate polyglutamates observed in the mFPGS cell line. By comparing the compartmental distribution and retention of folate polyglutamates in mFPGS cells with and without the MFT protein, we could study the origin of this cytosolic folate pool. A knock

down of the MFT protein should reduce the ability of mFPGS mitochondria to accumulate folates even when FPGS is induced. If the MFT permitted folate polyglutamate efflux from the mitochondrial matrix, the level cytosolic folate polyglutamate retention observed in the RNAi MFT doxycycline-induced mFPGS cell line should decrease when compared to the wild-type MFT doxycycline-induced mFPGS cell line because 1) the MFT protein responsible for folate polyglutamate efflux had been knocked down and less protein as available to mediate efflux, and 2) the pool of mitochondrial folate polyglutamates was decreased, meaning that there would be less matrix-associated folate polyglutamates available for efflux. However, if the levels of cytosolic folate polyglutamate retention were equivalent in doxycycline-induced mFPGS cells with and without (knocked down) the MFT, it would suggest that this pool of cytosolic folate polyglutamates was not dependent on the MFT. Therefore, one could conclude that the cytosolic folate pool was established by the cytosolic FPGS protein and did not arise from the mitochondrial folate polyglutamate pool.

How do cytosolic FPGS and the MFT coordinate the compartmentalization of folate metabolism?

If cytosolic polyglutamates are not substrates for the MFT, it would appear that the MFT and the cytosolic isoform of FPGS compete for cytosolic folate monoglutamates. However, in a single transfection experiment that was not presented in this thesis, the cytosolic isoform of FPGS in pcDNA 3.1(-), under a strong CMV promoter, was transfected in CHO cells that contain functional FPGS in both compartments. In a setup

identical to the glyB complementation assay, two plates of glyB cells that were identically transfected were challenged to grow either in the presence or absence of glycine using G418 as a selection agent. CHO cells transfected with cytosolic FPGS were able to grow equally as well in the absence of glycine compared to their growth in the presence of glycine. In these transfectants, apparent cytosolic overexpression of FPGS was not enough to impair mitochondrial folate accumulation and induce glycine auxotrophy. More definitive evidence could be obtained by a direct analysis of the folate levels in the cytosolic and mitochondrial compartments in CHO cells transfected with the cytosolic isoform of FPGS in pcDNA 3.1(-) compared with the levels in untransfected CHO cells. Other unpublished studies referenced by Lin *et al.* suggested that the overexpression of cytosolic FPGS in mammalian cells impaired the ability of mitochondria to accumulate folates (91). If the MFT and cytosolic FPGS are in competition for cytosolic monoglutamates, the cell must coordinate the activities of each of these proteins to permit simultaneous folate accumulation in the cytosol and mitochondria.

How to best identify the substrates and inhibitors of the MFT?

There is a need to directly identify the transport substrates and inhibitors of the MFT. The attempts made in this thesis and in two other studies (30, 61) suggest that methotrexate inhibits the mitochondrial folate transport process. However, methotrexate does not accumulate in mitochondria (77), which would suggest that methotrexate binds in the MFT transport cavity, but is not transported. In our hands, transport studies in isolated mitochondria were unable to provide an accurate kinetic analysis of transport events. The

isolation of intact mitochondria appears to be a delicate task, but is not impossible. Certainly, if additional attempts were made to study transport in isolated mitochondria, the buffer components and pH would require more attention. However, with a MFT purification protocol in place, the transport function of the MFT could be studied in reconstituted systems, a more ideal experimental system. We estimated that we were able to produce enough pure MFT protein for liposomal reconstitution from 1.5 L of cultured L1210 cells. Since the MFT does not appear to function as an exchanger, it is also unclear if these proteoliposomes would require the presence of folate substrate inside the liposome, or if the presence of substrate inside the liposome would hinder transport based on the disruption of a concentration gradient.

What CHO MFT residues should be experimentally investigated next?

Questions remain about the mechanism of transport of the MFT. The studies that were carried out over the course of this thesis have provided a much clearer understanding of the events that occur within the MFT transport cavity to permit mitochondrial folate transport. Characterizing the events that permit folate transport is an essential step towards understanding the substrate-specific transport mechanism of the MFT. Identifying the residues responsible for interaction with and coordination of the folate substrate is central to discovering the structural requirements for MFT substrates. MD simulations allowed the visualization of the THF trajectory in the MFT transport cavity and suggested that there was a very strict organization of amino acids and their side chains within the transport cavity. Three residues, CHO MFT W96, K235, and R288, which were not experimentally

examined in our mutagenesis studies, appeared essential in folate coordination at the top of the transport cavity. Mutagenesis of these residues would provide insight into their requirement and involvement in the positioning of folate substrates within the MFT transport cavity.

The residues investigated in this thesis were mostly residues that were charged or that were contained in the PxD/ExxK/R motifs in the MFT, but did not match the MCF consensus. Interestingly, the MFT was surprisingly tolerant to mutation of CHO MFT R249, W142, and Q246 in the glyB complementation assay, and yet these residues were thought to be indispensable to MCF protein function. Based on the studies presented in this thesis, we do not believe that these residues form a transport barrier, but rather we believe that they attract and position the substrate deep within the transport cavity for final passage into the mitochondrial matrix. Of particular interest are CHO MFT K47 and K145, which are basic residues predicted to be located in the PxD/ExxK/R motifs of the first and third transmembrane domains in the MFT. The MD simulations presented in this thesis were unable to capture tetrahydrofolate (THF) descent to the extent of interaction with either of these basic residues. We believe that one, or both, of these residues likely coordinate the α-carboxyl group of the glutamate tail of the folate substrate. It would also be of interest to examine the conserved motif residue, D44, on the first transmembrane domain. It is the only acidic residue that remains in the three PxD/ExxK/R motifs in the MFT. D44 is proposed to interact with CHO MFT R288 in the apo-MFT, and interact with K145 (in the second PxD/ExxK/R motif) in the tetrahydrofolate-bound MFT. The interaction of D44 with R288 may serve to hold R288 in place to contact the α-carboxyl of

THF higher up in the transport cavity. Once THF contacts R288, D44 may be released from R288, at which point D44 may coordinate and position K145 to receive the α-carboxyl group of THF from R288. Further investigation of the interactions between D44 and R288 and D44 and K145 is justified if it can further explain the role of these residues in folate transport.

What are the molecular events that occur to permit folate entry into the mitochondrial matrix?

The residues responsible for the final step of substrate translocation into the mitochondrial matrix are largely unknown. In contrast to our knowledge of substrate binding within the transport cavities of MCF proteins, our understanding of this final event is insufficient. The matrix-exposed loop regions of MCF proteins have been implicated in final substrate translocation (31, 75, 101, 102), but no amino acids have been specifically linked this event. The (D/E)Gxxxx(Y/F/W)(K/R)G motif of the Px(D/E)xx(K/R)x(K/R) - (20 to 30 amino acids) - (D/E)Gxxxx(Y/F/W)(K/R)G MCF conserved motif is contained in these loop regions. The MD simulations presented in this thesis predict that THF descent to the base of the transport cavity occurs in defined steps, where each preceding step appeared to be a prerequisite for further passage. Therefore, substrate bound to the Px(D/E)xx(K/R)x(K/R) sequence may be a required event to induce the stabilization of the (D/E)Gxxxx(Y/F/W)(K/R)G sequence. It is possible that the last basic residue in the Px(D/E)xx(K/R)x(K/R) sequence interacts with an acidic residue in one of the (D/E)Gxxxx(Y/F/W)(K/R)G sequences to hold these loop regions in place. This

interaction may function to hold the basic residue in the (D/E)Gxxxx(Y/F/W)(K/R)G sequence in place so that this K/R residue may establish contact with the substrate below the base of the transport carrier. The strict conservation of these residues across MCF proteins suggests that their conservation is likely not coincidental. The last basic residue in the Px(D/E)xx(K/R)x(K/R) motif and the charged residues in the (D/E)Gxxxx(Y/F/W)(K/R)G motif may contain some valuable information about the final translocation events and should be experimentally investigated.

Can the MFT be a useful therapeutic target?

Another aspect that is particularly interesting to speculate on is the potential or utility of the MFT as a drug target. Scientific research is in the middle of an enormous translational movement, where research discoveries and laboratory findings are being rapidly applied in a clinical setting. Receptors, enzymes, and transporters have all made for ideal pharmacological targets in disease therapy. GlyB cells grown in the absence of glycine do not survive longer than 24 hours (107). Hence, pharmacological inhibition of the MFT has the potential to induce rapid cell death. The development of an inhibitor would be quite feasible. In fact, nature has developed two inhibitors of the AAC. In our MD simulations, it appears the glutamate portion of the folate molecule proceeds first into the transport cavity and this glutamate tail would seem the most likely candidate for modification. Our current understanding of folate recognition by the MFT would have to be advanced further and likely complemented by a crystal structure of the MFT. One key to therapy is selectively targeting and treating malignancy, while leaving all other cells

untouched; a strong inhibitor of the MFT would be fairly non-specific and likely affect all cells, malignant and benign. Therefore, any agent developed to target the MFT would have to be accompanied by a cellular delivery method that could target this hypothetical agent specifically to malignant cells. Interestingly, the folate receptor is currently being exploited for targeted drug delivery (178).

List of References

List of References

1. Agrimi, G., Di Noia, M. A., Marobbio, C. M., Fiermonte, G., Lasorsa, F. M., & Palmieri, F. (2004). Identification of the human mitochondrial S-adenosylmethionine transporter: Bacterial expression, reconstitution, functional characterization and tissue distribution. *The Biochemical Journal, 379*(Pt 1), 183-190.

2. Aksimentiev, A., & Schulten, K. (2005). Imaging alpha-hemolysin with molecular dynamics: Ionic conductance, osmotic permeability, and the electrostatic potential map. *Biophysical Journal, 88*(6), 3745-3761.

3. Appling, D. R. (1991). Compartmentation of folate-mediated one-carbon metabolism in eukaryotes. *Faseb J, 5*(12), 2645-51.

4. Aquila, H., Eiermann, W., Babel, W., & Klingenberg, M. (1978). Isolation of the ADP/ATP translocator from beef heart mitochondria as the bongkrekate-protein complex. *European Journal of Biochemistry / FEBS, 85*(2), 549-560.

5. Aquila, H., Misra, D., Eulitz, M., & Klingenberg, M. (1982). Complete amino acid sequence of the ADP/ATP carrier from beef heart mitochondria. *Hoppe-Seyler's Zeitschrift Fur Physiologische Chemie, 363*(3), 345-349.

6. Aquila, H., Link, T. A., & Klingenberg, M. (1987). Solute carriers involved in energy transfer of mitochondria form a homologous protein family. *FEBS Letters, 212*(1), 1-9.

7. Babel, W., Wachter, E., Aquila, H., & Klingenberg, M. (1981). Amino acid sequence determination of the ADP,ATP carrier from beef heart mitochondria. the sequence of the C-terminal acidolytic fragment. *Biochimica Et Biophysica Acta, 670*(2), 176-180.

8. Baldwin, S. W., Tse, A., Gossett, L. S., Taylor, E. C., Rosowsky, A., Shih, C., & Moran, R. G. (1991). Structural features of 5,10-dideaza-5,6,7,8-tetrahydrofolate that determine inhibition of mammalian glycinamide ribonucleotide formyltransferase. *Biochemistry, 30*(7), 1997-2006.

9. Banerjee, R. K., Shertzer, H. G., Kanner, B. I., & Racker, E. (1977). Purification and reconstitution of the phosphate transporter from bovine heart mitochondria. *Biochemical and Biophysical Research Communications, 75*(3), 772-778.

10. Bas, D. C., Rogers, D. M., & Jensen, J. H. (2008). Very fast prediction and rationalization of pKa values for protein-ligand complexes. *Proteins, 73*(3), 765-783.

11. Baugh, C. M., & Krumdieck, C. L. (1971). Naturally occurring folates. *Annals of the New York Academy of Sciences, 186*, 7-28.

12. Beardsley, G. P., Moroson, B. A., Taylor, E. C., & Moran, R. G. (1989). A new folate antimetabolite, 5,10-dideaza-5,6,7,8-tetrahydrofolate is a potent inhibitor of de novo purine synthesis. *The Journal of Biological Chemistry, 264*(1), 328-333.

13. Bioinformatics Group, Department of Computer Science, University College London.*The PSIPRED protein structure prediction server.*, 2006, from http://bioinf4.cs.ucl.ac.uk:3000/psipred/

14. Block, M. R., Lauquin, G. J., & Vignais, P. V. (1979). Differential inactivation of atractyloside and bongkrekic acid binding sites on the adenine nucleotide carrier by ultraviolet light: Its implication for the carrier mechanism. *FEBS Letters, 10*4(2), 425-430.

15. Block, M. R., Lauquin, G. J., & Vignais, P. V. (1981). Chemical modifications of atractyloside and bongkrekic acid binding sites of the mitochondrial adenine nucleotide carrier. are there distinct binding sites? *Biochemistry, 2*0(9), 2692-2699.

16. Boritzki, T. J., Barlett, C. A., Zhang, C., & Howland, E. F. (1996). AG2034: A novel inhibitor of glycinamide ribonucleotide formyltransferase. *Investigational New Drugs, 1*4(3), 295-303.

17. Bower, M., Cohen, F. E. & R.L. Dunbrack, J.*SCWRL: A program for building sidechains onto protein backbones.*, 2006, from http://www.cmpharm.ucsf.edu/Bbower/scwrl.html

18. Brandolin, G., Doussiere, J., Gulik, A., Gulik-Krzywicki, T., Lauquin, G. J., & Vignais, P. V. (1980). Kinetic, binding and ultrastructural properties of the beef heart adenine nucleotide carrier protein after incorporation into phospholipid vesicles. *Biochimica Et Biophysica Acta, 59*2(3), 592-614.

19. Brandolin, G., Le Saux, A., Trezeguet, V., Lauquin, G. J., & Vignais, P. V. (1993). Chemical, immunological, enzymatic, and genetic approaches to studying the arrangement of the peptide chain of the ADP/ATP carrier in the mitochondrial membrane. *Journal of Bioenergetics and Biomembranes, 25*(5), 459-472.

20. Breneman, C. M., & Wiberg, K. B. (1990). *J. Comp. Chem., 1*1, 361-373.

21. Brigle, K. E., Spinella, M. J., Westin, E. H., & Goldman, I. D. (1994). Increased expression and characterization of two distinct folate binding proteins in murine erythroleukemia cells. *Biochem Pharmacol, 47*(2), 337-45.

22. Bryson, K., McGuffin, L. J., Marsden, R. L., Ward, J. J., Sodhi, J. S., & Jones, D. T. (2005). Protein structure prediction servers at university college london. *Nucleic Acids Research, 33*(Web Server issue), W36-8.

23. Calvert, H. (2002). Folate status and the safety profile of antifolates. *Seminars in Oncology, 29*(2 Suppl 5), 3-7.

24. Capobianco, L., Bisaccia, F., Michel, A., Sluse, F. E., & Palmieri, F. (1995). The N- and C-termini of the tricarboxylate carrier are exposed to the cytoplasmic side of the inner mitochondrial membrane. *FEBS Lett, 357*(3), 297-300.

25. Cappello, A. R., Curcio, R., Valeria Miniero, D., Stipani, I., Robinson, A. J., Kunji, E. R., & Palmieri, F. (2006). Functional and structural role of amino acid residues in the even-numbered transmembrane alpha-helices of the bovine mitochondrial oxoglutarate carrier. *Journal of Molecular Biology, 363*(1), 51-62.

26. Cappello, A. R., Miniero, D. V., Curcio, R., Ludovico, A., Daddabbo, L., Stipani, I., Robinson, A. J., Kunji, E. R., & Palmieri, F. (2007). Functional and structural role of amino acid residues in the odd-numbered transmembrane alpha-helices of the bovine mitochondrial oxoglutarate carrier. *Journal of Molecular Biology, 369*(2), 400-412.

27. Clewley, J. P., & Arnold, C. (1997). MEGALIGN. the multiple alignment module of LASERGENE. *Methods in Molecular Biology (Clifton, N.J.), 70*, 119-129.

28. Cook, R. J., & Blair, J. A. (1979). The distribution and chemical nature of radioactive folates in rat liver cells and rat liver mitochondria. *Biochem J, 178*(3), 651-9.

29. Cordes, F. S., Bright, J. N., & Sansom, M. S. (2002). Proline-induced distortions of transmembrane helices. *Journal of Molecular Biology, 323*(5), 951-960.

30. Cybulski, R. L., & Fisher, R. R. (1981). Uptake of oxidized folates by rat liver mitochondria. *Biochimica Et Biophysica Acta, 646*(2), 329-333.

31. Dahout-Gonzalez, C., Ramus, C., Dassa, E. P., Dianoux, A. C., & Brandolin, G. (2005). Conformation-dependent swinging of the matrix loop m2 of the mitochondrial saccharomyces cerevisiae ADP/ATP carrier. *Biochemistry, 44*(49), 16310-20.

32. David, C., Arnou, B., Sanchez, J. F., Pelosi, L., Brandolin, G., Lauquin, G. J., & Trezeguet, V. (2008). Two residues of a conserved aromatic ladder of the mitochondrial ADP/ATP carrier are crucial to nucleotide transport. *Biochemistry, 47*(50), 13223-13231.

33. Dehez, F., Pebay-Peyroula, E., & Chipot, C. (2008). Binding of ADP in the mitochondrial ADP/ATP carrier is driven by an electrostatic funnel. *Journal of the American Chemical Society, 130*(38), 12725-12733.

34. Dietrich, M., Brown, C. J., & Block, G. (2005). The effect of folate fortification of cereal-grain products on blood folate status, dietary folate intake, and dietary folate sources among adult non-supplement users in the united states. *Journal of the American College of Nutrition, 24*(4), 266-274.

35. Dixon, K. H., Lanpher, B. C., Chiu, J., Kelley, K., & Cowan, K. H. (1994). A novel cDNA restores reduced folate carrier activity and methotrexate sensitivity to transport deficient cells. *J Biol Chem, 269*(1), 17-20.

36. Dolan, M. A., Keil, M., & Baker, D. S. (2008). Comparison of composer and ORCHESTRAR. *Proteins, 72*(4), 1243-1258.

37. Dolinsky, T. J., Czodrowski, P., Li, H., Nielsen, J. E., Jensen, J. H., Klebe, G., & Baker, N. A. (2007). PDB2PQR: Expanding and upgrading automated preparation of biomolecular structures for molecular simulations. *Nucleic Acids Research, 35*(Web Server issue), W522-5.

38. Dotzlaf, J., Carpenter, J., Luo, S., Miles, R. R., Fisher, D., Qian, Y. W., Ehsani, M., Wang, X., Lin, A., McClure, D. B., Chen, V. J., & Zuckerman, S. H. (2007). Derivation and characterization of monoclonal antibodies against human folypolyglutamate synthetase. *Hybridoma (2005), 26*(3), 155-161.

39. Dougherty, D. A. (1996). Cation-pi interactions in chemistry and biology: A new view of benzene, phe, tyr, and trp. *Science, 271*(5246), 163-8.

40. Falconi, M., Chillemi, G., Di Marino, D., D'Annessa, I., Morozzo della Rocca, B., Palmieri, L., & Desideri, A. (2006). Structural dynamics of the mitochondrial ADP/ATP carrier revealed by molecular dynamics simulation studies. *Proteins, 65*(3), 681-691.

41. Farber, S., & Diamond, L. K. (1948). Temporary remissions in acute leukemia in children produced by folic acid antagonist, 4-aminopteroyl-glutamic acid. *The New England Journal of Medicine, 238*(23), 787-793.

42. Farber, S. (1949). Some observations on the effect of folic acid antagonists on acute leukemia and other forms of incurable cancer. *Blood,* 4(2), 160-167.

43. Fiermonte, G., Walker, J. E., & Palmieri, F. (1993). Abundant bacterial expression and reconstitution of an intrinsic membrane-transport protein from bovine mitochondria. *Biochem J, 294 (Pt 1*), 293-9.

44. Fiermonte, G., Palmieri, L., Todisco, S., Agrimi, G., Palmieri, F., & Walker, J. E. (2002). Identification of the mitochondrial glutamate transporter. *Journal of Biological Chemistry, 277*(22), 19289-19294.

45. Freemantle, S. J., Taylor, S. M., Krystal, G., & Moran, R. G. (1995). Upstream organization of and multiple transcripts from the human folylpoly-gamma-glutamate synthetase gene. *J Biol Chem, 270*(16), 9579-84.

46. Frisch, M. J., Trucks, G. W., Schlegel, H. B., Scuseria, G. E., Robb, M. A., Cheeseman, J. R., Montgomery, J., J. A., Vreven, T., Kudin, K. N., Burant, J. C., Millam, J. M., Iyengar, S. S., Tomasi, J., Barone, V., Mennucci, B., Cossi, M., Scalmani, G., Rega, N., Petersson, G. A., Nakatsuji, H., Hada, M., Ehara, M., Toyota, K., Fukuda, R., Hasegawa, J., Ishida, M., Nakajima, T., Honda, Y., Kitao, O., Nakai, H., Klene, M., Li, X., Knox, J. E., Hratchian, H. P., Cross, J. B., Bakken, V., Adamo, C., Jaramillo, J., Gomperts, R., Stratmann, R. E., Yazyev, O., Austin, A. J., Cammi, R., Pomelli, C., Ochterski, J. W., Ayala, P. Y., Morokuma, K., Voth, G. A., Salvador, P., Dannenberg, J. J., Zakrzewski, V. G., Dapprich, S., Daniels, A. D., Strain, M. C., Farkas, O., Malick, D. K., Rabuck, A. D., Raghavachari, K., Foresman, J. B., Ortiz, J. V., Cui, Q., Baboul, A. G., Clifford, S., Cioslowski, J., Stefanov, B. B., Liu, G., Liashenko, A., Piskorz, P., Komaromi, I., Martin, R. L., Fox, D. J., Keith, T., Al-Laham, M. A., Peng, C. Y., Nanayakkara, A., Challacombe, M., Gill, P. M. W., Johnson, B., Chen, W., Wong, M. W., Gonzalez, C., & and Pople, J. A. (2004). Gaussian 03.

47. Galivan, J., Ryan, T. J., Chave, K., Rhee, M., Yao, R., & Yin, D. (2000). Glutamyl hydrolase. pharmacological role and enzymatic characterization. *Pharmacology & Therapeutics, 85*(3), 207-215.

48. Garcia-Viloca, M., Truhlar, D. G., & Gao, J. (2003). Reaction-path energetics and kinetics of the hydride transfer reaction catalyzed by dihydrofolate reductase. *Biochemistry, 42*(46), 13558-13575.

49. Garrow, T. A., Brenner, A. A., Whitehead, V. M., Chen, X. N., Duncan, R. G., Korenberg, J. R., & Shane, B. (1993). Cloning of human cDNAs encoding mitochondrial and cytosolic serine hydroxymethyltransferases and chromosomal localization. *The Journal of Biological Chemistry, 268*(16), 11910-11916.

50. Geller, J., Kronn, D., Jayabose, S., & Sandoval, C. (2002). Hereditary folate malabsorption: Family report and review of the literature. *Medicine, 81*(1), 51-68.

51. Goldman, I. D., Lichtenstein, N. S., & Oliverio, V. T. (1968). Carrier-mediated transport of the folic acid analogue, methotrexate, in the L1210 leukemia cell. *J Biol Chem, 243*(19), 5007-17.

52. Goldman, I. D. (1971). The characteristics of the membrane transport of amethopterin and the naturally occurring folates. *Annals of the New York Academy of Sciences, 186*, 400-422.

53. Graham, F. L., & van der Eb, A. J. (1973). A new technique for the assay of infectivity of human adenovirus 5 DNA. *Virology, 52*(2), 456-467.

54. Gropp, T., Brustovetsky, N., Klingenberg, M., Muller, V., Fendler, K., & Bamberg, E. (1999). Kinetics of electrogenic transport by the ADP/ATP carrier. *Biophysical Journal, 77*(2), 714-726.

55. Halsted, C. H., Ling, E. H., Luthi-Carter, R., Villanueva, J. A., Gardner, J. M., & Coyle, J. T. (1998). Folylpoly-gamma-glutamate carboxypeptidase from pig jejunum. molecular characterization and relation to glutamate carboxypeptidase II. *The Journal of Biological Chemistry, 273*(32), 20417-20424.

56. Hediger, M. A., Romero, M. F., Peng, J. B., Rolfs, A., Takanaga, H., & Bruford, E. A. (2004). The ABCs of solute carriers: Physiological, pathological and therapeutic implications of human membrane transport proteinsIntroduction. *Pflugers Archiv : European Journal of Physiology, 447*(5), 465-468.

57. Heidkamper, D., Muller, V., Nelson, D. R., & Klingenberg, M. (1996). Probing the role of positive residues in the ADP/ATP carrier from yeast. the effect of six arginine mutations on transport and the four ATP versus ADP exchange modes. *Biochemistry, 35*(50), 16144-52.

58. Heimpel, S., Basset, G., Odoy, S., & Klingenberg, M. (2001). Expression of the mitochondrial ADP/ATP carrier in escherichia coli. renaturation, reconstitution, and the effect of mutations on 10 positive residues. *J Biol Chem, 276*(15), 11499-506.

59. Ho, S. N., Hunt, H. D., Horton, R. M., Pullen, J. K., & Pease, L. R. (1989). Site-directed mutagenesis by overlap extension using the polymerase chain reaction. *Gene, 77*(1), 51-9.

60. Horne, D. W., Patterson, D., & Cook, R. J. (1989). Effect of nitrous oxide inactivation of vitamin B12-dependent methionine synthetase on the subcellular distribution of folate coenzymes in rat liver. *Archives of Biochemistry and Biophysics, 270*(2), 729-733.

61. Horne, D. W., Holloway, R. S., & Said, H. M. (1992). Uptake of 5-formyltetrahydrofolate in isolated rat liver mitochondria is carrier-mediated. *The Journal of Nutrition, 122*(11), 2204-2209.

62. HUGO Gene Nomenclature Committee (HGNC).*HGNC database.* Retrieved 04, 2010, from http://www.genenames.org/

63. Humphrey, W., Dalke, A., & Schulten, K. (1996). VMD: Visual molecular dynamics. *Journal of Molecular Graphics, 1*4(1), 33-8, 27-8.

64. IJlst, L., van Roermund, C. W., Iacobazzi, V., Oostheim, W., Ruiter, J. P., Williams, J. C., Palmieri, F., & Wanders, R. J. (2001). Functional analysis of mutant human carnitine acylcarnitine translocases in yeast. *Biochemical and Biophysical Research Communications, 28*0(3), 700-706.

65. Indiveri, C., Iacobazzi, V., Giangregorio, N., & Palmieri, F. (1997). The mitochondrial carnitine carrier protein: CDNA cloning, primary structure and comparison with other mitochondrial transport proteins. *The Biochemical Journal, 321 (Pt 3*)(Pt 3), 713-719.

66. Institute of Medicine. (1998). *Dietary reference intakes for thiamin, riboflavin, niacin, vitamin B6, folate, vitamin B12, pantothenic acid, biotin, and choline*. Washington DC: National Academies Press.

67. Jackman, A. L., Taylor, G. A., Gibson, W., Kimbell, R., Brown, M., Calvert, A. H., Judson, I. R., & Hughes, L. R. (1991). ICI D1694, a quinazoline antifolate thymidylate synthase inhibitor that is a potent inhibitor of L1210 tumor cell growth in vitro and in vivo: A new agent for clinical study. *Cancer Research, 5*1(20), 5579-5586.

68. Johnston, J. M., Khalid, S., & Sansom, M. S. (2008). Conformational dynamics of the mitochondrial ADP/ATP carrier: A simulation study. *Molecular Membrane Biology, 25*(6-7), 506-517.

69. Kamen, B. A., & Capdevila, A. (1986). Receptor-mediated folate accumulation is regulated by the cellular folate content. *Proceedings of the National Academy of Sciences of the United States of America, 8*3(16), 5983-5987.

70. Kamen, B. A., Wang, M. T., Streckfuss, A. J., Peryea, X., & Anderson, R. G. (1988). Delivery of folates to the cytoplasm of MA104 cells is mediated by a surface membrane receptor that recycles. *The Journal of Biological Chemistry, 26*3(27), 13602-13609.

71. Kao, F., Chasin, L., & Puck, T. T. (1969). Genetics of somatic mammalian cells. X. complementation analysis of glycine-requiring mutants. *Proc Natl Acad Sci U S A, 6*4(4), 1284-91.

72. Kaplan, R. S., Mayor, J. A., & Wood, D. O. (1993). The mitochondrial tricarboxylate transport protein. cDNA cloning, primary structure, and comparison with other mitochondrial transport proteins. *The Journal of Biological Chemistry, 26*8(18), 13682-13690.

73. Kastanos, E. K., Woldman, Y. Y., & Appling, D. R. (1997). Role of mitochondrial and cytoplasmic serine hydroxymethyltransferase isozymes in de novo purine synthesis in saccharomyces cerevisiae. *Biochemistry, 3*6(48), 14956-14964.

74. Kieseritzky, G., & Knapp, E. W. (2008). Optimizing pKa computation in proteins with pH adapted conformations. *Proteins, 7*1(3), 1335-1348.

75. Kihira, Y., Majima, E., Shinohara, Y., & Terada, H. (2005). Cysteine labeling studies detect conformational changes in region 106-132 of the mitochondrial ADP/ATP carrier of saccharomyces cerevisiae. *Biochemistry, 4*4(1), 184-92.

76. Kikuchi, G., Motokawa, Y., Yoshida, T., & Hiraga, K. (2008). Glycine cleavage system: Reaction mechanism, physiological significance, and hyperglycinemia. *Proceedings of the Japan Academy.Series B, Physical and Biological Sciences, 8*4(7), 246-263.

77. Kim, J. S., Lowe, K. E., & Shane, B. (1993). Regulation of folate and one-carbon metabolism in mammalian cells. IV. role of folylpoly-gamma-glutamate synthetase in methotrexate metabolism and cytotoxicity. *The Journal of Biological Chemistry, 26*8(29), 21680-21685.

78. Kitamura, Y., Kusuhara, H., & Sugiyama, Y. (2010). Basolateral efflux mediated by multidrug resistance-associated protein 3 (Mrp3/Abcc3) facilitates intestinal absorption of folates in mouse. *Pharmaceutical Research, 2*7(4), 665-672.

79. Klingenberg, M., Grebe, K., & Heldt, H. W. (1970). On the inhibition of the adenine nucleotide translocation by bongkrekic acid. *Biochemical and Biophysical Research Communications, 3*9(3), 344-351.

80. Klingenberg, M., Falkner, G., Erdelt, H., & Grebe, K. (1971). On the relation between adenine nucleotide carrier sites and atractyloside binding in mitochondria. *FEBS Letters, 1*6(4), 296-300.

81. Klingenberg, M., Grebe, K., & Falkner, G. (1971). Interaction between the binding of 35S-atractyloside and bongkrekic acid at mitochondrial membranes. *FEBS Letters, 1*6(4), 301-303.

82. Klingenberg, M., Riccio, P., & Aquila, H. (1978). Isolation of the ADP, ATP carrier as the carboxyatractylate . protein complex from mitochondria. *Biochimica Et Biophysica Acta, 503*(2), 193-210.

83. Klingenberg, M. (1989). Molecular aspects of the adenine nucleotide carrier from mitochondria. *Archives of Biochemistry and Biophysics, 27*0(1), 1-14.

84. Kolbe, H. V., Costello, D., Wong, A., Lu, R. C., & Wohlrab, H. (1984). Mitochondrial phosphate transport. large scale isolation and characterization of the phosphate transport protein from beef heart mitochondria. *The Journal of Biological Chemistry, 25*9(14), 9115-9120.

85. Kramer, R., Aquila, H., & Klingenberg, M. (1977). Isolation of the unliganded adenosine 5'-diphosphate, adenosine 5'-triphosphate carrier-linked binding protein and incorporation into the membranes of liposomes. *Biochemistry, 16*(23), 4949-4953.

86. Krammer, E. M., Ravaud, S., Dehez, F., Frelet-Barrand, A., Pebay-Peyroula, E., & Chipot, C. (2009). High-chloride concentrations abolish the binding of adenine nucleotides in the mitochondrial ADP/ATP carrier family. *Biophysical Journal, 97*(10), L25-7.

87. Krishnamurthy, P. C., Du, G., Fukuda, Y., Sun, D., Sampath, J., Mercer, K. E., Wang, J., Sosa-Pineda, B., Murti, K. G., & Schuetz, J. D. (2006). Identification of a mammalian mitochondrial porphyrin transporter. *Nature, 443*(7111), 586-589.

88. LaNoue, K. F., & Tischler, M. E. (1974). Electrogenic characteristics of the mitochondrial glutamate-aspartate antiporter. *The Journal of Biological Chemistry, 249*(23), 7522-7528.

89. Liani, E., Rothem, L., Bunni, M. A., Smith, C. A., Jansen, G., & Assaraf, Y. G. (2003). Loss of folylpoly-gamma-glutamate synthetase activity is a dominant mechanism of resistance to polyglutamylation-dependent novel antifolates in multiple human leukemia sublines. *International Journal of Cancer.Journal International Du Cancer, 103*(5), 587-599.

90. Lin, B. F., Huang, R. F., & Shane, B. (1993). Regulation of folate and one-carbon metabolism in mammalian cells. III. role of mitochondrial folylpoly-gamma-glutamate synthetase. *J Biol Chem, 268*(29), 21674-9.

91. Lin, B. F., & Shane, B. (1994). Expression of escherichia coli folylpolyglutamate synthetase in the chinese hamster ovary cell mitochondrion. *J Biol Chem, 269*(13), 9705-13.

92. Lin, C. S., & Klingenberg, M. (1980). Isolation of the uncoupling protein from brown adipose tissue mitochondria. *FEBS Letters, 113*(2), 299-303.

93. Low, P. S., & Kularatne, S. A. (2009). Folate-targeted therapeutic and imaging agents for cancer. *Current Opinion in Chemical Biology, 13*(3), 256-262.

94. Lucas, M. L., Blair, J. A., Cooper, B. T., & Cooke, W. T. (1976). Relationship of the acid micro-climate in rat and human intestine to malabsorption. *Biochemical Society Transactions, 4*(1), 154-156.

95. Lucas, M. L., Cooper, B. T., Lei, F. H., Johnson, I. T., Holmes, G. K., Blair, J. A., & Cooke, W. T. (1978). Acid microclimate in coeliac and crohn's disease: A model for folate malabsorption. *Gut, 19*(8), 735-742.

96. Ma, C., Kotaria, R., Mayor, J. A., Remani, S., Walters, D. E., & Kaplan, R. S. (2005). The yeast mitochondrial citrate transport protein: Characterization of transmembrane domain III residue involvement in substrate translocation. *The Journal of Biological Chemistry, 280*(3), 2331-2340.

97. Ma, C., Remani, S., Sun, J., Kotaria, R., Mayor, J. A., Walters, D. E., & Kaplan, R. S. (2007). Identification of the substrate binding sites within the yeast mitochondrial citrate transport protein. *The Journal of Biological Chemistry, 282*(23), 17210-17220.

98. Ma, C., Remani, S., Sun, J., Kotaria, R., Mayor, J. A., Walters, D. E., & Kaplan, R. S. (2007). Identification of the substrate binding sites within the yeast mitochondrial citrate transport protein. *The Journal of Biological Chemistry, 282*(23), 17210-17220.

99. MacKerell, , A. D., Bashford, D., Bellott, Dunbrack, , R. L., Evanseck, J. D., Field, M. J., Fischer, S., Gao, J., Guo, H., Ha, S., Joseph-McCarthy, D., Kuchnir, L., Kuczera, K., Lau, F. T. K., Mattos, C., Michnick, S., Ngo, T., Nguyen, D. T., Prodhom, B., Reiher, W. E., Roux, B., Schlenkrich, M., Smith, J. C., Stote, R., Straub, J., Watanabe, M., Wiorkiewicz-Kuczera, J., Yin, D., & Karplus, M. (1998). All-atom empirical potential for molecular modeling and dynamics studies of proteinsâ€ . *The Journal of Physical Chemistry B, 102*(18), 3586-3616.

100. Majima, E., Koike, H., Hong, Y. M., Shinohara, Y., & Terada, H. (1993). Characterization of cysteine residues of mitochondrial ADP/ATP carrier with the SH-reagents eosin 5-maleimide and N-ethylmaleimide. *The Journal of Biological Chemistry, 268*(29), 22181-22187.

101. Majima, E., Shinohara, Y., Yamaguchi, N., Hong, Y. M., & Terada, H. (1994). Importance of loops of mitochondrial ADP/ATP carrier for its transport activity deduced from reactivities of its cysteine residues with the sulfhydryl reagent eosin-5-maleimide. *Biochemistry, 33*(32), 9530-9536.

102. Majima, E., Ikawa, K., Takeda, M., Hashimoto, M., Shinohara, Y., & Terada, H. (1995). Translocation of loops regulates transport activity of mitochondrial ADP/ATP carrier deduced from formation of a specific intermolecular disulfide bridge catalyzed by copper-o-phenanthroline. *The Journal of Biological Chemistry, 270*(49), 29548-29554.

103. Marobbio, C. M., Di Noia, M. A., & Palmieri, F. (2006). Identification of a mitochondrial transporter for pyrimidine nucleotides in saccharomyces cerevisiae: Bacterial expression, reconstitution and functional characterization. *The Biochemical Journal, 393*(Pt 2), 441-446.

104. Maurisse, R., De Semir, D., Emamekhoo, H., Bedayat, B., Abdolmohammadi, A., Parsi, H., & Gruenert, D. C. (2010). Comparative transfection of DNA into primary and transformed mammalian cells from different lineages. *BMC Biotechnology, 10*, 9.

105. Mauritz, R., Peters, G. J., Kathmann, I., Teshale, H., Noordhuis, P., Comijn, E. M., Pinedo, H. M., & Jansen, G. (2008). Dynamics of antifolate transport via the reduced folate carrier and the membrane folate receptor in murine leukaemia cells in vitro and in vivo. *Cancer Chemotherapy and Pharmacology, 62*(6), 937-948.

106. McBurney, M. W., & Whitmore, G. F. (1974). Isolation and biochemical characterization of folate deficient mutants of chinese hamster cells. *Cell, 2*(3), 173-82.

107. McCarthy, E. A. (2005). Structure and function of the mitochondrial folate transporter. (Ph.D. Dissertation, Virginia Commonwealth University, Virginia, United States).

108. McCarthy, E. A., Titus, S. A., Taylor, S. M., Jackson-Cook, C., & Moran, R. G. (2004). A mutation inactivating the mitochondrial inner membrane folate transporter creates a glycine requirement for survival of chinese hamster cells. *J Biol Chem, 279*(32), 33829-36.

109. McCloskey, D. E., McGuire, J. J., Russell, C. A., Rowan, B. G., Bertino, J. R., Pizzorno, G., & Mini, E. (1991). Decreased folylpolyglutamate synthetase activity as a mechanism of methotrexate resistance in CCRF-CEM human leukemia sublines. *The Journal of Biological Chemistry, 266*(10), 6181-6187.

110. McGuire, J. J., Hsieh, P., Coward, J. K., & Bertino, J. R. (1980). Enzymatic synthesis of folylpolyglutamates. characterization of the reaction and its products. *The Journal of Biological Chemistry, 255*(12), 5776-5788.

111. Moran, R. G., Werkheiser, W. C., & Zakrzewski, S. F. (1976). Folate metabolism in mammalian cells in culture. I partial characterization of the folate derivatives present in L1210 mouse leukemia cells. *The Journal of Biological Chemistry, 251*(12), 3569-3575.

112. Morozzo Della Rocca, B., Miniero, D. V., Tasco, G., Dolce, V., Falconi, M., Ludovico, A., Cappello, A. R., Sanchez, P., Stipani, I., Casadio, R., Desideri, A., & Palmieri, F. (2005). Substrate-induced conformational changes of the mitochondrial oxoglutarate carrier: A spectroscopic and molecular modelling study. *Molecular Membrane Biology, 22*(5), 443-452.

113. Muller, V., Basset, G., Nelson, D. R., & Klingenberg, M. (1996). Probing the role of positive residues in the ADP/ATP carrier from yeast. the effect of six arginine mutations of oxidative phosphorylation and AAC expression. *Biochemistry, 35*(50), 16132-43.

114. Muller, V., Heidkamper, D., Nelson, D. R., & Klingenberg, M. (1997). Mutagenesis of some positive and negative residues occurring in repeat triad residues in the ADP/ATP carrier from yeast. *Biochemistry, 36*(50), 16008-18.

115. Nakai, Y., Inoue, K., Abe, N., Hatakeyama, M., Ohta, K. Y., Otagiri, M., Hayashi, Y., & Yuasa, H. (2007). Functional characterization of human proton-coupled folate transporter/heme carrier protein 1 heterologously expressed in mammalian cells as a folate transporter. *The Journal of Pharmacology and Experimental Therapeutics, 322*(2), 469-476.

116. Narkewicz, M. R., Sauls, S. D., Tjoa, S. S., Teng, C., & Fennessey, P. V. (1996). Evidence for intracellular partitioning of serine and glycine metabolism in chinese hamster ovary cells. *The Biochemical Journal, 313 (Pt 3)*(Pt 3), 991-996.

117. Nelson, D. R., Lawson, J. E., Klingenberg, M., & Douglas, M. G. (1993). Site-directed mutagenesis of the yeast mitochondrial ADP/ATP translocator. six arginines and one lysine are essential. *Journal of Molecular Biology, 230*(4), 1159-1170.

118. Nelson, D. R. (1996). The yeast ADP/ATP carrier. mutagenesis and second-site revertants. *Biochim Biophys Acta, 1275*(1-2), 133-7.

119. Nelson, D. R., Felix, C. M., & Swanson, J. M. (1998). Highly conserved charge-pair networks in the mitochondrial carrier family. *J Mol Biol, 277*(2), 285-308.

120. Nijhout, H. F., Reed, M. C., Lam, S. L., Shane, B., Gregory, J. F.,3rd, & Ulrich, C. M. (2006). In silico experimentation with a model of hepatic mitochondrial folate metabolism. *Theoretical Biology & Medical Modelling, 3*, 40.

121. Nury, H., Dahout-Gonzalez, C., Trezeguet, V., Lauquin, G. J., Brandolin, G., & Pebay-Peyroula, E. (2006). Relations between structure and function of the mitochondrial ADP/ATP carrier. *Annu Rev Biochem, 75*, 713-41.

122. Palmieri, F., Quagliariello, E., & Klingenberger, M. (1972). Kinetics and specificity of the oxoglutarate carrier in rat-liver mitochondria. *European Journal of Biochemistry / FEBS, 29*(3), 408-416.

123. Palmieri, F., Indiveri, C., Bisaccia, F., & Iacobazzi, V. (1995). Mitochondrial metabolite carrier proteins: Purification, reconstitution, and transport studies. *Methods in Enzymology, 260*, 349-369.

124. Palmieri, F. (2004). The mitochondrial transporter family (SLC25): Physiological and pathological implications. *Pflugers Archiv : European Journal of Physiology, 447*(5), 689-709.

125. Palmieri, F. (2008). Diseases caused by defects of mitochondrial carriers: A review. *Biochimica Et Biophysica Acta, 1777*(7-8), 564-578.

126. Parker, N., Turk, M. J., Westrick, E., Lewis, J. D., Low, P. S., & Leamon, C. P. (2005). Folate receptor expression in carcinomas and normal tissues determined by a quantitative radioligand binding assay. *Analytical Biochemistry, 338*(2), 284-293.

127. Pasternack, L. B., Laude, D. A.,Jr, & Appling, D. R. (1994). 13C NMR analysis of intercompartmental flow of one-carbon units into choline and purines in saccharomyces cerevisiae. *Biochemistry, 33*(1), 74-82.

128. Pebay-Peyroula, E., Dahout-Gonzalez, C., Kahn, R., Trezeguet, V., Lauquin, G. J., & Brandolin, G. (2003). Structure of mitochondrial ADP/ATP carrier in complex with carboxyatractyloside. *Nature, 426*(6962), 39-44.

129. Perchiniak, E., Lawrence, S. A., Kasten, S., Woodard, B. A., Taylor, S. M., & Moran, R. G. (2007). Probing the mechanism of the hamster mitochondrial folate transporter by mutagenesis and homology modeling. *Biochemistry, 46*(6), 1557-1567.

130. Pfaff, E., Klingenberg, M., & Heldt, H. W. (1965). Unspecific permeation and specific exchange of adenine nucleotides in liver mitochondria. *Biochimica Et Biophysica Acta, 104*(1), 312-315.

131. Pfaff, E., & Klingenberg, M. (1968). Adenine nucleotide translocation of mitochondria. 1. specificity and control. *European Journal of Biochemistry / FEBS, 6*(1), 66-79.

132. Phelps, A., Briggs, C., Mincone, L., & Wohlrab, H. (1996). Mitochondrial phosphate transport protein. replacements of glutamic, aspartic, and histidine residues affect transport and protein conformation and point to a coupled proton transport path. *Biochemistry, 35*(33), 10757-10762.

133. Phelps, A., Briggs, C., Haefele, A., Mincone, L., Ligeti, E., & Wohlrab, H. (2001). Mitochondrial phosphate transport protein. reversions of inhibitory conservative mutations identify four helices and a nonhelix protein segment with transmembrane interactions and Asp39, Glu137, and Ser158 as nonessential for transport. *Biochemistry, 40*(7), 2080-2086.

134. Phillips, J. C., Braun, R., Wang, W., Gumbart, J., Tajkhorshid, E., Villa, E., Chipot, C., Skeel, R. D., Kale, L., & Schulten, K. (2005). Scalable molecular dynamics with NAMD. *Journal of Computational Chemistry, 26*(16), 1781-1802.

135. Pitkin, R. M. (2007). Folate and neural tube defects. *The American Journal of Clinical Nutrition, 85*(1), 285S-288S.

136. Pizzorno, G., Mini, E., Coronnello, M., McGuire, J. J., Moroson, B. A., Cashmore, A. R., Dreyer, R. N., Lin, J. T., Mazzei, T., & Periti, P. (1988). Impaired polyglutamylation of methotrexate as a cause of resistance in CCRF-CEM cells after short-term, high-dose treatment with this drug. *Cancer Research, 48*(8), 2149-2155.

137. Punta, M., Forrest, L. R., Bigelow, H., Kernytsky, A., Liu, J., & Rost, B. (2007). Membrane protein prediction methods. *Methods (San Diego, Calif.), 41*(4), 460-474.

138. Qiu, A., Jansen, M., Sakaris, A., Min, S. H., Chattopadhyay, S., Tsai, E., Sandoval, C., Zhao, R., Akabas, M. H., & Goldman, I. D. (2006). Identification of an intestinal folate transporter and the molecular basis for hereditary folate malabsorption. *Cell, 127*(5), 917-928.

139. Racanelli, A. C., Rothbart, S. B., Heyer, C. L., & Moran, R. G. (2009). Therapeutics by cytotoxic metabolite accumulation: Pemetrexed causes ZMP accumulation, AMPK activation, and mammalian target of rapamycin inhibition. *Cancer Research, 69*(13), 5467-5474.

140. Riccio, P., Aquila, H., & Klingenberg, M. (1975). Purification of the carboxy-atractylate binding protein from mitochondria. *FEBS Letters, 56*(1), 133-138.

141. Riccio, P., Aquila, H., & Klingenberg, M. (1975). Solubilization of the carboxy-atractylate binding protein from mitochondria. *FEBS Letters, 56*(1), 192-132.

142. Robinson, A. J., & Kunji, E. R. (2006). Mitochondrial carriers in the cytoplasmic state have a common substrate binding site. *Proc Natl Acad Sci U S A, 103*(8), 2617-22.

143. Robinson, B. H., Williams, G. R., Halperin, M. L., & Leznoff, C. C. (1971). The sensitivity of the exchange reactions of tricarboxylate, 2-oxoglutarate and dicarboxylate transporting systems of rat liver mitochondria to inhibition by 2-pentylmalonate, p-iodobenzylmalonate, and benzene 1,2,3-tricarboxylate. *European Journal of Biochemistry / FEBS, 20*(1), 65-71.

144. Said, H. M., & Redha, R. (1987). A carrier-mediated transport for folate in basolateral membrane vesicles of rat small intestine. *The Biochemical Journal, 247*(1), 141-146.

145. Sanbrook J, & Russel DW. (2001). Molecular cloning. A laboratory manual. *Molecular cloning. A laboratory manual.* (). Cold Spring Harbor, NY: Cold Spring Harbor Press.

146. Shafizadeh, T. B., & Halsted, C. H. (2007). Gamma-glutamyl hydrolase, not glutamate carboxypeptidase II, hydrolyzes dietary folate in rat small intestine. *The Journal of Nutrition, 137*(5), 1149-1153.

147. Shertzer, H. G., & Racker, E. (1974). Adenine nucleotide transport in submitochondrial particles and reconstituted vesicles derived from bovine heart mitochondria. *The Journal of Biological Chemistry, 249*(4), 1320-1321.

148. Shertzer, H. G., & Racker, E. (1976). Reconstitution and characterization of the adenine nucleotide transporter derived from bovine heart mitochondria. *The Journal of Biological Chemistry, 251*(8), 2446-2452.

149. Shih, C., Chen, V. J., Gossett, L. S., Gates, S. B., MacKellar, W. C., Habeck, L. L., Shackelford, K. A., Mendelsohn, L. G., Soose, D. J., Patel, V. F., Andis, S. L., Bewley, J. R., Rayl, E. A., Moroson, B. A., Beardsley, G. P., Kohler, W., Ratnam, M., & Schultz, R. M. (1997). LY231514, a pyrrolo[2,3-d]pyrimidine-based antifolate that inhibits multiple folate-requiring enzymes. *Cancer Research, 57*(6), 1116-1123.

150. Sohn, K. J., Smirnakis, F., Moskovitz, D. N., Novakovic, P., Yates, Z., Lucock, M., Croxford, R., & Kim, Y. I. (2004). Effects of folylpolyglutamate synthetase modulation on chemosensitivity of colon cancer cells to 5-fluorouracil and methotrexate. *Gut, 53*(12), 1825-1831.

151. Spinella, M. J., Brigle, K. E., Sierra, E. E., & Goldman, I. D. (1995). Distinguishing between folate receptor-alpha-mediated transport and reduced folate carrier-mediated transport in L1210 leukemia cells. *The Journal of Biological Chemistry, 270*(14), 7842-7849.

152. Stipani, I., & Palmieri, F. (1983). Purification of the active mitochondrial tricarboxylate carrier by hydroxylapatite chromatography. *FEBS Letters, 161*(2), 269-274.

153. Taylor, E. C., Kuhnt, D., Shih, C., Rinzel, S. M., Grindey, G. B., Barredo, J., Jannatipour, M., & Moran, R. G. (1992). A dideazatetrahydrofolate analogue lacking a chiral center at C-6, N-[4-[2-(2-amino-3,4-dihydro-4-oxo-7H-pyrrolo[2,3-d]pyrimidin-5- yl)ethyl]benzoyl]-L-glutamic acid, is an inhibitor of thymidylate synthase. *Journal of Medicinal Chemistry, 35*(23), 4450-4454.

154. Taylor, R. T., & Hanna, M. L. (1977). Folate-dependent enzymes in cultured chinese hamster cells: Folypolyglutamate synthetase and its absence in mutants auxotrophic for glycine + adenosine + thymidine. *Archives of Biochemistry and Biophysics, 181*(1), 331-334.

155. Taylor, R. T., & Hanna, M. L. (1982). Folate-dependent enzymes in cultured chinese hamster ovary cells: Impaired mitochondrial serine hydroxymethyltransferase activity in two additional glycine--auxotroph complementation classes. *Arch Biochem Biophys, 217*(2), 609-23.

156. Taylor, S. M., Freemantle, S. J., & Moran, R. G. (1995). Structural organization of the human folypoly-gamma-glutamate synthetase gene: Evidence for a single genomic locus. *Cancer Research, 55*(24), 6030-6034.

157. The PyMOL Molecular Graphics System.*PyMOL version 1.2r3pre.*www.pymol.org

158. Thompson, J. D., Higgins, D. G., & Gibson, T. J. (1994). CLUSTAL W: Improving the sensitivity of progressive multiple sequence alignment through sequence weighting, position-specific gap penalties and weight matrix choice. *Nucleic Acids Research, 22*(22), 4673-4680.

159. Tieleman, D. P., Shrivastava, I. H., Ulmschneider, M. R., & Sansom, M. S. (2001). Proline-induced hinges in transmembrane helices: Possible roles in ion channel gating. *Proteins, 44*(2), 63-72.

160. Titus, S. A., & Moran, R. G. (2000). Retrovirally mediated complementation of the glyB phenotype. cloning of a human gene encoding the carrier for entry of folates into mitochondria. *J Biol Chem, 275*(47), 36811-7.

161. Tripos International.*Sybyl 7.1.*, 2006, from www.tripos.com

162. Tripos International.*ORCHESTRAR.*, 2008, from http://www.tripos.com

163. Tripos International.*COMPOSER.*, 2006, from http://www.tripos.com

164. Tripos International.*Sybyl 8.0.*, 2008, from www.tripos.com

165. Walker, J. E., & Runswick, M. J. (1993). The mitochondrial transport protein superfamily. *J Bioenerg Biomembr, 25*(5), 435-46.

166. Walters, D. E., & Kaplan, R. S. (2004). Homology-modeled structure of the yeast mitochondrial citrate transport protein. *Biophysical Journal, 87*(2), 907-911.

167. Wang, X., Shen, F., Freisheim, J. H., Gentry, L. E., & Ratnam, M. (1992). Differential stereospecificities and affinities of folate receptor isoforms for folate compounds and antifolates. *Biochemical Pharmacology, 44*(9), 1898-1901.

168. Wang, Y., Zhao, R., & Goldman, I. D. (2004). Characterization of a folate transporter in HeLa cells with a low pH optimum and high affinity for pemetrexed distinct from the reduced folate carrier. *Clinical Cancer Research : An Official Journal of the American Association for Cancer Research, 1*0(18 Pt 1), 6256-6264.

169. Wang, Y., & Tajkhorshid, E. (2008). Electrostatic funneling of substrate in mitochondrial inner membrane carriers. *Proceedings of the National Academy of Sciences of the United States of America, 105*(28), 9598-9603.

170. Wani, N. A., Hamid, A., & Kaur, J. (2008). Folate status in various pathophysiological conditions. *IUBMB Life, 60*(12), 834-842.

171. Werkheiser, W. C. (1961). Specific binding of 4-amino folic acid analogues by folic acid reductase. *Journal of Biological Chemistry, 236*(3), 888-893.

172. Whetstine, J. R., Flatley, R. M., & Matherly, L. H. (2002). The human reduced folate carrier gene is ubiquitously and differentially expressed in normal human tissues: Identification of seven non-coding exons and characterization of a novel promoter. *The Biochemical Journal, 367*(Pt 3), 629-640.

173. Wohlrab, H. (2009). Transport proteins (carriers) of mitochondria. *IUBMB Life, 61*(1), 40-46.

174. Yamaguchi, R., Andreyev, A., Murphy, A. N., Perkins, G. A., Ellisman, M. H., & Newmeyer, D. D. (2007). Mitochondria frozen with trehalose retain a number of biological functions and preserve outer membrane integrity. *Cell Death and Differentiation, 14*(3), 616-624.

175. Yao, R., Rhee, M. S., & Galivan, J. (1995). Effects of gamma-glutamyl hydrolase on folyl and antifolylpolyglutamates in cultured H35 hepatoma cells. *Molecular Pharmacology, 48*(3), 505-511.

176. Zhao, R., Titus, S., Gao, F., Moran, R. G., & Goldman, I. D. (2000). Molecular analysis of murine leukemia cell lines resistant to 5, 10-dideazatetrahydrofolate identifies several amino acids critical to the function of folylpolyglutamate synthetase. *The Journal of Biological Chemistry, 275*(34), 26599-26606.

177. Zhao, R., Qiu, A., Tsai, E., Jansen, M., Akabas, M. H., & Goldman, I. D. (2008). The proton-coupled folate transporter: Impact on pemetrexed transport and on antifolates activities compared with the reduced folate carrier. *Molecular Pharmacology, 74*(3), 854-862.

178. Zhao, X., Li, H., & Lee, R. J. (2008). Targeted drug delivery via folate receptors. *Expert Opinion on Drug Delivery, 5*(3), 309-319.

VITA

Scott Alan Lawrence was born on August 21, 1981 in Columbus, Ohio. He graduated from St. Francis DeSales High School in 1999 and was admitted to the Pharmacy program at Ohio Northern University in the following fall. At Ohio Northern University, he was inducted into The Rho Chi Society and earned his Bachelor of Science in Pharmacy with distinction in 2004. He has been licensed to practice pharmacy since August of 2004. He started his graduate studies at Virginia Commonwealth University in the department of Pharmacology and Toxicology in the fall of 2004, where he joined the laboratory of Dr. Richard G. Moran. At Virginia Commonwealth University, he was awarded the Charles C. Clayton Award, the Anthony Ambrose Award, the Lauren A. Woods award, was inducted into Phi Kappa Phi and Golden Key International Honour Society and was nominated by his department for the Phi Kappa Phi Virginia Commonwealth University School of Medicine Graduate Scholarship. He has attended the American Association of Cancer Research meeting in 2006, the 2nd International Meeting on Folate Receptors and Carriers, and plans to attend and present his work in the upcoming American Association of Cancer Research meeting in 2010.